INFORMATION TO USERS

This manuscript has been reproduced from the microfilm master. UMI films the text directly from the original or copy submitted. Thus, some thesis and dissertation copies are in typewriter face, while others may be from any type of computer printer.

The quality of this reproduction is dependent upon the quality of the copy submitted. Broken or indistinct print, colored or poor quality illustrations and photographs, print bleedthrough, substandard margins, and improper alignment can adversely affect reproduction.

In the unlikely event that the author did not send UMI a complete manuscript and there are missing pages, these will be noted. Also, if unauthorized copyright material had to be removed, a note will indicate the deletion.

Oversize materials (e.g., maps, drawings, charts) are reproduced by sectioning the original, beginning at the upper left-hand corner and continuing from left to right in equal sections with small overlaps. Each original is also photographed in one exposure and is included in reduced form at the back of the book.

Photographs included in the original manuscript have been reproduced xerographically in this copy. Higher quality 6" x 9" black and white photographic prints are available for any photographs or illustrations appearing in this copy for an additional charge. Contact UMI directly to order.

UMI

UMI Number: 9605749

UMI

300 North Zeeb Road
Ann Arbor, MI 48103

ABSTRACT

THE EFFECT OF CHLORINE, SULFUR, AND PHOSPHOROUS COMPOUNDS ON DEACTIVATION OF PALLADIUM CATALYSTS

by
Tai-Chiang Yu

The effects of HCl, H_2S, tributyl phosphate (TBP), P_2O_5, and zinc dialkyldithophosphate (ZDP) as catalyst poisons for methane oxidation over palladium catalysts supported on γ-alumina were investigated in this study. The overall reaction rate of methane oxidation over palladium catalysts can be simplified into a pseudo first order reaction under excess oxidation conditions.

The deactivation of the catalyst poisoned by HCl is attributed to the loss of active sites due to volatilization of $PdCl_2$. H_2 treatment at 200 ^oC can reactivate the catalyst poisoned by HCl at temperatures of up to 300 ^oC, since no volatilization of $PdCl_2$ occurs at this relatively low temperature. It was found that 1.5 % water vapor in air can retard HCl induced catalyst poisoning and prolong catalyst life.

The effects of H_2S induced catalyst poisoning are attributed to a pore diffusion deactivation mechanism resulting from the reaction of the support with H_2S. Catalyst activity decreased with increasing H_2S concentration and temperature. Surface sulfite and sulfate groups were detected by FT-IR on poisoned catalysts and are believed to be the cause of the decrease of 25 % BET surface area. In the poisoning test at 400 ^oC, the decreases of activation energy suggest that the formation of $Al_2(SO_4)_3$ which transfers the reaction from surface reaction control to pore diffusion control. H_2 treatment at 600 ^oC removes the sulfite and sulfate from the surface of poisoned catalysts and regenerates most

of the fresh catalyst activity. The deactivation of methane oxidation can be described by first order deactivation rate law in presence of 80 ppm H_2S in the feed stream.

In the case of TBP induced poisoning, it is believed that the deposition of product P_2O_5 and other unburned phosphorous compounds cause a decrease of 64% BET surface area and catalyst activity. The catalyst activity decreases with increasing dose of TBP and temperature. The formation of $AlPO_4$ was detected by FT-IR on the aged catalyst. It is believed that a strong impervious film of phosphate blocks access to the pores and is the major deactivation mechanism.

In the case of P_2O_5 induced poisoning, a glass-like P_2O_5 film is produced at elevated temperatures that masks the catalyst surface as indicated for the TBP oxidation and causes a decrease of 92 % BET surface area and catalyst activity. The catalyst activity decreases with increasing dose of P_2O_5 and temperature. The formation of $AlPO_4$ is also detected by FT-IR indicating a similarity between the poisoning mechanism due to TBP oxidation and P_2O_5 addition. Thermal gravimetric analysis (TGA) shows that P_2O_5 can be partially removed by heat treatment in the range of 500 to 820 ^{o}C, but $AlPO_4$ is formed at these temperatures.

Studies of ZDP induced poisoning, treatment at 500 ^{o}C and 820 ^{o}C results in the deposition of a glaze containing a ZDP combustion product, β-$Zn_2P_2O_7$, which was identified by x-ray diffraction crystallography. The glaze masks the catalyst surface causing a decrease of BET surface area as well as catalyst deactivation. The catalyst activity decreases with increasing dose of ZDP and temperature. Heat treatment in air at 650 ^{o}C and H_2 treatment at 600 ^{o}C can slightly improve catalyst activity. TGA and FT-IR measurements show that β-$Zn_2P_2O_7$ is difficult to remove from the aged catalyst. However, H_2 treatment at 800 ^{o}C removes the $Zn_2P_2O_7$ from the catalyst surface, but the regenerated surface has poor catalytic activity. This may be due to palladium sintering at the severe reducing atmosphere used for regeneration.

THE EFFECT OF CHLORINE, SULFUR AND PHOSPHOROUS COMPOUNDS ON DEACTIVATION OF PALLADIUM CATALYSTS

by
Tai-Chiang Yu

A Dissertation
Submitted to the Faculty of
New Jersey Institute of Technology
in Partial Fulfillment of the Requirements for the Degree of
Doctor of Philosophy

Department of Chemical Engineering,
Chemistry and Environmental Science

October 1995

APPROVAL PAGE

THE EFFECT OF CHLORINE, SULFUR AND PHOSPHOROUS COMPOUNDS ON DEACTIVATION OF PALLADIUM CATALYSTS

Tai-Chiang Yu

Dr. Henry Shaw, Dissertation Advisor   Date
Professor of Chemical Engineering, NJIT

Dr. Robert J. Farrauto, Committee Member   Date
Research Fellow, Research and Development, Engelhard Corporation
Adjunct Professor of Chemical Engineering, NJIT

Dr. Dana E. Knox, Committee Member   Date
Associate Professor of Chemical Engineering, NJIT

Dr. Robert B. Barat, Committee Member   Date
Assistant Professor of Chemical Engineering, NJIT

Dr. Somenath Mitra, Committee Member   Date
Assistant Professor of Chemistry, NJIT

BIOGRAPHICAL SKETCH

Author: Tai-Chiang Yu

Degree: Doctor of Philosophy in Chemical Engineering

Date: October, 1995

Undergraduate and Graduate Education:

- Doctor of Philosophy in Chemical Engineering
  New Jersey Institute of Technology, New Jersey, 1995

- Master of Science in Chemical Engineering
  New Jersey Institute of Technology, New Jersey, 1991

- Bachelor of Science in Chemical Engineering
  Chinese Cultural University, Taipei, Taiwan, 1983

Major: Chemical Engineering

Presentations and Publications:

Yu, Tai-Chiang, 1995. "Catalytic Combustion of Methane in Presence of TBP and ZDP," Presented in Student Poster Session, 88th A&WMA Annual Meeting, San Antonio, TX.

Yu, Tai-Chiang, Henry Shaw and James Grow, 1995. "Catalytic Combustion of Methane in Presence of Phosphorous Compounds," Presented in Student Mini-Tech. Conference, NJIT, Newark, NJ.

Shaw, Henry, Yi Wang, Tai-Chiang Yu, and Anthony E. Cerkanowicz, 1993. "Catalytic Oxidation of Trichloroethylene and Methylene Chloride", *ACS Symposium Series 518*, Atlanta, GA.

Yu, Tai-Chiang, Henry Shaw and Robert J. Farrauto, 1992. "Catalytic Oxidation of TCE over PdO Catalyst on γ-Al$_2$O$_3$," *ACS Symposium Series 495*, NYC, NY.

Yu, Tai-Chiang, Henry Shaw and Robert J. Farrauto, 1991. "Catalytic Oxidation of TCE over PdO Catalyst on γ-Al$_2$O$_3$," Presented in Student Mini-Tech. Conference, NJIT, Newark, NJ.

Huang, Ta-Jen and Tai-Chiang Yu, 1991. "Calcination Conditions on Copper/Alumina Catalysts for Carbon Monoxide Oxidation and Nitric Oxide Reduction," *Applied Catalysis*, **71**, 275-282.

Huang, Ta-Jen, Tai-Chiang Yu and Shu-Hsiang Chang, 1989. " Effect of Calcination Atmosphere on CuO/Al$_2$O$_3$ Catalyst for CO Oxidation," *Applied Catalysis*, **52**, 157-163.

Huang, Ta-Jen, Tai-Chiang Yu, 1989. "Effect of Preadsorbed Oxygen Concentration on Activity and Selectivity of Methanol Reactions over Copper Surfaces," *Journal of the Chinese Institute of Chemical Engineers*,vol. **20**, No. 3.

This dissertation is dedicated to
my parents and my wife

ACKNOWLEDGMENT

TABLE OF CONTENTS

TABLE OF CONTENTS
(Continued)

TABLE OF CONTENTS
(Continued)

LIST OF TABLES

LIST OF TABLES
(Continued)

LIST OF FIGURES

LIST OF FIGURES
(Continued)

LIST OF FIGURES
(Continued)

LIST OF FIGURES
(Continued)

CHAPTER 1

INTRODUCTION

1.1 Catalytic Control of Air Pollution

Improving the quality of the environment has become a major concern in this country and around the world. Finding ways to reduce air pollution is critical to improving our environment and quality of life. Some promising methods to control of air pollution involve the use of catalysis. These catalytic control methods include reducing emissions from both mobile sources, such as automobiles, and stationary sources, such as power and manufacturing plants.

1.1.1 Mobile Sources-Control of Automotive Emissions

Gaseous emissions from automobiles contain CO, CO_2, water, unburned hydrocarbons and NO_x. The purpose of automotive three-way catalyst is to convert CO to CO_2, unburned hydrocarbons to CO_2 and water, and NO_x to N_2 and O_2. These three way catalysts are located in the automobile exhaust system so that all exhaust gases pass through them and are oxidized (except for NO_x). These catalysts were originally commercialized in 1975 in order to respond the Clean Air Acts of 1970. Due to the economic incentives in this area, many new catalysts or modified catalysts have been developed to meet the new auto emissions regulations not only for the light duty vehicles but also heavy duty vehicles such as diesel trucks.

1.1.2 Stationary Sources

1.1.2.1 NO_x Emissions Control: Nitrogen and oxygen exist as a variety of stable, but inter-convertible, oxides. They are known as NO_x. NO_x is a combination which includes NO, NO_2 and N_2O. A very large fraction of NO and NO_2 in the atmosphere is

1

anthropogenic. NO is primarily produced in the high temperature combustion of fossil fuels due to fixation of air (i.e., $N_2 + O_2$ or Zeldovitch Mechanism, 1946) and are emitted with the flue gas from power plant. NO_2 is produced from the air oxidation of NO at relatively low temperatures (Shaw, 1974). N_2O, on the other hand, is primarily produced in the biochemical decomposition of nitrogen fertilizers in the soil.

There are two general types of catalytic processes which can be used to control NO_x emissions. If exhaust streams contain an excess or equivalent concentration of reductants compared to the concentration of oxidants, NO_x can be controlled by avoiding the Zeldovitch Mechanism. This is similar to controlling NO_x by a three way automotive catalyst. This type of NO_x control process can be referred to as non-selective catalytic reduction (NSCR). If the exhaust stream is primarily oxidizing, then the second type of NOx control process comes into play. This process can be referred to as selective catalytic reduction (SCR). It is necessary to add ammonia as a reducing agent in this process. The ammonia is added in the presence of O_2 to preferentially react with NO and produce N_2 gas and water.

1.1.2.2 Volatile Organic Compounds (VOCs) and Toxic Emissions Control:

Manufacturing processes often involve organic solvents, feedstocks, or decomposition products that generate VOCs. During processing, small quantities of these VOCs may be released into the atmosphere. Table 1 shows a list of industries that are known to release VOCs into the atmosphere.

Table 1.1 Industries that are Known to have Air Pollution Problems.

Pharmaceutical	Dry cleaning	Breweries
Chemical plants	Paper	Coating process
Electronics industry	Petroleum storage	Food processing
Furniture manufacture	Power generation	Printing
Hazardous waste	Wood coating	Petrochemicals

Reference: (Summers, et al., 1992).

VOCs and toxic gaseous compound are usually controlled with granular activated carbon (GAC), condensing system, wet scrubbing, biodegradation, membranes separation, or incineration. The preferred technology for control of high concentrations of VOCs is incineration. The most often used method, destroys these compounds by burning them at temperatures greater than 1000 $^{\circ}C$ or by oxidation at temperatures between 300 and 350 $^{\circ}C$ over a catalyst. Catalytic oxidation is an energy efficient method to destroy VOC since the operating temperature is much lower than thermal incineration. Furthermore, in recent years, catalytic oxidation of chlorinated hydrocarbons has been demonstrated to be effective by Yu, et al., (1992); Wang, et al., (1992); Windawi (1993), etc. It is found that this process has good degradation efficiency and final product selectivity.

1.2 Potential Impacts of Catalyst Deactivation

In the process of air pollution control, the two major conditions leading to catalyst failure are thermal deactivation and poisoning by constituents in the gas stream.

1.2.1 Mobile Source-Automobile Emissions Control

When a catalyst experiences excessive temperature, the following catalyst deactivation processes may occur:

1. Sintering of the catalytically active component, reducing catalyst activity due to the loss of active sites.

2. Rapid changes of the temperature can result in thermal shock of honeycomb-supported catalysts due to the differences in the expansion/contraction of the surface versus the bulk of the substrate, causing cracking and decrepitation of the support.

3. Differences in expansion coefficients at elevated temperatures between the carrier and substrate can result in loss of adhesion between carrier and substrate.

The major compounds deposited during deactivation of automobile oxidation catalysts from the gas stream are grouped by four kinds of compounds: lead, sulfate,

phosphate, and halides (Williams, 1975). The lead problem has been solved since the abolishment of leaded gasoline. However, control of the other three components from both burning the fuel and lubricating oil is still needed. These components cause catalyst deactivation due to selective poisoning, adsorption on the active sites or interaction with active sites or carrier to produce an inactive compound, or non-selective poisons which are nondiscriminating in that accumulations of foreign substances on both active sites and carrier.

1.2.2 Stationary Sources

1.2.2.1 NO$_x$ Emissions Control: Thermal deactivation usually occurs at excessively elevated temperatures or due to rapid temperature changes which were mentioned above. In the SCR process, the operating temperatures range from 175 °C to 600 °C and depend on the catalyst used in the process. However, at temperatures above 600 °C, in a high water content process stream, zeolites tend to deactivate by a process called de-alumination whereby the Al^{+3} in the SiO_2-Al_2O_3 framework migrates out of the structure (Heck and Farrauto, 1995).

The major possible poisons in the process of NO$_x$ emission control are compounds of sulfur, chlorine, and particulates from the flue gas. The sulfur compounds are oxidized by oxygen to produce SO_2 and SO_3 which adsorb on the active component or react with the carrier to deactivate the catalyst. Small particulates from burning fossil fuels or coal may plug the catalyst pore entrance and deactivate the catalyst. In the SCR process, ammonia is introduced to reduce NO to N_2 but may also react with Cl⁻ to produce NH_4Cl or react with SO_3 to produce NH_4HSO_4 and $(NH_4)_2SO_4$ which deposit on the surface of catalyst or downstream on heat exchangers and other cool equipment. These low melting solids deactivate the catalyst and reduce the efficiency of the heat transfer equipment. Lubrication oil containing Zn, P from seals and compressors are responsible for catalyst deactivation in gas turbine SCR NO$_x$ emission control processes.

1.2.2.2 VOCs Emissions Control: The operating temperature of units designed for catalytic oxidation of VOC's normally range from 300 $^{\circ}$C to 350 $^{\circ}$C (Farrauto, 1992). Much higher temperatures, 450 $^{\circ}$C-600 $^{\circ}$C, are required for the catalytic oxidation of chlorinated hydrocarbons.

Thermal deactivation is not a major cause of catalyst replacement because modern catalysts are developed to be resistant to high temperature degradation. The major catalyst deactivation possibilities result from dust, lubricating oil and trace amount of organo-phosphorous, sulfur and metallic compounds in the gas stream. These impurities plug catalyst pore entrances or react with active sites as well as carrier to deactivate the catalyst.

Besides thermal deactivation and dust in the gas stream, the effect of chlorine, sulfur, and phosphorous compounds on catalyst deactivation is extremely important. In order to improve and expand the capabilities of these air pollution control processes, it is important to understand how catalyst deactivation occurs. This research is directed at explaining the mechanism by which chlorine, sulfur and phosphorous compounds affect PdO/γ-Al$_2$O$_3$ catalyst. In conducting this research, we hope to determine how catalysts are poisoned, and thus, how to avoid poisoning. Also, to the extent possible, we hope to find methods to regenerate deactivated catalysts.

CHAPTER 2

LITERATURE REVIEW

The literature study summarized in this chapter focuses on the fundamentals of catalyst deactivation and the research background for this thesis.

2.1 Palladium Catalysts

2.1.1 Palladium Chemistry

Palladium is a silver-white ductile metal which has a great affinity for hydrogen, being able to absorb that gas to a greater degree than any other metal. Palladium makes an excellent and versatile catalyst. Its merits have long been appreciated and its uses are constantly increasing in number. Palladium has been shown to have catalytic activity in many types of organic reactions, including hydrogenations, isomerizations, disproportionations, dehydrogenations and oxidations (Bailar Jr., 1973; Wise, 1968; Hartley, 1973). It has been widely used not only in organic chemistry but also in environmental catalysis (Farrauto, et al., 1992).

Most heterogeneous palladium catalysts are manufactured adsorbing one of two palladium aqueous salts, $PdCl_2$ or $Pd(NO_3)_2$ on a high surface area support. $PdCl_2$ is easily recovered during Pd refining and is less expensive. $Pd(NO_3)_2$ is derived from the chloride, and hence, is more expensive because it must be further processed. However, it is not easy to get rid of the Cl^- ion in preparing palladium catalyst by using $PdCl_2$ as precursor and the presence of chloride is known to have strong effects on catalyst performance (Simone, et al., 1991).

Once the catalyst is calcined on a high surface area substrate, the resultant catalyst has a brown color indicative of the presence of palladium oxide. Unlike platinum, palladium is oxidized to palladium oxide, PdO, in air at temperature above 500 °C, and it

6

dissociates to free metal and oxygen at above 875 $^{\circ}$C (Farrauto, et al., 1992; Wise, 1968). It glows on contact with hydrogen at room temperature, being reduced to the metal (Bailar, Jr., 1973). Its halogen salt, $PdCl_2$, is dark red color and melts at 500 $^{\circ}$C (Weast, 1974). PdS can be obtained as a grayish-black crystalline powder by heating palladium and sulfur together. The melting point of PdS is 970 $^{\circ}$C.

2.1.2 Palladium Catalysts in Environmental Applications

The excellence of palladium supported catalysts as a methane oxidation catalyst is well known in the literature (Hoyos, et al., 1993, Simone, et al., 1991, Farrauto, et al., 1992). This catalyst is used in the catalytic combustion of natural gas for energy production, produces very little NO_x because of the relatively low reaction temperature (Mouaddib, et al., 1992). Also, in catalytic oxidation of VOCs for treating industrial gases, it has high activity and good selectivity for the usual gas emissions.

In recent years, natural gas has received much more attention as an alternative fuel for automobiles because of its potential technical, economic and environmental advantages . Environmental benefits of natural gas include low photochemical reactivity, reduced cold start CO emissions and zero evaporative emission (Oh, et al., 1992). Furthermore, the relatively low content of carbon in methane can reduce CO_2 emissions for the same energy input from vehicular traffic. This leads to reduced greenhouse gas emissions. However, emissions of unreacted methane may be more hazardous because methane is a stronger infrared absorber causing a larger greenhouse contribution than CO_2. Palladium catalysts are considered the best approach for treating unreacted natural gas in compressed natural gas automobile applications.

In the case of three way catalysts, the performance of palladium-only three way catalysts was evaluated by Hepburn, et al., (1994). He showed significantly improved light-off characteristics and greatly enhanced thermal stability compared to currently produced Pt/Rh three way catalyst formulations. In fact, the new Pd-only washcoats have

better oxygen storage capacity which provide improved CO and NO_x conversion capability. As a result, Ford is planning to use a Pd-only catalyst in the production of a limited number of 1995 model vehicles in the North American market (Hepburn, et al., 1994).

2.2 Catalyst Characterization

In heterogeneous catalytic reactions, a number of physical and chemical properties are very important for the catalyst to perform as required. In this study, some of properties that must be measured will be discussed in order to investigate the effect of chlorine, sulfur and phosphorous on catalyst performance.

2.2.1 Physical Properties of Catalyst

2.2.1.1 Surface Area: The way of determining of internal surface area of porous materials is based on the adsorption of N_2 at liquid N_2 temperature onto the internal surface area. Each adsorbed molecule occupies an area of the surface comparable to its cross-sectional area of 0.162 nm^2. By measuring the number of N_2 molecules adsorbed in a monolayer coverage, one can calculate the available surface area.

The most common method of measuring surface area is that developed by Brunauer, Emmett and Teller (1938). The equation describes the relationship between volume adsorbed at a given partial pressure and the volume adsorbed at monolayer coverage:

$$\frac{P}{V(P_o - P)} = \frac{1}{V_m C} + \frac{(C-1)P}{V_m C P_o} \qquad (2-1)$$

where:

      P is partial pressure of N_2, mm Hg,

      P_0 is saturation pressure at the experimental temperature, mm Hg,

V is volume of N_2 adsorbed at P, cm^3,

V_m is volume adsorbed at monolayer coverage, cm^3,

C is a constant related exponentially to the heats of adsorption and liquefaction of the gas (Satterfield 1980).

where $C = exp[(q_1-q_L)/RT]$ (2-2)

   q_1 = heat of adsorption on the first layer, kcal/mole,

   q_L = heat of liquefaction of adsorbed gas on all other layers, kcal/mole

   R = gas constant, kcal/mole-K

   T = absolute temperature, K

By rearranging this equation, we obtain a straight line relationship $y = ax + b$, where y is equal to $P/V(P_0-P)$, x is equal to P/P_0, a is the slope $(C-1)/V_mC$ and b is the intercept $1/V_mC$. Therefore, V_m can be calculated by conducting experiment at different values of P/P_0 (Heck and Farrauto, 1995; Farrauto, 1974).

2.2.1.2 Pore Size Distribution: The equipment for measuring surface area also can be used to determine pore size distributions of materials with pore diameters less than 10 nm, except that relative high pressures are used to condense N_2 in the catalyst pores. The pressure at which a vapor will condense is determined by the curvature of the meniscus of the condensed liquid in the pores. This is given by the Kelvin equation for the variation of vapor pressure with surface curvature in a capillary tube closed at one end.

$$\ln \frac{P}{Po} = \frac{-2\sigma Vmcos\theta}{rRT}$$ (2-3)

where   P = vapor pressure of liquid over the curved surface, measured pressure,
         mm Hg,

   P_0 = vapor pressure of liquid over a plane surface, saturation pressure,
         mm Hg,

σ = surface tension of the liquid adsorbate, liquid N_2, erg/cm^2,

V_m = molar volume of the liquid adsorbate, liquid N_2, cm^3/mole,

θ = contact angle,

r = radius of the pore, cm,

R = gas constant, kcal/mole-K,

T = absolute temperature, K.

By either descending or ascending P/P$_o$, a value for V_m can be measured and pore size can be calculated from the Kelvin equation. The pore size distribution of a catalyst is usually presented in the form of a plot of the increment of pore volume per increment in pore size, versus pore size.

The pore size also can be measured by mercury intrusion. This is given by the Washburn equation: (Heck and Farrauto, 1995; Satterfield, 1980)

$$d = \frac{-4r\cos\theta}{P}$$

(2-4)

where d is pore size diameter, m,

r is surface tension, 0.48 N/m,

θ is contact angle, usually is 130°,

P is pressure in atmosphere, N/m^2.

By calculating it, the equation can be reduced to

$$d = \frac{15000}{P}$$

(2-5)

Therefore, pore size can be calculated by increasing pressure of mercury. Typical pore size distribution by the mercury intrusion method can be plotted by mercury penetration integration as a function of applied pressure.

Information on some other physical properties such as particles size, crush test, thermal shock are referred to in the literature (Satterfield, 1980) and will not be discussed here, since it was not used in the experimental program of this thesis.

2.2.2 Chemical Properties

2.2.2.1 Elemental Analysis: The proper combination of chemical components needed to make catalyst with good performance include promoters that are added to catalysts during preparation. The optimum contents of active compounds are essential in catalyst preparation. However, a small amount of impurity may cause catalysts to lose activity or selectivity. Therefore, an elemental analysis is important for projecting catalyst performance. By dissolving the catalyst, some typical instruments such as Atomic Absorption (AA), Inductively Coupled Plasma (ICP) can be applied to analyze for trace chemical components.

2.2.2.2 Chemisorption and Dispersion: Specific chemisorption methods have found considerable utility in determining the selective adsorption of a gas onto the active component of a supported catalyst. By using this method, one can understand the dispersion of active component on the carrier surface as well as metal surface area. Three kinds of analytical methods can be conducted in measuring chemisorption: static vacuum system, continuous flow apparatus, and plus flow method (Farrauto, 1974).

Pulse adsorption method is used in this research. An usual procedure is to inject a known volume of gas of known composition into a stream of carrier gas which passes through the catalyst bed. If the adsorbate is completely taken up by the catalyst, the detection system will not sense the change in thermal conductivity. When saturation of the catalyst is achieved, then additional adsorbate passes into the detector, and the area under the thermal conductivity response curve provides the volume of gas adsorbed. By knowing

the composition of the adsorbate, pulse volume, and the number of pulses, one can calculate the volume of adsorbate per an unit weight of catalyst.

In the case of palladium adsorption, CO is preferred as the adsorbate in pulse adsorption method (Farrauto, 1974). By assuming Pd-CO adsorption is linear, one can calculate the moles of Pd atoms on the surface of catalyst. Dispersion is defined as (Heck and Farrauto, 1995):

$$\text{Dispersion} = \frac{\text{Number of catalytic sites on the surface}}{\text{Theoretical number of sites present}} \qquad (2\text{-}6)$$

Basically, dispersion is an index which reflect crystalline size of active component on the surface of a substrate and is a diagnostic method used to understand how a catalyst is affected by some unusual condition such as high temperature, or presence of a poisons.

2.2.2.3 X-ray Diffraction Analysis: X-ray diffraction (XRD) can be used for qualitative and quantitative analysis of a material on the surface on catalyst, if the material is present in mass sufficient to diffract x-rays. Normally, the minimum limit of detection is approximately 5% for compounds and approximately 1% for elements (Satterfield, 1980). The bulk content can be identified by the angle of diffraction and relative intensity of each diffraction angle.

The size of crystalline material can be identified by the width of diffraction angle pattern. This is given by the Scherrer equation (Satterfield, 1980):

$$B = \frac{k\lambda}{l\cos\theta} \qquad (2\text{-}7)$$

where B is the net width at half height of an x-ray diffraction line due to a specific crystalline plane to the size of the crystallites, l, nm; λ is the wavelength of x-rays, nm; θ is Bragg angle and k is the constant, usually equal to one. Thus, as the crystallite size of a

catalyst increases, the diffraction patterns becomes increasingly sharper. This information allows the researcher to know if the active components are sintering and whether the carrier has undergone a phase change.

2.2.2.4 Thermal Gravimetric Analysis: In catalytic processes, a small amount of impurities which deposit or adsorb on the catalyst may affect catalyst activity. The deposition of carbon in coking is a common deactivation process for many organic catalytic process.

Thermal gravimetric analysis is a technique that provides understanding of microscopic catalyst changes by measuring the weight change of catalyst with changing experimental conditions. This method has been applied for adsorption-desorption studies and has been useful for studying the rate of coking, dehydration, sorption of poisons, and catalyst regeneration as a function of temperature (Satterfield, 1980).

2.2.2.5 Analysis of Surface Composition of Catalyst: Surface composition analysis, as opposed to elemental analysis, is a technique used to provide information on what compounds deposit on the surface of catalyst. It is helpful in diagnosing catalyst poisoning mechanism as well as chemical reactions that occur on the surface of a catalyst. X-ray photoelectron spectroscopy (XPS) is used more widely than others techniques for studying the surface composition and oxidation states of industrial catalysts (Heck and Farrauto, 1995).

In XPS, a sample is bombarded with monochromatic X rays, and photoelectrons of different energy are ejected from the various atomic shells. The intensity of electrons emitted from the first few atomic monolayer is high, but drop off from subsequent layers, falling exponentially as the limit of about 10 nm is approached (Satterfield, 1980). The electrons are resolved for their kinetic energy, which gives information on their binding energy. These binding energies are sensitive to the overall charge on the atom. Hence, the

composition of this thin layer can be determined by removing or sputtering away top layers and analyzing the underlying surfaces.

2.3 Catalyst Deactivation Mechanism

2.3.1 Fundamental Gas-Solid Phase Catalytic Reaction

In heterogeneous catalytic reaction, the overall reaction process can be separated into a sequence of individual steps which are shown below (Heck and Farrauto, 1995; Fogler, 1986):

1. Mass transfer of the reactants from the bulk fluid to the external surface of the catalyst.

2. Diffusion of the reactant from the pore mouth through the catalyst pores to the immediate vicinity of the internal catalytic surface.

3. Adsorption of reactant onto the catalyst surface.

4. Reaction on the surface of the catalyst.

5. Desorption of the products from the surface.

6. Diffusion of the products from the interior of the catalyst to the pore mouth at the external surface.

7. Mass transfer of the products from the external catalyst surface to the bulk fluid.

The overall reaction rate is determined by the slowest step in the mechanism. Figure 2.1 shows a typical reactant conversion as a function of temperature plot, assuming a first order reaction is occurring in a packed bed.

In the chemical kinetic region, where the diffusion steps 1, 2, 6, 7 are fast compared to the reaction step, the rate of equation is expressed by the following equation:

$$-r_A = \eta k S_a C_{AS} \qquad (2\text{-}8)$$

where, $-r_A$ is the rate of equation, mole/g catalyst sec

η is effectiveness factor, $0 \le \eta \le 1$.

k is the rate constant, cm^3/cm^2 sec.

S_a is surface area per gram of catalyst, cm^2/g

C_{AS} is the concentration of A on the surface of catalyst, mole/cm^3.

Since mass transfer resistance and pore diffusion resistance are neglected, C_{AS} is equal to bulk concentration of A, C_A and η is equal to one where the η is defined as follows:

$$\eta = \frac{\text{actual overall rate}}{\text{rate that would result if the entire surface were exposed to the external surface concentration } C_{As}} \qquad (2\text{-}9)$$
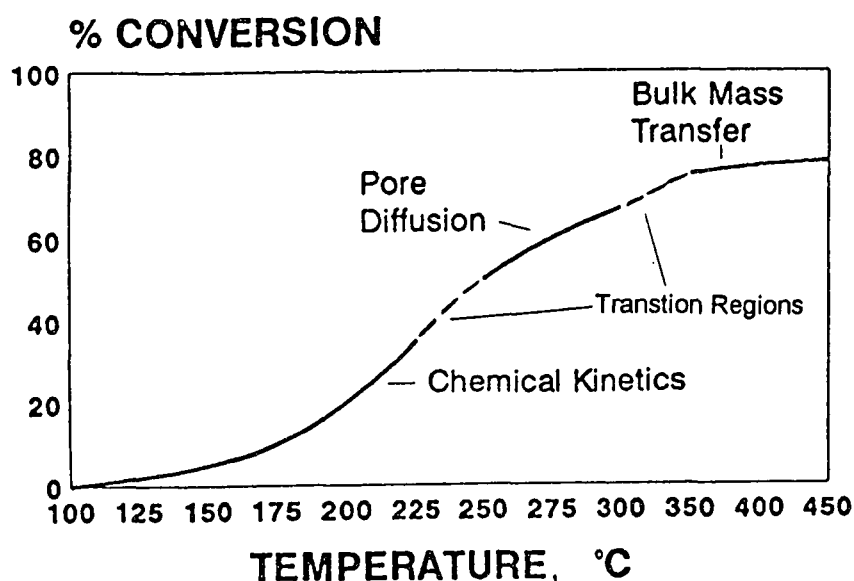
% CONVERSION

Chemical Kinetics, Ea > 10 Kcal/Mole
Pore Diffusion, Ea = 6-10 Kcal/Mole
Bulk Mass Transfer, Ea = 2-4 Kcal/Mole

Figure 2.1 Conversion versus Temperature Profile Illustrating Regions for Chemical Kinetics, Pore Diffusion, and Bulk Mass Transfer Control (Heck and Farrauto 1995).

Hence, equation (2-8) can be reduces to:

$$-r_A = kS_aC_A \qquad (2\text{-}10)$$

It is assumed that S_a is a constant. Then, equation (2-10) can be expressed as follows:

$$-r_A = k' C_A = A \exp(-E_a/RT)C_A \qquad (2\text{-}11)$$

where $k' = kSa = cm^3/g\text{-sec}$,

Ea is apparent activation energy, kcal/mole,

A is pre-exponential factor, 1/g-sec,

R is gas constant, kcal/mole-K,

T is absolute temperature, K.

Therefore, the reaction rate is proportional to the negative exponential of inverse temperature. So, the rate of conversion of A increases with temperature (see Figure 2.1).

In the pore diffusion region, steps 1, 3, 4, 5, 7 are fast compared to diffusion step 2 and 6, and the rate equation can be expressed by:

$$-r_A = \eta k S_a C_{AS} \qquad (2-12)$$

where η is the internal effectiveness factor,

C_{AS} is the concentration of A on the catalyst surface.

Since rate is internal pore diffusion limited, C_{AS} is assumed equal to $C_A \cdot \eta$ according to Fogler, 1986:

$$\eta = \frac{3}{R} \sqrt{\frac{D_e}{S_a k \rho_p}} \qquad (2-13)$$

Substitute equation (2-13) into equation (2-12), we obtain

$$-r_A = \frac{3}{R} \sqrt{\frac{D_e S_a k}{\rho_p}} C_A \qquad (2-14)$$

where R is radius of catalyst particle, cm,

D_e is effective diffusivity, cm^2/s

ρ_p is particle density, g/cm^3.

Equation (2-15) can be arranged as follows:

$$-r_A = \frac{3}{R} (\frac{D_e S_a A}{\rho_p})^{0.5} [\exp(-E_a/RT)]^{0.5} C_A$$

$$= A' [\exp(-E_a/RT)]^{0.5} C_A \qquad (2-15)$$

then, $-r_A$ is proportional to the square root of the negative exponential of inverse temperature. Hence, the rate of conversion of A increases with temperature but not very sensitive to temperature compared to chemical kinetic control region.

In bulk mass transfer region, steps 2, 3, 4, 5, 6, are faster than the bulk mass transfer step 1 and 7. The rate equation can be expressed as follows:

$$-r_A = a_c k_c (C_A - C_{AS}) \tag{2-16}$$

where k_c is mass transfer coefficient, m/sec

a_c is bulk surface area per gram, cm^2/g

For mass transfer limited reactions, C_{AS} approaches zero and equation (2-16) can be written as follows:

$$-r_A = a_c k_c C_A \tag{2-17}$$

where,

$$k_c = 0.6 \left(\frac{D_{AB}}{d_p}\right) Re^{1/2} Sc^{1/3}$$

$$= 0.6 \left(\frac{D_{AB}}{d_p}\right)\left(\frac{U d_p}{v}\right)^{1/2}\left(\frac{v}{D_{AB}}\right)^{1/3}$$

$$= 0.6 (D_{AB})^{2/3}(\upsilon)^{-1/6}(U)^{1/2}(d_p)^{-1/2} \tag{2-18}$$

where   Sc is Schmidt number, dimensionless,

Re is Reynolds number, dimensionless,

D_{AB} is gas phase diffusivity, m^2/s,

d_p is diameter of pellet, m,

U is free-stream velocity, m/s,

υ is kinematic viscosity, m^2/s.

Since D_{AB} is proportion to $T^{1.75}$ and υ is proportion to $T^{3/2}$, therefore, k_c is proportional to $T^{11/12}$ (Fogler, 1986). Hence, the rate equation, in the mass transfer control region, is almost linear with temperature.

Including temperature effects, the dependence of the rate of reaction on the velocity through the bed, particle diameter and temperature for the three types of limitations are listed in Table 2.1

Table 2.1 The Dependence of Rate of Reaction for Three Types of Limitations

Type of limitations	Velocity	Particle size	Temperature
Mass transfer	$U^{1/2}$	$(d_p)^{-2/3}$	~ Linear
Pore diffusion	Independent	$(d_p)^{-1}$	Exponential (not too strong)
Kinetic control	Independent	Independent	Exponential

Reference: (Fogler, 1986).

2.3.2 Catalyst Deactivation

There are many ways in which catalyst can be deactivated. There are at least four major deactivation mechanism. In the first, reactants may produce by-product which irreversibly adsorb on the surface of catalyst. This is called parallel deactivation. A second way occurs when the reaction products decompose or reacts further to produce a material which then deposited on the surface of the catalyst, deactivate the catalyst. This is called series deactivation. A third method involves the deposition of feed stream impurities which may deactivate the catalyst. This is called side-by-side deactivation. The fourth process for catalyst deactivation involves the structural modification or sintering of the catalyst caused by exposure of the catalyst to extreme conditions such as high temperature. This is called independent deactivation (Levenspiel, 1972). This reference does not deal with loss of active material due to volatilization or dissolution.

According to Butt (1988) and Satterfield (1980), catalyst deactivation mechanism may be grouped into the following categories:

1. Deactivation by poisoning

2. Deactivation by coking and fouling

3. Deactivation by sintering

4. Deactivation by loss of active catalytic materials.

Catalyst poisoning that occurs by strong selective adsorption on the active sites of the catalyst is called selective poisoning; or a nondiscriminating adsorption on the whole catalyst, non-selective poising. If adsorption is weak, then activity can be regenerated by

heat treatment or by chemical cleaning. If adsorption is strong, then poisoning is often permanent. Desorption may be enhanced by reaction with the fluid. Besides, the poisoning material may be adsorbed by the catalyst and react with active component, thus deactivating the catalysts. A poison can react with the carrier to shrink surface area, thus reducing activity.

The term fouling is generally used to describe a physical blockage such as deposition of dust, fine powder, or carbonaceous substance (coke). Sintering of supported metallic catalysts is often due to catalyst expose to high temperatures for extended periods of time. The active metal crystallites migrate together and grow to bigger crystallites which reduce metal surface area resulting in a loss of activity. In some cases, active metals react with impurities to produce a low melting compounds which can vaporize, resulting in the loss of the active catalytic component. This type of poisoning causes permanent catalyst deactivation because the active components are lost.

Loss of Active Sites = Sintering of Sites and Carrier
Pore Diffusion = Smaller Effective Pores
Masking = Some Surface Sites Covered and Pores Blocked
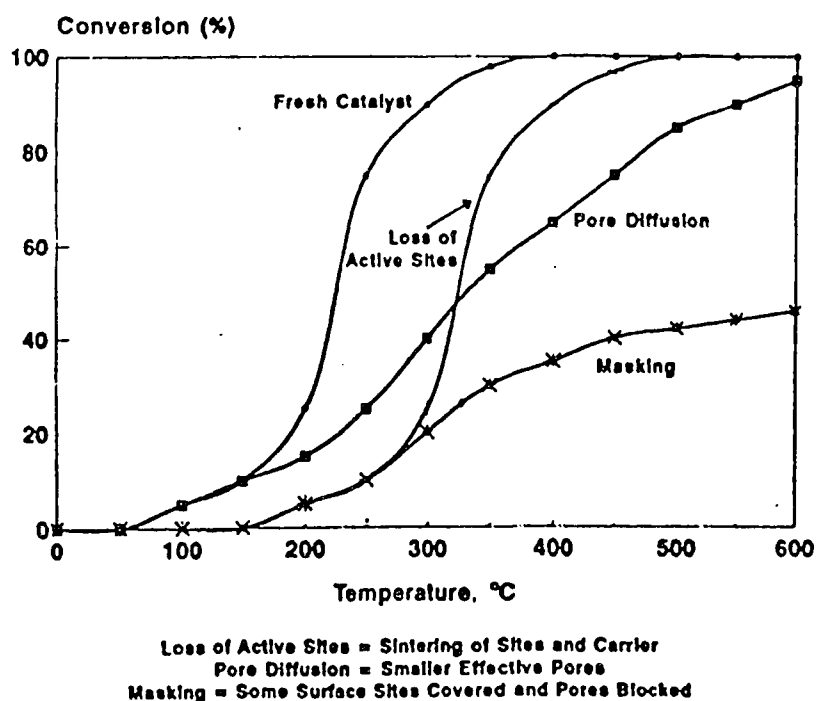
Figure 2.2 Relative Changes in the Conversion versus Temperature Profile for Various Deactivation Mechanisms (Heck and Farrauto 1995).

Figure 2.2 shows typical relative changes in conversion as a function of average bulk temperature for various deactivation mechanisms. It is often found that in order to maintain conversion, the curve for a catalyst that has lost active sites must be shifted to higher temperature. This shift does not affect the rate of pore diffusion or mass transfer. This process indicates that the reaction needs higher temperature to get the same conversion that is obtainable with fresh catalysts to compensate for loss of active sites. Since the curves very similar, but displaced down the conversion axis, the same mechanism seems to apply in the three zones (kinetics, diffusion and bulk mass transfer). The pore diffusion curve shows the temperature at which pore diffusion control is high enough to provide heat to the reaction, but the reactants can not easily penetrate into the pores, since the catalyst is deactivated by pore blocking. Therefore, the slope of the pore diffusion curve is lower than that for fresh catalysts. In the masking deactivation mechanism, the reactants have difficult accessing the catalyst surface since the catalyst surface is blocked by non catalytic materials and the catalyst geometric area is reduced due to coverage by this substance. Therefore, complete conversion can not be achieved, even though the temperature is more than adequate.

Catalyst deactivation may be caused by one or one more mechanisms. The detailed experimental study presented in the rest of this literature review will refer to these introductory concepts.

2.4 The Effect of Chlorine Compounds on Deactivation of Palladium Catalysts

2.4.1 Catalytic Oxidation of Chlorinated Hydrocarbons

Chlorinated hydrocarbons are widely used in dry cleaning, degreasing operations, and as solvents in the pharmaceutical industry, but their vapors are toxic to human beings, causing potential liver damage (Bond 1973). Some of chlorinated hydrocarbons such as trichloroethylene (TCE), and dichloromethane (DCM) are suspected a cancer causing

agent in humans (New Jersey Department of Health 1986). There may be no safe level of exposure for a carcinogen, so all contact should be minimized to the lowest possible level.

Catalytic oxidation is an energy efficient method to destroy chlorinated hydrocarbons (Lester, 1990). Numerous metal catalysts have been evaluated for their potential for oxidizing hydrocarbons and chlorinated hydrocarbons. These materials are usually divided into noble metals and transition metal oxides. The activity of noble metal catalysts for the complete oxidation of chlorinated compounds is reported by Ramanathan, et al., (1989) and Pope, et al., (1978). The transition metal oxide catalysts were also evaluated for treating chlorinated hydrocarbons by Senkan, et al., 1986; Ramanathan, et al., 1989 and Novinson, 1989. An investigation of catalytic oxidation of TCE and DCM on noble metal catalyst such as platinum and palladium, as well as metal oxide catalysts, such as iron oxides, and manganese oxides, is reported by Shaw, et al., 1991, 1992; Xu, 1994. These studies indicate that platinum is an excellent catalyst for treating chlorinated hydrocarbons and palladium, iron oxide catalyst are also suitable but manganese oxide is not suitable for oxidation of chlorinated hydrocarbons. Catalytic oxidation in conjunction with pneumatic fracturing, air striping, and heat injection will be demonstrated in 1995 under the EPA SITE program (EPA, 1994) for remediating a TCE contaminated site in New Jersey. Some of the TCE will be stripped from the water at the site.

A number of catalytic oxidation processes were also developed for destroying hazardous organics in aqueous waste streams (Baker, et al., 1989; Olfenbuttel, 1991). Consequently, catalytic oxidation dose not only solve air pollution problems but also can be used to solve water pollution problems.

2.4.2 The Effects of Chlorine Compounds on Deactivation of Catalysts

Complete catalytic oxidation of various chlorinated hydrocarbons in air or even in aqueous system is a useful technique. However, changes in activity and selectivity associated with

deactivation of these catalysts have important consequences for the performance of commercial and developmental control systems.

Products from the complete catalytic oxidation of chlorinated compounds are CO_2, H_2O and HCl if the reactant Cl/H ratio is less than one. If the ratio is large than one then, Cl_2 may also be a product. However, water or CH_4 added in the reaction provides H atoms to increase HCl selectivity at the expense of Cl_2 (Yu, et al., 1992; Windawi and Wyatt, 1993). Hence, appropriate treatment of effluent HCl is required for long term operation.

In deactivation studies conducted by Bond, 1975 for a number of chlorinated hydrocarbons over a series of Pt catalyst at 420 °C to 500 °C, it was found that no deactivation is observed for Pt on γ-alumina catalysts containing over 0.8 % Pt during a period of 12 hours at a conversion of 95% for feed containing 13,000 ppm C_2Cl_4. Mendyka, et. al., 1992 studied the deactivation of Pt oxidation catalysts by HCl vapor added to the inlet gas in order to simulate the HCl contribution from chlorinated hydrocarbons, and because HCl is often found in industrial flue gas, together with chloroorganic compounds and/or hydrocarbons. These studies showed that catalysts containing less than 0.15% were resistant to poisoning by chloroorganic compounds when xylene was present. One can infer that the production of water vapor as a source of hydrogen from the oxidation of xylene prevents catalyst poisoning.

Cullis, et al., 1970 reported on the partial oxidation of methane on a PdO sponge catalyst. Methylene chloride was added in pulses to the inlet gas stream, which contained methane. Methane oxidation was strongly inhibited and formaldehyde was formed. It was suggested that a strong interaction of chlorine with the catalyst leads to poisoning. However, pulses of pure CH_4 plus O_2 gradually restored the original activity, showing that the effect of this interaction is reversible. The effect of adding pulses of chloro- or bromo-hydrocarbons to the feed stream was examined for methane oxidation by Hucknall, et al., (1980). They found that halogenated hydrocarbons inhibit the oxidation of methane

over supported palladium catalysts. On alumina supported catalysts, the poisoning can be accounted for in terms of the interaction of the inhibitor with catalytically-active palladium (II) oxide to give metallic palladium. It was also found that adsorption of halogens on the metal and deposition of an organic residue on the catalyst surface also affect catalyst performance. Since these poisoning experiments due to halogenated hydrocarbons were performed in a helium atmosphere, no HCl effect on catalyst deactivation was reported.

In a recent study, Simone, et al., 1991 reported that catalyst containing chloride salts from the preparation methods produce catalysts that are inferior in performance for methane oxidation than others made without chloride containing salts. The results strongly suggest that localized site blockage and /or inductive effects are responsible for poor performance. The effects of chloride and water on propane and propene oxidation over platinum and palladium on alumina is reported by Barbier, et al., (1994). They find that for catalyst prepared from chloride containing precursor salts, chloride poisons the metallic activity regardless of particle size. Also, the effect of chloride is more detrimental under oxidizing conditions. Nevertheless, the poisoning effect disappears as a consequence of the removal of chloride from the catalyst surface by water produced during propane and propene oxidation.

2.5 The Effects of Sulfur Compound on Deactivation of Palladium Catalysts

Sulfur poisoning of noble metals has been widely studied (Hoyos, 1992, 1993; Gandhi and Shelef, 1991). In the catalytic control of air pollution processes, especially in automobile catalytic converters, low level amounts of sulfur compounds present in the exhaust gas are known to poison noble metal catalysts even though the poisoning is considerably less severe than base metal catalyst poisoning (Yao, et al., 1981).

There are a large number of papers describing studies the sulfur poisoning of platinum catalyst (Yao, et al., 1981; Ansell, et al., 1991; Hubbard, et al., 1993). In Yao's study, the SO_2 in the feed gas enhanced the propane oxidation but suppressed both

propylene and carbon monoxide oxidation over a Pt/γ-Al$_2$O$_3$ catalyst. The formation of surface sulfates on γ-Al$_2$O$_3$ could be interpreted to be the major reason for the enhancement of propane oxidation activity. The propane oxidation over platinum supported on various sulfation materials was studied by Hubbard, et al., (1993). They found that the acid strength did not have a major influence on propane oxidation activity. Also, the propane oxidation activity decreased in the order zirconia > silica > γ-alumina and the apparent activation energy for propane oxidation was independent of metal catalyst, support material and sulfation. It was suggested that the changes in activity were the result of a change in reaction-site density (Hubbard, et al., 1993).

Compared to platinum catalysts, palladium is capable of simultaneously converting significant quantities of hydrocarbons, carbon monoxide and nitrogen oxides and in an oxidizing atmosphere is more resistant to sintering than platinum. Also, its high methane oxidation activity is being used for preventing the emission of unburned methane from compressed natural gas automotive engines (Oh, et al., 1992) and from gas turbine for power generation. However, its resistance to sulfur poisoning has been less extensively studied than that of platinum.

The sulfur poisoning, recovery and related phenomena over supported palladium, rhodium and iridium catalysts for methane oxidation has been studied by Deng, et al. 1993. They reported the H$_2$S has a negative effect on methane oxidation activity over palladium, rhodium and iridium catalysts. This deactivation was due to the adsorption H$_2$S oxidized to sulfate under the reaction condition. Iridium catalyst at high temperature (> 500 $^\circ$C) show useful activity and are only slightly affected by H$_2$S at 200 ppm concentration.

The H$_2$S effect on methane oxidation over palladium supported on γ-alumina and silica has been studied by Hoyos, et al., 1993. Catalyst poisoning by H$_2$S at 400 $^\circ$C was investigated in this study. They reported that γ-alumina supported catalyst lowered the rate of deactivation due to the trapping of sulfate species. The formation of PdSO$_4$ was

identified by infrared spectroscopy but not detected by XRD on the surface of Pd/SiO$_2$ catalyst. This sulfate groups could be thermally eliminated under vacuum or under nitrogen flow at elevated temperature.

2.6 The Effect of Phosphorous Compounds on Catalyst Deactivation

2.6.1 Applications of TBP and ZDP

Tributylphosphate results in smoother combustion and improved engine performance when used as a fuel additive. One function of TBP is to combine with the lead from lead tetraethyl and expel it as relatively harmless lead orthophosphate. Also, TBP has anti-wear and corrosion inhibition properties when used as an oil additive (Corbridge, 1978).

Zinc dialkyldithiophosphate is a zinc salt of dialkyldithiophosphoric acid. It is used as a lubricating oils additive because of its anti-wear and anti-corrosion properties. Zinc salts of this kind, $Zn[(RO)_2PSS]_2$, are made by adding zinc oxide to the acid which is itself obtained from P_4S_{10} and an alcohol (Corbridge, 1978).

This material is a low hazard liquid and can burn upon heating to temperatures at or above the flash point (i.e. 110 ^oC). The actual molecular weight of ZDP is not known but the weight percent of P, S and Zn are 8.0%, 16.9% and 8.6% based on the data sheet provided by Exxon Co. (Exxon Chemical Americas 1994). By calculating it, the molecular weight is approximated 771.4 g/mole. According to the data sheet, the hazardous combustion products of ZDP are fumes, smoke, oxides of sulfur and carbon monoxide.

2.6.2 The Effect of Phosphorus Compounds on Catalyst Deactivation

A number of industrial processes produce trace qualities of hazardous gas mixtures which cannot be recovered economically. These gases containing volatile organic compounds (VOC) as well as compounds containing halogens, sulfur and phosphorous compounds. For some catalytic combustion of VOC processes, organic and phosphorus deposits had been observed on the surface of catalysts (Farrauto, et al., 1992). This catalyst

deactivation mechanism is caused by masking of the outer surface and possibly some pore plugging. Alkaline wash is an efficient method to regenerate the aged catalysts.

The P_2O_5 effects on γ-alumina was studied by Miciukiewicz, et al., 1989. The phosphorus-alumina samples with variable phosphorus content were prepared by impregnation of a γ-alumina support. It was found that P_2O_5 may block the support micropores, as a result of its interaction with the hydroxyl groups on alumina. Also, when phosphorus interacted with alumina, aluminum phosphate seemed to be preferentially formed. However, there are no further investigations of the P_2O_5 effect on metal supported on γ-alumina catalysts.

In the automotive three-way catalyst (TWC), many researchers expended great efforts to enhance the performance of the catalyst in order to comply the new Clean Air Act (CAA) Amendments in 1990. However, in the case of auto lubrication oil, oil-derived phosphorous compounds such as zinc dialkydithiophosphate (ZDP) have been reported to reduce the effects of pelleted oxidation catalysts, exhaust oxygen sensors, as well as monolithic three-way catalysts (Williamson, et al., 1979, 1984 1985). The deactivation of automotive catalysts by engine oil-derived components of phosphorus and zinc could occur by the formation of an amorphous zinc pyrophosphate, $Zn_2P_2O_7$, which is impervious to gas diffusion. Catalyst poisoning occurs at low-temperature (< 450 ^oC) environments. At elevated high temperatures (> 800 ^oC), chemically inert aluminum phosphate is the major product on the catalyst. The effects of phosphorus and ash contents of engine oils on deactivation of monolithic three way catalysts and oxygen sensors are reported by Inoue, et al., 1992. The catalysts and oxygen sensor were tested for a 100 hours in an engine. Phosphorus compounds retained on the catalyst deactivate the catalyst for CO oxidation and NO reduction ability, but have no effect on hydrocarbons oxidation. Also, engine oil with higher phosphorus contents produces higher concentrations of phosphorus compounds on the catalyst surfaces. The temperature effect on catalyst

deactivation were tested at 720 °C and 800 °C. The catalyst was more detrimentally affected when aged at 800 °C than if aged at 720 °C.

The effect on lubricant phosphorus level on exhaust emissions in a field trial of gasoline fueled vehicles was reported by Drury, et al., (1994). No significant lubricant effect on catalyst oxidation efficiency is observed in an 80,000 km test when ZDP content is lower than 0.12% by mass phosphorus in lubricating oil. An engine oil additive effect on deactivation of monolithic three way catalysts and oxygen sensors was studied by Ueda, et al., (1994). They found that engine oil additives such as Ca and Mg could prevent phosphorus from adhering to the catalysts and the sensors by forming a dense coating. The major function of Ca and Mg additives was to combine with phosphorus to form $Ca_3(PO_4)_2$ and $Mg_3(PO_4)_2$.

CHAPTER 3

EXPERIMENTAL

3.1 Catalysts and Materials

Laboratory evaluation were conducted using catalysts containing 2% to 4% PdO supported on gamma alumina powder. The particle size distribution of powder catalyst was under 200 mesh (75 μm) in order to minimize mass transfer resistance. The bulk density of catalyst is 0.282 g/cm^3. These catalysts were provided by Engelhard Corporation.

The chemicals for the experiment including tributyl phosphate (TBP), phosphorous pentaoxide (P$_2$O$_5$), octane, palladium chloride (PdCl$_2$), α-alumina and palladium (Pd) were purchased from Aldirich Chemicals Co. These chemicals are reagent grade. The zinc dialkyldithiophosphate (ZDP) was provided by Exxon Research and Engineering Co.

The analyzed gas mixtures and the pure inert gases for use a carrier gases were obtained from Matheson Gas Co. and used without further purification. Table 3.1 Shows the gases and their grades.

Table 3.1 Gases and Their Grades

Gases	Grade	Gases	Grade
Nitrogen	99.998%	1% Propane in Air	Analyzed
Hydrogen	99.99%	2% HCl in N$_2$	Analyzed
Air	Dry	2% Cl$_2$ in N$_2$	Analyzed
Carbon Monoxide	99.99%	500 ppm H$_2$S in N$_2$	Analyzed
Helium	99.995%	10 % N$_2$ in He	Analyzed
Argon	99.998%	20 % N$_2$ in He	Analyzed
5% H$_2$ in Ar	Analyzed	30 % N$_2$ in He	Analyzed
5% O$_2$ in He	Analyzed	0.1 % CO, 0.1 % CO$_2$, 0.1 % CH$_4$ in Air	Analyzed
1% CO in Air	Analyzed	1% CH$_4$ in Air	Analyzed

28

3.2 Laboratory Studies

3.2.1 The Effects of Chlorine Compounds on Catalyst Deactivation

The experimental apparatus flow schematic is shown in Figure 3.1 (All the Figures in Chapter 3 are shown in Appendix A). The catalyst deactivation experiments were conducted by using a one-inch diameter quartz tubular reactor. The catalyst bed temperature was maintained at $\pm$ 1°C in a 3 zone furnace (Applied Scientific Co.) by thermal controller and the temperature was monitored with calibrated Chromel-Alumel (K-type) thermocouples (Omega Engineering, Inc.).

3.2.1.1 Catalyst Deactivation Isotherms: Approximately 0.4 g of powder catalyst was used in each aging cycle of 24 hours. The temperature was varied from 300 $^{\circ}$C to 500 $^{\circ}$C. The feed mixture was diluted as required to prepare the desired gas stream composition. In order to accelerate catalyst deactivation and study the catalyst deactivation mechanism, a number of feed gas streams were prepared including 1% HCl in air, 1% Cl_2 in air and 1% HCl + 1.5% water vapor in air. The flow rate of the gas feed stream was set at 1040 cm^3/min (S.T.P.) and the flow rate was monitored with a rotormeter that was calibrated with a soap bubble meter. The concentration of HCl and Cl_2 was analyzed by chloride ion specific electrode pair and Drager tube.

3.2.1.2 Diagnostic Methane Oxidation Activity Test: The diagnostic methane oxidation activity test was conducted in a 1/4" stainless steel tubular reactor (see Figure 3.2). About 0.05g aged or fresh catalyst diluted with 0.45 g α-alumina was packed over 4 cm for methane oxidation activity test. The thermocouple was inserted inside the catalyst bed to monitor the reaction temperature. The 1% methane in air analyzed mixture was used as the diagnostic gas and the flow rate of the feed stream was 260 cm^3/min which is equivalent to 88,000 v/v/hr space velocity. The gas stream composition before and after the reactor was analyzed with an on-line gas chromatography (GC) using a 2 m porapak Q

column maintained at 40 °C and a flame ionization detector (FID) equipped with a methanization nickel catalyst reactor (Yu, 1991). The GC analysis followed the procedures described in section 3.3.

3.2.2 The Effect of H_2S on Catalyst Deactivation

3.2.2.1 Catalyst Deactivation Isotherms: The experimental apparatus flow schematic is shown in Figure 3.1. Approximately 0.3 g of powder catalyst was used in each aging cycle of 24 hours. The temperature was varied from 100 °C to 400 °C. The gaseous feed mixture was diluted as required to prepare the desired gas stream composition. In order to study the catalyst deactivation mechanism, 80 vppm H_2S in air was prepared for the feed gas stream. The flow rate of the gas feed streams was set at 260 cm^3/min (S.T.P.). The gas stream compositions before and after the reactor was analyzed with an on-line by gas chromatography (GC) using a flame photometric detector (FPD). The GC analysis followed the procedures described in section 3.3.

3.2.2.2 Kinetic Study and Activity Test of Methane Oxidation over Fresh Catalyst and H_2S Poisoned Catalyst: Approximately 10-50 mg of fresh or aged catalyst diluted with 0.25 g α-alumina were packed in a 1/4" quartz U-tube reactor (see Figure 3.3) for kinetic studies of methane oxidation. An analyzed 1% methane balanced with air mixture was feed stream mixture gas. The O_2/CH_4 ratio was therefore fixed at 20 in order to maintain a large excess of O_2. The flow rate of the feed stream was maintained constant at 52 cm^3/min. The thermocouple was inserted into the catalyst bed to monitor the reaction temperature. Methane conversion experiment were conducted as a function of residence time. Conversion was kept below 40 % in order to avoid distortions of the kinetics due to product-reactant reactions and mass transfer effects. The gas stream composition before and after the reactor was analyzed by using the on-line GC with FID.

3.2.2.3 Methane Oxidation over Palladium Catalysts in the Presence of H₂S: The methane oxidation over palladium catalysts in presence of H_2S was conducted in a 1/4" stainless steel tubular reactor (see Figure 3.2). About 0.05 g fresh catalyst diluted with 0.45 g α-alumina was packed over 4 cm for methane oxidation. The thermocouple was inserted inside the catalyst bed to monitor the reaction temperature. The 0.5% methane in air analyzed mixture was used as feed gas and the flow rate of the feed stream was 260 cm^3/min. Experiments were run at 300 and 400 ^oC. Once the reaction reached steady state, 80 ppm of H_2S was introduced into feed stream. At this time, we started to monitor methane activity change as a function of time. This procedure was developed to study the deactivation rate of the catalyst for methane oxidation in the presence of H_2S and to measure the degree of deactivation. The gas stream composition before and after the reactor was analyzed by on-line gas chromatography with FID and FPD.

3.2.3 The Effects of TBP and ZDP on Catalyst Deactivation

3.2.3.1 Catalyst Deactivation Isotherms: The experimental apparatus flow schematic diagram used for this set of experiments is shown in Figure 3.4. A bench scale pulse-flame reactor was designed to age catalyst with phosphorous compounds under oxidizing conditions to exam their impact on catalyst activity. A special designed one-inch diameter quartz tubular reactor was developed. It consists of two sections: the first was a pulse-flame combustion section and the other contained the catalyst bed. Each section was independently controlled with thermal controllers and the temperature was monitored with calibrated Chromel-Alumel (K-type) thermocouples (Omega Engineering, Inc.).

Approximately 0.4 g of powdered catalyst samples were used in studying this aging cycle. The aging substances, tributyl phosphate (TBP) which is non-zinc phosphorous compound and ZDP which is a zinc phosphorous compound, were used as poisons. Either catalyst poison was injected by syringe pump at a flow rate of 0.05 cm^3/min. The flow rate of air feed stream was 1040 cm^3/min which is equivalent to

44,000 v/v/hr space velocity during aging cycle. The ZDP, diluted with (1:1 volume ratio) in order to overcome the high viscosity of ZDP, was pumped into reactor. The temperature in the pulse flame section was set at 860 °C in order to ignite ZDP. This temperature was selected based on the research studies Williamson, et al., (1985). The catalyst bed temperature was controlled at either 500 °C or 820 °C. The catalyst aged at 500 °C represented normal automobile operating temperature and the catalyst aged at 820 °C represented the abnormal automobile operating temperature.

The dosage of phosphorous compounds was based on average automobile oil consumption estimated by Williamson, et al., (1985). In the laboratory aging tests, the simulated aging mileage was based on 48 kmph steady state vehicle operation. It was assumed that the oil consumption rate was 1 liter of oil per 3,400 km and 1 dm³ of oil contained 4 mg P. Table 3.2 shows P dosage levels in simulated miles for pulsator-aged catalysts.

Table 3.2 Phosphorous Dosage Levels in Simulated Miles for Pulsator-aged Catalysts

Simulated-aged time, hours	Simulated miles	P input, g	TBP, g	ZDP, g	P_2O_5, g
400	12000	0.023	0.2	028	0.05
800	24000	0.046	0.4	0.56	0.11
1200	36000	0.069	0.6	0.84	0.16
1600	48000	0.092	0.8	1.12	0.21
2000	60000	0.115	1.0	1.40	0.26
2400	72000	0.138	1.2	1.68	0.32
2800	84000	0.161	1.4	1.96	0.37
3200	96000	0.184	1.6	2.24	0.42
3600	108000	0.207	1.8	2.52	0.47
4000	120000	0.23	2.0	2.80	0.52

1. Basic assumption: average speed = 48 kmph(30 mph), average oil consumption = 1dm³/3400 km, phosphorous content = 4 mg/dm³.
2. Density of TBP is 0.979 g/cm³, P content of TBP is 11.6 wt %
3. Density of ZDP is 1.12 g/cm³, P content of ZDP is 8.0 wt %
4. P content of P_2O_5 is 43.7 wt %

3.2.3.2 Diagnostic Methane Oxidation Activity Test: Following the pulsator aging, the 1% CH_4 in air analyzed mixture was used as diagnostic gas to measure changes in catalyst activity. The catalytic activity was determined as percent methane conversion as a function of temperature. The gas mixture was passed over the catalyst at the flow rate of 1040 cm^3/min (S.T.P.) which is equivalent to 44,000 v/v/hr. The reactants and products were analyzed the HP 5890 on-line gas chromatography FID.

3.2.4 The Effects of P_2O_5 on Catalyst Deactivation

3.2.4.1 Catalyst Deactivation Isotherms: Williamson, et al., (1985) reported that the products from the combustion of organo-phosphorous compounds were CO_2, H_2O and gas phase phosphorous pentaoxide, P_2O_5. In this part of the research, we assumed that all P_2O_5 was deposited on the catalyst bed. Therefore, P_2O_5 mixed with catalyst at the same dosage as TBP (see Table 3.1) was designed for testing the effect of P_2O_5 on catalyst deactivation.

Approximately 0.4 g catalyst mixed with various weights of P_2O_5 were thermally aged at 500 °C and 820 °C for 3 hours. The flow rate of air feed stream was set at 1040 cm^3/min (STP) during the aging cycle.

3.2.4.2 Diagnostic Methane Oxidation Activity Test: Following the aging cycle, the catalytic activity was determined by comparing changes in methane conversion as a function of temperature from that determined for fresh catalysts. The test was performed at 44,000 v/v/hr space velocity. The reactants and products were analyzed by on-line gas chromatography.

3.2.5 Catalyst Deactivated by Incipient Wetness with P_2O_5 Aqueous Solution

3.2.5.1 Catalyst Deactivation Isotherms: Since P_2O_5 mixed with catalyst was not completely uniform, catalyst samples containing the desired weight of P_2O_5 were prepared by incipient wetness. These samples were tested for the effect of P_2O_5 on catalyst deactivation. Each 0.4 g catalyst sample was saturated with a desired concentration of P_2O_5 in aqueous solution and calcined at 500 °C or 820 °C for 3 hours. Each catalyst sample was weighed before and after calcination in order to measure how much weight percent of P_2O_5 was retained on each catalyst sample.

3.2.5.2 Diagnostic Methane Oxidation Activity Test: Approximately 10 mg of fresh or aged catalyst sample were diluted with 90 mg α-alumina and packed into a 1/4" quartz tubular reactor. A thermocouple was inserted into the catalyst bed. Methane conversion was tested at 88,000 v/v/hr space velocity and 460 °C as a function of P_2O_5 content on the catalyst. The methane conversion was analyzed by GC.

3.3 Analytical Methods

3.3.1 Gas Chromatography (GC)

The CH_4, CO and CO_2 were analyzed by flame ionization detector (FID). The sample gas is introduced into a nickel hydrogenation catalytic reactor to produce methane allowing the use of the very sensitive FID system. The detection limit for FID is 5×10^{-6} to 10×10^{-6} mole fraction (5 vppm to 10 vppm). Figure 3.5 illustrates the flow schematic for the methanation reactor in the GC. The operating conditions are as follows:

Detector: FID, HP 5890

Detector Temperate: 200 °C

Injection Temperature: 150 °C

Oven Temperature: 40 °C

Carrier Gas: Helium, 30 cm^3/min

Packing Material: Porapak Q 80/100, 1/8" x 6' SS

Ni Catalyst Reaction Temperature: 350 ^{o}C

Air: 400 cm^3/min

H$_2$: 35 cm^3/min

Integrator: HP 3396 A

The H$_2$S and SO$_2$ were analyzed by flame photometric detector (FPD) and the operating conditions are as follows:

Detector: FPD, HP 5890

Detector Temperature: 250 ^{o}C

Injection Temperature: 150 ^{o}C

Oven Temperature: 40 ^{o}C

Column Packing Material: Porapak Q 80/100, 1/8" x 6' SS

Carrier Gas: N$_2$, 20 cm^3/min

Air: 380 cm^3/min

H$_2$: 40 cm^3/min

Figure 3.6 and 3.7 show typical peak resolution and retention times for the reactants and products.

3.3.2 HCl and Cl$_2$ Measurement

Mixture of 2% HCl in N$_2$ and 2% Cl$_2$ in N$_2$ were diluted with air by using rotormeters to obtain desired mixtures feed mixture to ± 10%. The concentration of HCl in the feed stream was double checked by absorbing it in two bottles of de-ioned water. Each bottles contains 50 ml of de-ioned water. This scrubbing solution is analyzed by chloride ion specific electrode pair. This pair was calibrated by 0.1 to 0.001 mole/dm^3 NaCl solution. The concentrations of Cl$_2$ were determined by using Drager gas color-detector tubes. This

method of analysis was reported to be accurate with a tolerance of less than 10 percent according to the manufacturer.

3.4 Catalyst Characterizations Analysis

3.4.1 Temperature Programmed Reduction (TPR) and CO Chemisorption

This experiment was conducted using the Altamira Instrument. A 0.05 g sample was packed in a U tube for CO chemisorption. The flow schematic diagram for TPR and CO chemisorption is shown in Figure 3.3. The experimental procedure for CO chemisorption can be summarized as follows: (Yu, 1991):

(1) Load 0.05 g powder catalyst into U-tube.

(2) Install U-tube on the Altamira Catalyst Characterization Instrument.

(3) Set operating parameters:

    Step 1:

        Temperature: 40 ^{o}C,

        Carrier gas: Argon, 30 cm^3/min.

    Step 2:

        Temperature: programmed temperature, 40 ^{o}C to 350 ^{o}C, ramp rate 10 ^{o}C/min,

        Carrier gas: 5% H_2 in argon.

    Step 3:

        Hold the temperature at 350 ^{o}C for 5 minutes.

    Step 4:

        Cool down to room temperature and shift carrier gas to argon.

        Inject adsorbate gas, CO for 5 pulses.

    Step 5:

        Calculate total volume of CO adsorbed on the surface of the catalyst.

Step 6:

Convert the volume of CO which adsorbed on the surface of catalyst per 0.05g to the volume of CO per gram.

3.4.2 BET Surface Area

The BET surface area was measured by using Altamira Instrument, see Figure 3.8. This N_2 adsorption measurements was conducted by a continuous flow method (Nelsen, et al., 1958). This method does not involve vacuum techniques. Also, it can be extended to a lower range of surface areas, because of the high sensitivity of thermal conductivity detection. The theory of BET surface area measurement was reviewed in Chapter 2. The experimental procedure for BET surface area measurements are as follows:

(1) Load 0.05g of catalyst sample into quartz U-tube.

(2) Install U-tube on the Altamira Catalyst Characterization Instrument (Altamira Instrument, Inc.).

(3) Pre-treat the catalyst sample by using helium at 20 cm^3/min for 5 minutes.

(4) Measure the vapor pressure of liquid nitrogen, P_o.

(5) Measure the ambient pressure, P.

(6) Introduce 10% N_2 in helium gas through the U-tube at 20 cm^3/min. Once the TCD baseline is stable, immerse the sample tube onto the liquid nitrogen Dewar. Since the N_2 molecules condense onto the catalyst surface at liquid N_2 temperature, the response of TCD shows a negative peak. The TCD signal goes back to the baseline when N_2 molecules saturate the catalyst surface. Remove the liquid N_2 Dewar when the baseline is stable. The response of the TCD shows a positive peak when the temperature reaches room temperature. This peak indicates that the desorption of N_2 molecules from catalyst is complete.

(7) Inject two pulse of known volumes of N_2 into the carrier gas flow. Comparing the adsorption and desorption peak area with the calibration peak, one can obtain the actual volume of N_2 adsorbed on the catalyst sample.

(8) Repeat (6) and (7) with 20 % N_2 in helium and 30 % N_2 in helium adsorbate gas and measure the actual volume of N_2 adsorbed on the catalyst sample.

(9) By rearranging equation (2-1) and plotting $1/V[(P_0/P)-1]$ versus P/P_0, we obtain a straight line $y = ax + b$, where a is the slope $(C-1)/V_m C$ and b is the intercept $1/V_m C$. V_m can then be calculated as follows Altamira Instruction Manual 1989:

$$V_m = \frac{1}{Slope + Intercept}$$ (3-1)

and the surface area is given by

$$SA = \frac{V_m\ N\ Acs}{V'}$$ (3-2)

where:

SA = total surface area, m^2/g,

V_m = volume of adsorbate at monolayer coverage, cm^3/g,

N = Avagadro's number, $6.02 * 10^{23}$ molecules/mole,

Acs = cross sectional area of adsorbate molecule, $0.162\ nm^2$,

V' = molar volume of adsorbate at 25 ^oC, 24500 cm^3/mole.

Figure 3. 9 shows a typical $1/V[(P_0/P)-1]$ versus P/P_0 plots for catalyst sample BET surface area.

3.4.3 Thermal Gravimetric Analysis

The thermal gravimetric analysis of sample weight gain or loss was conducted by using a Perkin-Elmer thermal gravimetric analyzer (TGA). The initial weight of catalyst samples used varied between 2 mg and 10 mg. The schematic flow diagram of TGA is shown in

Figure 3.10 and the detail outline of TGA is shown in Figure 3.11. The experimental procedures are as follows (TGA-7 series Instruction Manual 1993):

(1) Clean the platinum sample pan and zero the microbalance.

(2) Load the catalyst sample on the sample pan and raise the furnace to the sample pan.

(3) Wait for 2-5 minutes till the balance is stable.

(4) Record the sample weight.

(5) Set the temperature program as required by the experiment.

(6) Switch on the reactive gas and measure the flow rate (HCl, H_2S, Air, N_2,etc.)

(7) Double check the sample weight.

(8) Press "start" to begin the experiment.

3.4.3.1 Thermal Gravimetric Analysis of HCl over Palladium Catalysts: The air feedstream containing 300 ppm HCl was introduced into furnace when the weight of catalyst sample become stable at the desired reaction temperature. The 300 ppm HCl in air was calibrated by using chloride ion specific electrode pair. The total HCl feedstream flow rate was 60 cm^3/min and the time of exposure of the catalyst sample was 30 minutes.

3.4.3.2 Thermal Gravimetric Analysis of H_2S over Palladium Catalysts: The air feedstream containing 250 ppm H_2S was introduced into furnace when the weight of catalyst sample become stable at desired reaction temperature. The total feedstream flow rate was 60 cm^3/min and the time of exposure of the catalyst sample to H_2S was 30 minutes.

3.4.3.3 Thermal Gravimetric Analysis of TBP, P_2O_5 and ZDP over Palladium Catalysts: The weight change of the sample containing TBP, P_2O_5, ZDP as a function of temperature or time was performed by using TGA. The following experiment procedure was used:

(1) Load approximately 5 mg of catalyst sample on the sample pan and weigh it.

(2) Record the sample weight, add the catalyst poison and reweigh.

(3) Record the total weight and subtract the catalyst weight. Calculate the poison material weight.

(4) Flow the reactive gas.

(5) Set the temperature program.

(6) Press "Start" to run.

By using this method, one can determine if the catalyst poison can be removed by thermal treatment.

3.4.4 Fourier Transform Infrared (FT-IR) Spectroscopy

The FT-IR spectroscopy analysis was conducted by GC-FT-IR (BIO-RAD FTS-40). The sample was prepared by adding 5 mg of catalyst sample mixed with 295 mg KBr and was pressed as a thin disk under 8 kg/cm^2. The sample disc was placed in a sample holder and introduced into a cell. The infrared spectra were recorded at room temperature at a resolution of 8 cm^{-1}. Every spectrum was the sum of 64 scans. The plot function was set to absorbance. The operating conditions are listed below:

Detector: Internal

Scan Speed: 5 kHz

Delay: 1.0 sec

Aperture: 2 cm^{-1}

Sample Beam: Internal

Controller Signal Path: Auto

Low Pass Filter: 1.12 kHz

Collect Sensitivity: 3

Scan Wave Number: 4000-450 cm^{-1}

3.4.5 Elemental Analysis of the Catalyst Deactivated by TBP and ZDP

The phosphorous and zinc contents were measured using the Mehlich 2 Extraction Method (Hach Co., 1994). Approximately 0.05 g aged catalyst was extracted by 10 cm^3 of diluted HF extraction solution (Hach Co.) for 30 minutes. After shaking and extraction, the solution was diluted by de-ionized water 1:20 and analyzed by inductively coupled plasma spectrometer (VG/FISONS-Plasma Quad II). This analysis was used to determine the weight percent of zinc and phosphorous retained on the catalyst surface.

3.4.6 X-Ray Diffraction Crystallography

X-ray diffraction (XRD) was used to measure the surface bulk content of catalyst poisons. The model is Rigaku-VS-DXR 3000. Approximately 0.25 g of powder catalyst sample was loaded into a sample holder and was packed tightly in order to be held in a vertical position. Then, the sample holder was placed into the cell to start x-ray scanning. The scan speed was 0.2 degree per min. and the target was copper. The voltage was set at 30 KV and the current was set 20 mA. These powder catalyst sample was analyzed with the help of Professor Grow.

CHAPTER 4

RESULTS

4.1 The Effect of Chlorine Compounds on Catalyst Deactivation

4.1.1 Methane Oxidation Activity

The comparisons of the effects on methane oxidation activity, the diagnostic reaction, of chemically poisoned, thermally degraded, and fresh catalysts is shown in Table 4.1. There is no significant change in activity and chemisorption capacity between fresh catalyst and catalysts aged at 500 °C in flowing air for 24 hours. This is a blank test to determine if the catalyst is deactivated thermally during 24 hour exposure to air at 500 °C. The effect of water vapor on catalyst activity was examined at 500 °C and space velocity of 44,000 v/v/hr. The results show that activity and chemisorption are almost the same between aged and fresh catalysts. The water vapor effect was also studied by Mendyka (1992) in catalytic oxidation of trichloroethylene (TCE) on Pt catalyst, who reported water had no significant effect on the efficiency of TCE oxidation.

Table 4.1 Effect of Different Catalyst Treatment on Oxidation Activity

Treatments	Temperature, °C/time	CO chemisorption, cm^3/g-catalyst	Activity[1], °C
Fresh	Room Temperature	1.12	333
Air	500/24 h	1.14	332
1.5 % H_2O in air	500/24 h	1.07	332
1.0 % Cl_2 in air	500/24 h	1.0	343
1.0 % HCl in air	500/24 h	0.32	377
1.5 % H_2O + 1 % HCl in air	500/24 h	0.65	350
1.0 % HCl in air	300/24 h	1.09	362
1.5 % H_2O + 1% HCl in air	300/24 h	1.15	348

1. Temperature for 30% conversion of methane

The temperature for converting 30 % CH_4 increases from 333 ^oC to 377 ^oC when catalyst is aged with 1% HCl gas for 24 hours at 500 ^oC. The CO chemisorption drops for the same two treatments from 1.12 cm^3/g to 0.32 cm^3/g. These results suggest that the decrease in activity is due to losing metal surface area. The catalyst is also aged by 1% Cl_2 gas in air at 500 ^oC for 24 hours. The activity changes from 333 ^oC to 343 ^oC for 30% conversion of methane and CO chemisorption is reduced from 1.12 to 1.0 cm^3/g, which indicates that the catalyst does not significantly lose active sites. In the catalytic oxidation of chlorinated hydrocarbons, only small concentrations of Cl_2 are found in the off-gas since chlorine is primarily converted to HCl by adding water vapor or other hydrogen sources (Shaw, et al., 1992; Windawi, et al., 1993). Since the production of Cl_2 in catalytic oxidation process is small compared, to the production of HCl, it is not the predominant catalyst deactivator in catalytic oxidation of chlorinated hydrocarbons. Furthermore, it has no significant effect on catalytic oxidation of methane.

4.1.2 Temperature Effect

The effect of temperature and exposure to HCl on deactivation of palladium catalyst is summarized in Table 4.1. The catalyst aged by 1% HCl at 300 ^oC for 24 hours was tested for methane oxidation activity. The temperature for 30% conversion of methane is 362 ^oC compared to 333 ^oC for fresh catalyst. The temperature needed to be increased by about 30 ^oC to maintain the same oxidation activity. However, at these temperatures, CO chemisorption drops from 1.12 to 1.09 cm^3/g. These results indicate that activity decays slightly while minimally affecting metal surface area at this temperature. Figure 4.1 (All the figures in Chapter 4 are shown in Appendix B) shows the effect of temperature and HCl exposure on methane oxidation over 4% PdO/γ-alumina catalyst. It should be noted that the 300 ^oC and 500 ^oC HCl curves are displaced to higher temperature compared to the fresh catalyst curve, but no apparent significant effect on pore diffusion and mass transfer region has occurred. The shape of these curves have remained fairly similar to the fresh

catalyst curve. This indicates that the reaction needs a higher temperature to light off because the active sites were poisoned by HCl. Also, the results show activity decreased as the temperature is increased.

A poisoning mechanism was proposed by Simone, et al., (1991), who reported the Cl⁻ present from catalyst preparation procedures results in reversible poisoning. Low activity is not due to poor metal distribution or enhanced thermal sintering, but by localized site poisoning. In this case, it can be shown that HCl chemisorbed by the catalyst results in poisoning and causes poor activity performance.

4.1.3 Water Effect

The Effect of water vapor added to the HCl gas steam was examined since water vapor is a constituent in the effluent of hydrocarbon combustion. Also, water vapor is added to enhance HCl selectivity in catalytic oxidation of chlorinated hydrocarbons. Figure 4.2 shows the effect of water vapor and HCl pretreatment on methane oxidation. The results show the temperature for 30 % conversion of methane is 350 $^{\circ}$C which indicates that water vapor retards catalyst deactivation by HCl. The water vapor effect can also be measured by CO chemisorption, i.e., 30 % conversion of methane is achieved at 350 $^{\circ}$C, and CO chemisorption corresponds to 0.65 cm^3/g. The corresponding effect in the absence of water is 377 $^{\circ}$C and 0.32 cm^3/g. These results suggest that water vapor inhibits HCl adsorption on the surface of the catalyst. However, the CO chemisorption still drops from 1.12 to 0.65 cm^3/g because of the volatilization of PdCl$_2$. In aging tests at 300 $^{\circ}$C, see Table 4.1, water vapor also retards catalyst deactivation but CO chemisorption remains the same as that obtained for fresh catalyst. This evidence was also found by Spivey and Butt (1992), who reported that the addition of water vapor to the inlet gas stream containing vinyl chloride significantly retarded the deactivation process without altering the oxidation reaction rate. Unfortunately, the mechanism by which water vapor retarded deactivation was not examined by these authors. However, Mendyka, et al.,

(1992) reported that H_2O produced during oxidation of the hydrocarbon aided in desorbing HCl from the catalyst. This is indicative of why water minimizes catalyst deactivated by HCl.

Figure 4.3 summarizes the water effect on regeneration of catalyst aged with 1% HCl in air at 500 °C. The fresh catalyst activity was tested at 377 °C and thermal aging was conducted at 500 °C for 15 hours. It was found that the activity did not significantly change at 377 °C. Then, the catalyst was aged in 1% HCl for 2 hours at 500 °C. It was found that conversion dropped from 90 % to 23 % at 377 °C. This was followed by water vapor treatment for 23 hours, the catalyst activity improved from 23 % to 55 % and could not be further regenerated by additional water vapor treatment since apparently part of PdO reacted with HCl and volatilized during the aging period. The results show that a fraction of HCl adsorbed by catalyst can be removed by water. Similar findings were reported by Marecot, et al., (1994), who found that the chloride on the catalyst surface was removed by water which was produced by propane and propene combustion. However, the regeneration was limited because palladium metal surface area had decreased as evinced by a decrease in adsorption of CO from 1.12 to 0.32 cm^3/g.

4.1.4 BET Surface Area and Chemical Identification

The temperature and HCl effects on BET surface area and CO chemisorption are summarized in Table 4.2. The effect on BET surface area of aging the catalyst thermally and with HCl was about 20 %. for 24 hours. CO chemisorption, on the other hand, showed a large variability. Hence, this shows that HCl selectively chemisorbs on the surface of the catalyst and does not impact on pore diffusion.

Table 4.2 The Temperature and HCl Effect on BET Surface Area and CO Chemisorption

Treatment	BET surface area, m^2/g	CO Chemisorption, c.c./g
Fresh catalyst	67	1.12
1% HCl in air, 300 °C/24 hours	53	1.09
1% HCl in air, 500 °C/24 hours	66	0.32

Figure 4.4 and Figure 4.5 show how the quartz wool and reactor turned dark red after finishing HCl aging tests at 500 °C. The red color was found that coated on the end of the reactor was due to a temperature gradient that occurred in that area. It is suspected that $PdCl_2$ is formed during the experiment since $PdCl_2$ is dark red color. The quartz wool was washed with de-ioned water for 4 hours and was analyzed by Inductively Coupled Plasma Mass Spectroscopy (ICP-MS) for qualitative analysis of palladium and was analyzed by selective ion electrode for qualitative analysis of Cl. It was found that palladium and chloride ions were present in the solution. The result indicates that the catalyst aged by HCl at 500 °C produced $PdCl_2$ which vaporized and was transported to colder parts of the reactor where it condensed on the wall of the reactor and quartz wool. The $PdCl_2$ melting point is 500 °C. Hence, the CO chemisorption measurements of HCl aged catalyst at 500 °C showed a sharp drop due to loss of the active metal.

4.1.5 Thermal Gravimetric Analysis

Figure 4.6 shows that no weight change of γ-Al_2O_3 occurs when HCl gas is introduced into TGA reactor at 300 °C for 30 minutes. The weight loss of 18% during the first 5 minutes was due to surface moisture. Figure 4.7 shows the weight change of 2% PdO/γ-alumina as HCl gas is introduced into TGA reactor at 300 °C for 30 minutes. In the first 20 minutes, the weight loss as temperature increased to 300 °C was due to the removal of moisture from the catalyst sample. After that, no further weight changes were observed as temperature reached 300 °C. After 45 minutes, HCl gas was introduced into reactor and a

weight gain from 93.95% to 94.71% was determined for the next 30 minutes. This result suggests that PdO reacted with HCl to produce $PdCl_2$.

The thermal gravimetric analysis of the interaction of 4% PdO/γ-alumina with 300 ppm HCl is shown in Figure 4.8. The weight change of 4% PdO/γ-alumina sample is from 93.45% to 94.57%. The difference in weight gain from 2% PdO/γ-alumina and the 4% PdO/γ-alumina was 0.76 % and 1.12%, respectively. These results indicated that the weight gain increase as palladium content increases. This suggests that PdO reacts with HCl to produce $PdCl_2$ and H_2O. Normally, the difference of the weight gain from PdO to $PdCl_2$ is 0.90% for 2% PdO; 1.80% for 4% PdO. However, one can concluded that 84.7% of 2% PdO catalyst was converted to $PdCl_2$ and 62.6% of 4% PdO catalyst was converted to $PdCl_2$. This could be explained by the inaccessibility of some of the PdO in pores which do not react with HCl, particularly since the outer surface forms $PdCl_2$ which enhances the difficulty for HCl to penetrate inside the pores to react with PdO or to cause volatilization of $PdCl_2$ which decreases the percentage of weight gain (Sreeramamurthy, et al., 1974).

Figure 4.9 shows the difference of weight change as a function of temperature for 30 minutes reaction time. The difference of weight change increases as the temperature is increased from 200 °C to 300 °C reaches a maximum region between 300 °C to 400 °C, and decreases sharply to 500 °C. The decrease is due to $PdCl_2$ volatilization at the higher temperatures.

Figure 4.10 shows the weight change of 4% PdO/γ-alumina as a function of temperature in H_2 reductive atmosphere. Curve (I) shows that the weight change as a function of temperature. Curve (II) shows that the first derivative of weight change as a function of temperature. At 82 °C, the PdO started to be reduced to Pd metal. Figure 4.11 shows that the weight change of pure PdO and $PdCl_2$ as a function of temperature in reductive atmosphere. Curve (I) shows that the reduction of PdO starts at 60 °C and is essentially complete at 110 °C. Curve (II) shows that the reduction of $PdCl_2$ starts at 50

$^\circ$C and is essentially complete at 110 $^\circ$C. This indicates that a catalyst poisoned by HCl can be reduced with H_2 at a lower temperature to produce Pd which could then be reoxidized to PdO at 500 $^\circ$C.

Figure 4.12 shows the results of an activity test of a catalyst poisoned with HCl at 300 $^\circ$C, regenerated with H_2 at 200 $^\circ$C, and reoxidized at 500 $^\circ$C. The results show that activity after regeneration approaches that of fresh catalysts. It appears that HCl adsorbs on the surface of catalyst and reacts with PdO to produce $PdCl_2$ at 300 $^\circ$C. At this temperature, $PdCl_2$ is not volatile, but strongly affects catalytic activity. The CO chemisorption is minimally affected by the presence of HCl.. This is because the standard test for chemisorption requires that the catalyst be run in the temperature programmed reduction (TPR) mode to reduce PdO to Pd before measuring CO chemisorption. The $PdCl_2$ remaining on the catalyst is reduced by hydrogen to Pd under the same conditions as PdO is reduced. Therefore, one cannot distinguish between a catalyst aged by HCl at 300 $^\circ$C and residual PdO in a chemisorption study. However, a combination of TGA, elemental analysis and CO chemisorption studies can give better insight to understand the poisoning mechanism. At 500 $^\circ$C, a large number of chlorinated active metal sites are volatilized, which cause permanent catalyst deactivation although the catalyst can be partially regenerated by H_2.

4.2 The Effect of Sulfur Compound on Catalyst Deactivation

4.2.1 Kinetics Study of Methane Oxidation over Palladium Catalyst

The mechanism of methane oxidation over palladium catalyst under oxidizing conditions was proposed by Oh, et al., (1991, 1992). They reported that the noble metal surface is predominating covered with oxygen and thus the critical step in the methane oxidation is the dissociative adsorption of CH_4 onto the oxygen-covered surface. This mechanism postulated that O_2 adsorbs more strongly than CH_4 onto the surface of palladium catalyst. As a result of the substantial difference in the strength of adsorption, O_2 inhibits

CH_4 oxidation under oxidizing conditions by preventing the weaker CH_4 adsorption on the active sites.

Berg and Jaras (1994) proposed that methane and oxygen are adsorbed on different sites (S1 and S2) in the methane oxidation over magnesium oxide catalyst. Based on this mechanism and Langmuir-Hinshelwood kinetics, they proposed the following mechanism:

$$CH_4 (g) + S1 <---> CH_4 (a) \qquad (4-1)$$

$$O_2 (g) + S2 <---> O_2 (a) \qquad (4-2)$$

$$CH_4 (a) + O_2 (a) ---> CH_3\cdot (a) + HO_2\cdot (a) \qquad (4-3)$$

$$CH_3\cdot (a) + HO_2\cdot (a) + O_2 ---> CO_2 (a) + H_2O (a) + H_2O \qquad (4-4)$$

$$CO_2 (a) + H_2O (a) ---> CO_2 (g) + H_2O (g) + S1 + S2 \qquad (4-5)$$
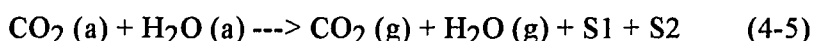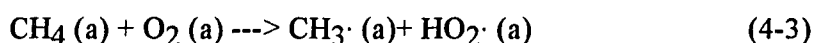
In Oh, et al., (1992) studies, the concentration of CO_2 and H_2O has no effect on methane conversion. Therefore, we assume that the rate of desorption of CO_2 and H_2O is very fast or adsorption sites not needed for O_2 and CH_4 are involved in CO_2 and H_2O desorption. Finally, the mechanism represented by Eqs. (4-1)-(4-5) would lead to the rate equation:

$$-r_{CH_4} = k\ CH_4(a)\ O_2(a) \qquad (4-6)$$

where $CH_4(a)$ and O_2 (a) are the surface coverage of methane and oxygen, respectively. The surface coverage also can be written as follows:

$$CH_4 (a) = K_a\ C_{CH_4}/(1 + K_a C_{CH_4}) \qquad (4-7)$$

$$O_2 (a) = K_b\ C_{O_2}/(1 + K_b\ C_{O_2}) \qquad (4-8)$$

Therefore, Eq. (4-6) can written as follows:

$$-r_{CH_4} = k\ K_a\ C_{CH_4}/(1 + K_a C_{CH_4}) * K_b\ C_{O_2}/(1 + K_b\ C_{O_2}) \qquad (4-9)$$

According to a pervious study (Oh, et al., 1991), under oxidizing conditions, methane conversion is independent of O_2 concentration when O_2/CH_4 ratio larger than 5. This indicates that the high concentration of bulk O_2 and strong adsorption of O2 causes the last term in Eq. (4-9) to approach 1 (Atkins, 1982). In other hands, $K_b C_{O_2} >> 1$ and K_b

$C_{O_2}/(1 + K_b\, C_{O_2}) \cong 1$. In our study, the O_2/CH_4 ration is 20. Therefore, Eq. (4-9) can be written as follows:

$$-r_{CH_4} = k\, K_a\, C_{CH_4}/(1 + K_a C_{CH_4}) \qquad (4\text{-}10)$$

$$-r_{CH_4} = k'\, C_{CH_4}/(1 + K_a C_{CH_4}) \qquad (4\text{-}11)$$

where $-r_{CH_4}$ = rate of reaction, gmole/g-cat. s

$k' = k\, K_a$ = rate constant, cm^3/g-cat. s

K_a, K_b = adsorption constants, cm^3/gmole

C_{CH_4} = bulk gas phase concentration of CH_4, mole/cm^3

C_{O_2} = bulk gas phase concentration of O_2, mole/cm^3

For a packed-bed reactor, we obtain

$$\frac{W}{F_{Ao}} = \int_0^{X_a} \frac{dX_a}{-r_A} \qquad (4\text{-}12)$$

Substituting Eq. (4-11) into Eq. (4-12), we obtain

$$\frac{W}{F_{Ao}} = \int_0^{X_a} \frac{1 + K_a\, C_{CH_4}}{k'\, C_{CH_4}} dX_a \qquad (4\text{-}13)$$

Integrating Eq. (4-13), we obtain

$$\frac{W}{V} = \frac{-\ln(1 - X_a)}{k'} + \frac{K_a}{k'} C_{Ao}\, X_a \qquad (4\text{-}14)$$

where W = weight of catalyst, g

F_{Ao} = molar flow rate of CH_4, gmole/s

V = volumetric flow rate of feed stream, cm^3/s

C_{Ao} = P_{Ao}/RT = initial concentration of methane, mole/cm^3

X_a = conversion of methane, ($C_{Ao} - C_A$)/ C_{Ao}.

P_{Ao} = partial pressure of methane, atm

R = gas constant = atm-l/mole-K

T = reaction temperature, K

By using non-linear regression method, we can solve for k' and K_a.

Table 4.3 The Rate Constants and Adsorption Equilibrium Constants for Methane Oxidation over Palladium Catalysts at Various Reaction Temperatures

Temperature, °C	k', cm³/g-s	K_a, cm³/mole	k', cm³/g-s	R Square
250	1.0	0.204	1.00	0.98
260	1.54	0.160	1.54	0.94
270	2.63	0.107	2.62	0.96
280	4.25	0.055	4.22	0.99
290	8.0	0.040	7.98	0.99
300	12.97	0.020	12.81	0.93

Figure 4.13 to 4.18 show methane conversion versus W/V on the temperature range of 250 °C to 300 °C. The results show the experimental data fit the postulated model. Table 4.3 shows rate constant, k' and adsorption constant K_a at various reaction temperatures. The results show the K_a values is very small compared to k' thus the second term in Eq.(4-14) can be neglected. As an alternate mechanisms, one can assume that in equation (4-11), the denominator term, $K_a C_{CH_4}$, is much smaller than 1 since C_{CH_4} is also small (~2.1-2.3 x10 $^{-7}$ mole/cm³). Therefore, Eq(4-11) can be simplified into a pseudo first order reaction rate expression.

$$-r_{CH_4} = k' \, C_{CH_4} \tag{4-15}$$

Substituting Eq. (4-15) into (4-13), we obtain

$$\frac{W}{V} k' = -\ln(1 - Xa) \tag{4-16}$$

Figure 4.19 shows the plots of -ln(1-Xa) vs. W/V for methane oxidation over palladium catalyst. The pseudo first order rate constant, k,' value can be obtained from the slope of the lines at each constant temperature. The slopes were calculated by linear regression. The rate constants, k', and R square of the linear regression are listed in Table 4.3. The dotted lines of Figure 4.13-4.18 show methane conversion versus W/V at various reaction temperatures by assuming pseudo first order kinetics. The results show the pseudo first order rate equation also provides a good fit of the experimental data. The rate constants, k', from Eq.(4-14) and Eq. (4-16) are almost identical. These results prove that the second

term of Eq. (4-14) is not significant. Therefore, the second term of Eq. (4-14) can be truncated as Eq. (4-16).

In Hoyos, et al., (1993) study, the methane oxidation over palladium catalysts is described by first-order kinetics with respect to methane and zero order with respect to oxygen. Similar kinetics were found for methane oxidation over platinum (Otto, 1989). They reported that the reaction can be described by first-order kinetics with respect to methane and is independent of oxygen pressure under excess oxygen conditions. Compared to the literature studies, the experimental data is quite consistent to the literature findings. It is concluded that methane oxidation reaction described by first order kinetics is simplified from Langmuir-Hinshelwood kinetics.

4.2.2 Catalyst Deactivation Isotherms

The catalytic oxidation of H_2S over 4% PdO/γ-alumina as a function of temperature is shown in Figure 4.20. After steady state was achieved at each desired temperature, H_2S was reacted for 20 minutes. The temperature was then increased to the next desired temperature. At 200 ^oC, 95% H_2S had been consumed. However, no other sulfur compounds were found in the off-gas. It appears that H_2S is adsorbed by either PdO or alumina or both. At lower temperatures, 100 ^oC to 200 ^oC, it appears that H_2S is adsorbed by PdO or reacts with PdO. After H_2S treatment, the catalyst turned black from brown as it was taken out from the reactor. At higher temperatures, 300 to 400 ^oC, it appears that H_2S is oxidized to SO_2 and SO_3 and these gases react with alumina. This is also reported by Hoyos, et al., (1993) that alumina is able to store sulfur as a surface sulfate, under oxidizing condition.

The catalytic oxidation of H_2S over 4% PdO/γ-alumina isotherms at 200 ^oC as a function of time is shown in Figure 4.21. It appears that a H_2S break through point occurs at 21 hours. The total accumulation of H_2S is about 1.02 milimoles based on 95 % H_2S

conversion. The PdO and alumina content used in this experiment are about 0.1 milimole and 2.82 milimole, respectively. This indicates that the H_2S is not only adsorbed by PdO but also reacts with alumina.

4.2.3 Methane Oxidation Activity Test

Figure 4.22 presents data on methane conversion as a function of temperature over the H_2S treated catalyst at 200 ^oC and 400 ^oC for 24 hours. It is clear that the catalyst treated at 400 ^oC has deactivated more than the one treated at 200 ^oC. It is found that the slopes of the 200 ^oC curve and 400 ^oC curve in the pore diffusion control regime decreased when compared to the fresh catalyst. These results suggest that there is increased pore diffusion resistance with increased treatment temperature possibly due to a reduction in pore size due to $Al_2(SO_4)_3$ formation.

Figure 4.23 shows the BET surface area change as a function of H_2S treatment temperature. The results show that the BET surface area decrease slightly with increasing treatment temperature. This also suggests formation of surface sulfate groups on the catalyst. The reduction of BET surface area may increases the diffusion resistance and deactivates methane oxidation activity (see Figure 4.22).

The treatment temperature effects on methane oxidation conversion, CO chemisorption and BET surface area are listed in Table 4.4. It is found the methane oxidation conversion is deactivated monotonically with H_2S treatment temperature. However, the CO chemisorption does not follow this trend. The CO chemisorption at 100 ^oC and 200 ^oC is lower than the CO chemisorption at 300 ^oC and 400 ^oC. Furthermore, methane oxidation conversion temperature increases with treatment temperature. These results shows that H_2S may be adsorbed by catalyst and reacts with PdO, preventing CO from adsorbing on the PdS sites. However, methane oxidation conversion for catalysts poisoned at 100 ^oC and 200 ^oC is higher than that at 300 ^oC and 400 ^oC. After testing

methane oxidation activity, the CO chemisorption was measured again for the sample catalysts which are poisoned at 200 °C and 400 °C.

The comparison of CO chemisorption before and after the methane oxidation activity test is provided in Table 4.5. The results show the CO chemisorption improves after the test for the catalyst poisoned at 200 °C, but only slight changes are found for the catalyst poisoned at 400 °C. It is hypothesized that the sulfur present on the active sites at the 200 °C treatment temperature is partially removed by air oxidation during the methane oxidation activity test. However, little if any sulfur is removed from the catalyst poisoned at 400 °C because all the sulfur adsorbed on the active sites is converted to SO_2 and reacts with Al_2O_3 forming $Al_2(SO_3)_3$ and $Al_2(SO_4)_3$ at this temperature.

Table 4.4 The Poisoned Temperature Effects on Methane Oxidation Conversion, CO Chemisorption and BET Surface Area

Catalyst poisoned temperature, °C	Methane oxidation activity T_{30}, °C	Methane oxidation activity T_{90}, °C	CO chemisorption, cm^3/g	BET surface area, m^2/g
Fresh catalyst	283	332	1.12	67
100 °C/24 hrs	343	400	0.53	55
200 °C/24 hrs	352	415	0.16	64
300°C/24 hrs	353	430	0.60	53
400 °C/24 hrs	362	448	0.51	50

T_{30} and T_{90} each indicates the temperature at 30 % and 90 % methane conversion

Table 4.5 The Comparison of CO Chemisorption Before and After Methane Oxidation Activity Test

Poisoned Temperature, °C	Before test, CO cm^3/g	After test, CO cm^3/g
200	0.16	0.69
400	0.51	0.53

4.2.4 Thermal Gravimetric Analysis

Figure 4.24 shows the thermal gravimetric analysis over 4% PdO/γ-alumina in presence of 250 ppm H_2S with air at 200 ^oC. At the beginning, the catalyst sample is heated to 200 ^oC at 40 ^oC/min and keep constantly at 200 ^oC. The initial catalyst sample weight loss is due to the removal of moisture. Once the balance reaches steady state at 200 ^oC, then 250 ppm H_2S gas is introduced to reactor and the weight starts to increase until the gas stream is switched to dry air after 30 minutes. The total weight gain in 30 minutes test is about 0.82 %. Figure 4.25 shows the thermal gravimetric analysis over 4% PdO/γ-alumina in presence of 250 ppm H_2S with air at 400 ^oC. The total weight gain in 30 minutes is about 2.09 %. Theoretically, if 4% PdO reacts with H_2S to produce PdS and H_2O then the weight gain should be 0.52%. The results suggest that H_2S is adsorbed by PdO and oxidized to SO_3 then reacts with alumina. In Figure 4.26, it is shown that the total weight gain is 0.67 % on the pure alumina with 250 ppm H_2S in presence of air stream. Compared to 2.1 % weight gain on 4% PdO/γ-Al_2O_3 catalyst, this indicates that the H_2S needs to adsorb on PdO first and then reacts with alumina. Therefore, PdO catalyzes the oxidation of H_2S to SO_2 and SO_3 (see Figure 4.20).

Figure 4.27 shows the weight gain as a function of temperature in 30 minutes with 250 ppm H_2S in presence of air stream. It is observed that catalyst weight increases with temperature increase. It is consistent with the results of methane oxidation conversion and BET surface area. It is indicated that the more weight gains, the more sulfur is reacted with the catalyst, there for the less methane oxidation activity.

4.2.5 FT-IR Spectroscopy of the Poisoned Catalyst

Figure 4.28 shows the FT-IR spectra of the H_2S effect on catalyst deactivation as a function of temperature for 24 hours. An absorbance band at 1145 cm^{-1} is assigned a strong $Al_2(SO_4)_3$ absorbance band (Nyquist, et al., 1971) and the absorbance band at

1070 cm^{-1} is attributed to the surface sulfite group (Yao, et al., 1981). The intensity of these two bands become stronger as the treatment temperature is increased. These results suggest that H$_2$S is first adsorbed by PdO and oxidized to SO$_2$ and then oxidized to SO$_3$ and finally reacts with Al$_2$O$_3$ to produce Al$_2$(SO$_4$)$_3$ (Farrauto, et al., 1992).

Figure 4.29 shows the thermal gravimetric analysis of the catalyst poisoned at 200 ^{o}C in presence of air. Generally, for fresh catalyst, the initial sample weight loses as the temperature increased is due to the removal of moisture from catalyst. However, the poisoned catalyst stops loosing the weight when the temperature reached 375 ^{o}C. On the contrary, the weight of poisoned catalyst gained as the temperature increased and the color of the catalyst turns brown from black. This is attributed to the air oxidation of the H$_2$S adsorbed on the catalyst producing sulfite and sulfate groups with the alumina.

Figure 4.30 shows the comparison of IR spectra of poisoned catalyst before and after thermal treatment with air. It is shown that the absorbance of the bands at 1145 cm^{-1} and 1070 cm^{-1} are stronger after thermal treatment with air. This is consistent with the observations using thermal gravimetric analysis.

4.2.6 H$_2$ Regeneration of H$_2$S Poisoned Catalyst

Figure 4.31 compares the methane oxidation conversion of H$_2$ regenerated catalyst with catalyst poisoned by H$_2$S in air at 400 ^{o}C, and fresh catalyst. The results show that catalyst activity for methane conversion is partially recovered by H$_2$ treatment. The results suggest that the surface sulfate and sulfite groups are reduced by H$_2$ at 600 ^{o}C. Figure 4.32 shows that no gases evolve from the 400 ^{o}C H$_2$S poisoned catalyst tested by temperature programmed oxidation. Results from temperature programmed reduction of the 400 ^{o}C H$_2$S poisoned catalyst are provided in Figure 4.33. The peak at 58 ^{o}C is H$_2$ consumption for reduction of PdO. The broad peak starting at 400 ^{o}C and ending at 600 ^{o}C is believed to be desorption of SO$_2$ from surface sulfite and sulfate groups due to the

H_2 reduction. Hence, the methane oxidation conversion is improved by H_2 treatment which remove SO_2 and SO_3 from the surface.

Figure 4.34 compares FT-IR spectra of the 400 °C H_2S poisoned catalyst before and after H_2 regeneration. The results show that the bands absorbance of regeneration catalyst at 1145 cm^{-1} and 1070 cm^{-1} are smaller than the catalyst before regeneration. This indicates that the sulfate and sulfite group are removed by H_2 treatment.

4.2.7 Comparisons of Activation Energies and Pre-exponential Factor over Fresh Catalyst, H_2S Poisoned Catalyst and the Catalyst Regenerated by H_2

By assuming pseudo first-order kinetics, the rate constants of methane oxidation can be calculated by using Eq. (4-16). Table 4.6 shows the rate constants of methane oxidation over fresh, H_2S poisoned and H_2 regeneration catalysts.

Table 4.6 The Rate Constants of Methane Oxidation over Fresh, H_2S Poisoned and H_2 Regeneration Catalysts

Temperature, °C	Fresh Catalyst k', cm^3/g-s	H_2S Poisoned Catalyst k', cm^3/g-s	H_2 Regeneration Catalyst k', cm^3/g-s
250	1.00		---
260	1.54		0.50
270	2.62		0.85
280	4.22		1.25
290	7.98		2.52
300	12.81	0.77	3.9
320		1.63	
340		3.06	
360		5.57	
380		8.67	

According to the Arrhenius equation, the rate constant can be described as follows:

$$k' = A \exp(-E_a/RT) \qquad (4-17)$$

where A is the pre-exponential factor, cm^3/g cat.-sec,

E_a is apparent activation energy, kcal/mole,

R is gas constant, kcal/mole-K.

By taking natural logarithm of both sides of Eq. (4-17), we obtain

$$\ln k' = \ln A + (-E_a/R) \, 1/T \qquad (4\text{-}18)$$

Figure 4.35 shows three plots of the logarithm of the rate constants versus $1/T$ for methane oxidation over fresh, H_2S poisoned and H_2 regeneration catalysts. The E_a and A are obtained from the slope and intercept. The apparent activation energy and pre-exponential factor for methane oxidation over fresh, H_2S poisoned and H_2 regeneration catalysts are listed in Table 4.7. The results show Ea and A values decrease as the catalyst is poisoned by H_2S at 400 ^oC. These results suggest that sulfur retained on the catalyst surface as sulfate and sulfite, affecting the Arrhenius parameters by decreasing activation energy and pre-exponential factor. As the poisoned catalyst is regenerated by H_2, the activation energy reverts back to that of fresh catalyst, but the pre-exponential factor achieves only half of fresh catalyst. These indicate that mostly sulfur are removed from poisoned catalyst surface by H_2 treatment. However, the sulfur poisoned catalyst can not be regenerated completely. Hence, the A value is smaller than the fresh catalyst indicative the permenant loss of some active sites. These results are consistent with the FT-IR analysis of fresh, H_2S poisoned and H_2 treatment catalysts.

Table 4.7 The Activation Energies and Pre-exponential Factor for Methane Oxidation over Fresh, H_2S Poisoned and H_2 Regenerated Catalysts

Catalysts	Activation Energy, kcal/mole	Pre-exponential Factor, $cm^3/g\text{-}s$
Fresh	30.82	7.02×10^{12}
H_2S Poisoned at 400 ^oC	21.82	1.78×10^8
H_2 Regeneration at 600 ^oC	31.39	3.63×10^{12}

4.2.8 Methane Oxidation as a Function of Temperature over Fresh and H_2S Poisoned Catalysts

In the pack-bed reactor and pseudo first order reaction, the methane conversion can be described as follows:

$$Xa = 1 - \exp(-k'*W/V) \qquad (4\text{-}19)$$

Substitute Eq.(4-17) into Eq.(4-19), we obtain

$$Xa = 1 - \exp[-A*(-E_a/RT)*W/V] \qquad (4\text{-}20)$$

Figure 4.36 shows methane oxidation conversion as a function of temperature over fresh catalyst by plugging fresh catalyst's Ea and A values. The results show that Eq. (4-20) describes very well the experimental data for each value of W/V. The results suggest that the reaction is governed by chemical kinetics. Figure 4.37 shows the relationship of methane oxidation conversion as a function of temperature for the catalyst poisoned by H_2S at 400 $^\circ C$ by substituting the poisoned catalyst's E_a and A value into Eq. (4-20). The results show that Eq. (4-20) agrees very well with the experimental data for each value of W/V. Based on these results, it is concluded that methane oxidation can be described by a pseudo first-order reaction rate law and the conversion can be expressed by Eq. (4-20) when the reaction is conducted at low conversions under oxidizing conditions and the catalyst particle size is so small that can avoid pore diffusion effects.

4.2.9 Methane Oxidation over Palladium Catalyst in Presence of H_2S

In our study, the deactivation of methane oxidation over palladium catalyst can be attributed to H_2S which adsorbs onto palladium active sites is oxidized to SO_3 and reacts with alumina forming $Al_2(SO_4)_3$. It is assumed that H_2S is an impurity in the feed stream. Therefore, the main reaction is methane oxidation and the poisoning reaction is that H_2S adsorbs onto the active sites is converted to SO_3 and reacts with Al_2O_3. The reaction rate law for methane oxidation under oxidation conditions has been derived and simplified as a pseudo-first order reaction.

$$-r_{CH_4} = k' C_{CH_4} \qquad (4-15)$$

A catalyst decay rate law was proposed by Fogler (1986) and Butt (1988). The deactivation rate law can be expressed as follows:

$$-r_d = - da/dt = k_d'C_p^m a^q \qquad (4-21)$$

In our study, the H_2S in the feedstream is held constant at 80 ppm. Therefore, Eq (4-21) becomes

$$-r_d = - da/dt = k_d a^q \qquad (4-22)$$

where $-r_d$ = deactivation rate = activity min^{-1}

a = catalytic activity, time dependent

k_d = decay constant, min^{-1}

q = order of deactivation

Integrating Eq.(4-22), we have

$$a = [1-(1-q)k_d t]^{1/(1-q)} \qquad (4-23)$$

where $q \neq 1$.

In the deactivation study, Eq.(4-15) has to be multiplied by a "activity term, a". Therefore, Eq.(4-22) becomes

$$-r_{CH_4} = a \ k' \ C_{CH_4} \qquad (4-24)$$

In our case, we have to determine the decay order by trial and error. Therefore, let q = 0, 2 and substitute them into Eq.(4-23), we have

$$q = 0, a = 1-k_d t \qquad (4-25)$$

$$q = 2, a = 1/(1+k_d t) \qquad (4-26)$$

Let q = 1 and substitute it into Eq.(4-22), we have

$$q = 1, a = exp(-k_d t) \qquad (4-27)$$

Since the reaction time is faster than the deactivation time one can use the pseudo-steady state forms of the mole balances. For the pack-bed reactor, we have

$$k's(W/V) = -ln (1-Xa) \qquad (4-28)$$

Substituting Eq. (4-25, 26, 27) into Eq. (4-28) respectively, we have

$$k'(1-k_d t)^* W/V = -\ln (1-Xa) \qquad (4\text{-}29)$$

$$k'^* \exp(-k_d t)^* W/V = -\ln (1-Xa) \qquad (4\text{-}30)$$

$$k'^* 1/(1+k_d t)^* W/V = -\ln (1-Xa) \qquad (4\text{-}31)$$

The k_d and k' can be obtained by non-linear regression under fixed reaction temperatures and residence time. Table 4.8 shows k_d and k' at various deactivation order and reaction temperatures.

Table 4.8 k_d and k' at Various Deactivation Order and Reaction Temperatures

Deactivation Order	Zero Order	First Order	Second Order
k', cm^3/g-s, 400 °C	215.6	306.5	336.6
k_d, min^{-1}, 400 °C	0.003	0.010	0.025
k', cm^3/g-s, 300 °C	19.7	24.6	24.8
k_d, min^{-1}, 300 °C	0.007	0.015	0.029

Figure 4.38 and 4.39 show the methane oxidation over palladium catalyst in presence of H_2S at 300 °C and 400 °C. The results show the first order deactivation law fits the experimental data better than zero or second order. This indicates that methane oxidation activity decay in exponential forms (Fogler, 1986) when H_2S is presented in the methane/air feedstream. In Figure 4.38, since the temperature at 300 °C is not high enough to compensate the catalyst deactivated by H_2S, the methane conversion finally approach to zero. In Figure 4.39, the results indicate that the H_2S adsorbs onto the active sites and reacts with Al_2O_3 as surface sulfate species in the beginning which makes the deactivation of methane oxidation. After a while, since the catalyst surface is saturated by sulfate species and the methane oxidation activity approach to steady state gradually.

In Hoyos et al. study (1993), although there is no kinetic study of deactivation of methane oxidation, the experimental data show that a exponential decay trend of methane oxidation as a function of time. Therefore, it is concluded that the deactivation of methane oxidation over palladium in presence of H_2S is followed by the first order deactivation rate law. By having this deactivation rate law, the effect of temperature and H_2S

concentration on methane oxidation can be applied into this deactivation rate law to predict the reaction temperature which maintain the same methane conversion during long term operation. However, it is not primary objects of this study and this will be considered a future study.

4.3 The Effect of Tributyl Phosphate on Deactivation of Catalysts

4.3.1 Effects of TBP Poisoning on Methane Oxidation over Palladium Catalysts

Normally, the operating temperature of the catalytic converter in the exhaust system of a natural gas fuel vehicle ranges from 400 ^{o}C to 600 ^{o}C. Therefore, catalyst aging at 500 ^{o}C was chosen for evaluation of normal catalyst durability performance and catalyst aging at 820 ^{o}C was chosen as representative of extreme operating conditions. Figure 4.40 provides the results of a simulation of automotive catalyst poisoned by TBP on methane oxidation over 4% PdO/γ-Al$_2$O$_3$ catalyst. This activity test was performed at 500 ^{o}C. It was found that methane conversion decreased with increasing of TBP dosage. The result clearly indicate that TBP is detrimental to the catalytic oxidation of methane over palladium catalysts.

Methane oxidation activity for fresh and TBP aged catalyst are compared as a function of temperature in Figure 4.41. The slope in the pore diffusion regime of aged catalyst curve is much lower than the slope of fresh catalyst curve. These results suggest that the rate of pore diffusion is reduced due to pore blocking by the TBP and the reactants are not easy to diffuse inside the porous to access the active sites (Heck and Farrauto, 1995).

4.3.2 Effect of Phosphorous Retention on Methane Oxidation Activity and BET Surface Area

After finishing the activity test, the catalyst sample was taken out from the reactor. It was found that the catalyst was covered by dark brown material which might be the major poison species on the catalyst surface. Part of aged catalyst sample were digested to analyze for elemental phosphorous and the rest was used to determine BET surface area and CO chemisorption. Table 4.9 shows the effects of phosphorous retention on methane oxidation activity, BET surface area and CO chemisorption of catalyst after aging test at 500 °C. It is found that elemental phosphorous remains on the surface of catalyst and increases in proportion to added TBP. The methane oxidation activity, BET surface area and CO chemisorption decreased in proportion to the quantity of TBP added into the reactor. The results show that phosphorous compounds, retained on the surface of catalyst, decrease methane oxidation activity. Also, phosphorous poisons affect catalyst surface since not only the BET surface area is decreased, but also the metal surface area (CO chemisorption). By investigating the methane conversion curve as a function of temperature (Figure 4.41) and BET surface area, it is believed that the residue of incompletely burned phosphorous compounds and P_2O_5 (Williamson, et al., 1985) result in the deactivation of catalysts.

Table 4.9 The Effect of Phosphorous Retention on Methane Oxidation Conversion, BET Surface Area and CO Chemisorption

Simulated-aged Mileage, miles	Phosphorous retention, wt %	Methane oxidation conversion, %	CO Chemisorption, c.c./g	BET surface area, m^2/g
Fresh catalyst	0	95.2	0.63	103
Fresh catalyst[1]	0	96.0	0.62	107
60,000	2.2	76.7	0.52	58
120,000	2.8	66.0	0.30	37

1. Fresh catalyst treated with air at 500 °C for 6 hours.
2. Methane oxidation activity was tested at 500 °C, 44,000 v/v/hr.

4.3.3 Temperature Effect on Methane Oxidation Activity and BET Surface Area

Figure 4.42 shows the temperature effect on methane oxidation activity over 4% PdO/γ-Alumina. The temperature has no effect on the blank test of methane oxidation activity but has negative effect when TBP has been added into reaction. The higher the aged temperature the lower the methane oxidation activity. Table 4.10 compares the temperature effect on methane oxidation activity with BET surface area and CO chemisorption. The results show the surface area at 820 °C is slightly larger than that at 500 °C. Also, the CO chemisorption is slightly improved at 820 °C due to the increased BET surface area. The results suggest that the TBP is burned completely at 820 °C. However, the combustion product, P_2O_5 may easily react with Al_2O_3 forming $AlPO_4$ which contribute to the catalyst deactivation mechanism at 820 °C.

Table 4.10 The Temperature Effects on Methane Oxidation Conversion, BET Surface Area and CO Chemisorption of TBP Aged Catalyst.

Simulated-aged Mileage, miles	Aged temperature, °C	Methane oxidation conversion, %	CO Chemisorption, c.c./g	BET surface area, m^2/g
Fresh catalyst	----	95.2	0.63	103
Fresh catalyst[1]	500	96.0	0.62	107
Fresh catalyst[2]	820	93.4	0.60	102
120,000	500	66.0	0.30	37
120,000	820	30.0	0.32	41

1. Fresh catalyst treated with air at 500 °C for 6 hours
2. Fresh catalyst treated with air at 820 °C for 6 hours
3. Methane oxidation activity was tested at 500 °C, 44,000 v/v/hr.

4.3.4 Thermal Gravimetric Analysis and FT-IR

The catalyst was loaded in the sample pan and weighed by the microbalance as a function of temperature. Figure 4.43 shows the comparison of weight change of TBP combustion in air and over catalyst. In the curve #1, the TBP evaporates completely when temperature

reaches 230°C. It is noted that the boiling point of TBP is 185 °C. In the curve #2 and curve #3, by calculating the weight change, the TBP is removed completely. It can be derived that TBP can be easily removed by thermal treatment if TBP is deposited on the surface of catalyst below 200 °C. However, at higher temperature, if TBP is combusted to produce P_2O_5 and deposits on the catalyst surface then another deactivation mechanism will be occurred during thermal treatment. This will be discussed in the next section.

The catalyst aged by TBP recovered from pulsator reactor was examined by FT-IR. The color of catalyst aged by TBP at 500 °C is a black and brown mixture and the color becomes dark brown in the test at 820 °C. Figure 4.44 shows the comparison of FT-IR spectra with the catalyst aged by TBP at 500 °C and 820 °C. In the wave number range from 1,000 to 1,200 cm^{-1}, there is an IR absorbance band. Comparing to fresh catalyst FT-IR spectra, a strong $AlPO_4$ IR absorbance is identified based on standard IR spectra (Nyquist, et al., 1971). In the test at 820 °C, this band is much bigger than the test at 500 °C, which indicates the TBP is burned at 860 °C to produce P_2O_5 which reacts with Al_2O_3 to produce $AlPO_4$ at 820 °C. Also, the methane oxidation conversion is decreased from 66 % to 30 % compared to the aged test at 500 °C. However, the temperature has a slight effect on BET surface area but gives a different catalyst deactivation mechanism from physical blocking at 500 °C to chemical interaction with support at 820 °C.

4.3.5 Heat Treatment Effect on Aged Catalyst

Table 4.11 shows the post heat treatment effect on the catalyst aged by TBP. The result shows that methane activity over the TBP aged catalyst has been slightly improved when the TBP aged catalyst is thermally treated by air at 650 °C for 2 hours. These results suggest that some residue material retained on the catalyst surface is removed during heat treatment. Hence, it is much easier for methane to access the active sites. However, the

aged catalyst can only be partially regenerated since P_2O_5 is difficult to remove. Furthermore, the higher temperature may affect the formation of $AlPO_4$. In the next section, we will focus on P_2O_5 effect on catalyst deactivation.

Table 4.11 Heat Treatment Effect on Methane Oxidation over TBP Aged Catalyst

	Fresh Catalyst	TBP Aged Catalyst [1]	Heat Treatment at 650 °C for 2 hours
T_{30}, °C	336	365	360
T_{90}, °C	400	425	415

1. The catalyst was aged by TBP for 60,000 simulated miles at 500 °C

4.4 The Effect of P_2O_5 on Catalyst Deactivation

4.4.1 Methane Oxidation Activity and BET Surface Area

In this section, we assumed that all doses of TBP in the reactor are oxidized to P_2O_5 since gaseous P_2O_5 is usually found in the automobile combustion of fuel doped with phosphorous hydrocarbons (Williamson, et al., 1985). Therefore, the equivalent amounts of P_2O_5 mixed with catalysts were tested for the study of P_2O_5 effect on methane oxidation.

The effect of P_2O_5 and treatment temperatures on methane oxidation are summarized in Table 4.12. Fresh catalyst treated in air at 500 °C and 820 °C for 6 hours has no significant effect on methane conversion and BET surface area. The test results show that as a consequence of the presence of P_2O_5, methane conversion and BET surface area decreased. Aging at 820 °C is more detrimental on the catalyst activity than aging at 500 °C, even though BET surface area does not significant change. These results show a strong catalyst support interaction with P_2O_5 at 820 °C. These results are similar to those found in the TBP aging tests.

Table 4.12 The Effect of P_2O_5 Concentration and Aged Temperatures on Methane Oxidation over 4% PdO/γ-Al_2O_3 Catalyst

P_2O_5 Contents	Treatment	Methane oxidation conversion, %	BET surface area, m^2/g
Fresh catalyst	---	95.2	103
Fresh catalyst	500 °C/6 hrs	96.0	107
Fresh catalyst	820 °C/6 hrs	93.4	102
0.26 g P_2O_5 + 0.4 g catalyst	500 °C/3 hrs	82.0	19
0.52 g P_2O_5 + 0.4 g catalyst	500 °C/3 hrs	65.7	8
0.52 g P_2O_5 + 0.4 g catalyst	820 °C/3 hrs	29.7	9

1. The activity was tested at space velocity 44,000 v/v/hr, 500 °C, and 1% methane in air.

Figures 4.45 and 4.46 compare methane oxidation conversion as a function of temperature for catalyst aged with P_2O_5 at 500 °C and 820 °C with fresh catalysts at the same temperatures. The results show that the slopes of 500 °C and 820 °C curves are lower than fresh catalyst curve and the maximum conversion of 500 °C and 820 °C curves are dropped compared to fresh catalyst curve. This is due to the masking of P_2O_5 and loss in geometric area, which impact the bulk mass transfer area. (Heck and Farrauto, 1995). After the test, the catalysts were visually inspected. It was observed that a visible glassy products and a small clot of P_2O_5 covered the catalyst surface. These observations provide support that the deposition of P_2O_5 on the catalyst surface impedes methane access to the catalyst surface and increases mass transfer and pore diffusion resistance...

4.4.2 Thermal Gravimetric Analysis

Figure 4.47 provides the TGA results of weight change of P_2O_5 as a function of temperature in air. As temperature increases from room temperature to 320 °C weight increases. This indicates that some of the moisture present in the equipment is absorbed by P_2O_5. This is followed by a gradual decrease in weight as temperature increases until a sharp weight decrease is observed when temperature reaches 600 °C. This is followed by a gradual to zero weight change as temperature reaches 890 °C. This thermal treatment

sequence indicates that the P_2O_5 is dehydrated at temperature ranging from 320 ^oC to 600 ^oC and sublimes into the gas phase until there is none left. Figure 4.48 shows the weight change of fresh catalyst in air as a function of temperature. The results show that the temperature has a slight effect on the weight change of fresh catalyst. PdO decomposes to Pd metal at temperatures above 800 ^oC (Farrauto, et al., 1992). The 6.7 % weight change is due to volatilization of adsorbed water on the Al_2O_3 support when temperature is below 800 ^oC.

The weight change of P_2O_5 mixed with catalyst as a function of time is shown in Figure 4.49. The total weight of mixture is 12.958 mg and the catalyst weight is 6.9 mg. So, the weight of P_2O_5 is 6.058 mg in the beginning. According to the results of Figure 4.47, all the pure P_2O_5 should sublime to gas phase and the weight should decrease from 12.958 mg to 6.9 mg as temperature increases above 800 ^oC. However, the weight changes from 12.958 mg to 11.568 mg and the weight does not change with exposure time. These results show that the behavior of P_2O_5 in the presence of catalyst is not the same as pure P_2O_5. There appears to be is a strong adsorption between catalyst and P_2O_5. Catalyst active sites and pores are blocked by P_2O_5 causing a loss in activity.

Figures 4.50 and 4.51 show the weight change as a function of temperature of P_2O_5 mixed with PdO and pure γ-Al_2O_3, respectively. It appears that P_2O_5 in both mixture does not sublime. In the mixture of P_2O_5 with PdO, the total weight change is 0.689 mg. Comparing this weight loss to the total weight of P_2O_5, 2.963 mg, there are 2.274 mg of P_2O_5 retained on the catalyst surface. In the mixture of P_2O_5 with pure γ-Al_2O_3, the total weight change is 1.875 mg resulting in the retention of 5.645 mg of P_2O_5 on the catalyst surface. These results show that P_2O_5 is a non discriminative adsorption. Once it is adsorbed by the catalyst, it may form a glassy high molecular weight oligomer and $AlPO_4$ compound (Miciukiewicz, 1989 and Williamson, 1985).

4.4.3 Catalyst Deactivated by Incipient Wetness with P_2O_5 Aqueous Solution

In the previous study, we found that P_2O_5 had very strong adsorption interaction with the catalyst and physically blocked the catalyst surface. However, it is not easy to mix uniformly P_2O_5 with catalyst. Using the incipient wetness technique with P_2O_5 solution can uniformly disperse P_2O_5 on the catalyst surface. (Miciukiewicz, 1989). Table 4.13 shows the effect of P_2O_5 content and treatment temperatures on methane oxidation and BET surface area. These results show the P_2O_5 retention leads to catalyst deactivation and decreases in BET surface area. The more P_2O_5 is retained on the catalyst surface, the lower the methane oxidation activity and BET surface area. High temperatures can remove more P_2O_5 from the catalyst surface and leads to renovation of BET surface area, but cannot contribute to enhanced activity for methane oxidation.

Table 4.13 The P_2O_5 Contents and Aged Temperatures Effect on Methane Oxidation and BET Surface Area

P_2O_5 wt. %	Treatment	P_2O_5 retention, wt. %	Methane oxidation conversion, %	BET surface area, m^2/g
Fresh	----	0	92.6	103
2.9	500 ^oC/3h	0.6	65.4	80
4.7	500 ^oC/3h	3.8	30.0	62
4.7	820 ^oC/3h	2.4	24.9	70

1. The catalyst is deactivated by incipient wetness of P_2O_5 aqueous solution.
2. The activity is tested at 460 ^oC, 88,000 v/v/hr.

4.4.4 Thermal Gravimetric Analysis of Catalyst Deactivated by P_2O_5 Aqueous Solution

Figure 4.52 shows the weight change of catalyst poisoned via incipient wetness with P_2O_5 solutions as a function of temperature. The total weight changed from 17.773 mg at room temperature to 9.219 mg at about 120 ^oC. This indicates that the water is removed from the sample. The sample weight decreased slightly from 9.219 mg to 8.787 mg with temperature increases to 500 ^oC. There are 0.432 mg of P_2O_5 that sublimes and 0.647 mg

of P_2O_5 still remains on the catalyst surface. Therefore, about 60.0 % of P_2O_5 is retained on the catalyst surface.

Figure 4.53 shows the same experiment as Figure 4.52 but the temperature is programmed to 820 °C. The sample weight changed from 23.028 mg at room temperature to 12.205 mg at about 120 °C. This indicates the water is removed from the sample. The sample weight decreased slightly from 12.205 mg to 11.607 mg when temperature is increased to 820 °C. Therefore, 56.2 % of P_2O_5 is retained on the catalyst surface. These results suggest that heat treatment can remove part of P_2O_5 but induces another deactivation mechanism.

4.4.5 IR Spectroscopy of Fresh Catalyst and Aged Catalyst

Figure 4.54 shows the FT-IR spectra of P_2O_5 effect on the catalyst surface at different temperature. The FT-IR spectra (A), (B), and (C) which indicate the fresh catalyst, the catalyst sample taken from TGA at 500 °C, and at 820 °C, respectively. The band at 1630 cm^{-1} is due to the bending vibration of adsorbed water molecules (Yao, et al., 1981). The broad band at 1,110 cm^{-1} is $AlPO_4$ absorbance (Nyquist, et al., 1971). It should be noted that no absorbance at 1,110 cm^{-1} is observed for fresh catalyst. For the aged catalyst, the higher the treatment temperature the higher the absorbance band at 1110 cm^{-1}. The band below 1,000 cm^{-1} is the complete absorption band of the alumina (Chang, 1978). These results provide evidence of similar findings in the TBP aged catalyst. The formation of $AlPO_4$ can be found not only in the reaction of Al_2O_3 and P_2O_5 but also in the TBP aged catalyst surface. Therefore, it can be determined that P_2O_5 is the major combustion product of TBP and that P_2O_5 reacts with Al_2O_3 forming $AlPO_4$, when the catalyst is exposed to high temperatures.

4.5 The Effect of ZDP on Deactivation of Catalyst

4.5.1 ZDP Effects on Methane Oxidation over Palladium Catalyst

Figure 4.55 shows the simulation of automotive catalyst poisoned by ZDP for methane oxidation over palladium catalyst. The results show that thermal aging does not affect catalyst activity, but ZDP deactivates palladium catalysts. The methane oxidation activity decreases with increasing P input.

Methane oxidation activity as a function of temperature on fresh catalyst and aged catalyst is plotted in Figure 4.56. It is shown that catalyst deactivation occurred in both the low-temperature (<400 °C) kinetic regime, as well as the mass transfer regime (>400 °C). In the kinetic regime, this implies that the catalyst active sites are blocked by the poison. Hence, the reaction needs high temperature to light off methane oxidation. In the pore diffusion and mass transfer regime, the temperature is high enough to oxidize methane but pore diffusion and mass transfer mechanisms are hindered by the deposition of the poison. Therefore, methane is not easy to access the catalyst surface and diffuse into the pores of the catalyst. Comparing the slopes of these two curves in the pore diffusion and mass transfer regimes, the slope of aged-catalyst is much lower than that of the fresh catalyst. It is believed that the poison not only blocked the active sites of catalyst, but blocked the entrance to pores and covered the entire catalyst surface.

4.5.2 Comparisons of Methane, Propane and CO Oxidation Activity over Fresh and Aged Catalyst

Figures 4.57 and 4.58 show the CO and propane oxidation activity as a function of temperature over fresh catalyst and aged catalyst respectively. The results show that ZDP has negative effects on propane and CO oxidation activity. The comparisons of methane, propane and CO oxidation activity over fresh catalyst and aged catalyst are listed in Table 4.14. The conversion of CO and Propane oxidation could reach 90 % under 500 °C. The

difference of T_{90} between fresh and aged catalyst is over 150 °C for methane oxidation activity. It is observed that ZDP is more detrimental to methane oxidation than to propane and CO oxidation.

Table 4.14 The Comparisons of Methane, Propane and CO Oxidation Activity over Fresh and Aged Catalyst.

Reactants	Methane	Methane	Propane	Propane	CO	CO
	T_{50}, °C	T_{90}, °C	T_{50}, °C	T_{90}, °C	T_{50}, °C	T_{90}, °C
Fresh Catalyst	345	460	310	340	130	138
Aged Catalyst	538	>600	348	436	195	238

1. T_{50} and T_{90} indicate the temperature at conversion 50% and 90 % receptively.
2. The aged catalyst indicates the catalyst was aged 120,000 simulated miles at 500 °C.

4.5.3 Activation Energies and Rate Constants of Methane Oxidation over Fresh and Aged Catalysts

In methane oxidation reaction, 20% O_2 is in large stoichiometric excess over 1% methane. Hence, it is assumed that the reaction is pseudo first order with respect to methane and zero order with respect to oxygen. This assumption is justified by the study of Hoyos, et al., (1993). The rate of reaction can be written as follows:

$$-r_A = k'C_{CH4} \tag{4-15}$$

where $-r_A$ is rate of reaction of methane, gmole/g of catalyst-s

k' is a rate constant, cm^3/gm of catalyst-s

C_{CH4} is methane concentration, gmole/cm^3

In these experiments, the packed bed reactor is assumed to be a plug flow reactor system and all the reactions are run under kinetic control regime, i.e., the methane conversion is under 30 %. Therefore, the integral form of the packed catalyst bed equation can be derived as follows:

$$\frac{Wk}{V} = -\ln(1-X_A) \tag{4-16}$$

where W is weight of catalyst, gram

V is volumetric feed rate, cm^3/sec

X_A is conversion of methane

k' is rate constant, cm^3/g of catalyst-s

Figures 4.59 and 4.60 show the plots of -ln $(1-X_A)$ versus W/V for methane oxidation over fresh catalyst and aged catalyst. The rate constants are obtained from the slope of the lines. The slopes were calculated by linear regression.

According to the Arrhenius equation, the rate constant also can be described as follows:

$$k' = A \exp(-Ea/RT) \quad\quad\quad (4-17)$$

where A is the pre-exponential factor, cm^3/g-s,

Ea is apparent activation energy, kcal/mole,

R is gas constant, kcal/mole-K.

then,

$$\ln k' = \ln A + (-Ea/R)(1/T) \quad\quad\quad (4-18)$$

Figure 4.61 shows two plots of the logarithm of the rate constants versus 1/T for methane oxidation over fresh catalyst and aged catalyst. The Ea and A are obtained from the slope and intercept. The Arrhenius apparent activation energy, Ea and pre-exponential factor, A for methane oxidation over fresh catalyst and aged catalyst are listed in Table 4.15. The results show that the Ea value for the fresh catalyst and aged catalyst are almost identical, but the A value of aged catalyst is one third lower than the A value of fresh catalyst. It is suggested that the nature of reaction pathway for fresh and aged catalyst remained unchanged but the decrease in internal surface area did affect the pre-exponential factor as well as the reaction rate (Satterfield 1980). These results imply that the catalyst is deactivated by loss of active sites to phosphorous compounds.

Table 4.15 The Arrhenius Apparent Activation Energy and Pre-exponential Factor for Methane Oxidation over Fresh and Aged Catalyst.

Treatment	Apparent activation Energy, Ea, kcal/mole	Pre-exponential factor, A, cm^3/g-sec
Fresh catalyst	19.99	17.49×10^7
Pulsator aged 120,000 simulated miles	20.48	6.18×10^7

4.5.4 Effect of Phosphorous and Zinc Retention on Methane Oxidation Activity, BET Surface Area and CO Chemisorption

Table 4.16 shows the effects of phosphorous and zinc retention on pulsator activity and BET surface area of catalyst in the aged test at 500 °C. It is shown that zinc and phosphorous are retained on the surface of the ZDP aged-catalyst as the dose of ZDP is increased. These results suggest that a zinc phosphorous compound or phosphorous compound are formed on the catalyst surface. The BET surface area and metal surface area (CO chemisorption) are decreased as the doses of ZDP are increased. Obviously, the methane conversion drops as the BET surface area and metal surface area decrease. The results suggest that the retention of zinc and phosphorous causes the blockage of the catalyst surface and results in catalyst deactivation.

Table 4.16 The Effect of Zinc and Phosphorous Retention on Methane Oxidation Conversion, BET Surface Area and CO Chemisorption

Simulated-aged Mileage, miles	Phosphorous retention, wt. %	Zinc retention, wt. %	Methane oxidation conversion, %	CO Chemisorption, cm^3/g	BET surface area, m^2/g
Fresh catalyst	0		95.2	0.63	103
Fresh catalyst[1]	0		96.0	0.62	107
60,000	3.0	0.6	54.0	0.40	56
120,000	4.2	1.0	41.9	0.19	35

1. Fresh catalyst treated with air at 500 °C for 6 hours
2. The activity was tested at space velocity 44,000 v/v/hr, 500 °C, and 1% methane in air.

4.5.5 Temperature and Phosphorous Dosage Effect on Methane Oxidation Activity, BET Surface Area and CO Chemisorption

Figure 4.62 shows the temperature effects on methane conversion due to catalyst deactivation. The results show the higher the aged temperature, the lower the methane conversion.

Table 4.17 The Aged Temperature Effects on the Methane Conversion, BET Surface Area and CO Chemisorption

Simulated-aged Mileage, miles	Aging temperature, ^{o}C	Methane oxidation conversion, %	CO Chemisorption, cm^3/g	BET surface area, m^2/g
Fresh catalyst	----	95.2	0.63	103
Fresh catalyst[1]	500	96.0	0.62	107
Fresh catalyst[2]	820	93.4	0.60	102
120,000	500	41.9	0.19	35
120,000	820	34.0	0.31	39

1. Fresh catalyst treated with air at 500 ^{o}C for 6 hours
2. Fresh catalyst treated with air at 820 ^{o}C for 6 hours
3. The activity was tested at space velocity 44,000 v/v/hr, 500 ^{o}C, and 1% methane in air.

Table 4.17 shows the aging temperatures effects on the BET surface area and CO chemisorption of the aged catalyst. In the aging tests at 820 ^{o}C, the BET surface area and CO chemisorption are slightly increased. This indicates that the residue of unburned organo-phosphorous compounds are burned completely at 820 ^{o}C. However, the methane oxidation conversion is less than at 500 ^{o}C. Similar findings were reported by Inoue, et al., (1992) in his study of ZDP effects on three way catalyst. They found that the deactivation of the catalyst at 800 ^{o}C was greater than at 720 ^{o}C. Also, they indicated that the drop in activity at 800 ^{o}C may have been caused by the different types of compounds that were formed during the aging test.

4.5.6 Results of Thermal Gravimetric Analysis

Figure 4.63 shows the comparison of ZDP with catalyst or without catalyst in the weight change as a function of temperature. In the test of ZDP only, see curve #1, the reaction starts at 200 °C and the weight of ZDP drops sharply as temperature is increased. It was found that 26 % of sample weight remained on the sample pan at temperature over 400 °C, and still retained on the sample pan when the temperature reached 900 °C. Similarly, in the test of ZDP with catalyst, see curve #2, the reaction starts at 170 °C and the weight of ZDP drops sharply as the temperature is increased. It is found that curve #2 is shifted to lower temperature compared to curve #1. This is because the ZDP is catalyzed and the ignition temperature is lowered by catalytic oxidation. About 25.7 %, excluding catalyst weight, of sample weight remained on the sample pan at temperatures over 360 °C, and still retained on the catalyst when the temperature reached 900 °C. It is concluded that unburned ZDP which condensed on the surface of catalyst at room temperature cannot be removed by post heat treatment even when the temperature reaches 900 °C. In a previous study, Williamson, et al., (1984, 1985) reported that $Zn_2P_2O_7$ was the major product of ZDP combustion. Once it was formed on the surface of catalyst, it could be removed by H_2 treatment at 800 °C but might cause severe sintering of the catalyst and also deactivation of the catalyst.

4.5.7 Results of FT-IR and XRD Analysis

Figure 4.64 shows the comparisons of FT-IR spectra of the catalyst deactivated by ZDP at 500 °C and 820 °C . It is found that the IR spectra at 500 °C has 6 major absorbance bands located at 1,000-1,200 cm⁻¹ which are 1,030, 1,070, 1,100, 1,140, 1,180, 1,200 respectively. Those bands almost matched the standard $Zn_2P_2O_7$ IR spectra which are 1,030, 1,080, 1,100, 1,130, 1,160 and 1,190 cm⁻¹ (Nyquist, et al., 1971). However, The IR absorbance bands 1,225, 1,275, 1,285 and 1,340 cm⁻¹ could not be identified. These

are probably due to unburned phosphorous compounds. The FT-IR spectra at 820 $^\circ$C has 5 major absorbance bands located at 1,000-1,200 cm^{-1} which are 1,060, 1,100, 1,120, 1,167 and 1,196 cm^{-1}. Those almost matched the standard $Zn_2P_2O_7$ IR spectra. The bands at 1,275, 1,285 and 1340 cm^{-1} disappeared at 820 $^\circ$C IR spectra. This is because unburned residue are burned off at 820 $^\circ$C. These results suggest that the formation of $Zn_2P_2O_7$ was deposited on the aged catalyst surface. However, it needs more evidence to support the hypothesis of the formation of $Zn_2P_2O_7$. Figure 4.65 shows the XRD patterns of the catalyst deactivated by ZDP at 820 $^\circ$C. The 2-theta of 3 major peaks 29.5, 35.2 and 42.95 and each relative intensity 100%, 30%, and 25% showed the formation of beta-$Zn_2P_2O_7$ on the surface of aged catalyst. Similar findings were reported by Williamson, et al., (1984, 1985). They found that $Zn_2P_2O_7$ was the major combustion product of ZDP. This evidence was also referred to by Inoue, et al., (1992) in their study of effects of phosphorous and ash contents of engine oils on deactivation of monolithic three-way catalysts and oxygen sensors.

Figure 4.66 shows the FT-IR spectra of ZDP combustion products which were collected on the fritted disc while the blank test was running at 500 $^\circ$C. It is shown that those spectra are almost identical with the spectra of the catalyst deactivated by ZDP at 500 $^\circ$C. It is concluded that those combustion products which are carried from combustion zone to the catalyst bed are deposited on the surface of catalyst and result in the deactivation of the catalyst.

In the previous thermal gravimetric analysis of ZDP combustion, see Figure 4.63, the weight change of ZDP combustion is from 100 % to 26 % at 860 $^\circ$C. If all the ZDP is converted to $Zn_2P_2O_7$ then the weight change is from 100 % to 19.8%. Therefore, 6.2% residue remained on the sample pan which indicated some portions of ZDP residue could not be precisely identified by FT-IR or XRD. This probably is a formation of higher molecular amorphous phosphorous oligomers (Williamson, et al., 1985).

4.5.8 Thermal Treatment and H_2 Treatment Effects on ZDP Aged Catalyst

Figure 4.67 shows post thermal treatment effect on methane oxidation activity as a function of temperature over ZDP aged catalyst . The results show that methane oxidation activity is partially improved after heat treatment. These results suggest that some residue on ZDP aged catalyst can be removed from the catalyst surface. However, in TGA test, $Zn_2P_2O_7$ cannot be removed when temperature reaches 900 ^oC. Figure 4.68 shows the FT-IR spectra of different treatment of ZDP aged catalyst. The results show the thermal treatment spectra is almost the same as the ZDP aged spectra. This is coincident with the results of TGA. Therefore, the heat treatment can slightly regenerate the catalyst activity.

Figure 4.69 shows H_2 treatment temperature effect on methane oxidation over ZDP aged catalyst. The results show the catalyst activity is slightly improved when the ZDP aged catalyst has been treated at 600 ^oC in reductive atmosphere. However, the catalyst activity decreases when ZDP aged catalyst is treated at 800 ^oC. Figure 4.70 shows the temperature programmed reduction of ZDP aged catalyst. At 70 ^oC, the H_2 consumption peak represents the reduction of PdO. The broad desorption peak started from 400 ^oC to 800 ^oC is believed due to the material desorbing from the surface of aged catalyst during H_2 treatment. The reactor was taken out from the furnace when the experiment had done. It is found that white color solid deposits on the wall of the reactor. It is believed that the zinc is replaced by H_2 in the H_2 reduction reaction. Figure 4.71 shows the FT-IR spectra of the comparison of different H_2 treatment temperature effect on ZDP aged catalyst. The results show the H_2 treatment at 600 ^oC can not remove $Zn_2P_2O_7$. However, at 800 ^oC H_2 treatment, the $Zn_2P_2O_7$ is removed but inducing the formation of another compound which is believed to be $AlPO_4$ (Nyquist, et al., 1971).

CHAPTER 5

DISCUSSION

5.1 The Effect of Chlorine Compounds on Catalyst Deactivation

The discussion of the effect of HCl on deactivation of PdO/γ-alumina for methane oxidation over PdO/γ-alumina catalysts is based on the results presented in Chapter 4.

The catalyst aged with HCl at 300 ^{o}C had lower activity than fresh catalysts but no significant changes of active metal were found. It appeared that HCl gas was adsorbed and reacted with PdO to produce PdCl$_2$, which remained on the surface of the catalyst. Simone, et al., (1991) found that catalysts prepared using a PdCl$_2$ precursor salt had lower activity compared with catalysts prepared with a Pd(NO$_3$)$_2$ salt. These researcher showed that chlorine remaining on the surface inhibits methane oxidation. They also demonstrated that once the chlorine was removed, the methane oxidation activity improved. Accordingly, our results of temperature programmed reduction of pure PdCl$_2$ indicated that catalyst poisoned by HCl can be regenerated with hydrogen. The reduced Pd metal was then oxidizes with oxygen to produce PdO. The results show that methane oxidation activity is regenerated close to fresh catalyst when the chlorine is removed. This evidence is consistent with the finding of Simone, et al., (1991).

When the catalyst was aged with HCl at 500 ^{o}C, it showed lower activity and metal surface area than fresh catalyst or catalyst aged at 300 ^{o}C. There are two possible mechanisms associated with the loss of active metal, one is catalyst sintering and the other is evaporation. Thermal treatment at 500 ^{o}C showed no significant change of metal surface. Also, the PdO decomposition temperature is about 840-870 ^{o}C therefore no PdO volatilization occurred. Satterfield (1980) pointed out in his book that chloride may poison metal by forming a surface metal chloride, or it may enhance sintering via the formation of volatile metal chlorides. Lisitsyn, et al., (1989) report that chloride containing palladium

catalyst with the highest dispersion of palladium were the least active. Hence, metal chloride volatilization is a possible way of losing methane oxidation activity. Our results show that the catalyst is poisoned by HCl and produces $PdCl_2$. Then, the $PdCl_2$ volatilizes and deposits on the colder walls of the reactor.

The effect of water addition to a gas stream containing HCl is to retard catalyst deactivation. A mechanism proposed by Mendyka, et al., (1992) who found that H_2O produced during catalytic oxidation of hydrocarbons by platinum catalyst aided in desorbing HCl from the catalyst. Marecot, et al., (1994) also found that using chloride containing precursor salts to synthesize catalysts tended to poison the catalyst for propane oxidation. Nevertheless, the poisoning effect disappears in continuous use in catalytic oxidation of propane because the water produced removed chloride from the catalyst surface. This may be the same mechanism that occurs on palladium catalyst. One can speculate that water vapor may hinder the following reaction rate by

$$PdO\ (s) + 2\ HCl\ (g) <\text{-------}> PdCl_2\ (s) + H_2O\ (g) \qquad (5\text{-}1)$$

favoring the reverse reaction. Also, the addition of water vapor can minimize the Cl_2 formation in catalytic oxidation of chlorinated hydrocarbons (Yu, et al., 1992, Windawi, et al., 1993).

5.2 The Effect of Sulfur Compound on Catalyst Deactivation

5.2.1 Catalyst Deactivation Mechanism

As was pointed out in Chapter 4, H_2S poisons PdO on $\gamma\text{-}Al_2O_3$ catalysts for methane oxidation. The different H_2S treatment temperatures give insight on of how catalyst are poisoned.

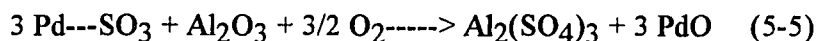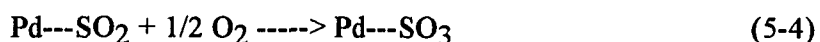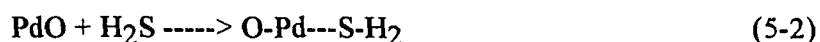At 200 ^{o}C, H_2S is adsorbed by palladium metal. Therefore, the color of catalyst turns black from brown. In CO chemisorption experiments, H_2S occupies catalyst active sites, which leads a decrease of CO chemisorption from 1.12 cm^3/g to 0.19 cm^3/g. However, thermal treatment of the catalyst at 400 ^{o}C cam regenerate the active metal

dispersion 0.19 to 0.69 cm^3/g. These results suggest that Pd---SH$_2$ is oxidized by air forming Pd--SO$_2$ and Pd---SO$_3$ which reacts with Al$_2$O$_3$ to produce Al$_2$(SO$_4$)$_3$. This is confirmed by finding surface sulfite and sulfate group absorbance bands in the FT-IR spectra.

Additional evidence for these results were found using thermal gravimetric analysis (see Figure 4.29). The 200 ^{o}C poisoned catalyst sample weight decreased as the temperature increased. However, the sample weight gains when the temperature increased to 375 ^{o}C. Above 375 ^{o}C, the sample showed a gain in weight indicating that Pd---SH$_2$ reacts with O$_2$ forming Pd---SO$_2$ and the sulfur was retained on the support.

At 400 ^{o}C treatment temperature, the color of the catalyst sample is brown (the usual color of PdO) and the CO chemisorption, i. e., metal dispersion is larger than the catalyst treated at 200 ^{o}C (see Table 4.4). This indicates that the temperature is sufficiently high to rapidly oxidize Pd---SH$_2$ to Pd---SO$_2$ and Pd---SO$_3$. Also, the Pd---SO$_3$ can react with Al$_2$O$_3$ forming Al$_2$(SO$_4$)$_3$. That is why the surface sulfite and sulfate absorbance bands in the FT-IR spectra are bigger than the spectra of the catalyst treated at 200 ^{o}C.

Combining these findings, a deactivation mechanism can be proposed as follows:

$$PdO + H_2S -----> O\text{-}Pd\text{---}S\text{-}H_2 \qquad (5\text{-}2)$$

$$O\text{-}Pd\text{---}S\text{-}H_2 + O_2 -----> Pd\text{---}SO_2 + H_2O \qquad (5\text{-}3)$$

$$Pd\text{---}SO_2 + 1/2 \ O_2 -----> Pd\text{---}SO_3 \qquad (5\text{-}4)$$

$$3 \ Pd\text{---}SO_3 + Al_2O_3 + 3/2 \ O_2 -----> Al_2(SO_4)_3 + 3 \ PdO \qquad (5\text{-}5)$$

At 200 ^{o}C, the temperature is so low that the rate of reaction (5-3) is slow. Therefore, most of catalysts sites stay at reaction (5-3) and just little sulfite and sulfate is produced. At high temperature, 400 ^{o}C, the temperature is high enough to speed up reaction (5-3). Therefore, the color of catalyst sample turns brown and the rate of production of sulfite and sulfate is higher than at 200 ^{o}C. Reactions (5-3) and (5-4) are reactions in series and reaction (5-5) indicates that surface sulfite reacts with Al$_2$O$_3$ to produce Al$_2$(SO4)$_3$. Due

to the formation of sulfite and sulfate, BET surface area and CO chemisorption decrease and pore diffusion resistance increase leading to catalyst deactivation.

H_2 treatment at 600 °C induces catalyst regeneration. It is found that the surface sulfate and sulfite group are removed at 600 °C. The aluminum sulfate groups are reduced by H_2 and produce alumina, SO_2 and H_2O according to the reaction:

$$Al_2(SO_4)_3 + 3 H_2 \text{-----> } Al_2O_3 + 3 SO_2 + 3 H_2O \qquad (5\text{-}6)$$
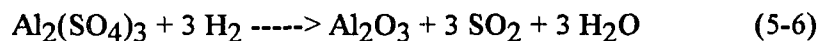
The surface sulfite groups can be thermally removed at around 600 °C (Chang, 1978).

5.2.2 Comparisons of Activation Energy over Fresh and H_2S Poisoned Catalysts

Hicks, et al., (1990) reported that the activation energy may change slightly as the palladium particle size changes. The activation energy for methane oxidation over palladium catalyst has been reported to be in the range from 17 kcal/mole to 33 kcal/mole according to Hicks, et al., (1990). However, for the same catalyst and same reaction conditions, the activation energy should be identical. The discrepancy in activation energy needs to be explained.

According to Satterfield's study (1980), the strong adsorption of a poison on the active sites increases the apparent activation energy of the reaction. However, in our study, the activation energy for H_2S poisoned catalyst decreases. These results suggest that sulfur is adsorbed on the active sites and quickly reacts with Al_2O_3 forming aluminum sulfate. Therefore, the activation energy does not increase when the catalyst has been poisoned by H_2S at 400 °C for 24 hours.

The activation energy decrease can be attributed by the formation of $Al_2(SO_4)_3$ which enhances the internal diffusion resistance and shifts the rate determining step from surface reaction domain to pore diffusion domain. If the reaction rate is completely controlled by pore diffusion under first-order reaction conditions, then the rate equation can be expressed by Eq. (2-16).

$$-r_A = 3/R(D_e S_a A/\rho_p)^{0.5}[exp(-E_t/RT)]^{0.5} C_A$$

$$= A' [exp (-E_t/RT)]^{0.5} C_A$$

$$= A' [exp (-E_{app}/RT)] C_A \qquad (2\text{-}16)$$

Therefore, $\quad E_{app} = 1/2 E_t, \qquad\qquad\qquad (5\text{-}7)$

where E_{app} = measured activation energy, kcal/mole,

E_t = true activation energy, kcal/mole.

R = radius of catalyst particle, cm,

D_e = effective diffusivity, cm^2/s

ρ_p = particle density, $g/\ cm^3$.

S_a = surface area per gram of catalyst, cm^2/g

This measurement of the apparent activation energy results primarily when internal diffusion limitations are present. However, if the reaction is in the transition region, between kinetic control and pore diffusion control, the measured activation energy should be in the ranges of 30.82 kcal/mole (the E_t of fresh catalyst) and 15.41 kcal/mole (half E_t of fresh catalyst). In our findings, the measured activation energy is 21.82 kcal/mole. This indicates that the methane oxidation over H_2S poisoned catalyst is influenced by pore diffusion effects but is not completely limited by pore diffusion controls.

5.2.3 External Mass Transfer Effects

In industrial applications, the catalyst particle size can not be so small to cause high pressure drop in the reactor. Therefore, large particle size catalyst may experience external and internal pore diffusion transfer resistance. The mass transfer coefficient and reaction rate constant are the key parameters used to determine if the reaction is mass transfer limited or chemical reaction limited. If $k''\gg k_c$ then mass transfer control the overall reaction. If $k''\ll k_c$ then mass transfer effects are not important when the reaction rate is limiting.

The mass transfer coefficient, k_c can be expressed by Thoenes-Kramers correlation

$$k_c = (1-\varepsilon_b)/\varepsilon_b *(D_{AB}*Sh''/d_p) \tag{5-8}$$

where D_{AB} = diffusivity of methane in air = 0.183 cm^2/s,

d_p = catalyst particle size = 7.5 * 10^{-3}cm,

Sh'' = Sherwood number = $Re''^{0.5}Sc^{1/3}$,

Re'' = Reynold numbers Re'' = $Udp/(1- \varepsilon_b)*v$,

U = linear velocity = 6.9 cm/s,

v = kinematics viscosity = 0.65 cm^2/s,

Sc = Schmit number, Sc = v/D_{AB}= 0.65/0.183 = 3.55,

ε_b = bed porosity = 0.25.

The mass transfer coefficient at 400 ^{o}C can be calculated as follows:

Re'' = $6.9*7.5*10^{-3}/(1-0.25)* 0.65 = 0.11$

Sh'' = $(0.11)^{0.5} * (3.55)^{1/3} = 0.51$

k_c = $(1-0.25)/0.25*(0.183/7.5*10^{-3})*3.55 = 259.86$ cm/s

The specific reaction rate at 400 ^{o}C can be calculated by Arrhenius equation where

k' = A exp (-Ea/RT)

= $7.02*10^{12}$ exp [-30.82 /(1.987 *673)]

= 687 cm^3/g-s,

Since k' = k'' * Sa, then

k'' = $687/67*10^4$ cm^2/g

= $1.03 * 10^{-3}$ cm/s.

where Sa = surface area = $67*10^4$ cm^2/g.

Consequently, for small particle size catalyst, the reaction is governed by surface reaction controls when temperature reaches 400 ^{o}C. Hence, the plots of methane conversion as a function of temperature in Figure 4.37 and 4.38 are governed by chemical reaction kinetics. If the reaction is operated by using pellet or honeycomb catalysts then the internal and external mass-transfer effects could be observed in a plot of conversion versus
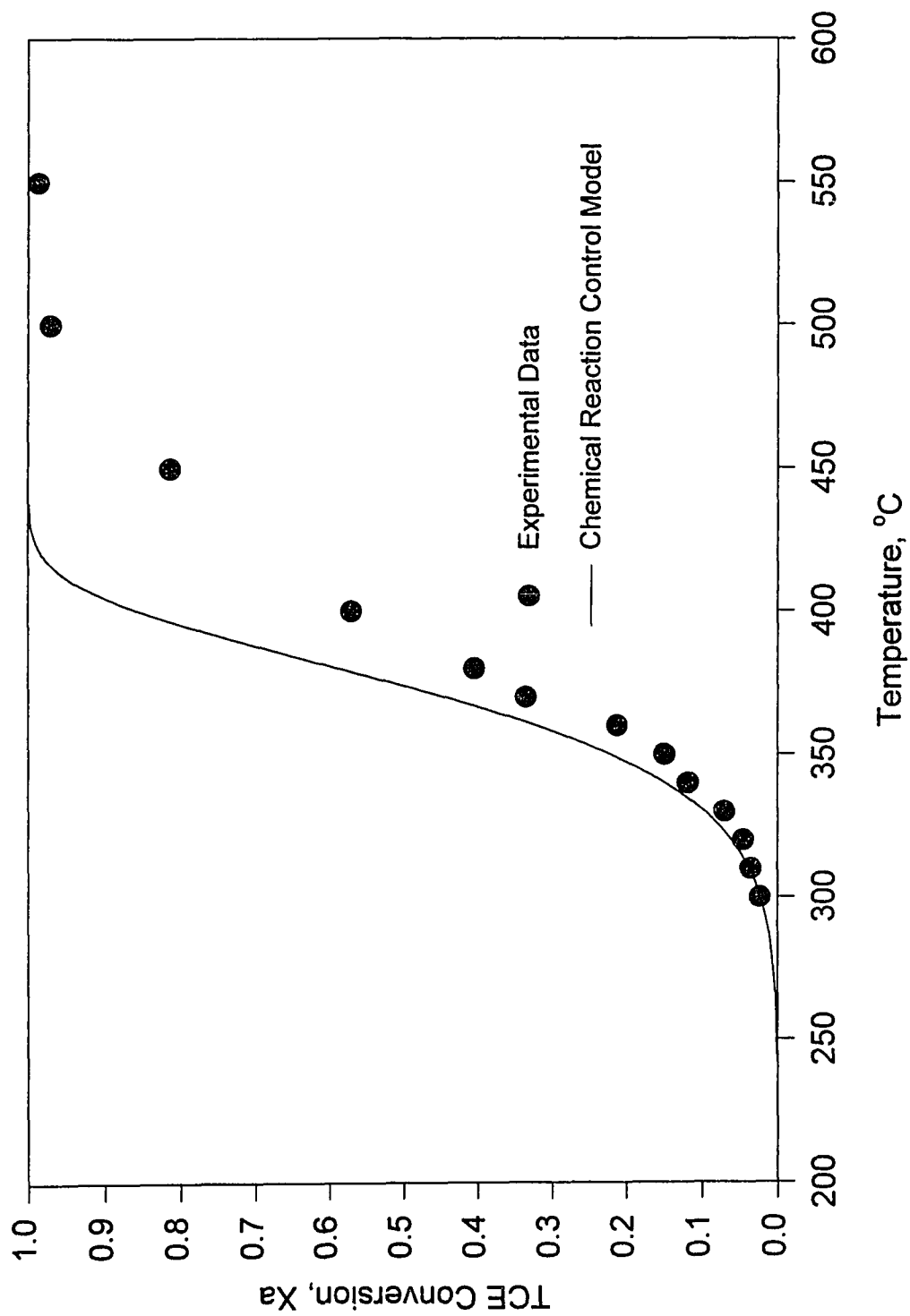
Figure 5.1 Catalytic Oxidation of TCE over 4% PdO/γ-Alumina on a Monolith as a Function of Temperature (Yu, et al., 1991)

temperature. Figure 5.1 shows such a plot of conversion versus temperature for the profile of catalytic oxidation of TCE over palladium on a monolith. The line represents the chemical reaction kinetics model. At lower conversion (<30 %), conversion follows the kinetic model. However, at higher conversion (>40 %), deviations from the kinetic model are observed. This occurs because the reaction is affected by internal and external mass transfer controls.

5.3 The Effect of Phosphorous Compounds of Catalyst Deactivation

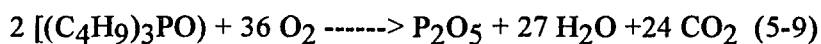#### 5.3.1 TBP and P_2O_5 Effects on Catalyst Deactivation

The results show that TBP and P_2O_5 poison PdO/γ-alumina for methane oxidation. In aging tests at 500 °C, the larger the dose of TBP, the lower the resulting methane oxidation activity. From the conversion of methane versus temperature curves, it is found that the slope of the curves in the pore diffusion regime and mass transfer regime are lower for phosphorous treated catalysts than for fresh catalysts. These results suggest that phosphorous poison deposits on the catalyst surface leading to a loss in geometric area which impacts on the mass transfer area. Also, phosphorous compounds penetrate into the pore network coating the inside of the pores, increasing pore diffusion resistance (Heck and Farrauto 1995).

The BET surface area decreases by more than 60 % in the aging with TBP test at 500 °C, when compared with fresh catalyst. These results confirm the hypothesis that the poisons which deposit on the catalyst surface cause a reduction in specific surface area. The decrease in metal chemisorption is due to the deposition of the phosphorous compounds. It is concluded that this deactivation mechanism causes non-discriminating poisoning. Heat treatment results show that catalyst activity improves, but can not be regenerated completely to fresh catalyst activity. This indicates that some portion of unburned phosphorous compound is removed by heat treatment but P_2O_5 remains on the

catalyst surface. The IR spectra results show that the remaining P_2O_5 reacted with Al_2O_3 forming $AlPO_4$.

In aging tests at 820 °C, the specific surface area of the aged catalyst has been slightly affected by the temperature, but methane oxidation activity drops to half compared to aging at 500 °C. Checking the metal chemisorption, there is no specific sintering which occurred at 820 °C. But, the IR spectra results show a strong $AlPO_4$ absorbance band at 1110 cm^{-1}. The formation of $AlPO_4$ can be assumed to occur as follows:

$$2 [(C_4H_9)_3PO) + 36 O_2 ------> P_2O_5 + 27 H_2O +24 CO_2 \quad (5\text{-}9)$$

$$P_2O_5 + Al_2O_3 ------> 2 AlPO_4 \quad (5\text{-}10)$$

It is believed that the formation of $AlPO_4$ leads to catalyst deactivation at 820 °C.

A sequence of experiments were designed to investigate the P_2O_5 effects on catalyst deactivation. The results show that P_2O_5 sticks to the catalyst surface regardless of what the metal sites or the support happens to be. It can be partially removed by heat treatment. However, some portions of P_2O_5 reacted with Al_2O_3 and forms $AlPO_4$ during the heat treatment. Similar findings were found by Miciukiewicz, et al., (1989). They reported that P_2O_5 is adsorbed on Al_2O_3 forming a monolayer and some portions of P_2O_5 react with Al_2O_3 to produce $AlPO_4$ at 500 °C. The catalyst deactivation at 820 °C is greater than that at 500 °C. These results are similar with TBP aging tests and are coincident with the assumption of reaction (5-10).

5.3.2 ZDP Effects on Catalyst Deactivation

ZDP effects on catalyst deactivation are more complicated than those with TBP, since the catalyst is deactivated not only by phosphorous compound, but also by zinc and sulfur compounds. The sulfur effects on catalyst deactivation has been discussed in Chapter 4. The formation of sulfate and sulfite groups on the catalyst surface lead to the deactivation of catalyst.

The zinc and phosphorous effects on catalyst deactivation are attributed to the poisoning compounds depositing on the surface of the catalyst. Consequently, the retention of zinc and phosphorous on the catalyst surface blocks the pore entrance and leads to the reduction of specific surface area and thus methane oxidation activity. By checking the activation energy and pre-exponential factor of both fresh and aged catalyst, it is found there is no significant change in activation energy but there is a big drops of pre-exponential factor. This indicates that the rate determining step for the catalytic oxidation of methane is the same between the fresh and aged catalyst. But, the decrease of BET surface area and metal surface area (CO chemisorption) result to a decrease in the pre-exponential factor.
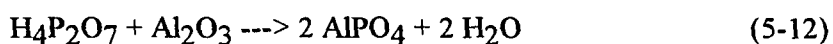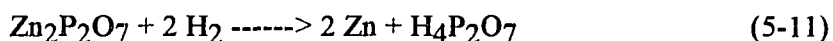
This ash like poisoning material on the catalyst surface is analyzed by FT-IR and XRD. The results suggest that a substantial part of the catalyst poisoning is due to β-zinc pyrophosphate. Similar findings were reported by Williamson, et al., (1984, 1985) and Inoue, et al., (1992). They found that the deactivation of automotive catalysts by engine oil-derived components of phosphorous and zinc occur by the formation of an amorphous zinc pyrophosphate ($Zn_2P_2O_7$) that is impervious to gas diffusion. Also, Williamson, et al., reported that the catalyst poison was derived from ZDP at low-temperatures (<450 ^{o}C) and that by increasing catalyst temperatures from 450 ^{o}C to 730 ^{o}C delayed the rate of catalyst deterioration from ZDP.

In our study, since the ZDP is ignited at 860 ^{o}C before being carried to the catalyst bed, the combustion product is identified by XRD to be β-$Zn_2P_2O_7$ which has a linear crystalline structure. Generally, neutral anhydrous pyrophosphates are thermally quite stable. When heated, however, many pyrophosphates undergo polymorphic phase changes until they melt (Bailar, 1973). Therefore, what they found is an amorphous compound simply because the temperature is below 450 ^{o}C and when heated, like in our finding, is a crystalline structure. This phase change (from amorphous to crystalline) may lead to an

increase in catalyst surface area which the reactants can easily access. This is why they reported increasing catalyst temperature delays the rate of catalyst deterioration.
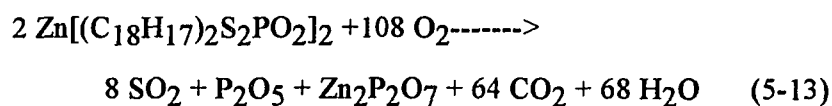
In our TGA studies, the residue of ZDP combustion products, $Zn_2P_2O_7$, is stable and not easy to remove from the catalyst surface even at temperature as high as 900 °C. Hydrogen reduction at 600 °C slightly improved catalyst activity, but does not remove $Zn_2P_2O_7$ from the catalyst surface. However, treatment at 800 °C can remove the $Zn_2P_2O_7$ but has poor catalyst activity performance and induces other compound formation which is believed to be $AlPO_4$. Similar findings were reported by Williamson, et al., (1984). They found H_2 treatment between 800 °C and 1000 °C remove Zn, P and Pb in the sample. However, treatment at the severe reductive atmosphere caused significant sintering of the catalyst.

Based on the result of H_2 treatment, the formation of $AlPO_4$ can be proposed as follows:

$$Zn_2P_2O_7 + 2\ H_2 \text{------>}\ 2\ Zn + H_4P_2O_7 \qquad (5\text{-}11)$$

$$H_4P_2O_7 + Al_2O_3 \text{--->}\ 2\ AlPO_4 + 2\ H_2O \qquad (5\text{-}12)$$

Some part of $H_4P_2O_7$ is vaporized and desorbs from the catalyst surface since the melting point is 67 °C and some parts of $H_4P_2O_7$ reacts with Al_2O_3 to produce $AlPO_4$. Therefore, the broad peak shown in Figure 4.62 is believed the desorption of $H_4P_2O_7$.

From the above results and the literature reviews, the complete combustion reaction of ZDP follows reaction (5-13):

$$2\ Zn[(C_{18}H_{17})_2S_2PO_2]_2 + 108\ O_2 \text{------>}$$

$$8\ SO_2 + P_2O_5 + Zn_2P_2O_7 + 64\ CO_2 + 68\ H_2O \qquad (5\text{-}13)$$

Therefore, the catalyst is not only deactivated by $Zn_2P_2O_7$ deposited on the catalyst surface, but may also be affected by SO_2 and P_2O_5. However, the major finding on the catalyst surface is $\beta\text{-}Zn_2P_2O_7$ which is consistent with the data from Williamson, et al., (1985) and Inoue, et al., (1992). Also, sulfur and P_2O_5 effects were individually

investigated in this study. The effect of these compounds are believed to be the key reasons for catalyst deactivation.

5.3.3 Comparisons of TBP and ZDP Effects on Catalyst Deactivation

The comparison of TBP and ZDP effects on catalyst deactivation are listed in Table 5.1. The ZDP effect on catalyst deactivation is more detrimental than the TBP effect. This is due to the sulfur content of the ZDP compound. When burned, it produces oxides of sulfur which add another poison mechanism. However, in the mass transfer control regime, zinc and phosphorous compounds were found to be the predominant catalyst deactivators.

Table 5.1 The Comparison of TBP and ZDP Effects on Methane Oxidation Conversion, BET Surface area, CO Chemisorption

Simulated-aged Mileage, miles	Methane oxidation conversion, %	CO Chemisorption, c.c./g	BET surface area, m^2/g
Fresh catalyst	95.2	0.63	103
Fresh catalyst[1]	96.0	0.62	107
Fresh catalyst[2]	93.4	0.60	102
6,000, TBP/500 °C	76.7	0.52	58
120,000, TBP/500 °C	66.0	0.30	37
120,000, TBP/820 °C	30.0	0.32	41
60,000, ZDP/500 °C	54.0	0.40	56
120,000, ZDP/500 °C	41.9	0.19	35
120,000, ZDP/820 °C	34.0	0.31	39

1. Fresh catalyst treated with air at 500 °C for 6 hours
2. Fresh catalyst treated with air at 820 °C for 6 hours

The chemisorption of CO on the catalyst aged with ZDP is lower than the catalyst aged with TBP at 500 °C. This is due to the sulfur effect on catalyst deactivation. However, in the 120,000 pulsator-aged simulated miles, temperature gives a different deactivation mechanism. In TBP aged test, the BET surface area is regenerated from 37 to

41 m^2/g and the CO chemisorption is regenerated from 0.30 to 0.32 cm^3/g but methane oxidation activity drops by half. This is due to the formation of $AlPO_4$ which deactivates the catalyst. Similarly, in the ZDP aging tests, although the BET surface area and CO chemisorption are regenerated, the methane oxidation activity has also dropped from 41.9 to 34 %. This effect is more sensitive in the TBP aged test because all of TBP is converted to P_2O_5, and reacts with Al_2O_3 to produce $AlPO_4$. Also, no other poison interferes with the diagnostic reaction of methane oxidation. In the ZDP aged test, sulfur, zinc pyrophosphate and P_2O_5 reduce catalyst activity and also interfere with methane oxidation activity. Therefore, this effect is not sensitive to the ZDP aging.

CHAPTER 6

CONCLUSIONS

The effects of chlorine, sulfur and phosphorous compounds on palladium supported on γ-alumina catalyst have been investigated. All of these compounds caused catalyst deactivation as measured by the diagnostic reaction of methane oxidation over palladium catalyst. From the experimental results it can be concluded that:

The catalyst is poisoned by HCl due to the reaction of PdO with HCl. At 500 ^oC aging temperature, the catalyst loses its activity due to the volatilization of $PdCl_2$. At 300 ^oC, the catalyst is reversibly poisoned by HCl since $PdCl_2$ formed does not volatilize at this temperature and $PdCl_2$ can be regenerated by H_2 treatment. HCl has a strong effect on metal surface area (dispersion) but no significant effect on BET surface area. The addition of water vapor can retard the rate of catalyst deactivation and is believed to prevent HCl from adsorption on the catalyst surface.

The poisoning effect of H_2S on methane oxidation over palladium catalyst is due to the reaction of PdO with H_2S, SO_2 and SO_3. At low temperature (200 ^oC), H_2S is first adsorbed by PdO forming Pd---SH_2 and is further oxidized by O_2 to form SO_2 and SO_3 which can react with Al_2O_3 forming aluminum sulfate. However, the reaction rate at low temperature is so slow that only a small amount of surface sulfite and sulfate group can be identified by FT-IR. At high temperature (400 ^oC), the rate of formation of surface sulfite and sulfate groups as determined by FT-IR spectra is much larger. Due to the formation of aluminum sulfate, the BET surface area decreases as well as metal dispersion. The major deactivation mechanism can be attributed to active site poisoning induced by the formation of surface sulfite and sulfate group and causing an increased pore diffusion resistance. Temperature programmed reduction of H_2 from room temperature to 600 ^oC can remove the surface sulfite and sulfate groups from catalyst surface and rejuvenate the

catalyst activity. In the kinetic study of methane oxidation over palladium catalysts, methane oxidation can be described by a pseudo first order reaction under excess oxidation conditions. The deactivation of methane oxidation can be described as a first order deactivation rate law in presence of 80 ppm H_2S in the feedstream. In the H_2S poisoning test at 400 ^{o}C, the decreases of activation energy suggest that the formation of $Al_2(SO_4)_3$ which transfers the reaction from surface reaction control to pore diffusion control reaction.

The TBP poisoning effect on methane oxidation over palladium catalyst is due to the unburned phosphorous compounds and the combustion product, P_2O_5. The higher dose of TBP gives the lower catalyst activity for methane oxidation. The aging temperature at 820 ^{o}C has greater deactivation than 500 ^{o}C. The decrease of BET surface area is a result of fouling by phosphorous compounds which lead to the catalyst deactivation. The formation of $AlPO_4$ on the surface of the catalyst induces another deactivation mechanism when catalyst is aged at 820 ^{o}C. Thermal treatment of the 500 ^{o}C aged catalyst with air at 650 ^{o}C can partially recover catalyst activity. It is believed that some unburned phosphorous residues are removed during the thermal treatment.

The P_2O_5 effect on methane oxidation over palladium catalyst are believed due to surface coverage of a glass-like P_2O_5 which deactivates the catalyst for methane oxidation. The higher doses of P_2O_5 leads to the lower methane oxidation activity. Thermal gravimetric analysis shows that P_2O_5 can be partially removed by thermal treatment. However, most of the P_2O_5 remain on the catalyst surface. The presence $AlPO_4$ is identified by FT-IR on the surface of catalyst aged at 500°C and 820 ^{o}C. The catalyst aged at 820 ^{o}C produces more $AlPO_4$ than is found at 500 ^{o}C. Consistently, the catalyst aged at 820 ^{o}C has less activity than 500 ^{o}C.

The ZDP effect on methane oxidation over palladium catalyst is due to the retention of zinc and phosphorous on the catalyst surface and leads to deactivation of the catalyst. ZDP has a stronger effect on methane oxidation than it has for CO and propane

oxidation. The higher dose of ZDP in the experimental test leads to lower catalyst activity for methane oxidation. The major combustion product on the surface of catalyst is β-$Zn_2P_2O_7$ which is identified by XRD. The major deactivation mechanism is believed due to the deposition of β-$Zn_2P_2O_7$ on the catalyst surface which covers the catalyst surface area and reduces the geometric surface area, which leads to the catalyst deactivation. The estimation of activation energy and pre-exponential factor for fresh catalyst and ZDP aged catalyst shows that the loss of BET surface area is responsible for the decreases of pre-exponential factor but no effects on activation energy. The deactivation at 820 $^{\circ}$C is greater than at 500 $^{\circ}$C. Thermal treatment of the 500 $^{\circ}$C aged catalyst can partially improve the catalyst activity. However, the thermal gravimetric analysis shows that the residue on the catalyst surface can not be removed at 900 $^{\circ}$C. H_2 treatment at 600 $^{\circ}$C can slightly improve catalyst activity, but can not remove the $Zn_2P_2O_7$. However, H_2 treatment at 800 $^{\circ}$C can remove the $Zn_2P_2O_7$ from catalyst surface, but do not improve catalyst activity performance. This may be due to sintering of palladium in the severe reductive atmosphere and the formation of $AlPO_4$. These results confirm that it is desirable to have low phosphorous content engine oil in order to prevent catalyst deactivation.

APPENDIX A

FIGURES FOR CHAPTER 3
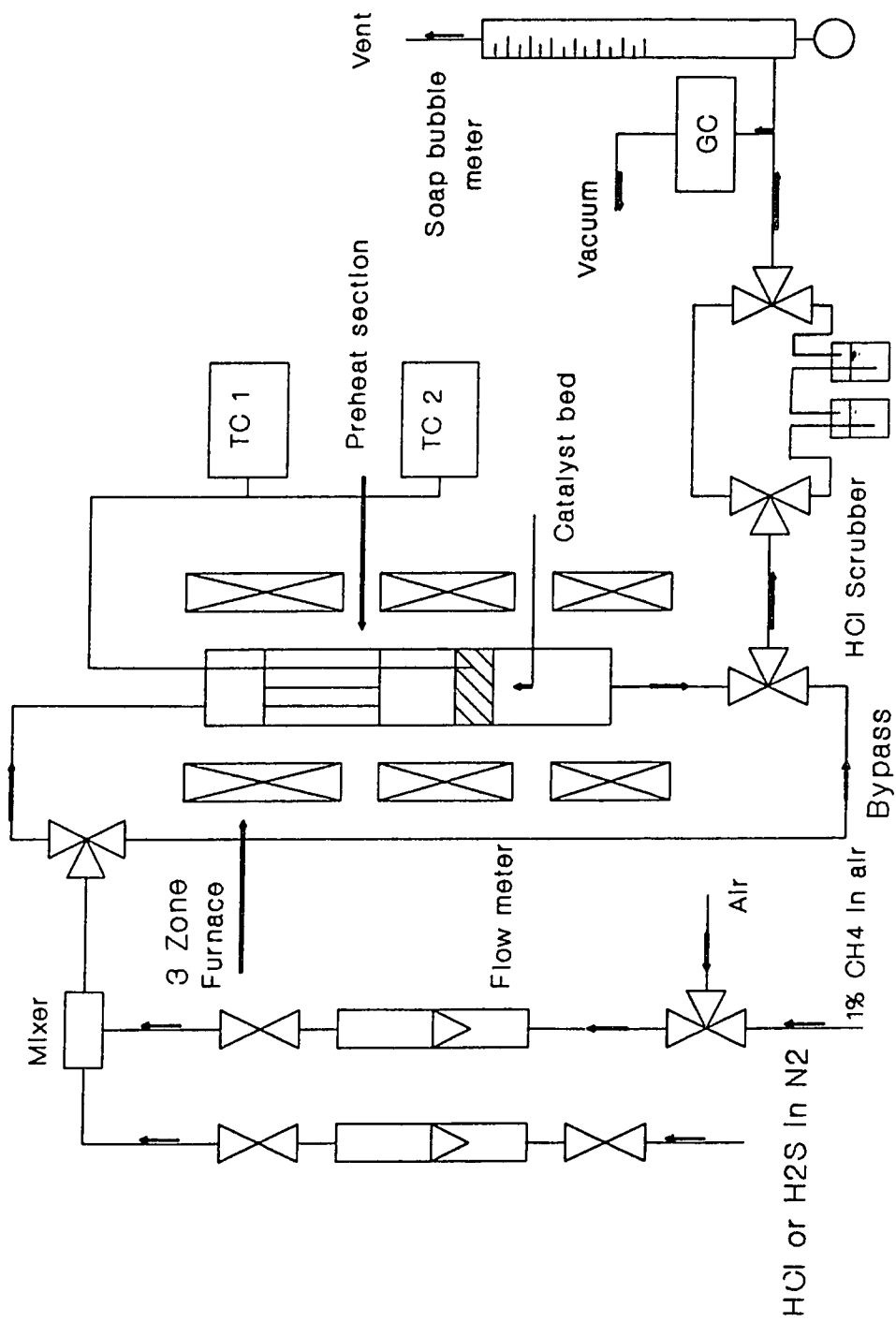
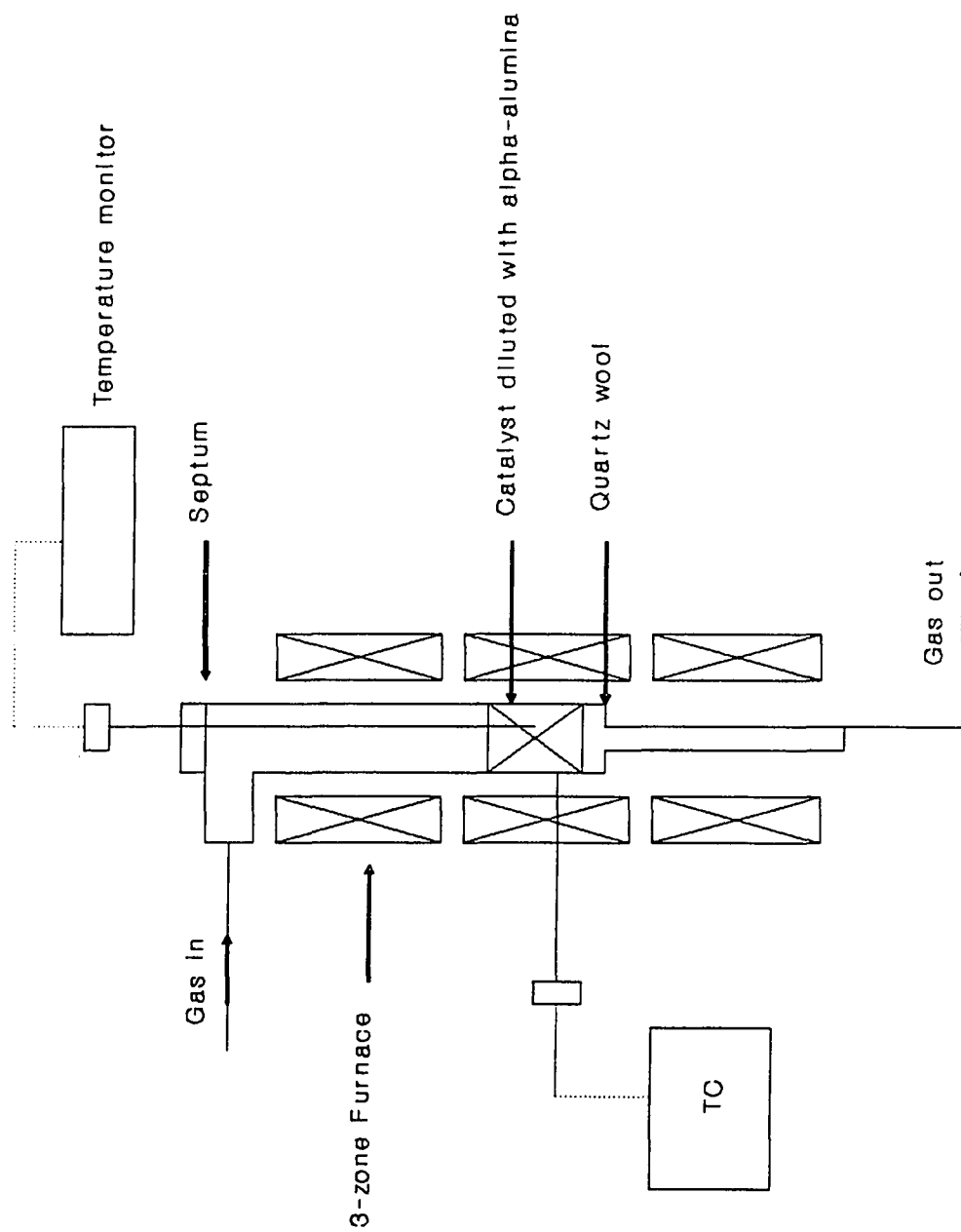**Figure 3.1 Experimental Flow Schematic Diagram.**
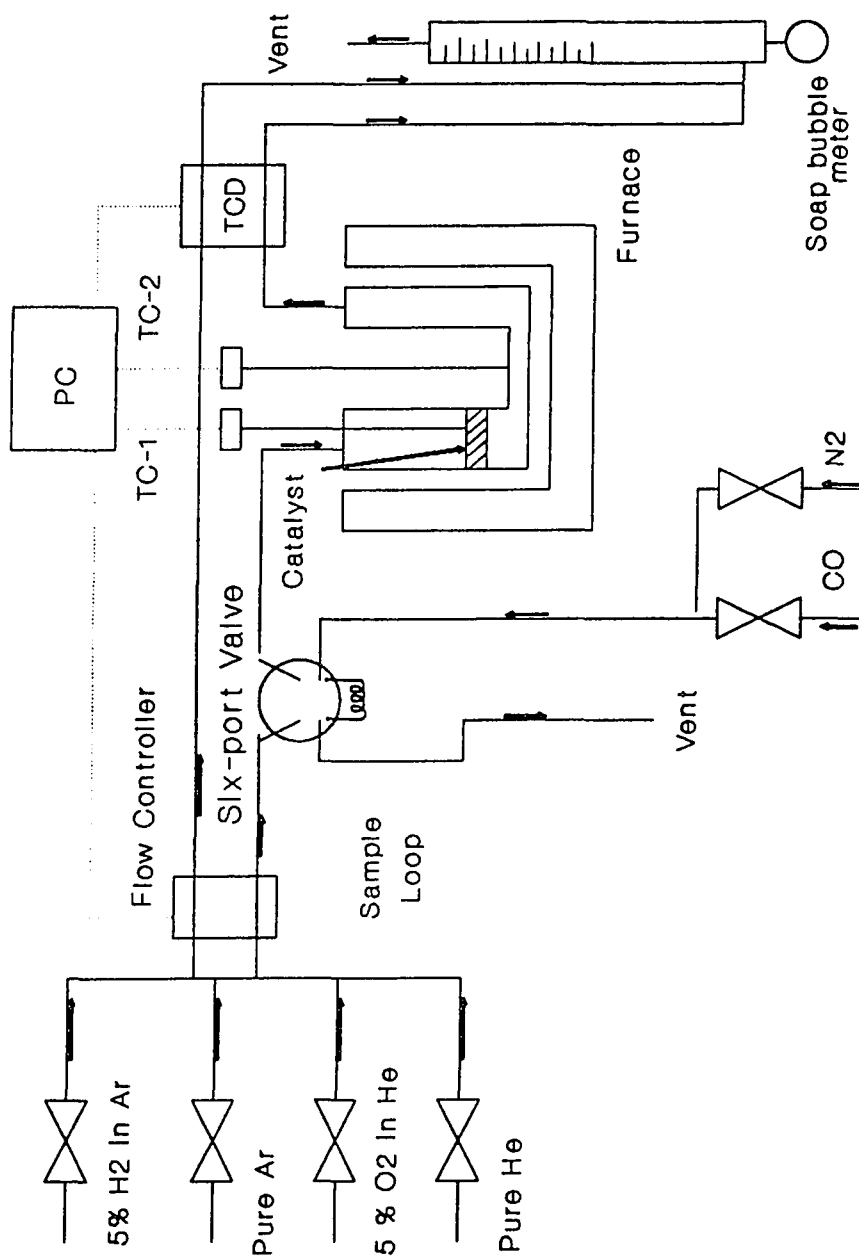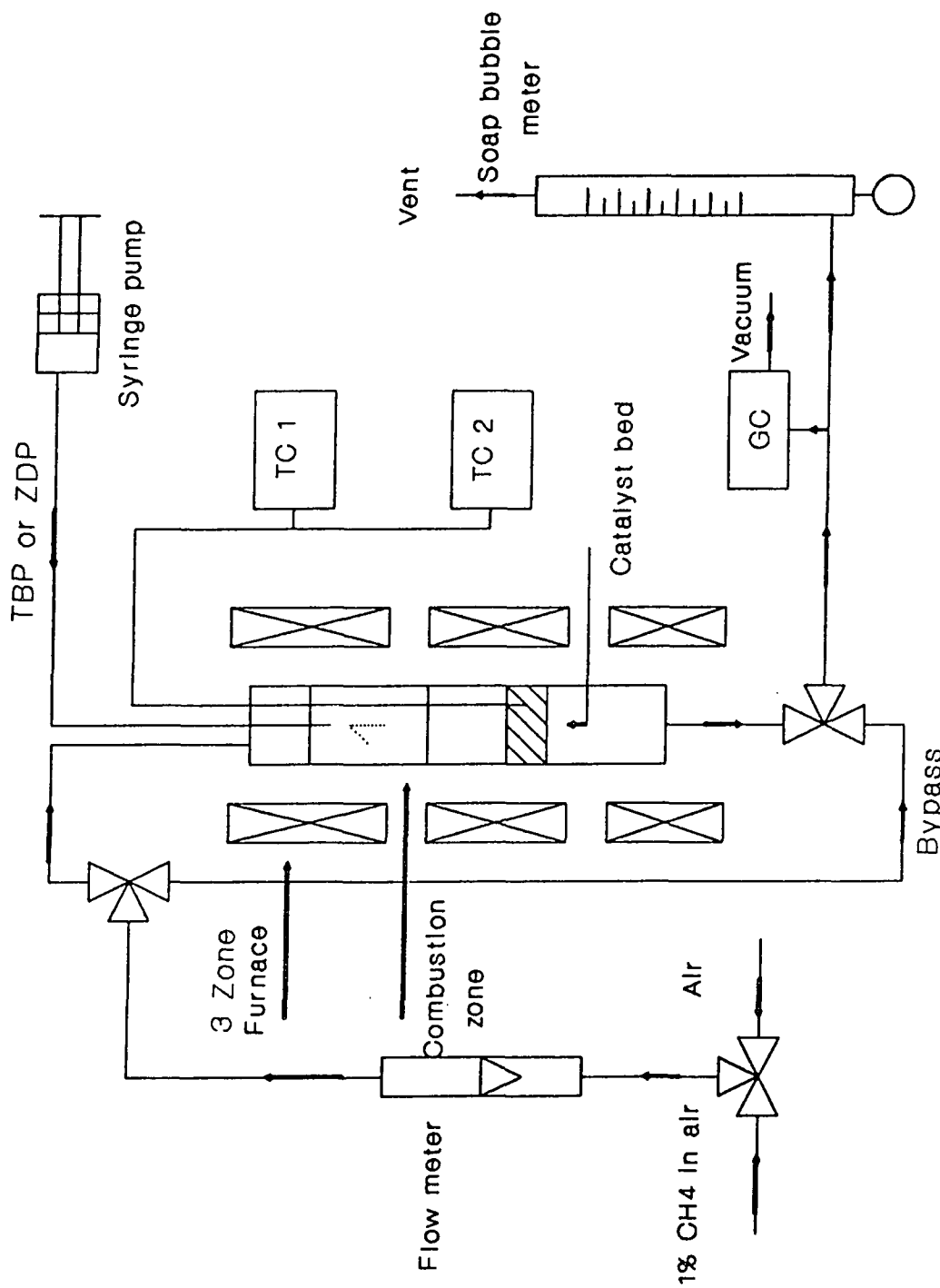
Figure 3.2 Diagnostic Activity Test Reactor.

Figure 3.3 Flow Schematic Diagram of Altamira Instruments for TPR and Pulse Chemisorption.

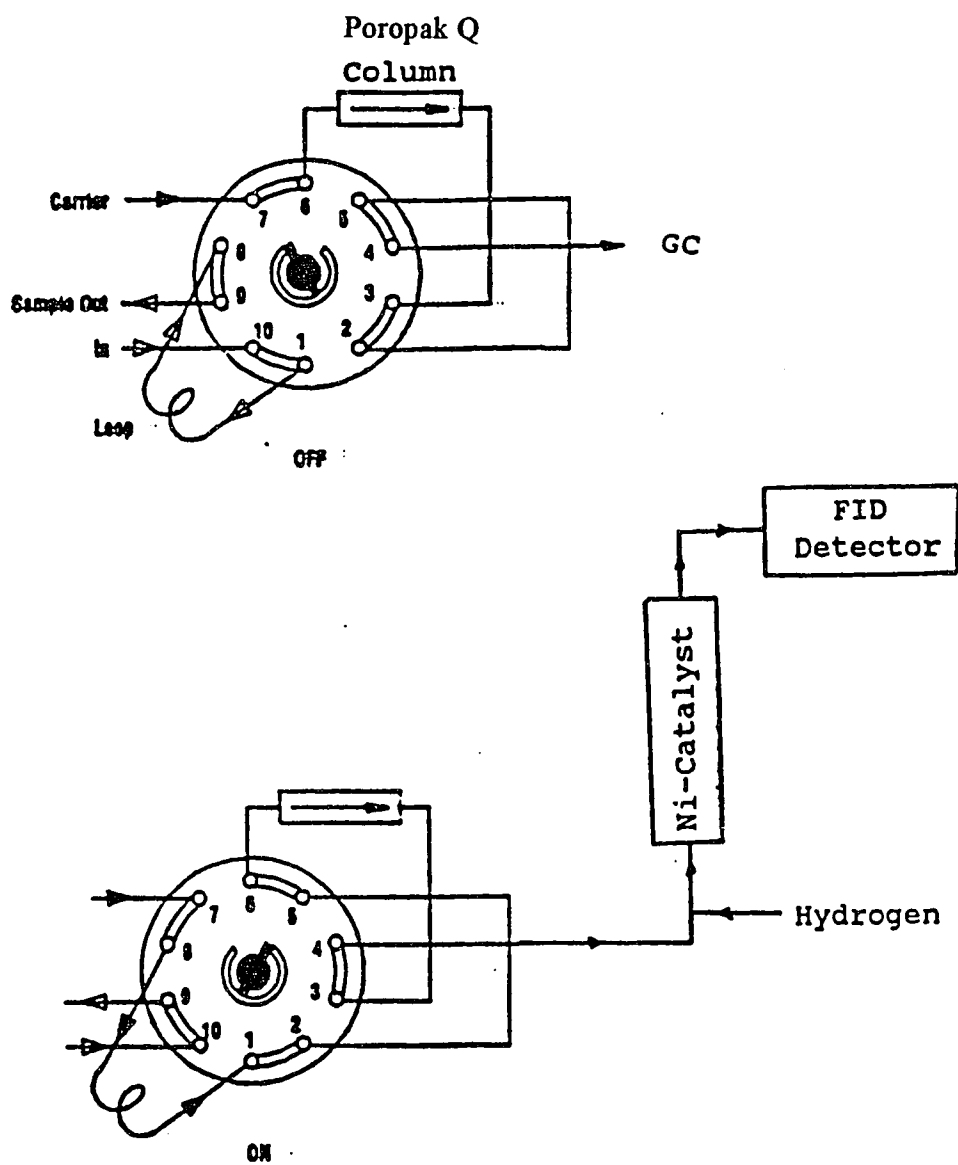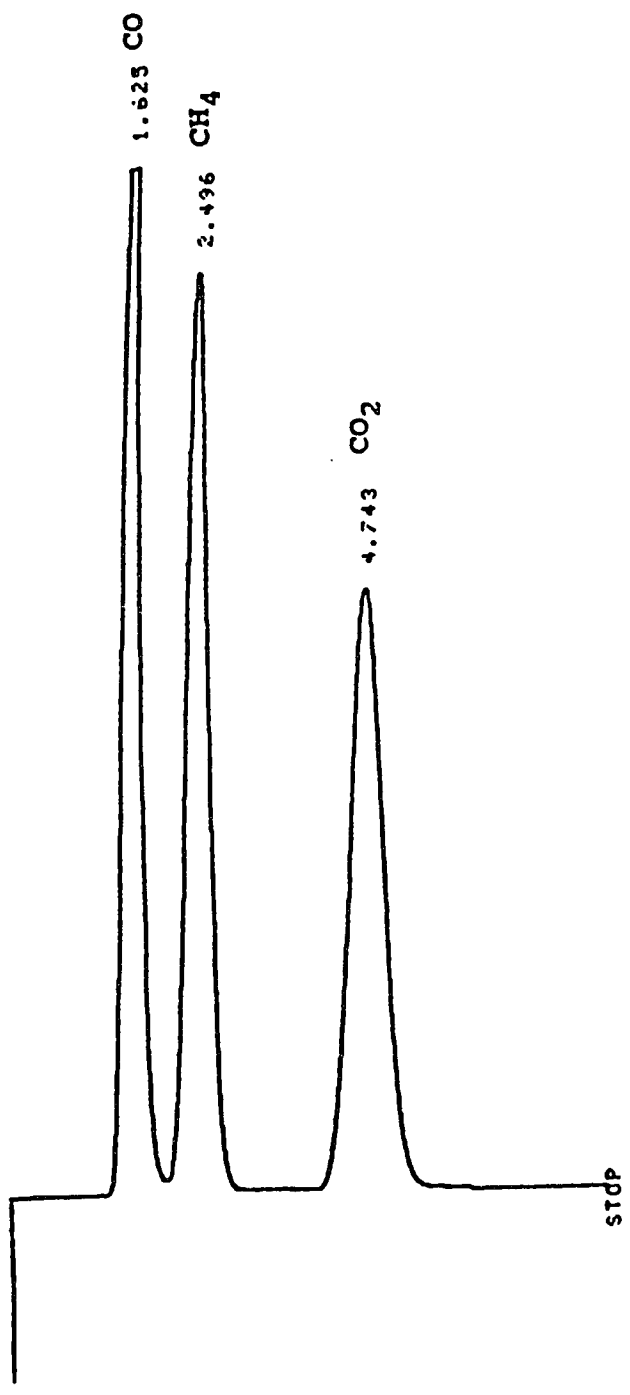**Figure 3.4** Experimental Pulse-flame Flow Schematic Diagram.

Poropak Q

Column

Carrier

GC

Sample Out

In

Loop

OFF

FID
Detector

Ni-Catalyst

Hydrogen

ON

Figure 3.5 Nickle Hydrogenation Catalyst System.

Figure 3.6 Typical Peak Resolution and Retention Time for CO, CO_2 and CH_4 with Poropak Q Column and FID.

START

H₂S

1.415

TIMETABLE STOP

SO₂
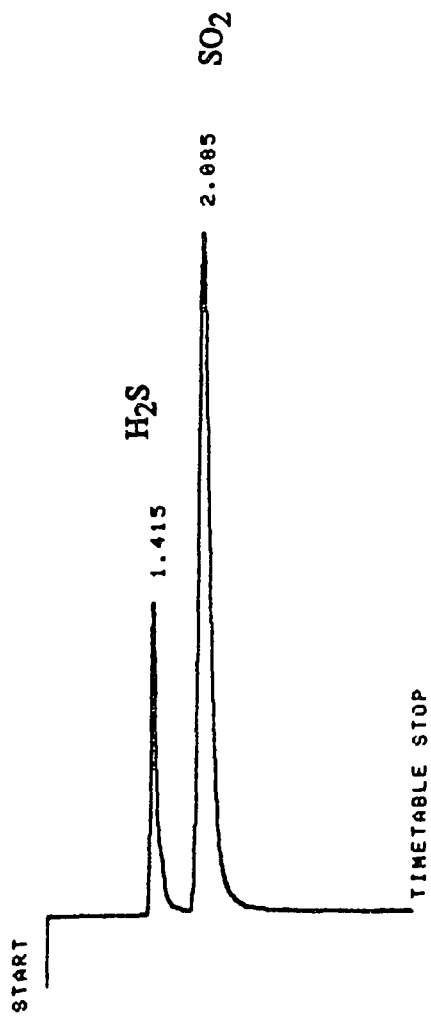
2.085

RUN# 27   JAN   7, 1981   03:46:29

AREA%

RT   AREA   TYPE   WIDTH   AREA%
1.415   6317818   BB   .089   18.39378
2.085   28026208   BB   .182   81.60624

TOTAL AREA=3.4343E+07
MUL FACTOR=1.0000E+00

Figure 3.7 Typical Peak Resolution and Retention Time for H₂S and SO₂ with Poropak Q Column and FPD.
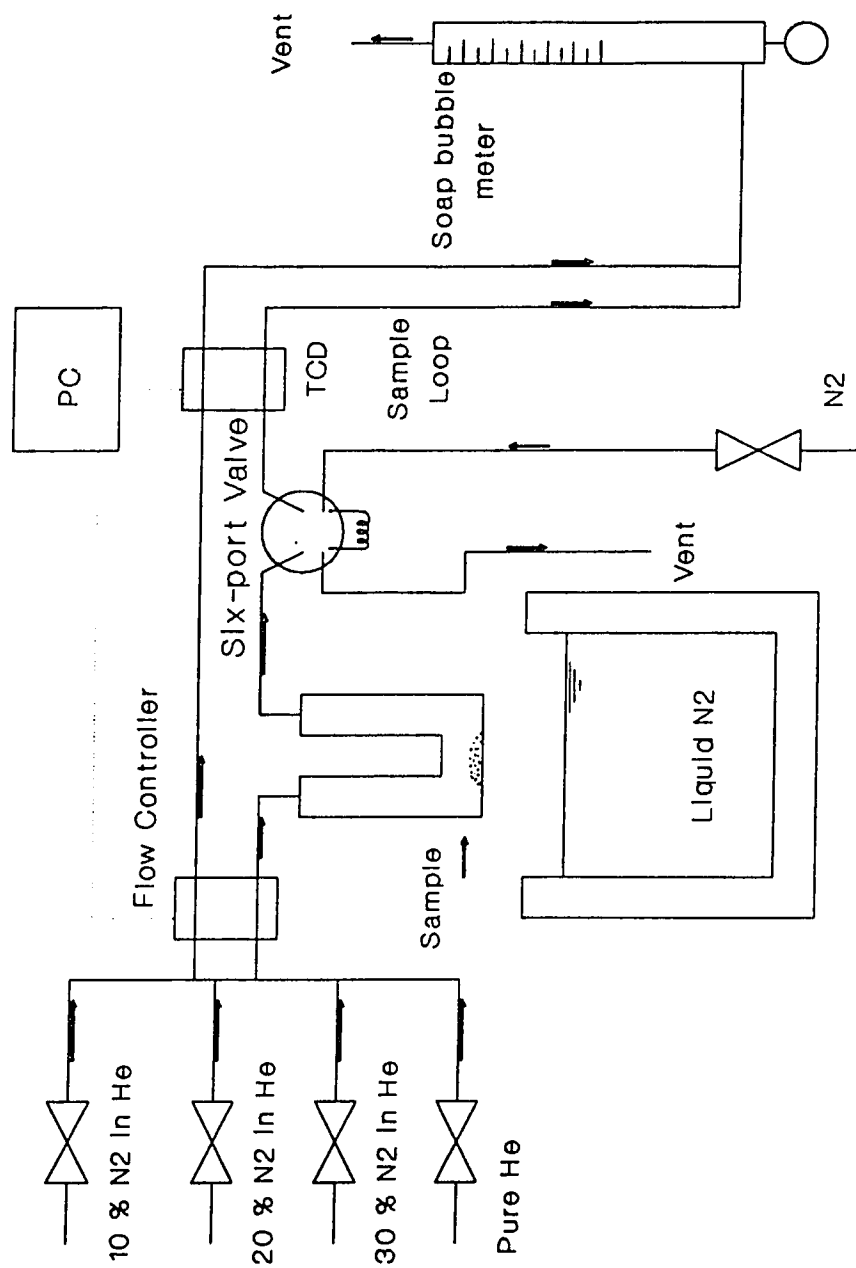
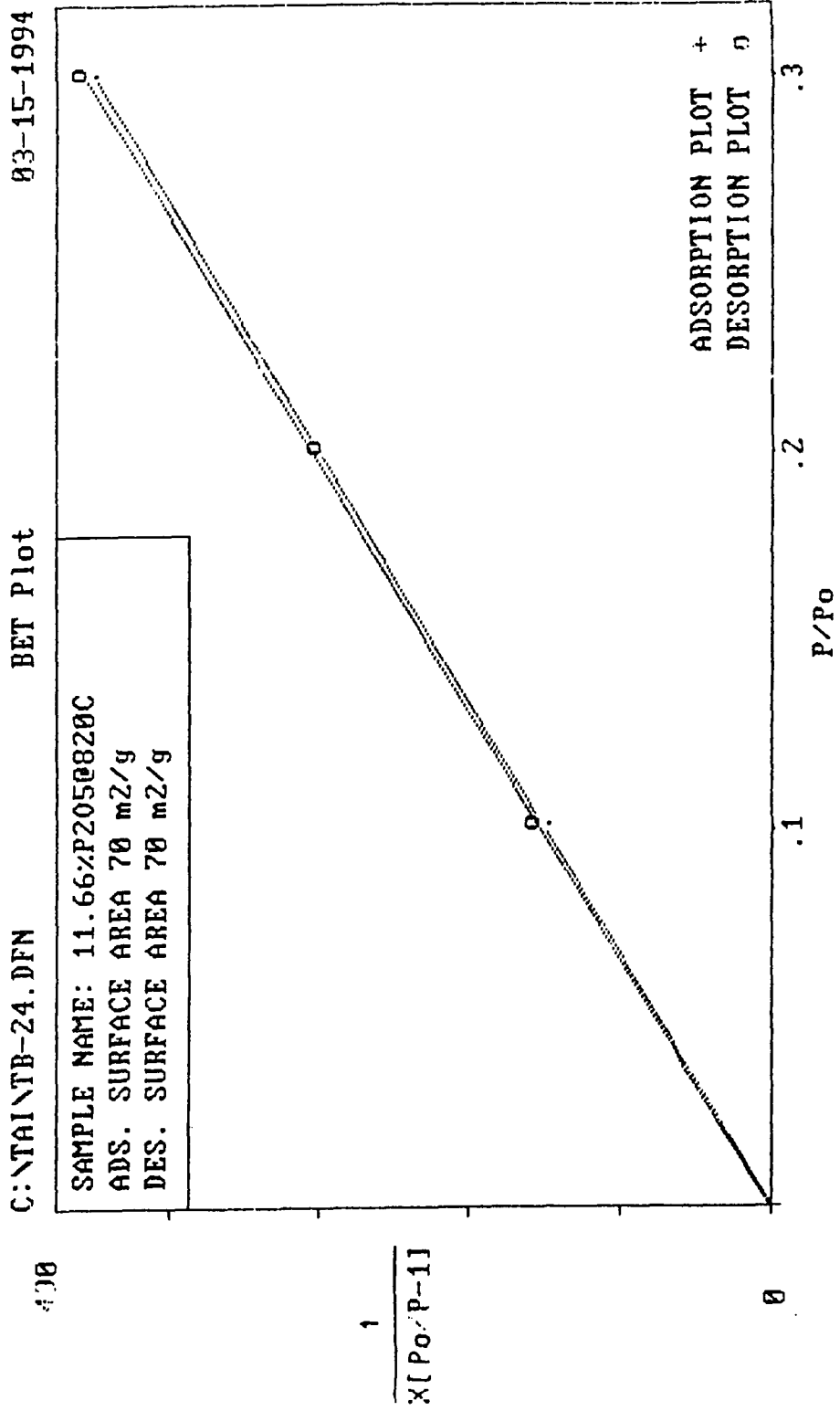**Figure 3.8** Flow Schematic Diagram of Altamira Instruments for BET Surface Area Measurements.
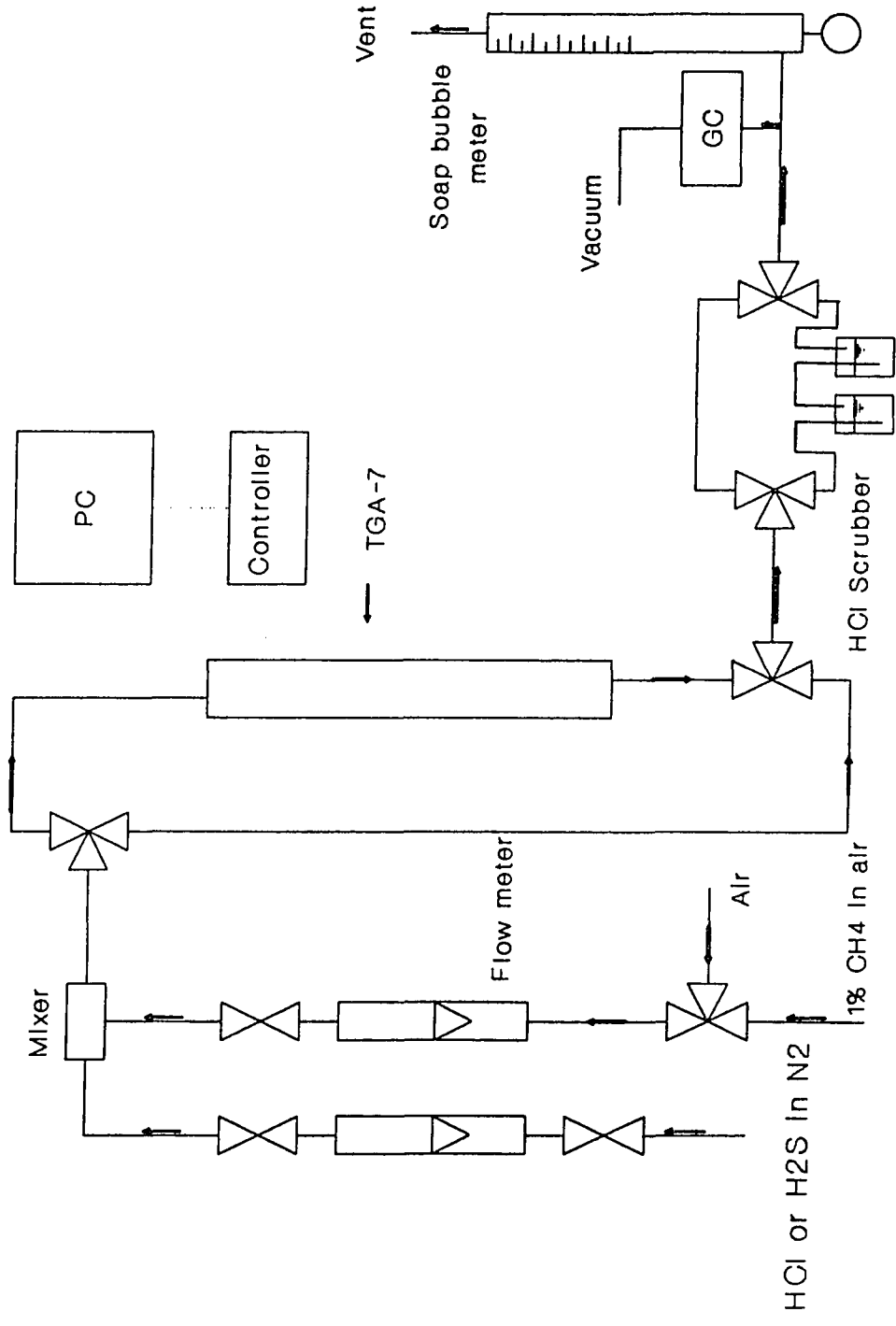
Figure 3.9 Typical Plots of BET Surface Area Measurements.

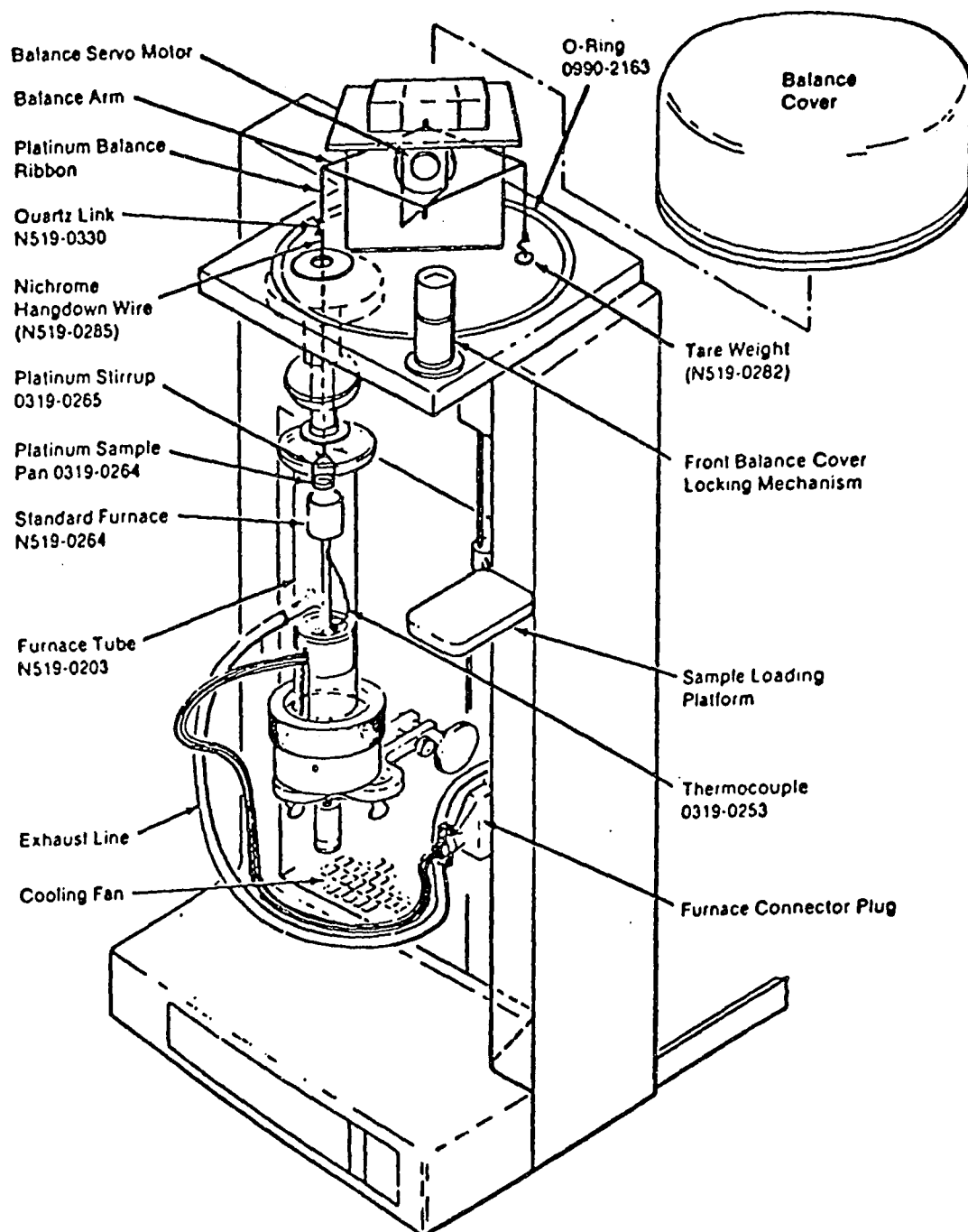**Figure 3.10** Flow Schematic Diagram of Thermal Gravimetric Analyzer.

Balance Servo Motor

Balance Arm

Platinum Balance
Ribbon

Quartz Link
N519-0330

Nichrome
Hangdown Wire
(N519-0285)

Platinum Stirrup
0319-0265

Platinum Sample
Pan 0319-0264

Standard Furnace
N519-0264

Furnace Tube
N519-0203

Exhaust Line

Cooling Fan

O-Ring
0990-2163

Balance
Cover

Tare Weight
(N519-0282)

Front Balance Cover
Locking Mechanism

Sample Loading
Platform

Thermocouple
0319-0253

Furnace Connector Plug

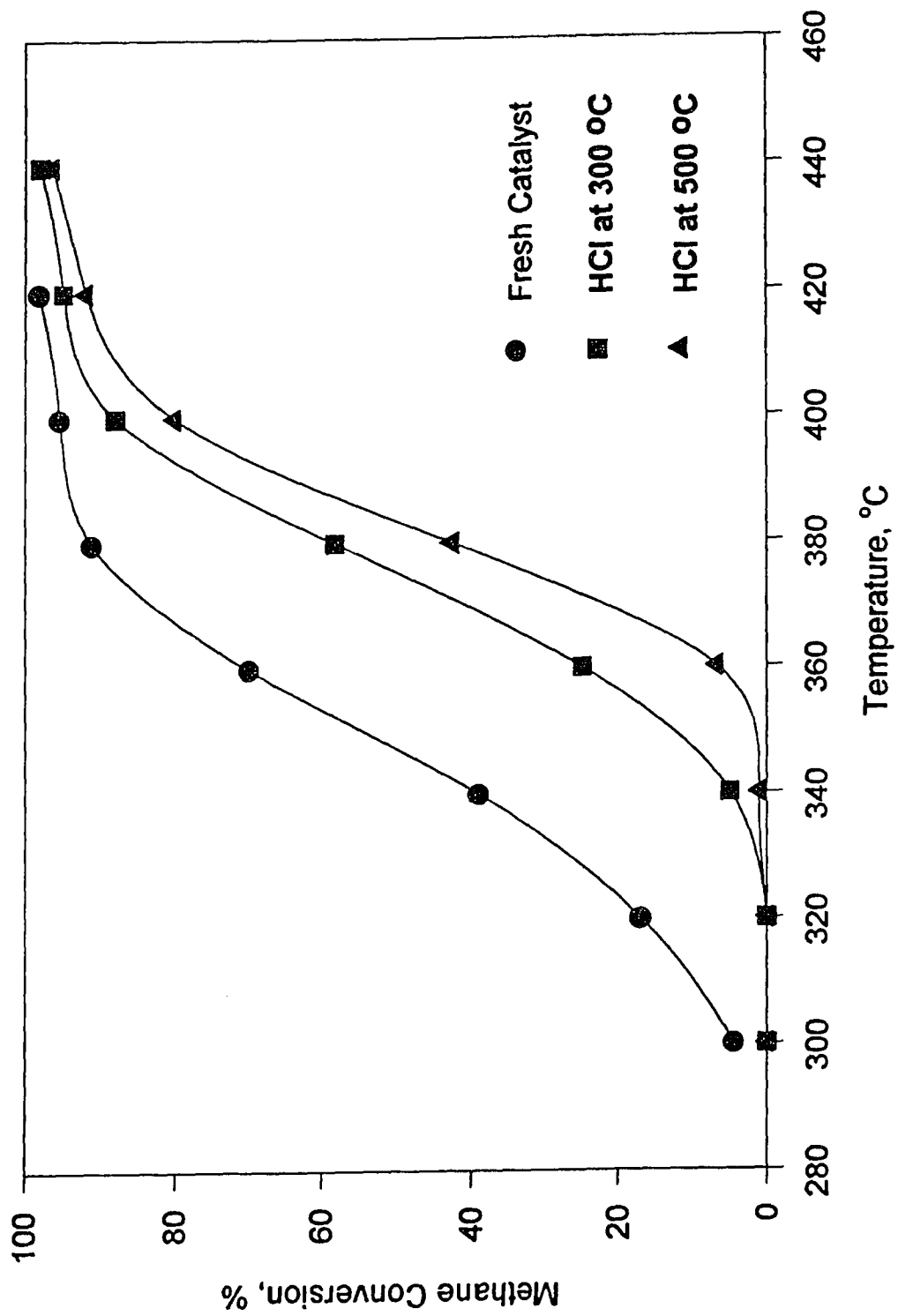**Figure 3.11** Schematic of TGA Unit.

APPENDIX B

FIGURES FOR CHAPTER 4

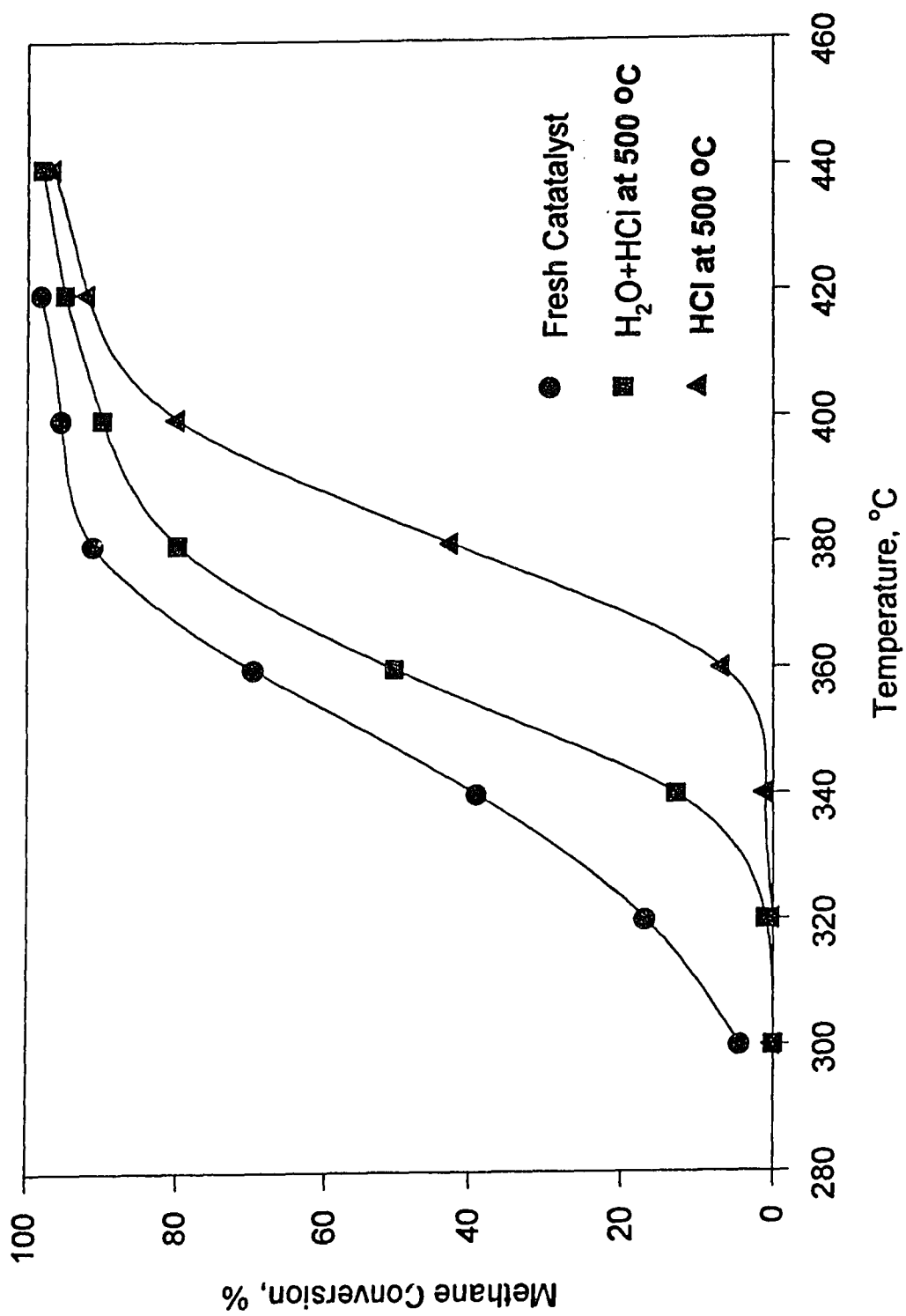Figure 4.1 Temperature and HCl Effects on Methane Oxidation over 4% PdO/γ-Alumina Catalyst

Figure 4.2 Water Vapor and HCl Effects on Methane Oxidation over 4% PdO/γ-Alumina Catalyst
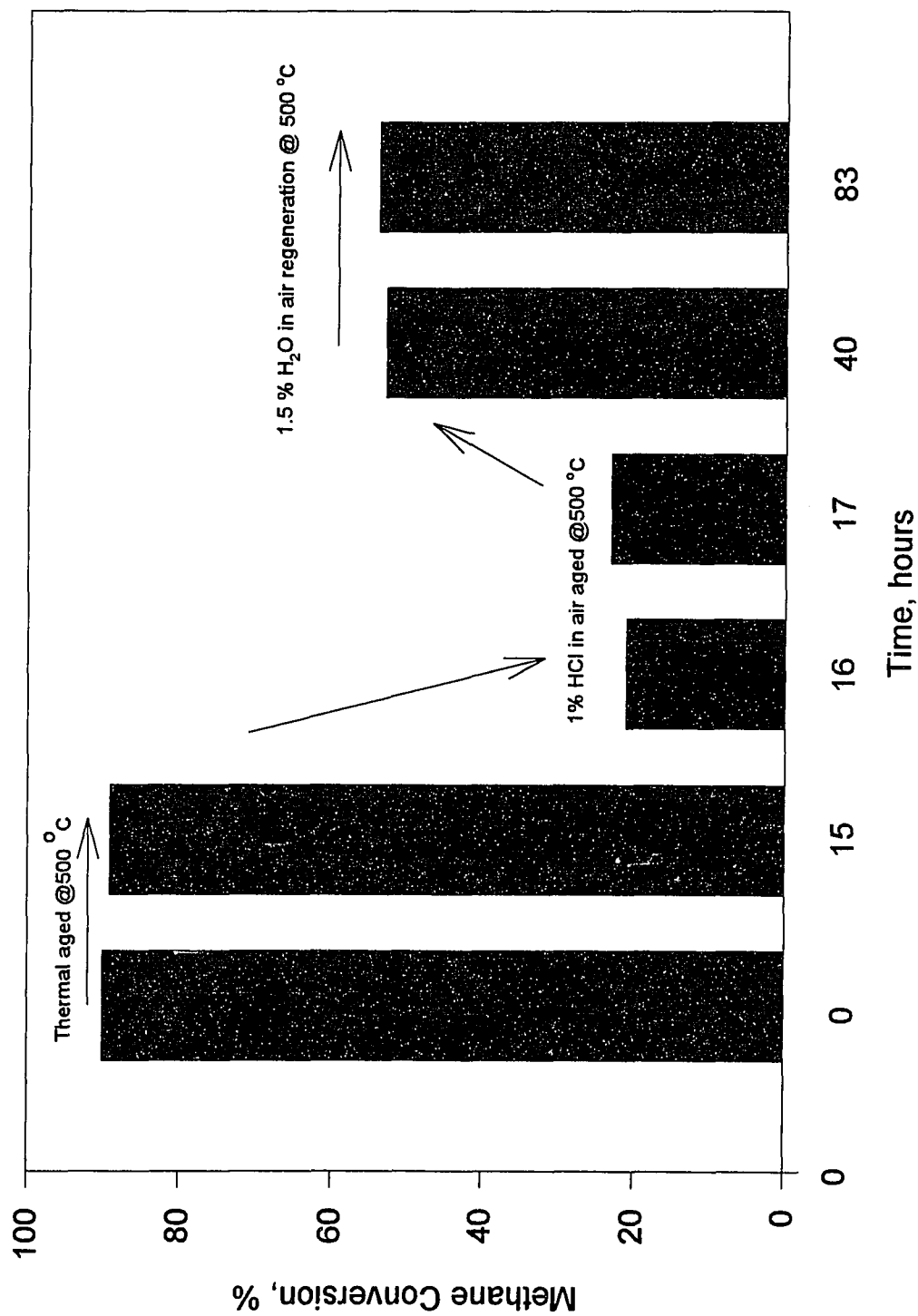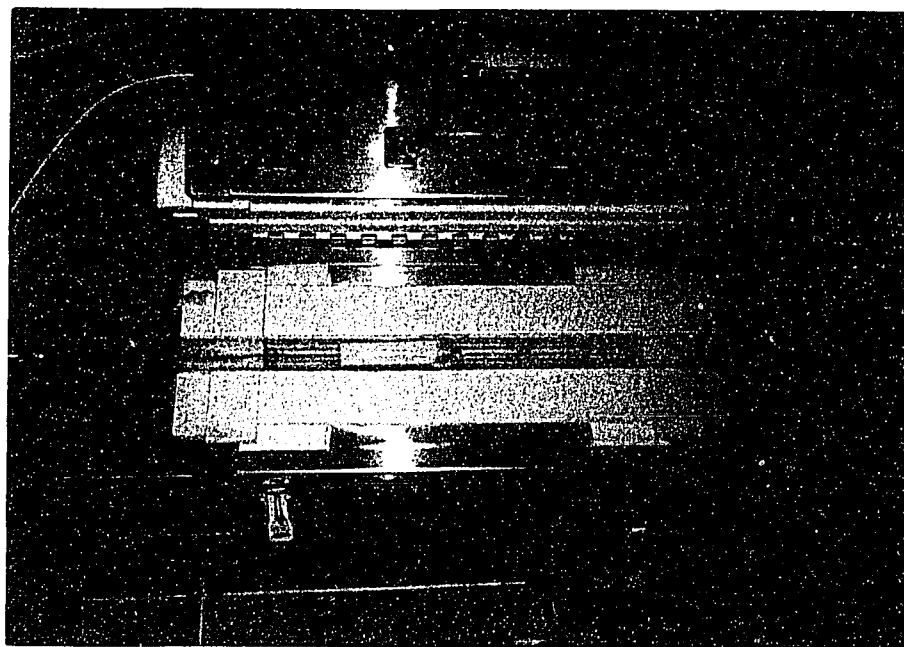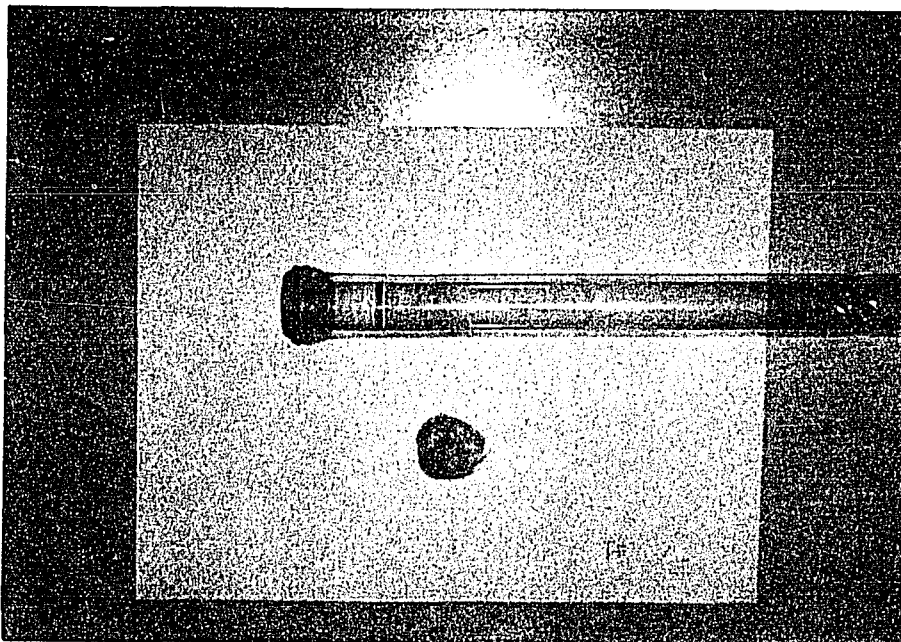
Figure 4.3 Water Effect on Regeneration of Catalyst Aged by HCl at 500 °C.
Methane oxidation activity was tested at space velocity 88,000 v/v/hr, 377 °C

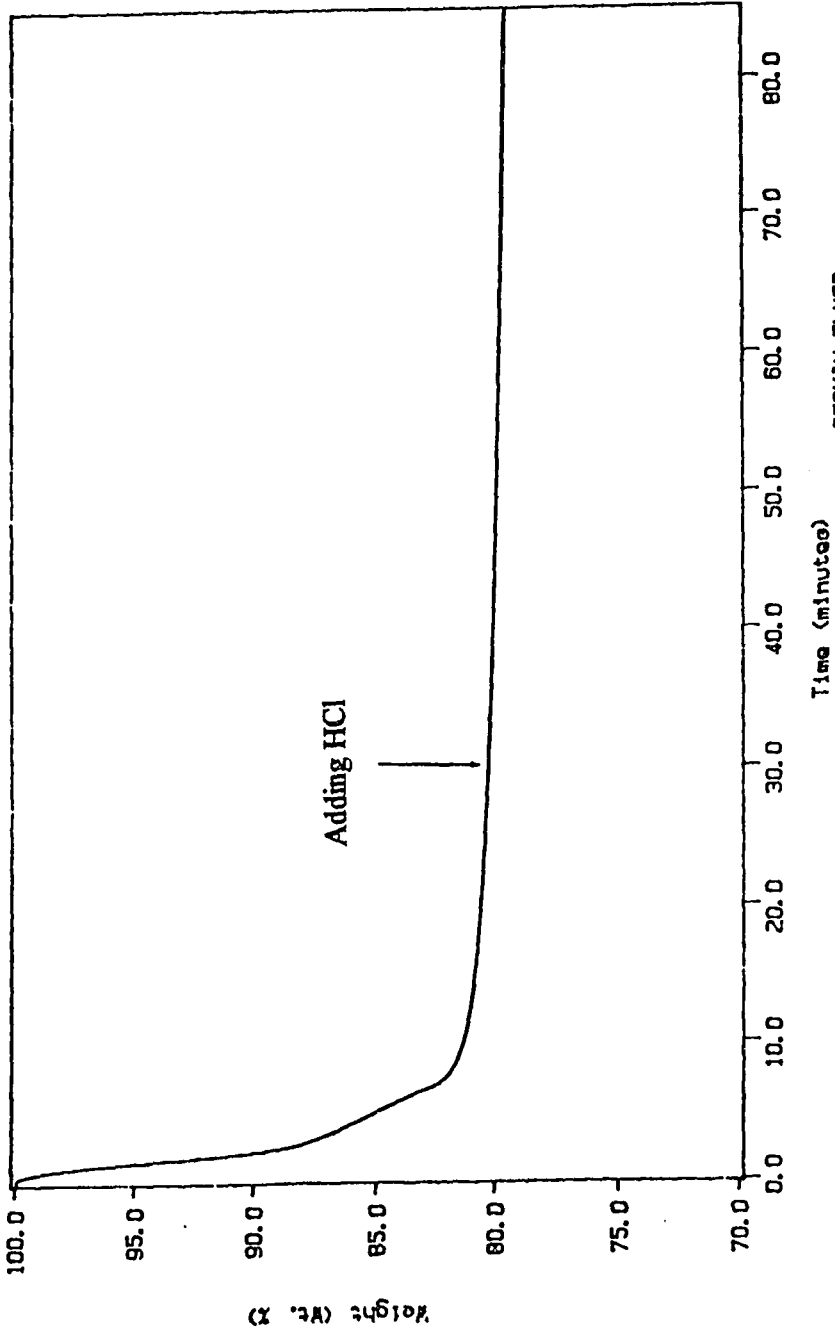**Figure 4.5** Photograph of the Reactor and Quartz Wool After the Completion of the Catalyst Aging Test with HCl at 500 ºC.

Figure 4.4 Photograph of the Reactor was Taken After the Completion of the Catalyst Aging Test with HCl at 500 ºC.

Figure 4.6 Weight Change of Pure γ-Alumina Due to the Flow of 300 ppm HCl in Air at 300 °C for 30 Minutes.

Curve 1: TGA
File Info: yu047   Fri Jun 18 17:46:09 1993
Sample Weight: 3.488   mg
2% PdO/Al2O3 300 ppm HCl 830C C
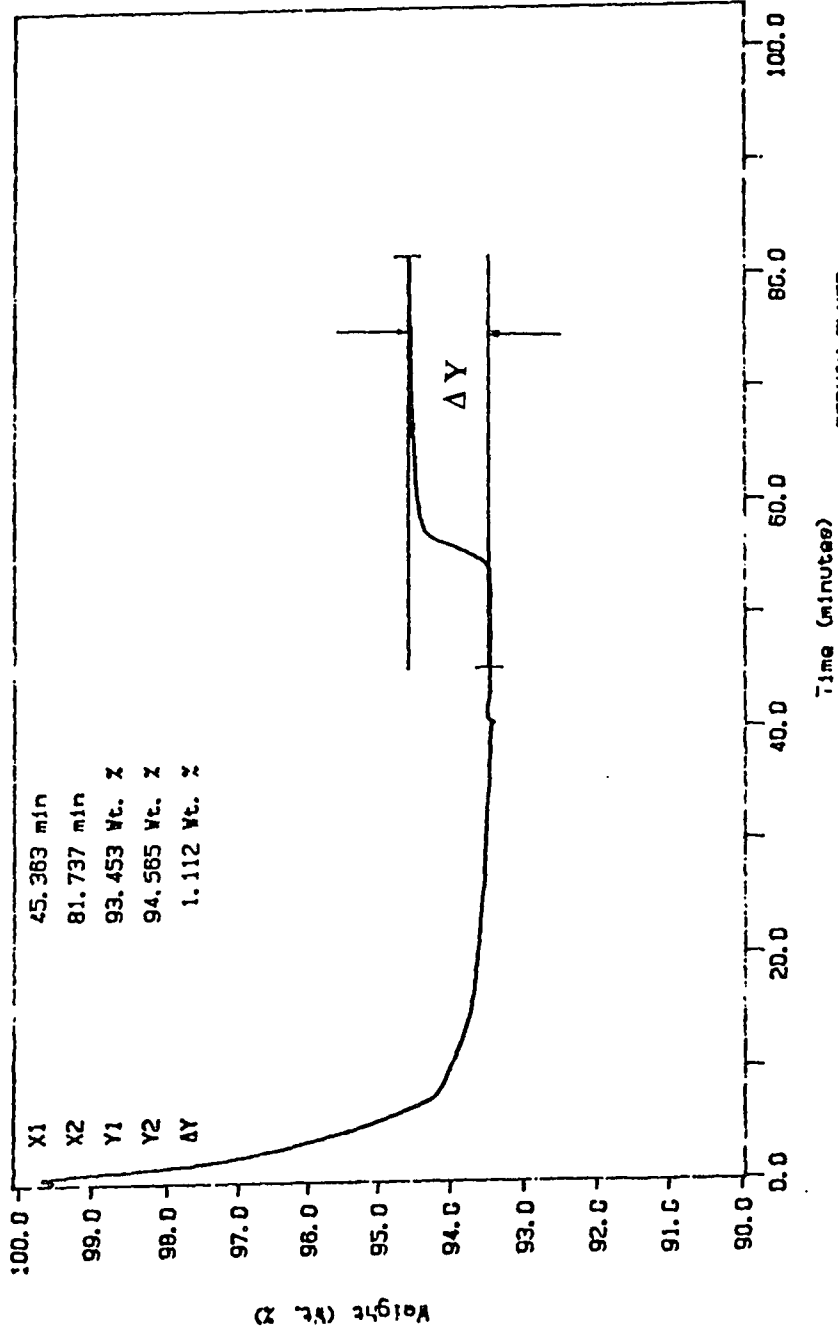
X1	52.200 min	
X2	78.500 min	
Y1	93.949 Wt. %	
Y2	94.708 Wt. %	
ΔY	0.758 Wt. %	

Figure 4.7 Weight Change of 2% PdO/γ-Alumina Due to the Flow of 300 ppm HCl in Air at 300 °C for 30 Minutes.

Figure 4.8 Weight Change of 4% PdO/γ-Alumina Due to the Flow of 300 ppm HCl in Air at 300 °C for 30 Minutes.
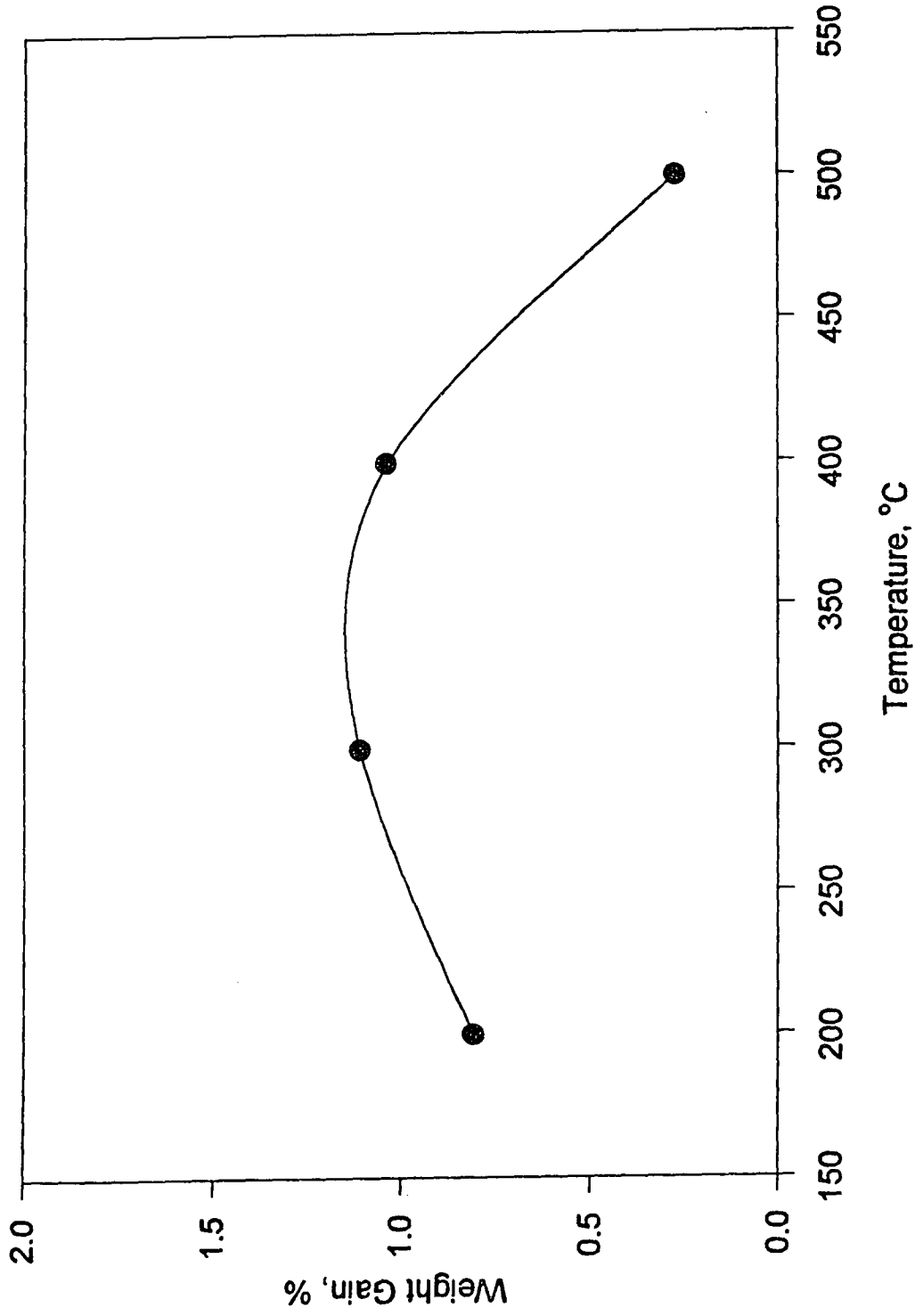
Figure 4.9 Weight Gain of 4% PdO/γ-Alumina as a Function of Temperature Due to Reaction with 300 ppm HCl in Air for 30 Minutes.

TPR1. FRESH CATALYST

1st Derivative (%/min x 10⁻²)

Temperature (°C)

Curve (II)

Curve (I)

Curve 1: TGA
File Info: YU053   Fri Jul 30 08:42:27 1993
Sample Weight: 2.287   mg
TPR1. FRESH CATALYST

X1	81.883	°C
X2	92.518	°C
Y1	98.173	Wt. %
Y2	97.818	Wt. %
ΔY	-0.554	Wt. %

4% PDO/AL2O3
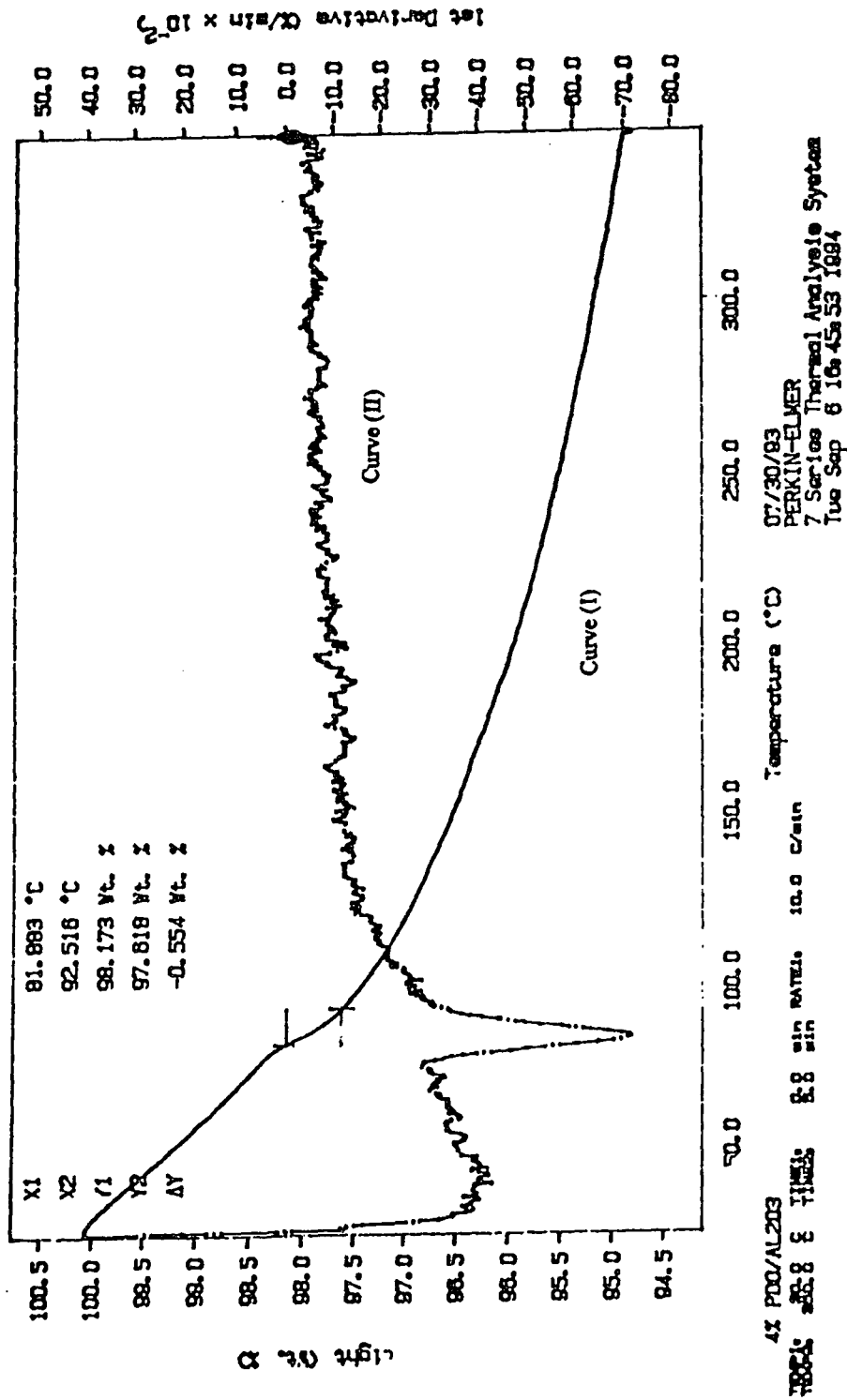
Figure 4.10 Weight Change of 4% PdO/γ-Alumina as Function of Temperature Due to the Flow of 5% H₂ in Argon.
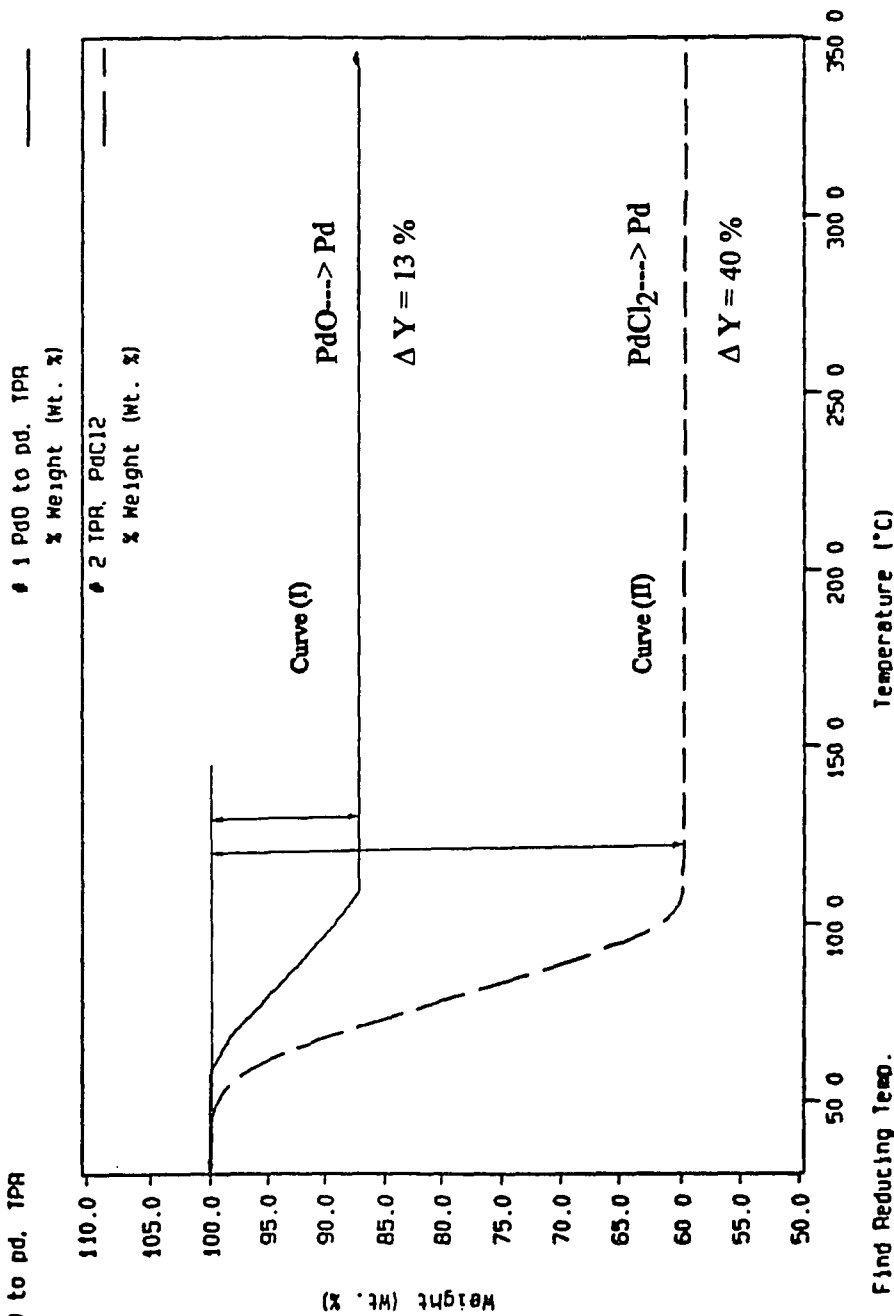
Figure 4.11 Weight Change of Pure PdO and $PdCl_2$ as a Function of Temperature Due to the Flow of 5% H_2 in Argon.
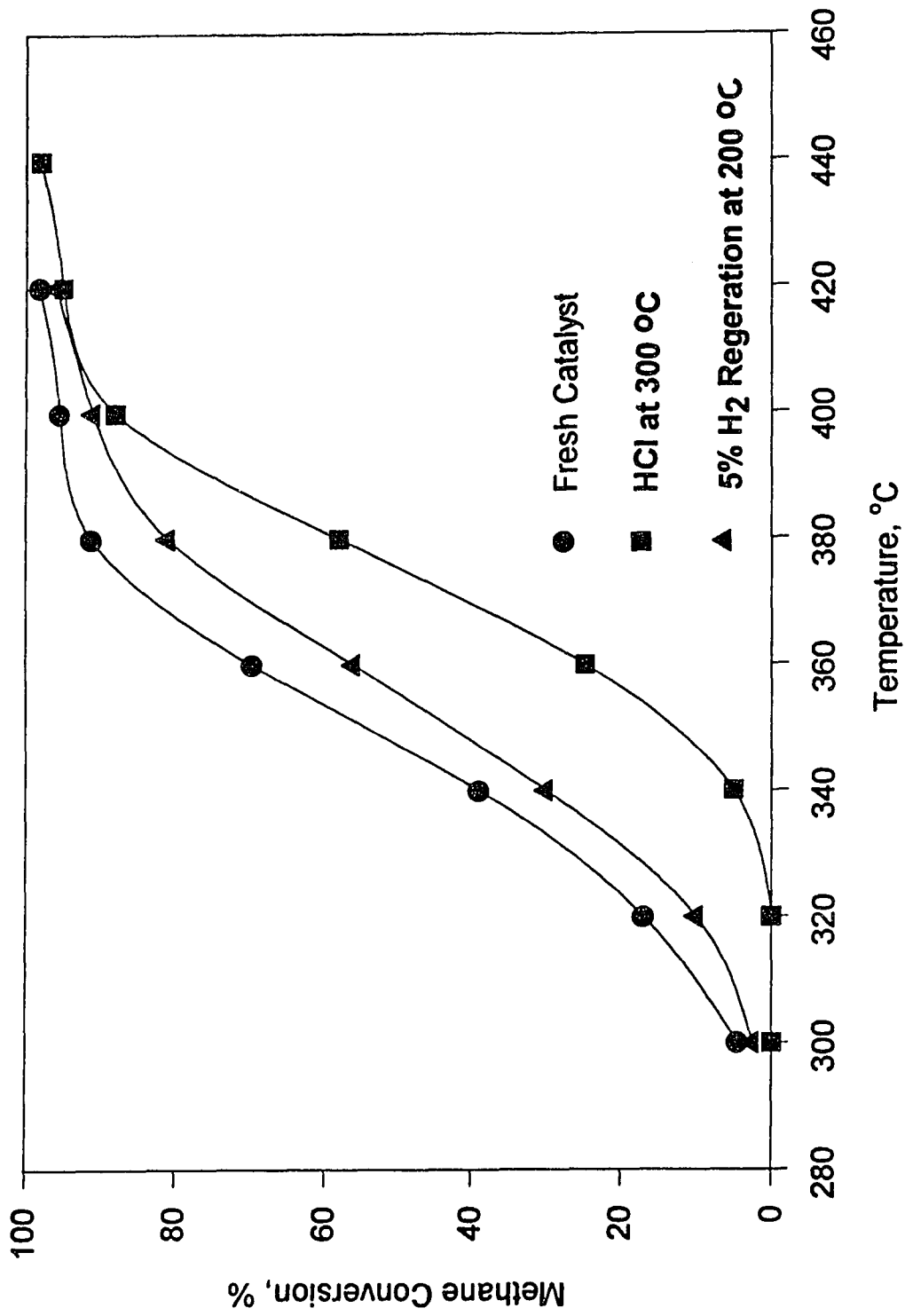
Figure 4.12 Effect of H_2 Regeneration of HCl Poisoned 4% PdO/γ-Alumina Catalyst on Methane Oxidation Activity.
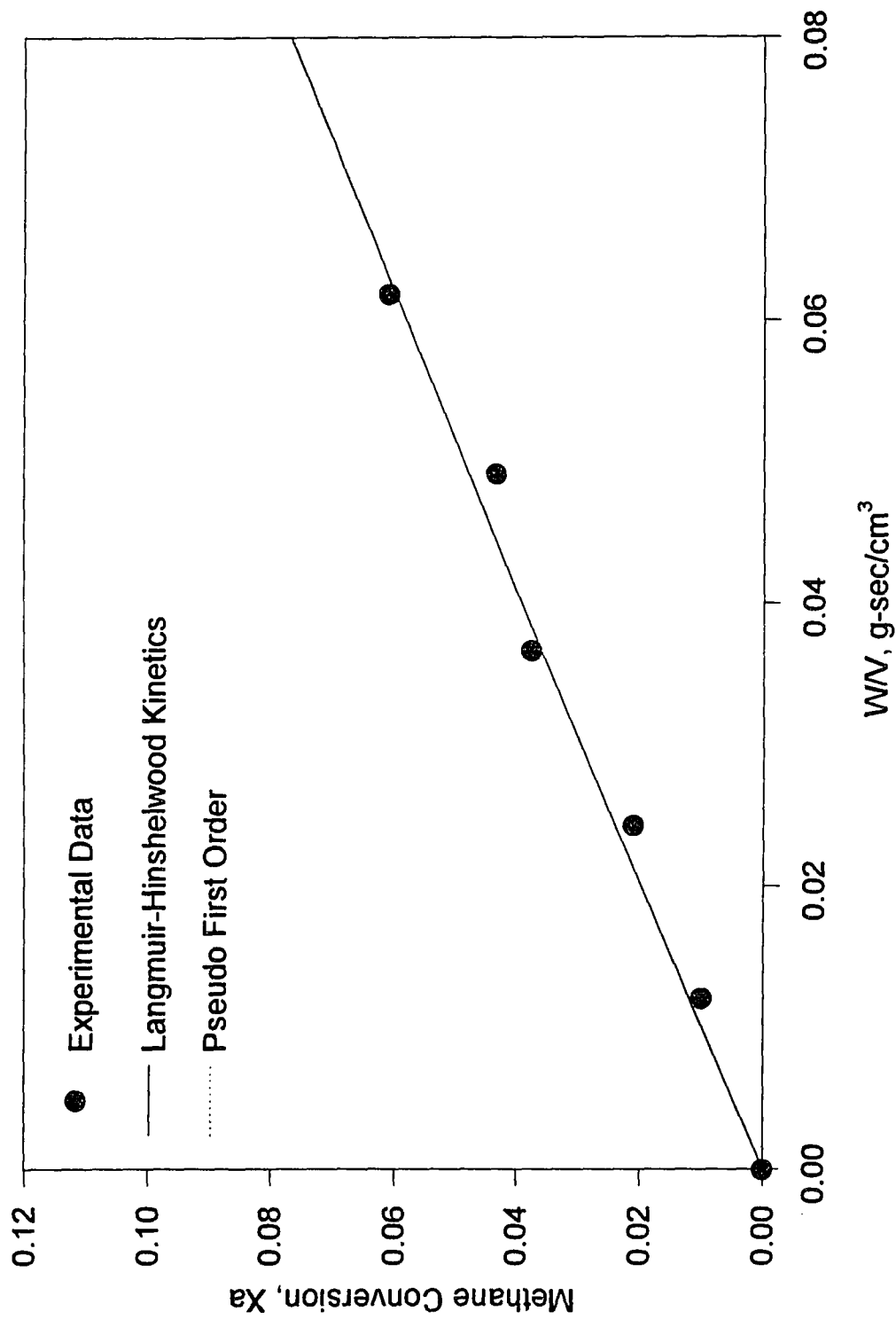
Figure 4.13 Comparison of Methane Oxidation Kinetic Mechanisms over Palladium Catalyst at 250 °C
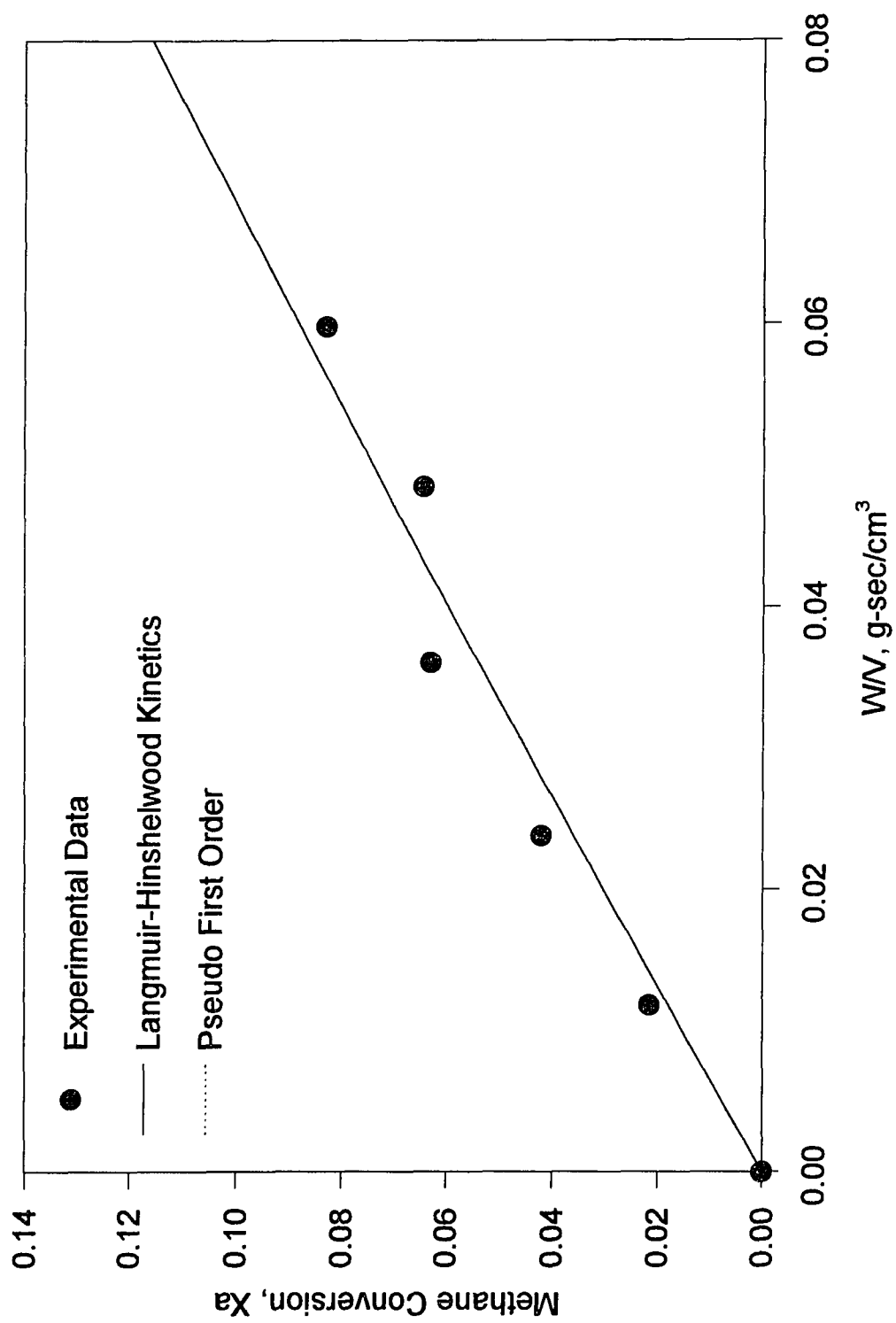
Figure 4.14 Comparison of Methane Oxidation Kinetic Mechanisms over Palladium Catalyst at 260 °C
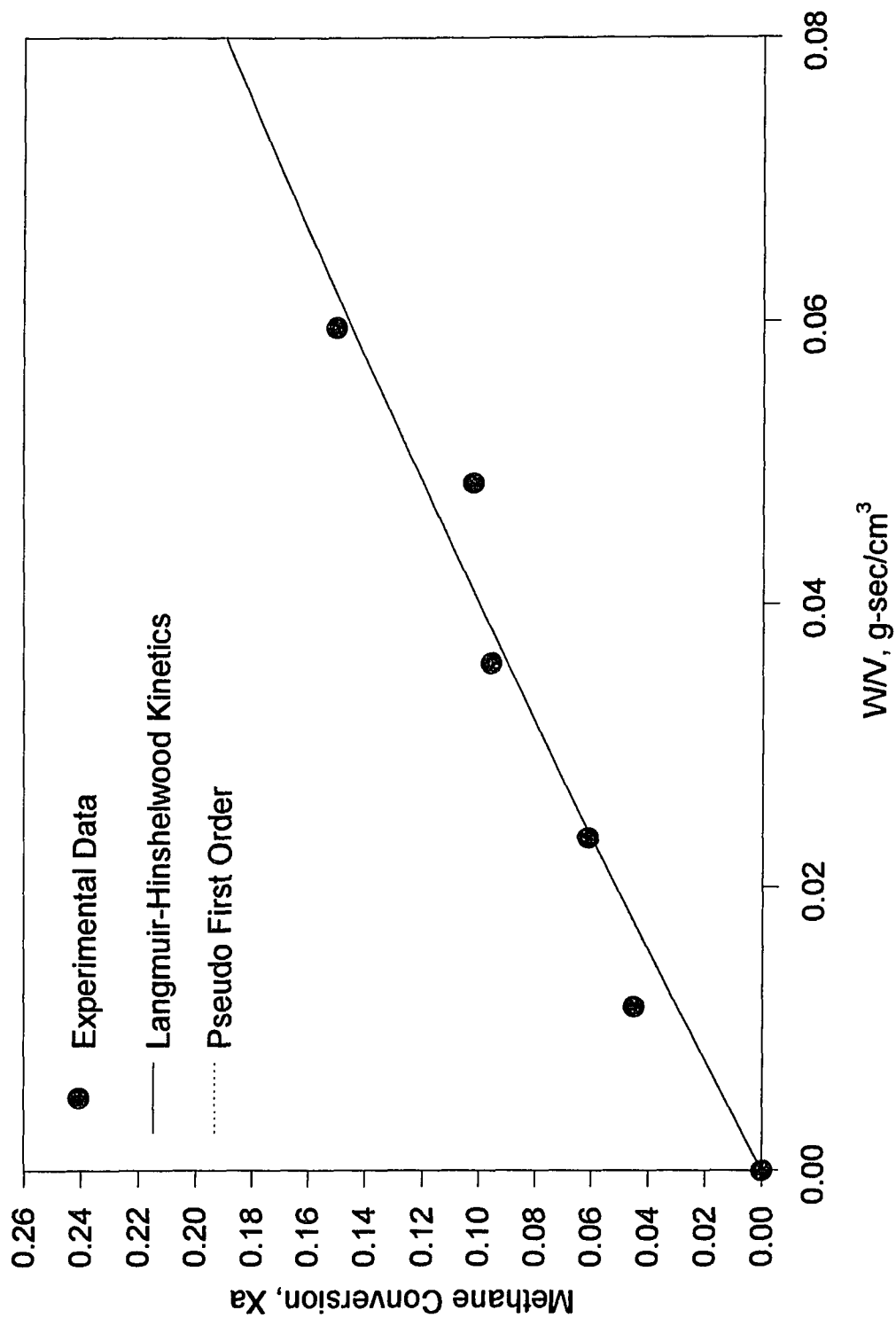
Figure 4.15 Comparison of Methane Oxidation Kinetic Mechanisms over Palladium Catalyst at 270 ^{o}C
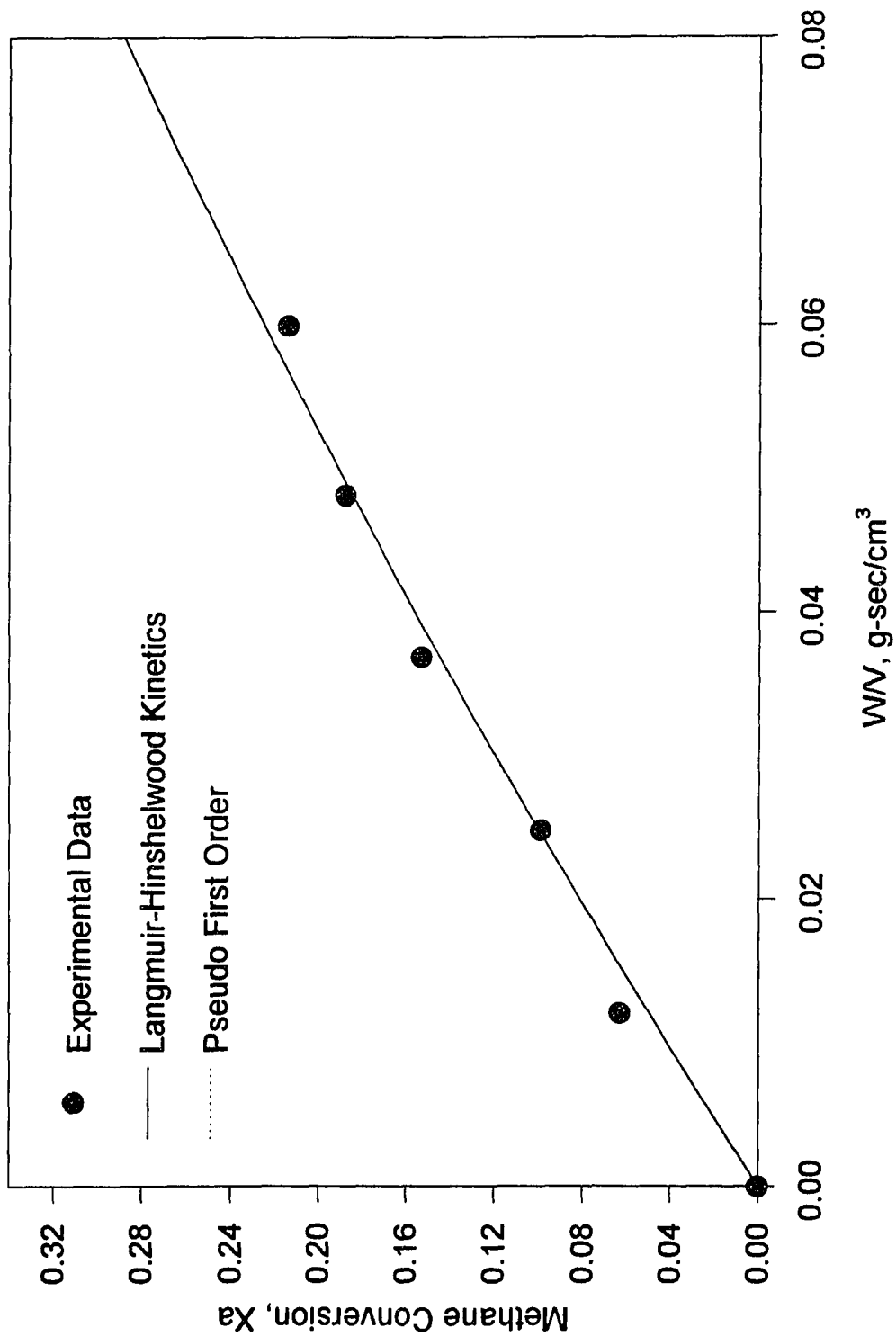
Figure 4.16 Comparison of Methane Oxidation Kinetic Mechanisms over Palladium Catalyst at 280 °C
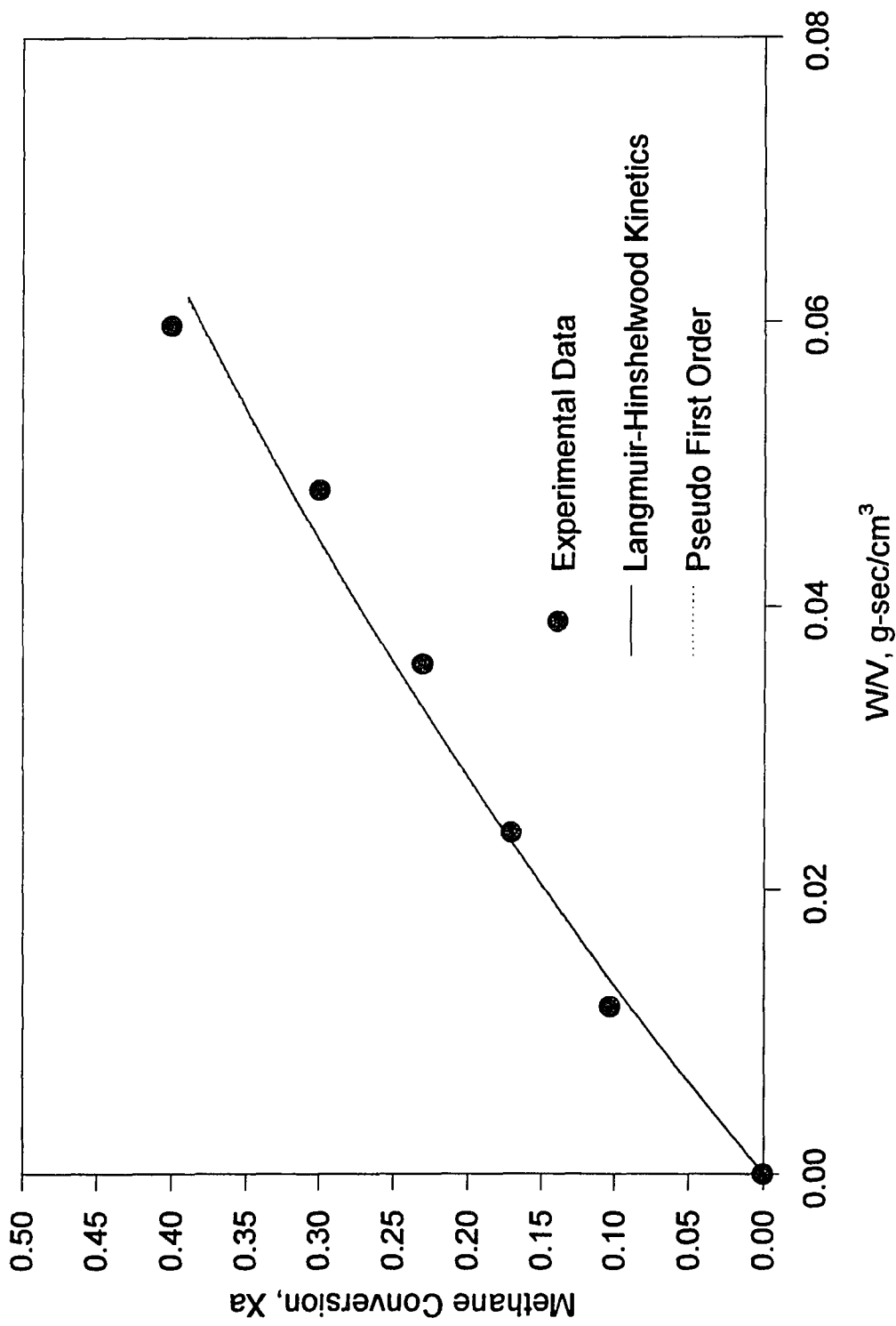
Figure 4.17 Comparison of Methane Oxidation Kinetic Mechanisms over Palladium Catalyst at 290 °C
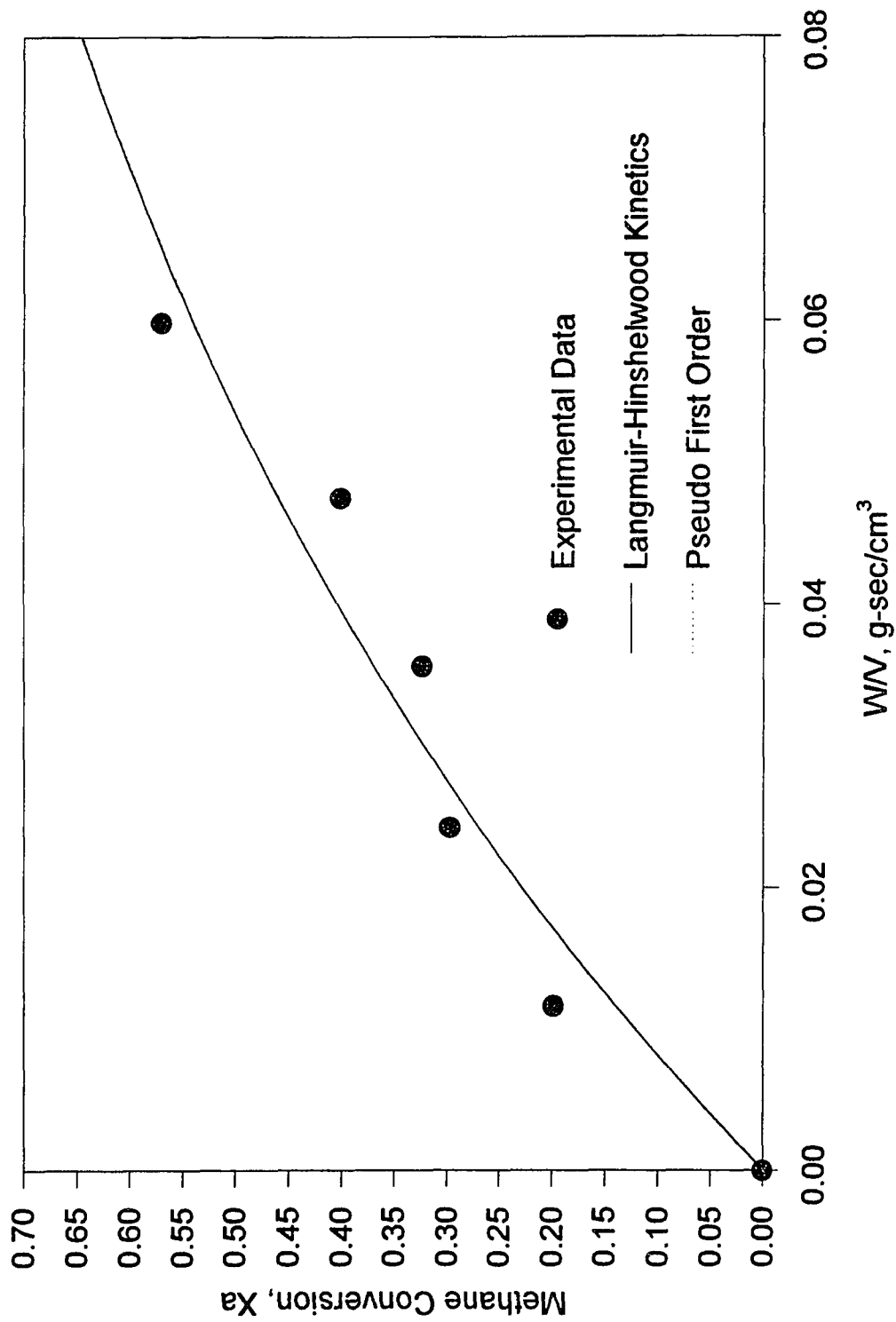
Figure 4.18 Comparison of Methane Oxidation Kinetic Mechanisms over Palladium Catalyst at 300 °C
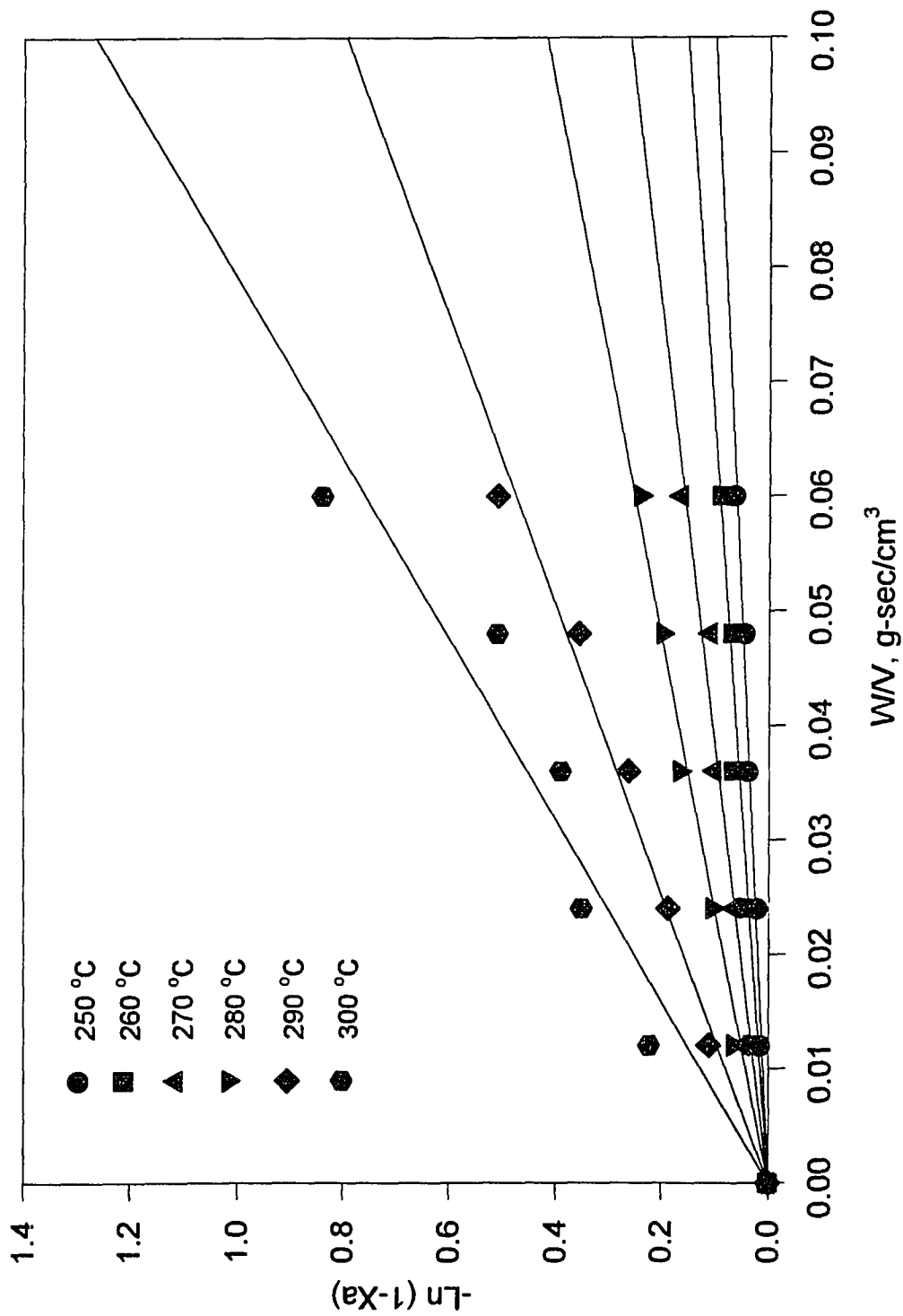
Figure 4.19 The Plots of -Ln (1-Xa) Versus W/V for Methane Oxidation over Palladium Catalysts
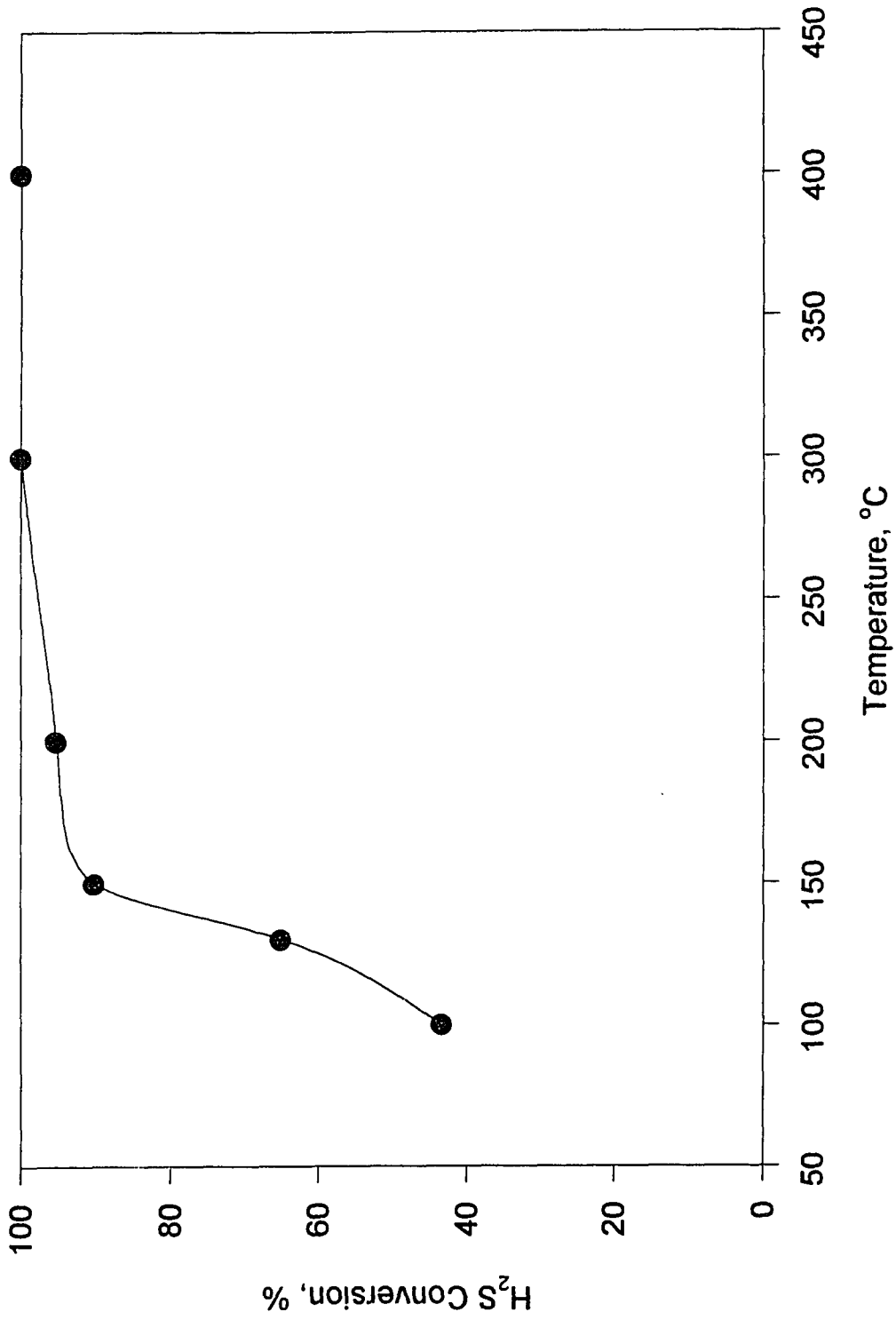
Figure 4.20 H$_2$S Oxidation over 4% PdO/γ-Alumina Catalyst as a Function of Temperature
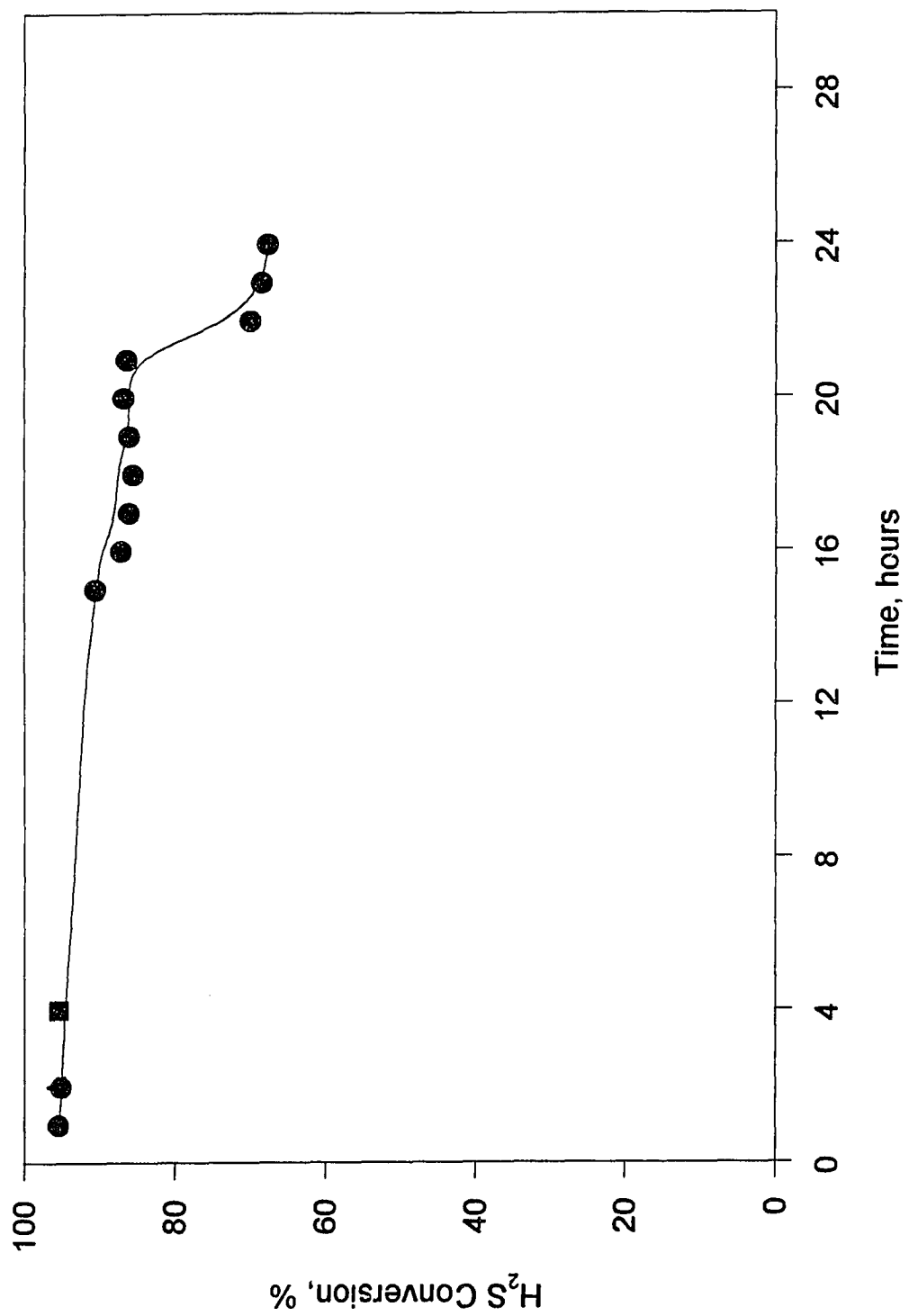
Figure 4.21 H_2S Oxidation over 4% PdO/γ-Alumina Catalyst at 200 °C as a Function of Time
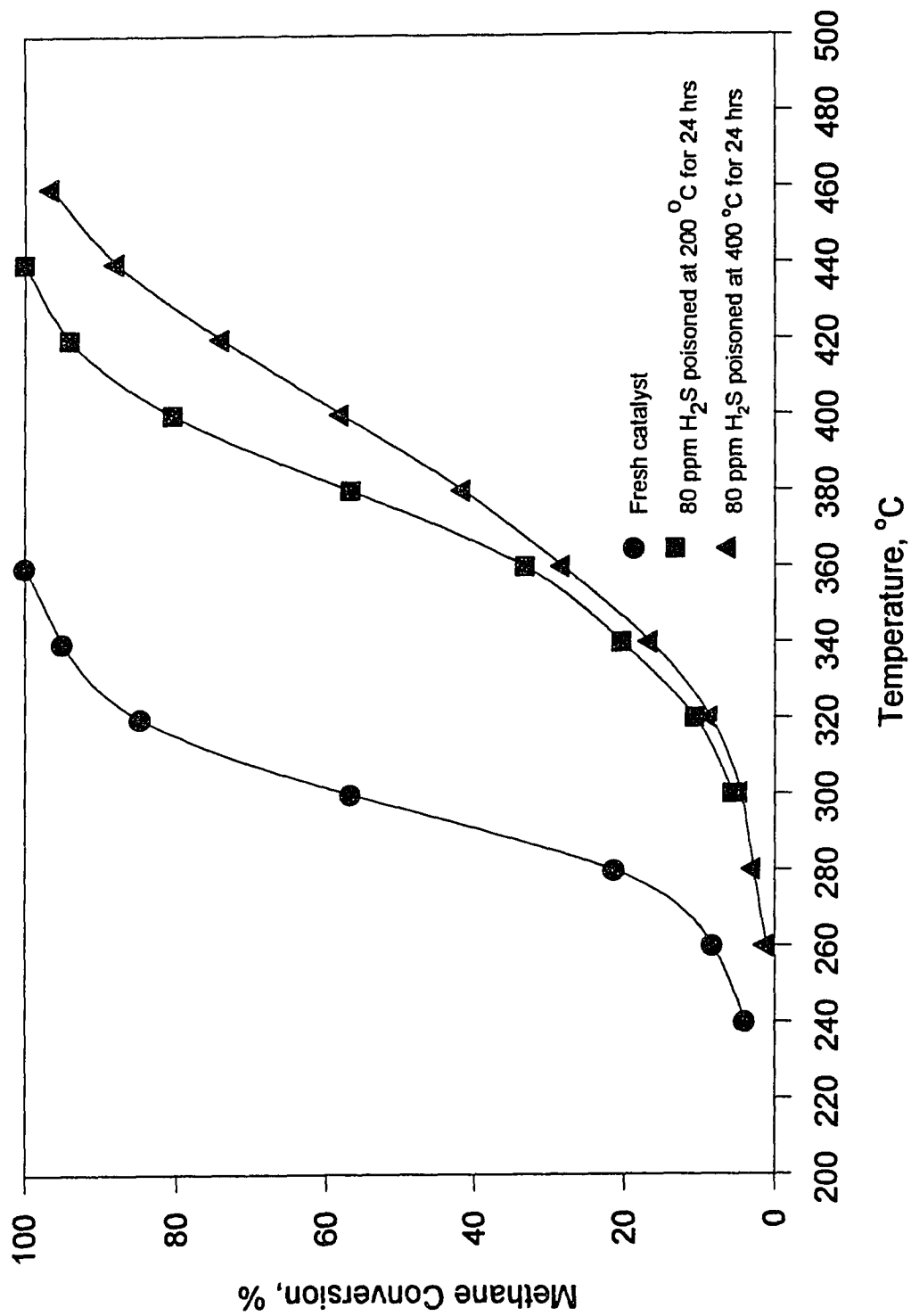
Figure 4.22 Methane Oxidation over 4% PdO/γ-Alumina Fresh and Poisoned Catalysts as a Function of Temperature.
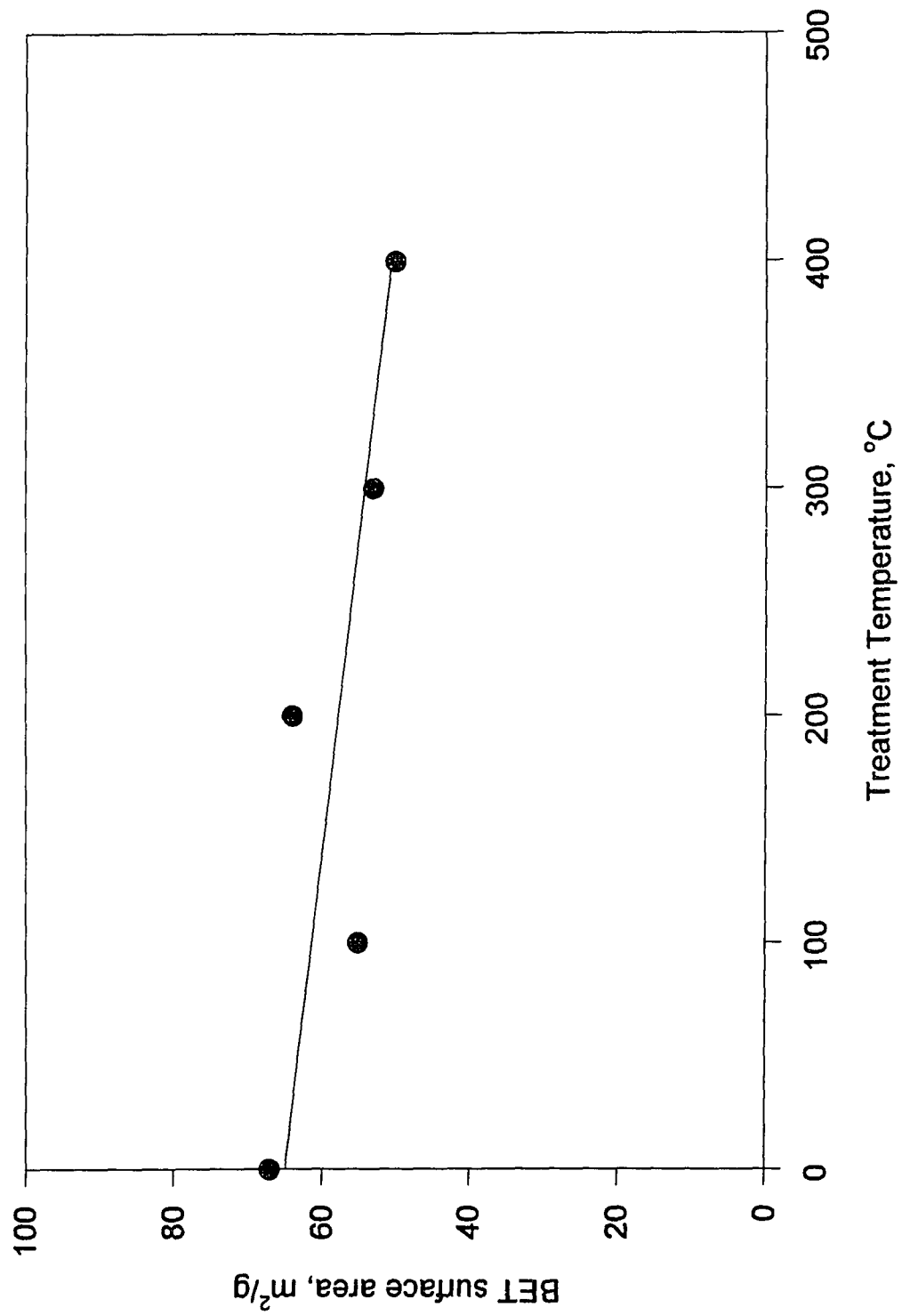
Figure 4.23 H_2S Treatment Temperature Effect on BET Surface Area of 4% PdO/γ-Alumina Catalyst

Figure 4.24 Thermal Gravimetric Analysis of 4% PdO/γ-Alumina Due to the Flow of 250 ppm H_2S in Air at 200 °C.

Curve 1: TGA
File Info: yu022   Mon May 10 13:48:01 1993
Sample Weight: 3.800   mg
4%PdO/Al2O3+250 ppm H2S+Air

X1   18.133 min
X2   60.933 min
Y1   94.872 Wt. %
Y2   96.960 Wt. %
ΔY   2.088 Wt. %

ΔY

Adding H_2S

Weight (Wt. %)

104.0

102.0

100.0

98.0

96.0

94.0

92.0

90.0

88.0

0.0   10.0   20.0   30.0   40.0   50.0   60.0   70.0

Time (minutes)

400 oC Adsorption+TPD

TEMP1: 20.0 C   TIME1:   0.0 min   MIN RATE1:   40.0 C/min
TEMP2: 400.0 C   TIME2: 60.0 min

PERKIN-ELMER
7 Series Thermal Analysis System
Mon Apr 10 15:40:29 1995
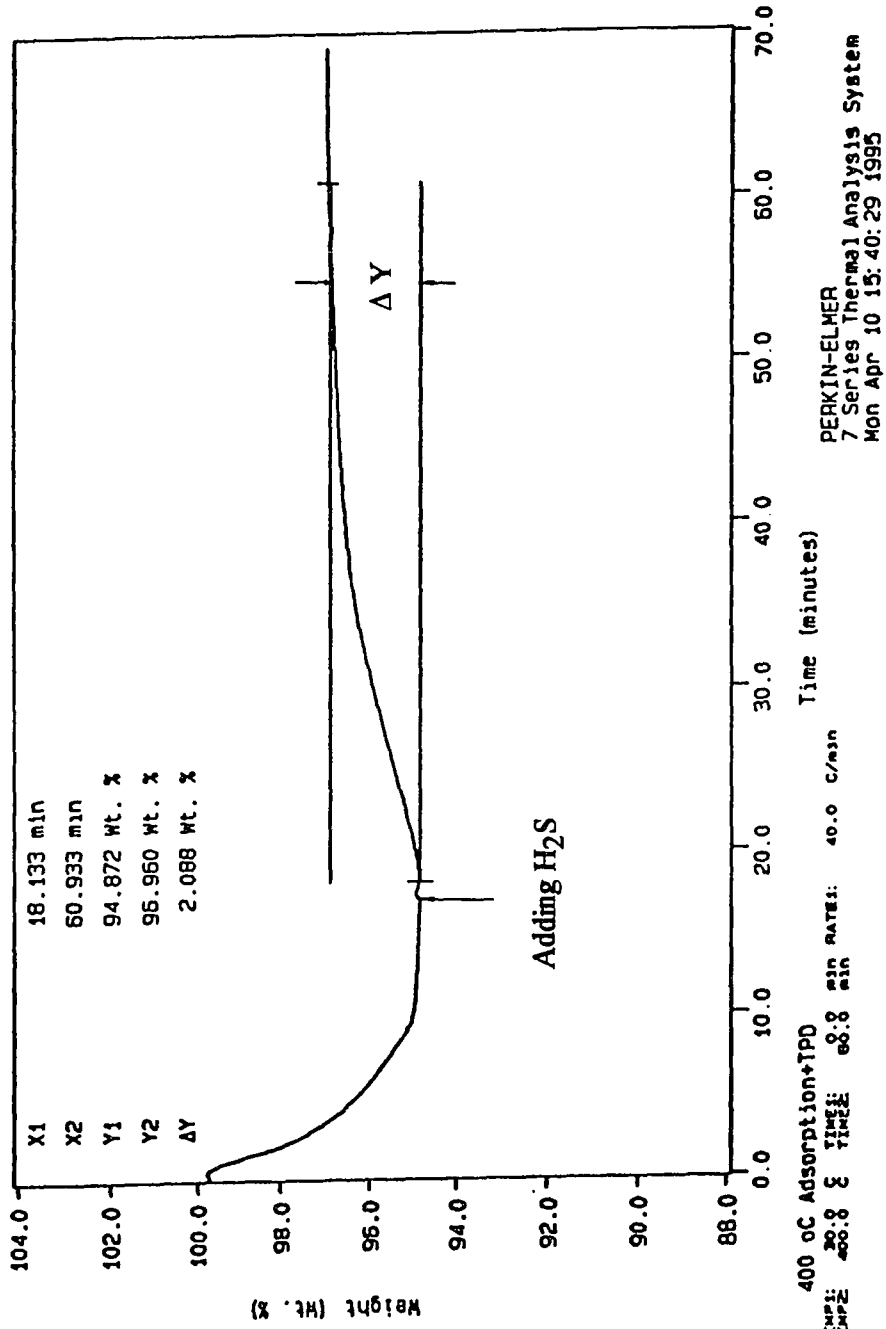
Figure 4.25 Thermal Gravimetric Analysis of 4% PdO/γ-Alumina Due to the Flow of 250 ppm H_2S in Air at 400 °C.

132

Curve 1: TGA
File Info: yu019   Mon May 3 11:29:08 1993
Sample Weight: 5.990   mg
A1203+250ppm H2S+Air

X1   54.947 min
X2   89.223 min
Y1   76.088 Wt. %
Y2   76.759 Wt. %
ΔY   0.671 Wt. %

Weight (Wt. %)

Adding H2S

ΔY

Time (minutes)

400 oC

TEMP1: 28.8 C TIME1: 0.0 min RATE1: 40.0 C/min
TEMP2: 408.8 C TIME2: 60.0 min

PERKIN-ELMER
7 Series Thermal Analysis System
Mon Apr 10 15:48:06 1995.
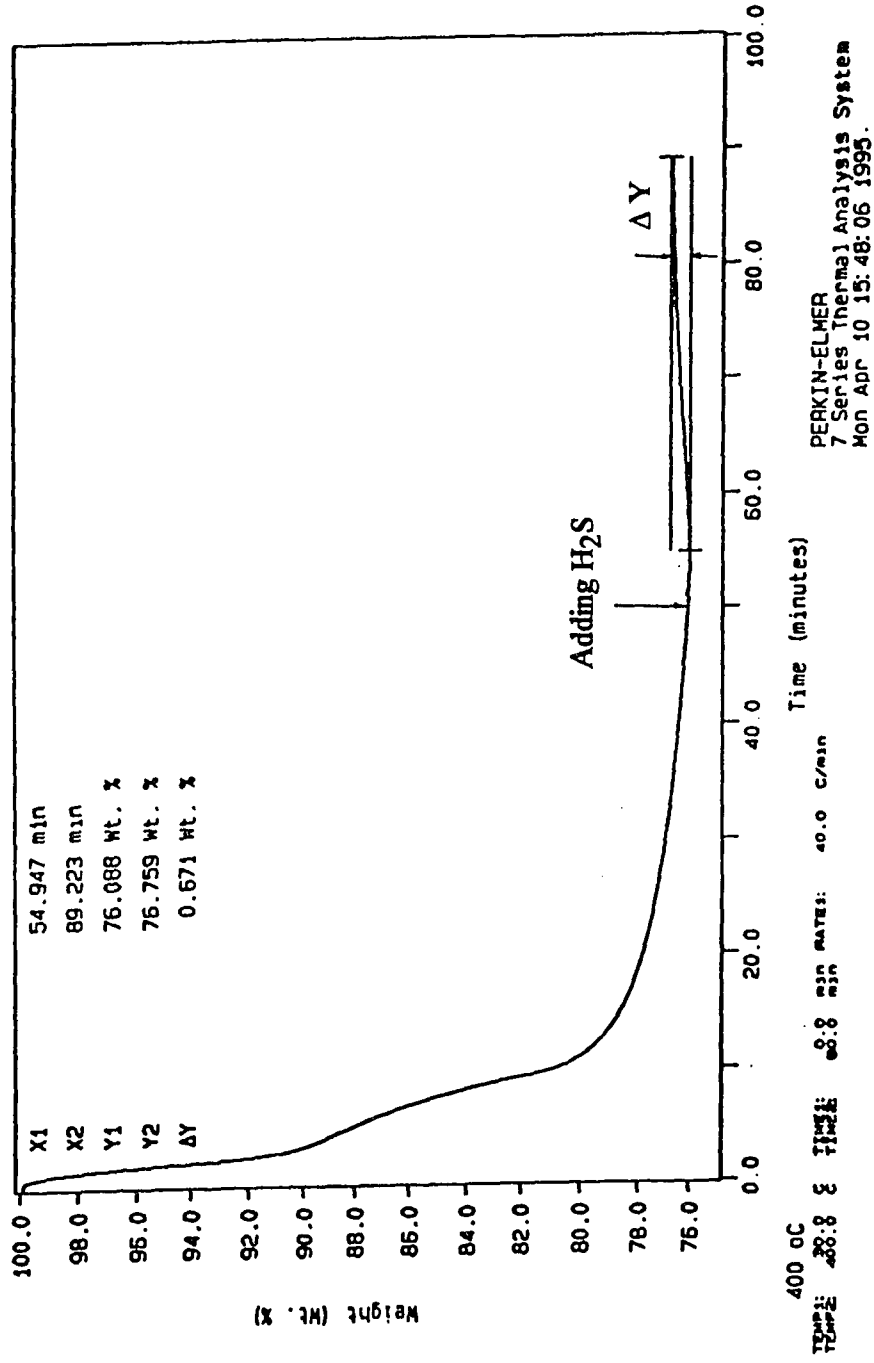
Figure 4.26 Thermal Gravimetric Analysis of Pure γ-Alumina Due to the Flow of 250 ppm H₂S in Air at 400 ºC.
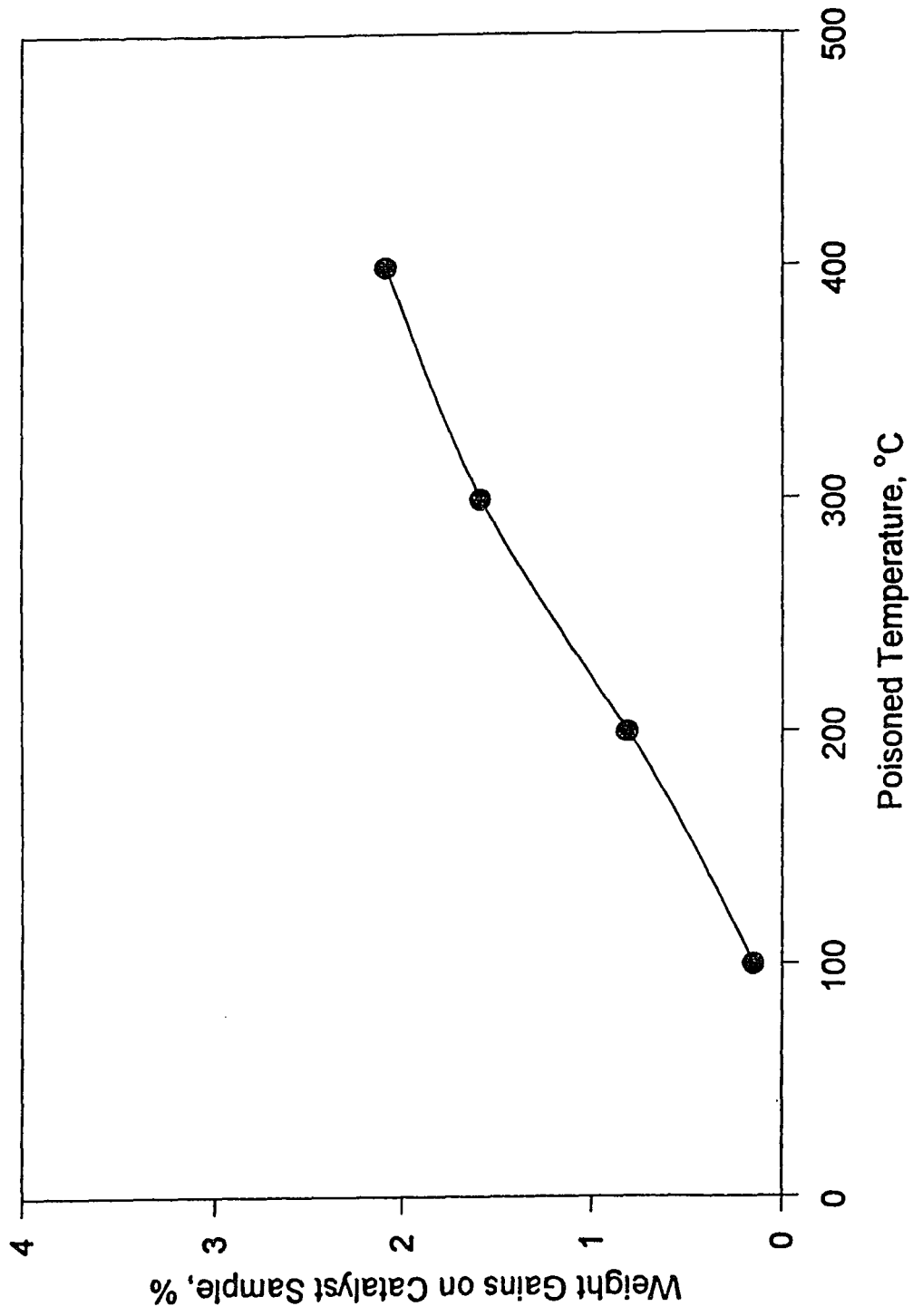
Figure 4.27 Thermal Gravimetric Analysis of 4% PdO/γ-Alumina Due to the Flow of 250 ppm H$_2$S in Air for 30 Minutes.
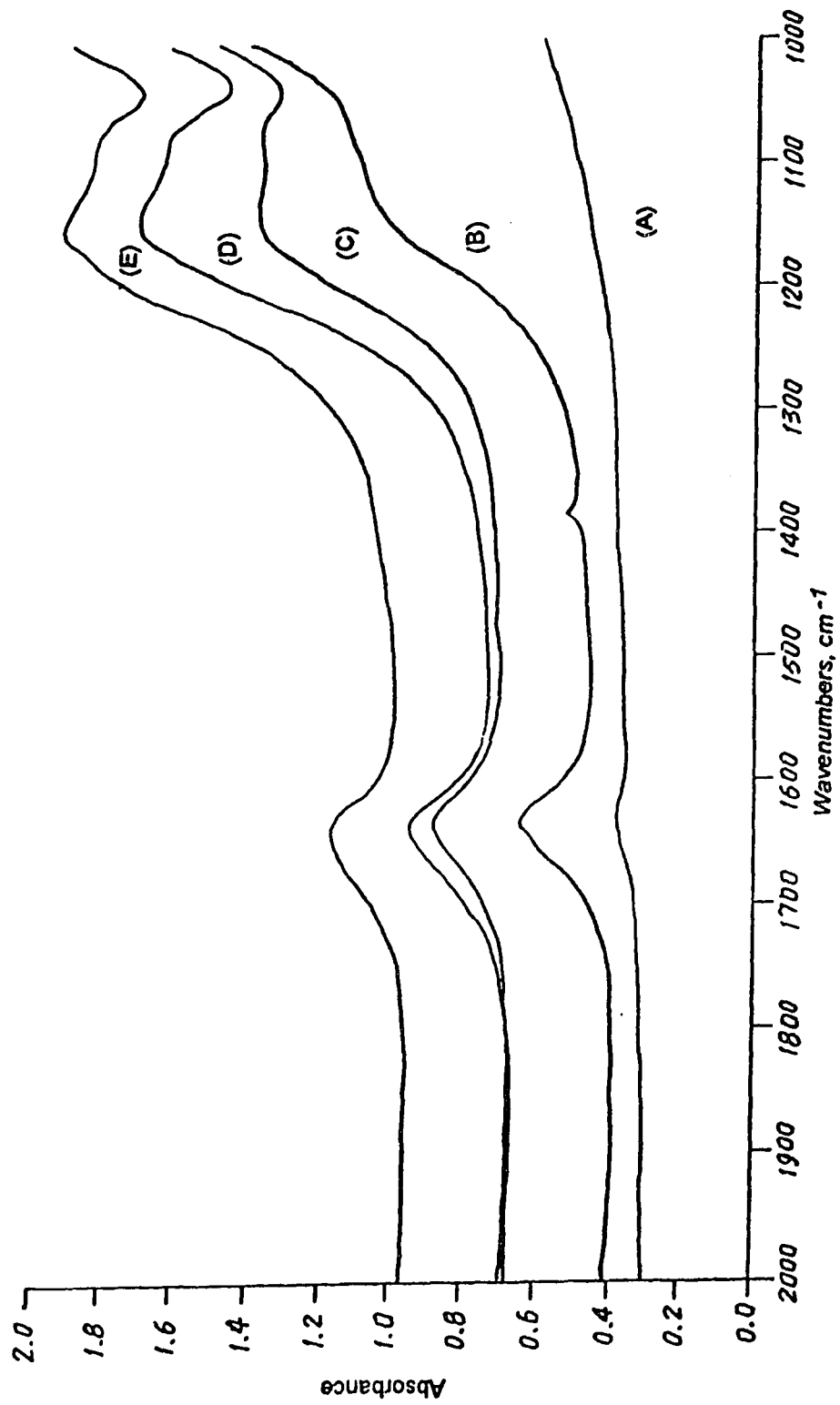
Figure 4.28 FT-IR Spectra of SO_2 and SO_3 Due to the Catalytic Oxidation of H_2S as A Function of Treatment Temperature (A) Fresh Catalyst, (B) Poisoned at 100 °C, (C) Poisoned at 200 °C, (D) Poisoned at 300 °C, (E) Poisoned at 400 °C.

135
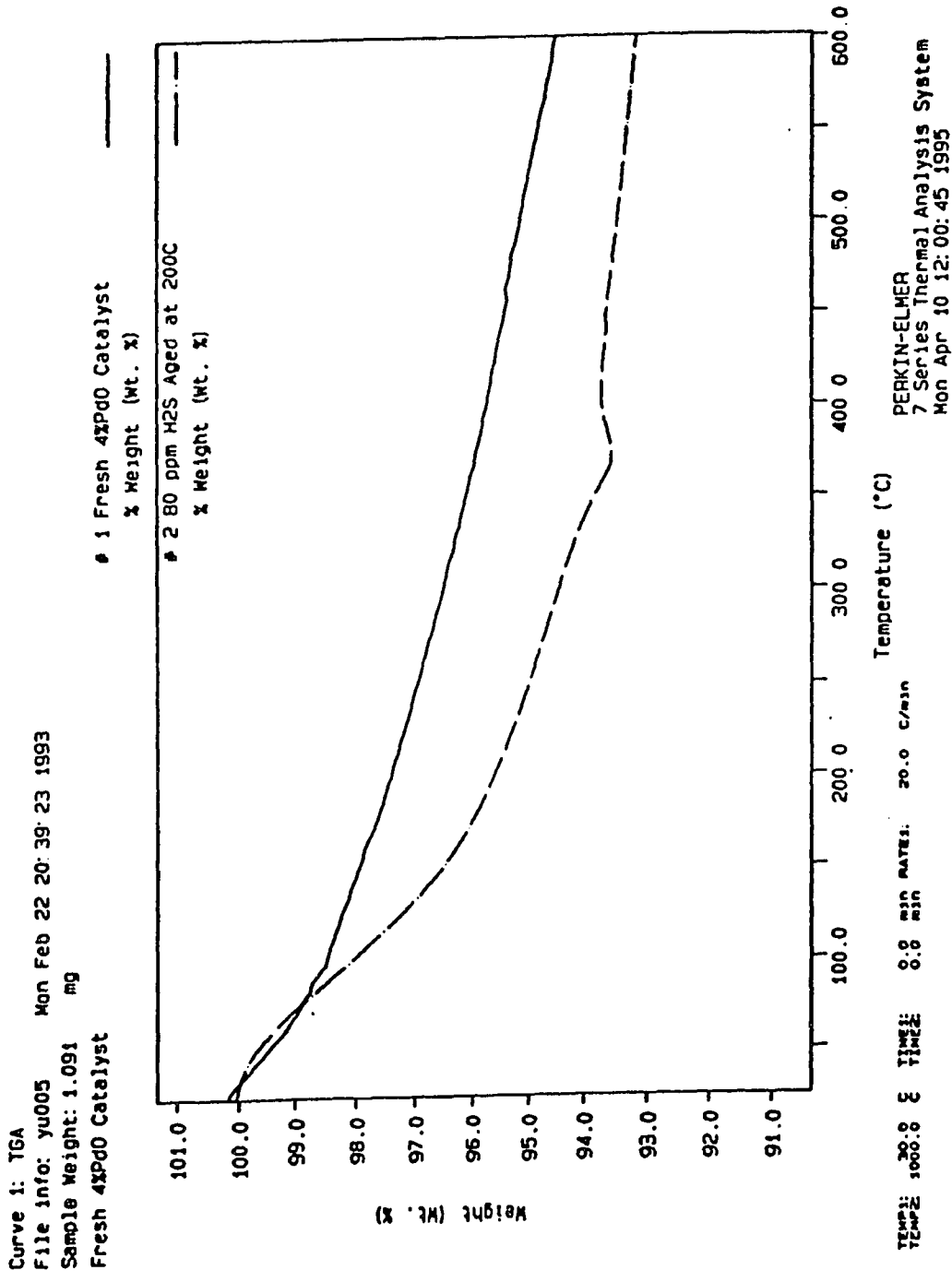
Figure 4.29 Thermal Gravimetric Analysis of the 200 °C H_2S Poisoned Catalyst Due to Air Flow.
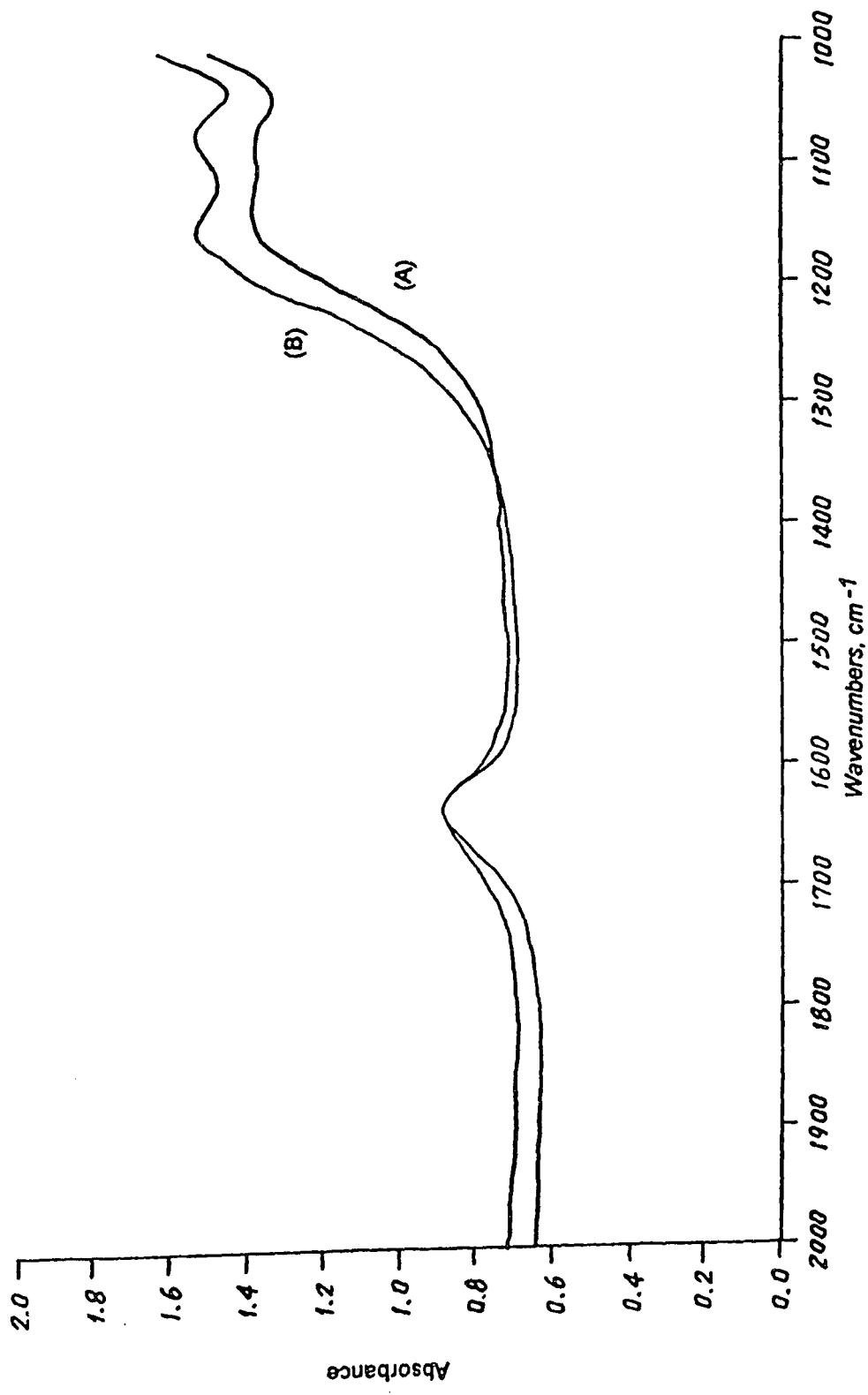
Figure 4.30 Comparison of FT-IR Spectra of the 200 °C H_2S Poisoned Catalyst Before and After Thermal Treatment with Air: (A) Before Thermal Treatment, (B) After Thermal Treatment
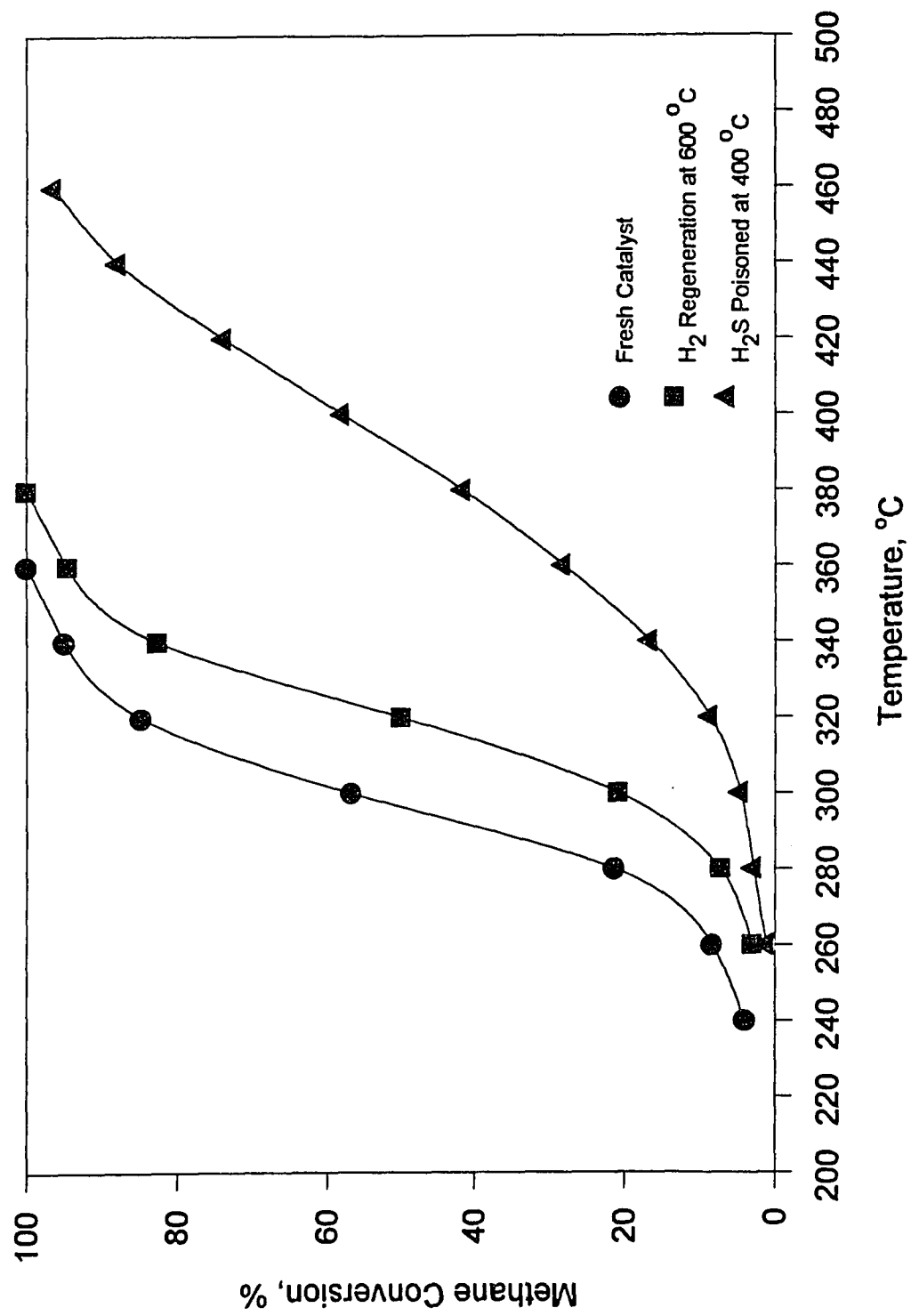
Figure 4.31 H$_2$ Treatment Effect on Methane Oxidation over H$_2$S Poisoned 4% PdO/γ-Alumina Catalyst as a Function of Temperature.

Figure 4.32 Temperature Programmed Oxidation of the 400 °C H2S Poisoned Catalyst on the Altamira Instrument.

Temperature Programmed Reduction   TCD SIGNAL: -258

H2S400CRE-OXIDIZED
4/3/95-1
C:\TAi\yu216.DFN

58 C

478 C

537 C

SIGNAL

TIME (MINUTES)
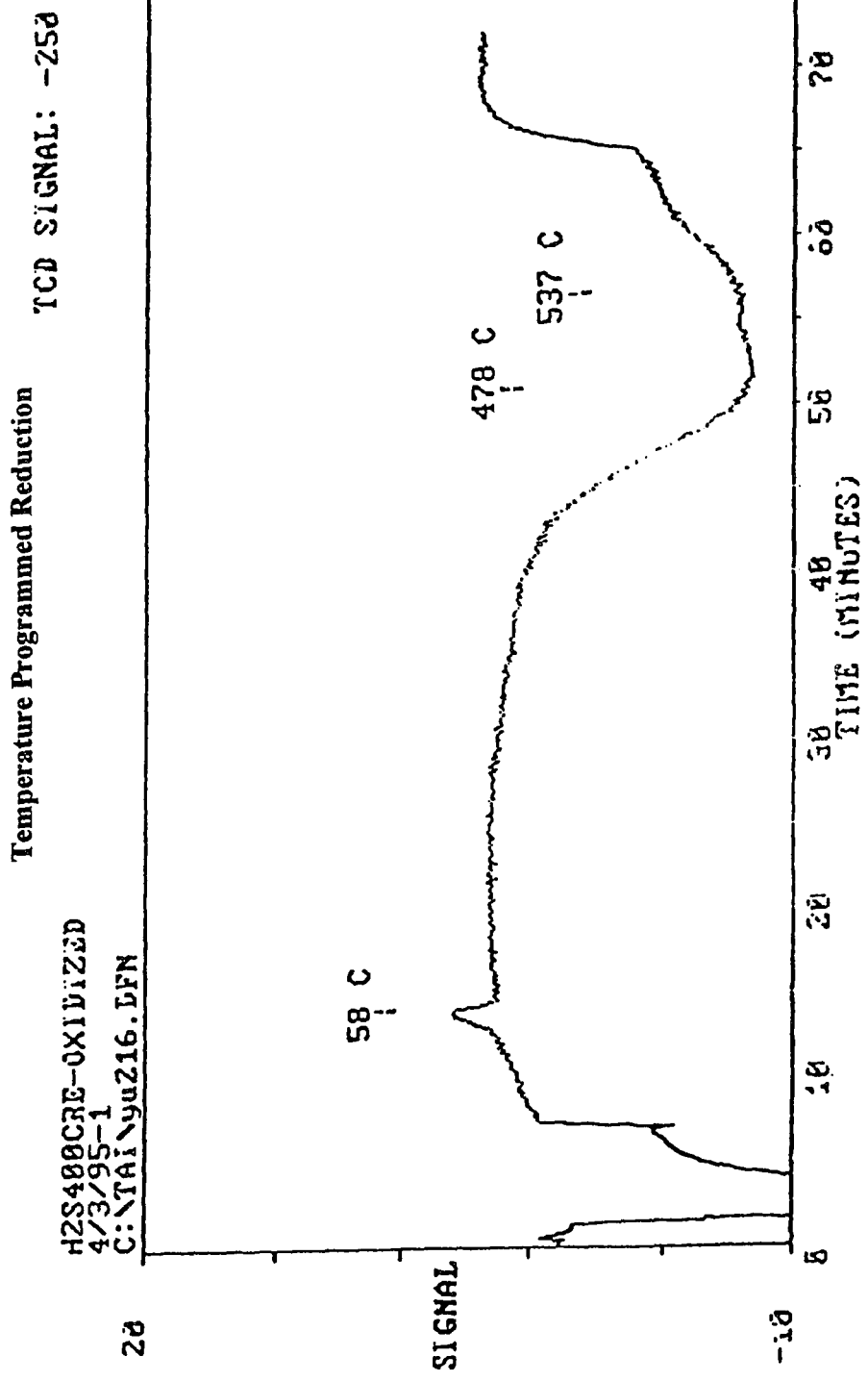
Figure 4.33 Temperatue Programmed Reduction of the 400 °C H_2S Poisoned Catalyst on the Altamira Instrument.
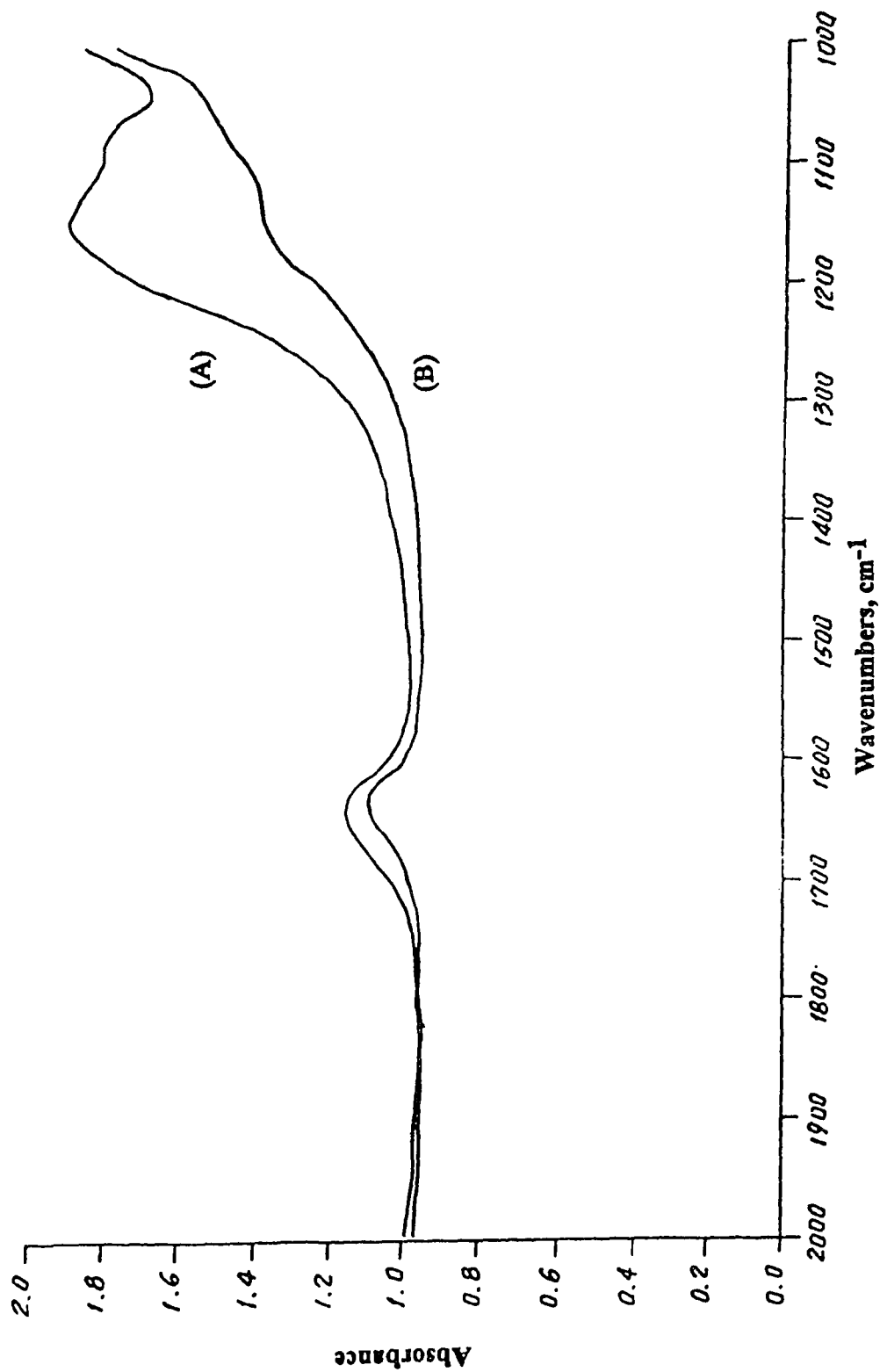
Figure 4.34 Comparison of the FT-IR Spectra of H_2S Poisoned PdO Catalyst Before and After H_2 Regeneration (A) Before H_2 Regeneration, (B) After H_2 Regeneration.
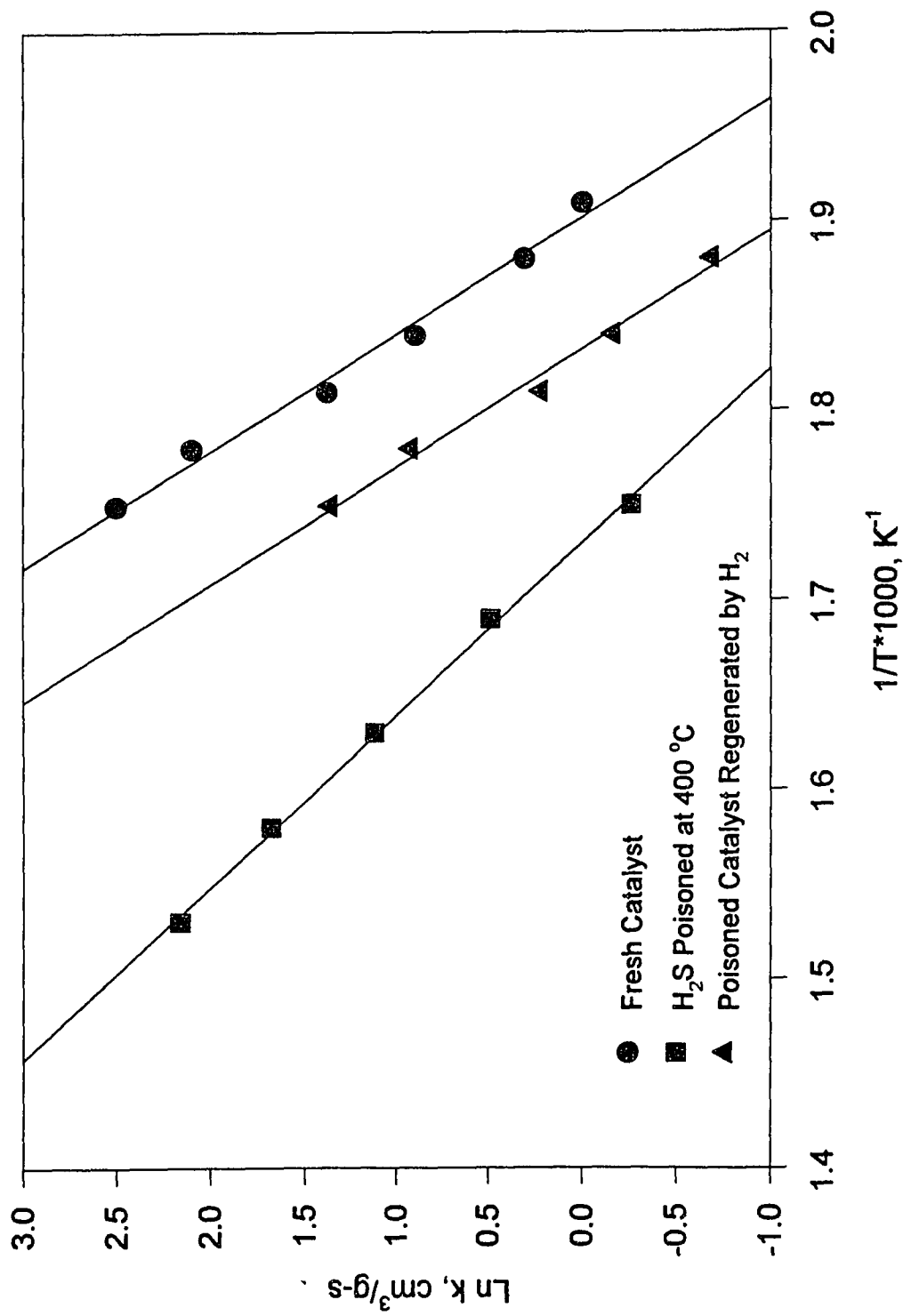
Figure 4.35 *Arrhenius Plots for Methane Oxidation over Fresh, H_2S Poisoned and H_2 Regenerated Catalysts.*
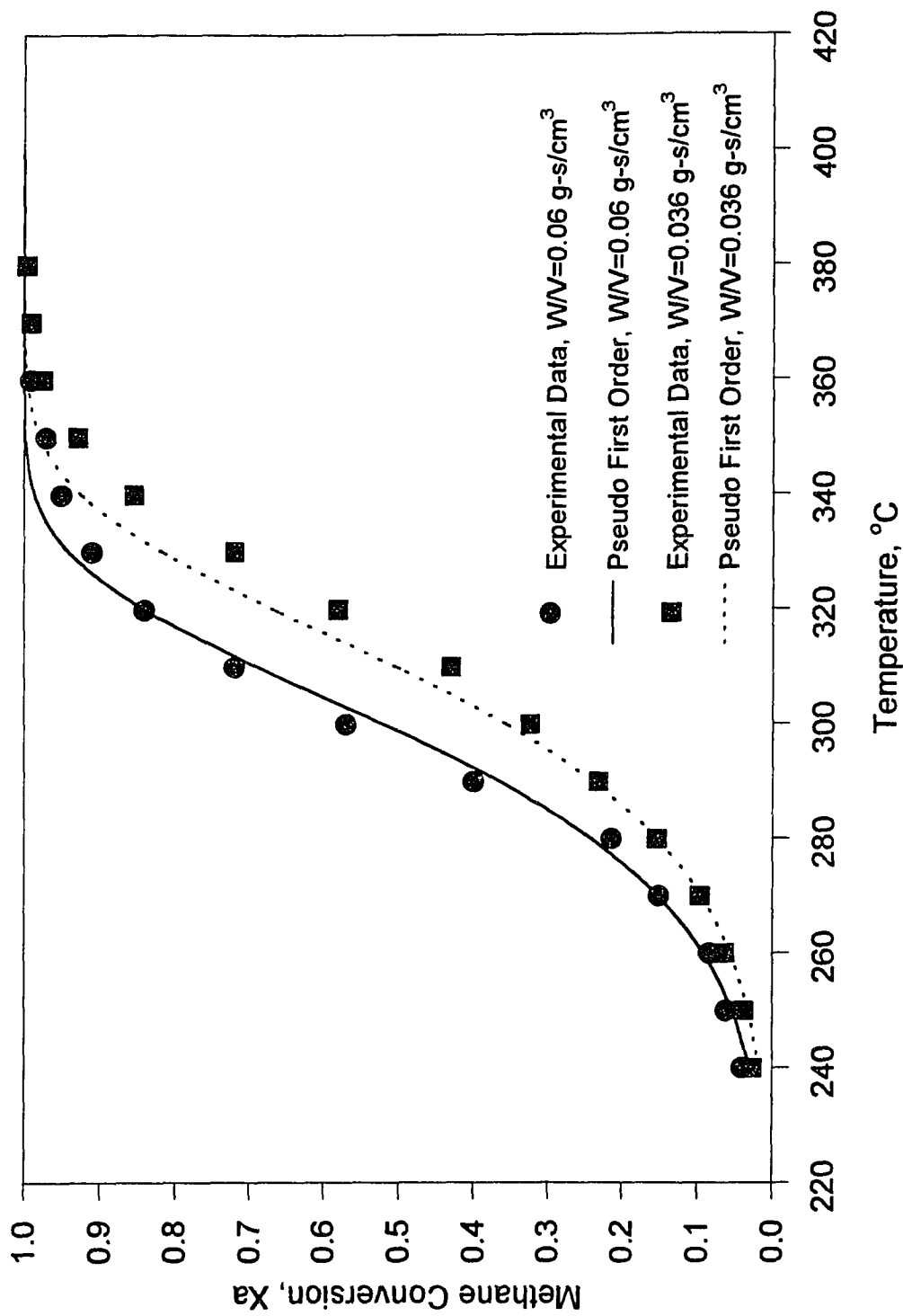
Figure 4.36 Agreement with Kinetic Mechanism of Methane Oxidation over Fresh Palladium Catalysts as a Function of Temperature
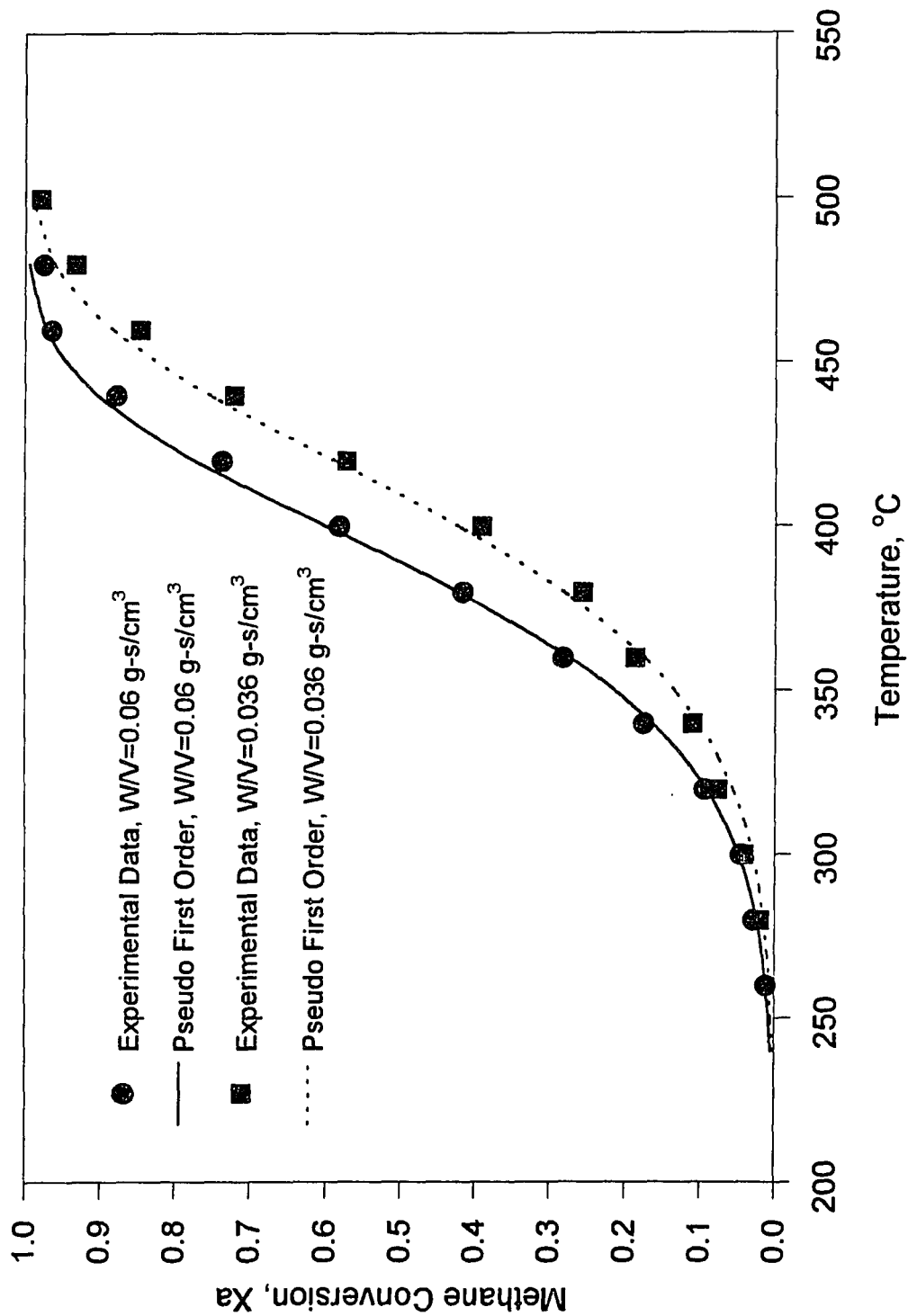
Figure 4.37 Agreement with Kinetic Mechanism of Methane Oxidation over H_2S Poisoned Palladium Catalysts as a Function of Temperature
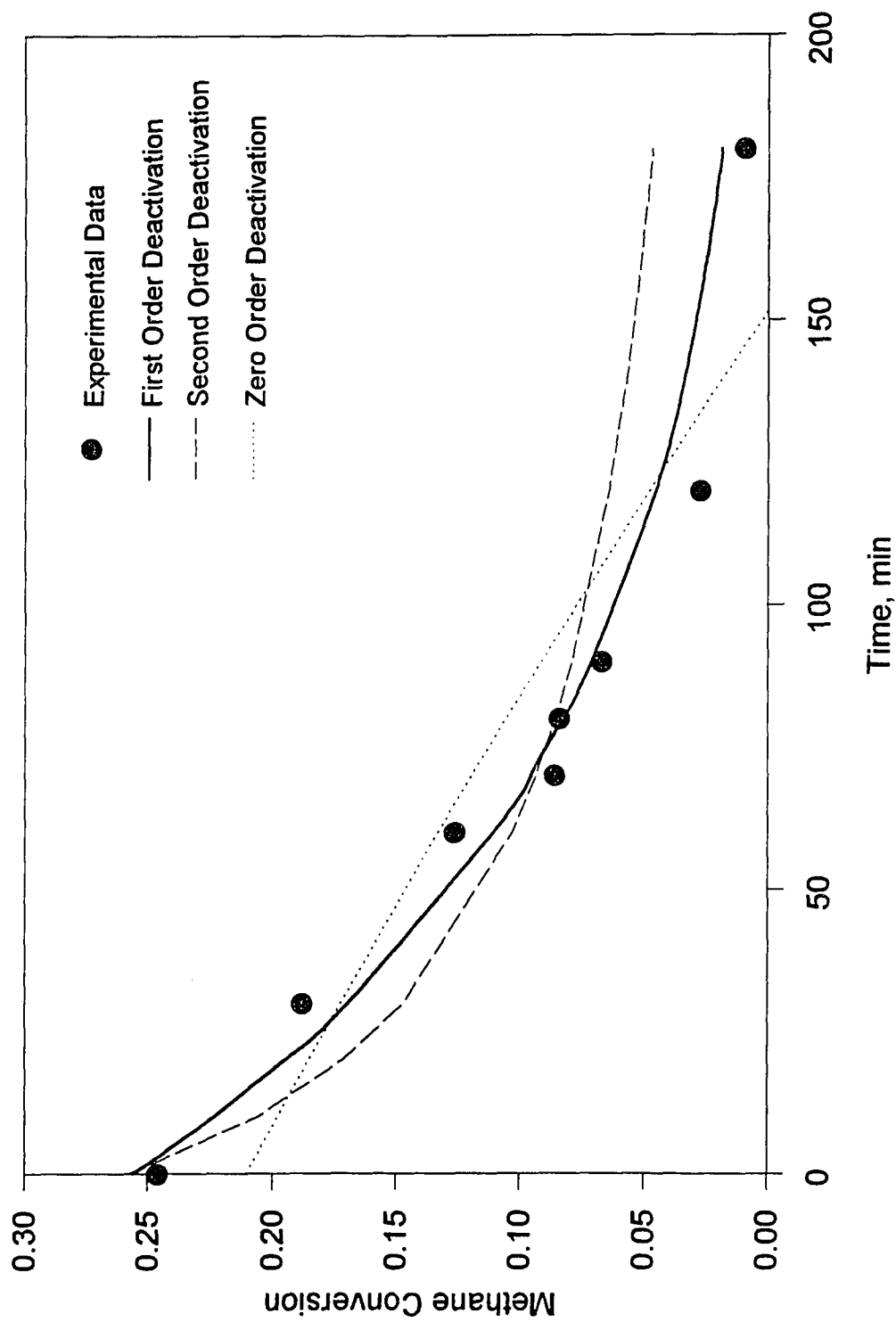
Figure 4.38 Methane Oxidation over Palladium Catalyst in Presence of H_2S at 300 °C
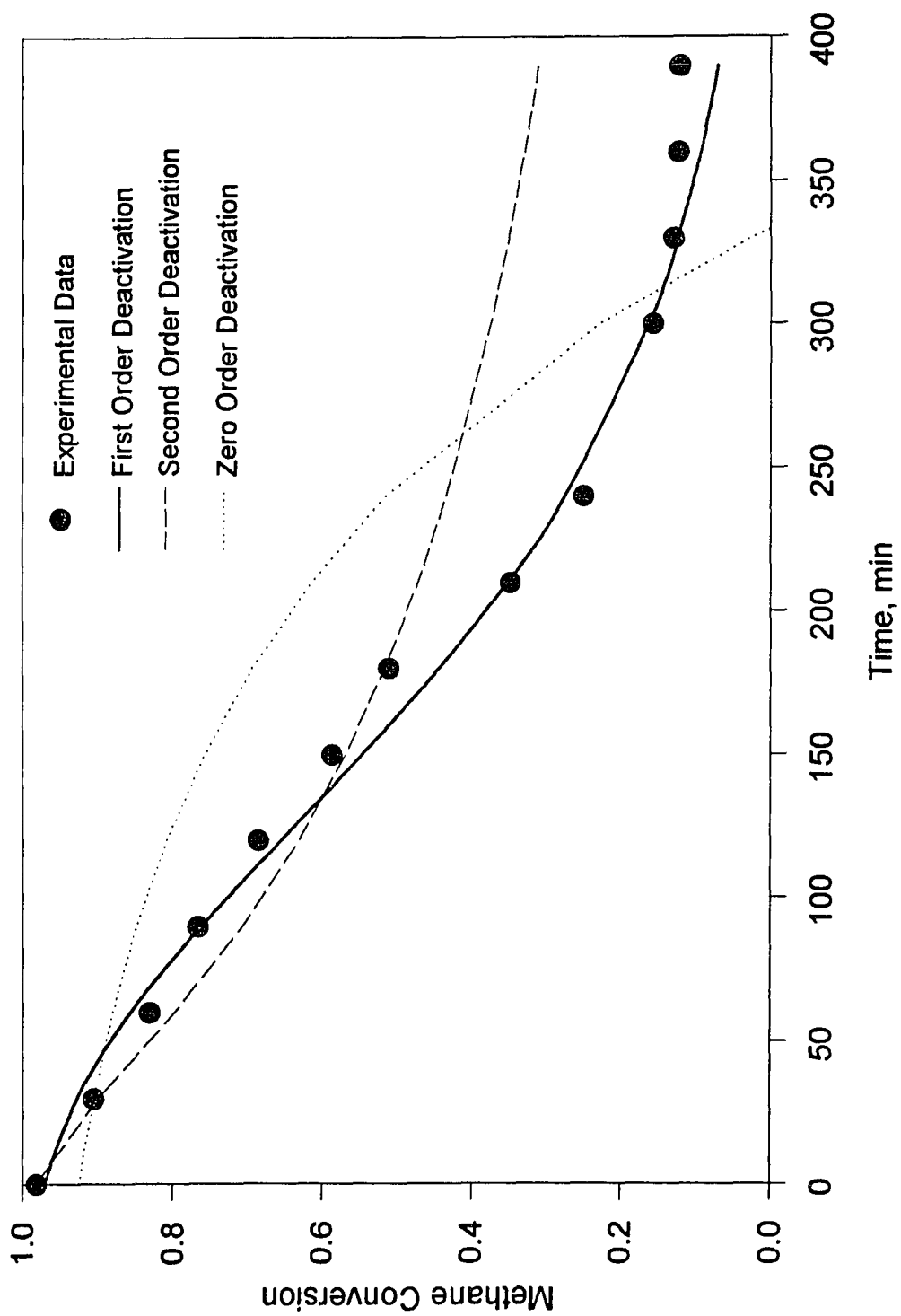
Figure 4.39 Methane Oxidation over Palladium Catalyst in Presence of H_2S at 400 °C
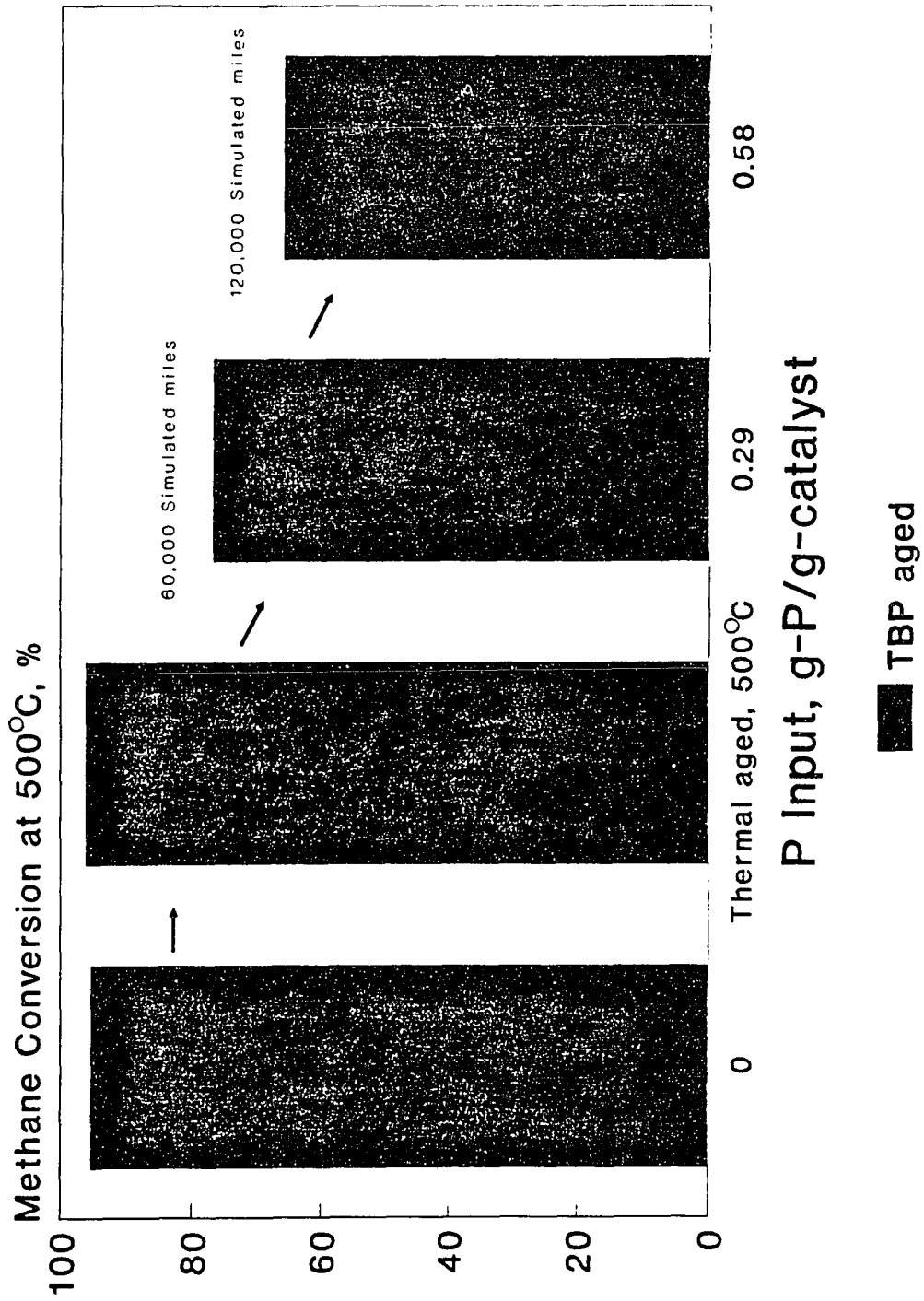
Figure 4.40 Simulation of TBP Poisoning Effect on Methane Oxidation in Automotive Applications

Figure 4.41 Methane oxidation Activity as a Function of Temperature for Fresh and TBP Aged Catalyst. The catalyst was aged with TBP for 120,000 simulated miles.

Figure 4.42 Temperature Effect on Methane Oxidation over 4% PdO/γ-Alumina Catalyst as a Function of Pulsator-aged Simulated Miles.

Curve 1: TGA
File Info: yu073   Wed Nov 17 08:52:38 1993
Sample Weight: 8.810   mg
TBP in Air, @10 C/min, 500 C

1 TBP in Air, @10 C/min, 500 C ————
    % Weight (Wt. %)

2 TBP+4%PdO/Al2O3 in Air —··—
    % Weight (Wt. %)

3 TBP+4%PdO/Al2O3 in Air —·—
    % Weight (Wt. %)

Weight (Wt. %)

Temperature (°C)

TEMP1: 30.0 C   TIME1:   0.0 min RATE1:   10.0 C/min
TEMP2: 500.0 C   TIME2: 10.0 min

PERKIN-ELMER
7 Series Thermal Analysis System
Wed Jan 18 17:30:17 1995
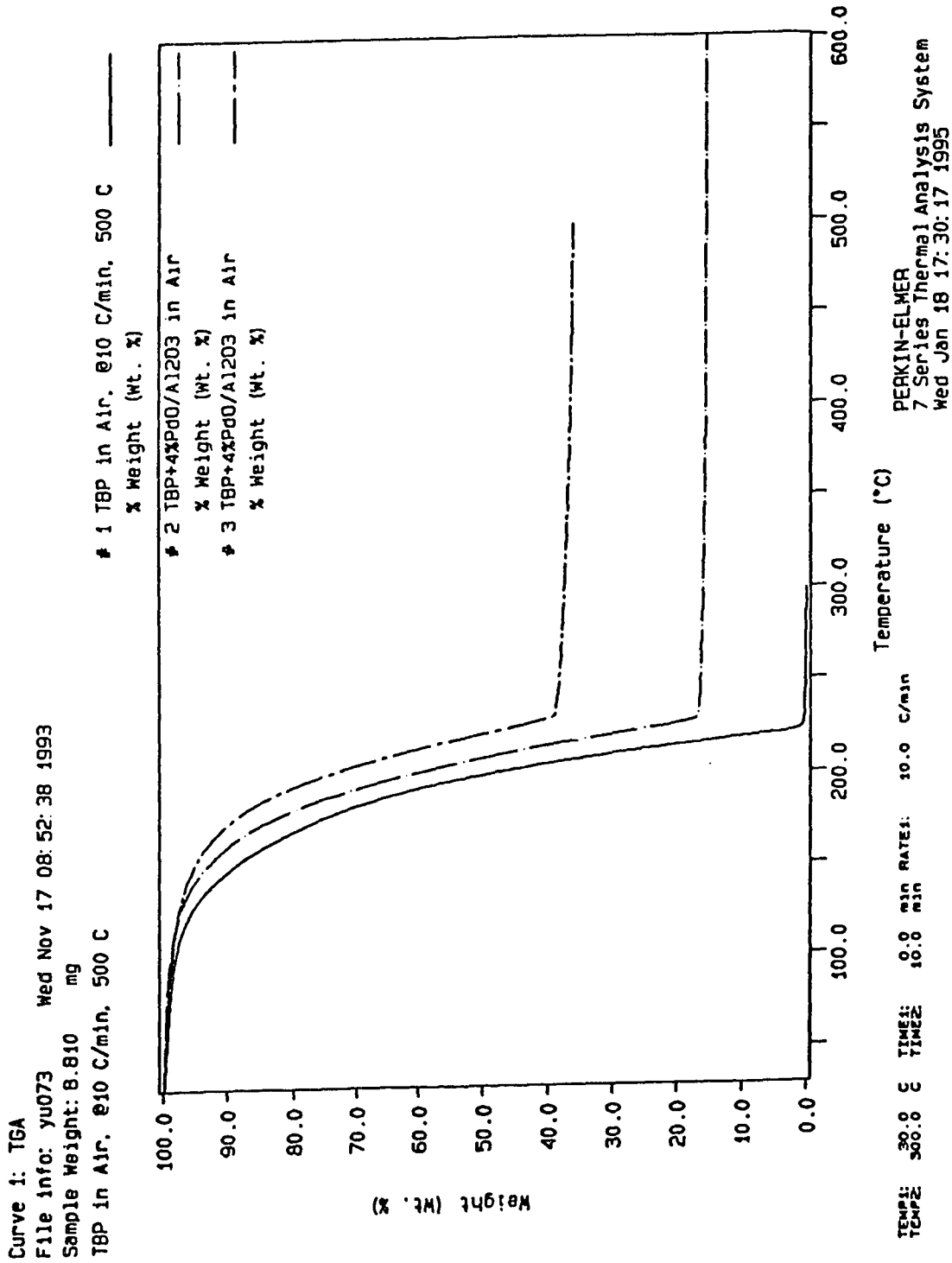
Figure 4.43 Thermal Gravimetric Analysis of TBP Combustion in Air and over PdO Catalyst.
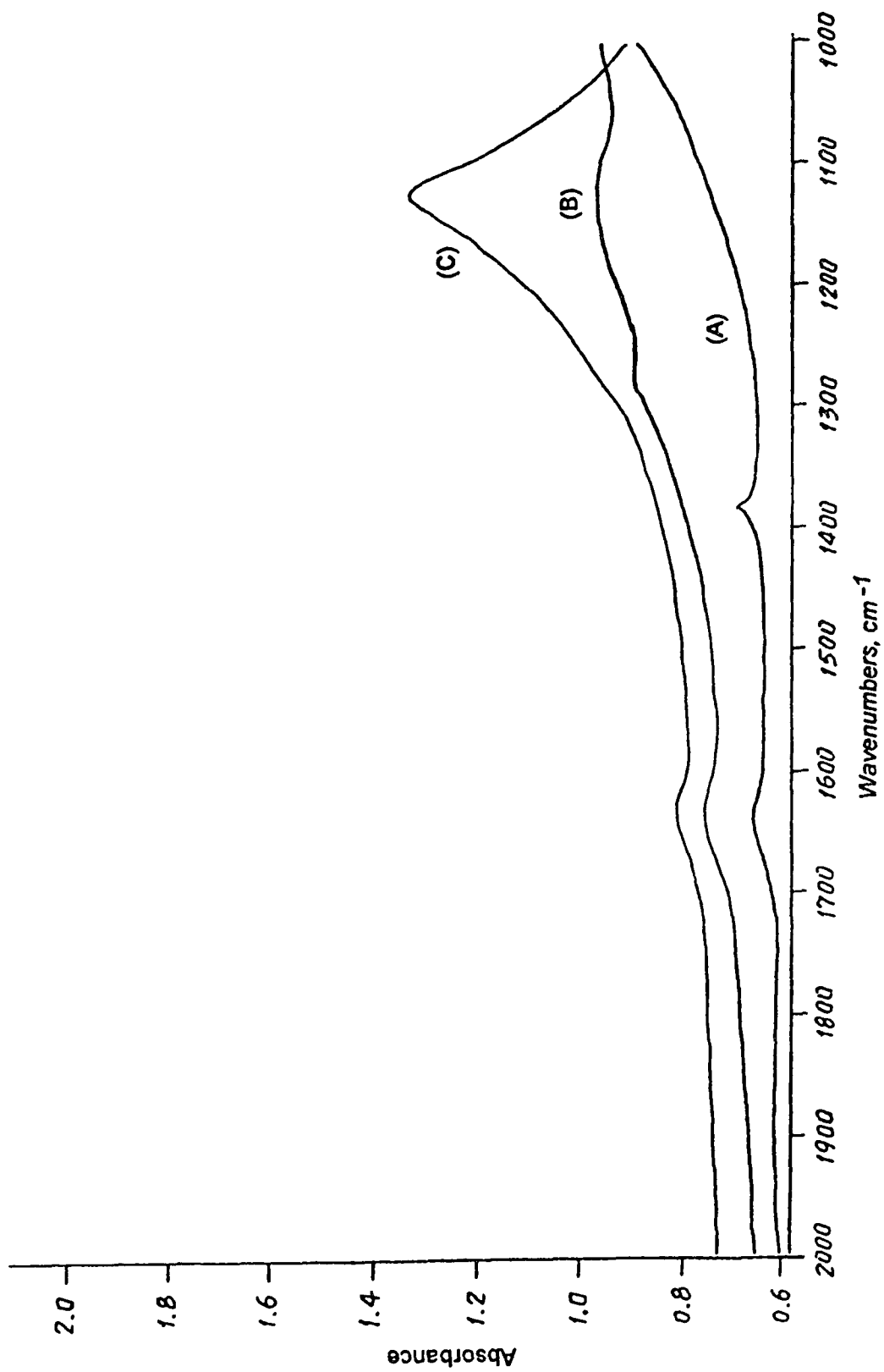
Figure 4.44 FT-IR Spectra of TBP Effect on Catalyst Deactivation as Function of Temperature: (A) Fresh Catalyst, (B) Treatment at 500 °C, (C) Treatment at 820 °C
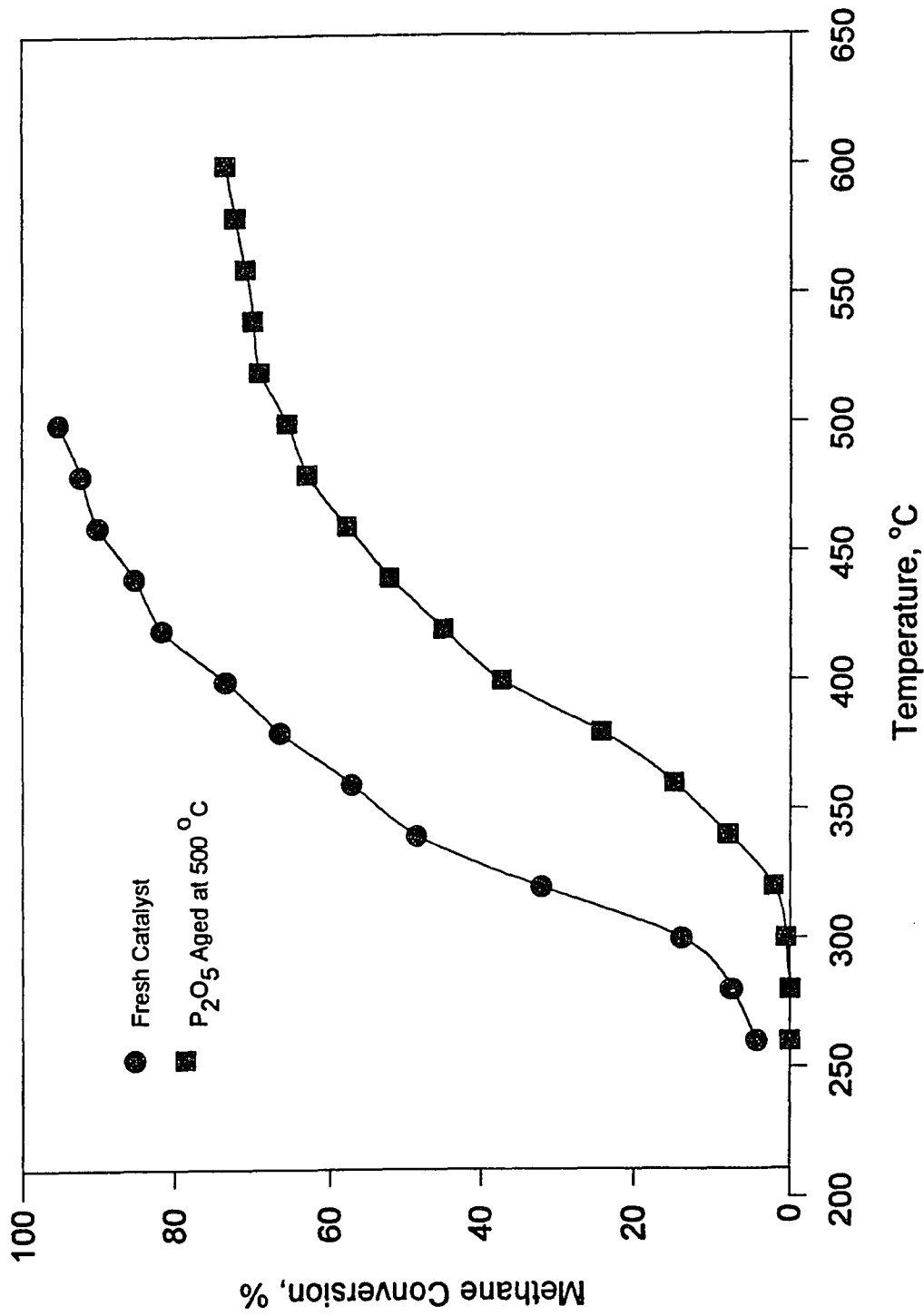
Figure 4.45 Methane Oxidation Activity as a Function of Temperature over Fresh and P_2O_5 Aged Catalyst

A mixture of 0.52 g P_2O_5 and 0.4 g PdO catalyst was aged for 120,000 simulated miles at 500 °C
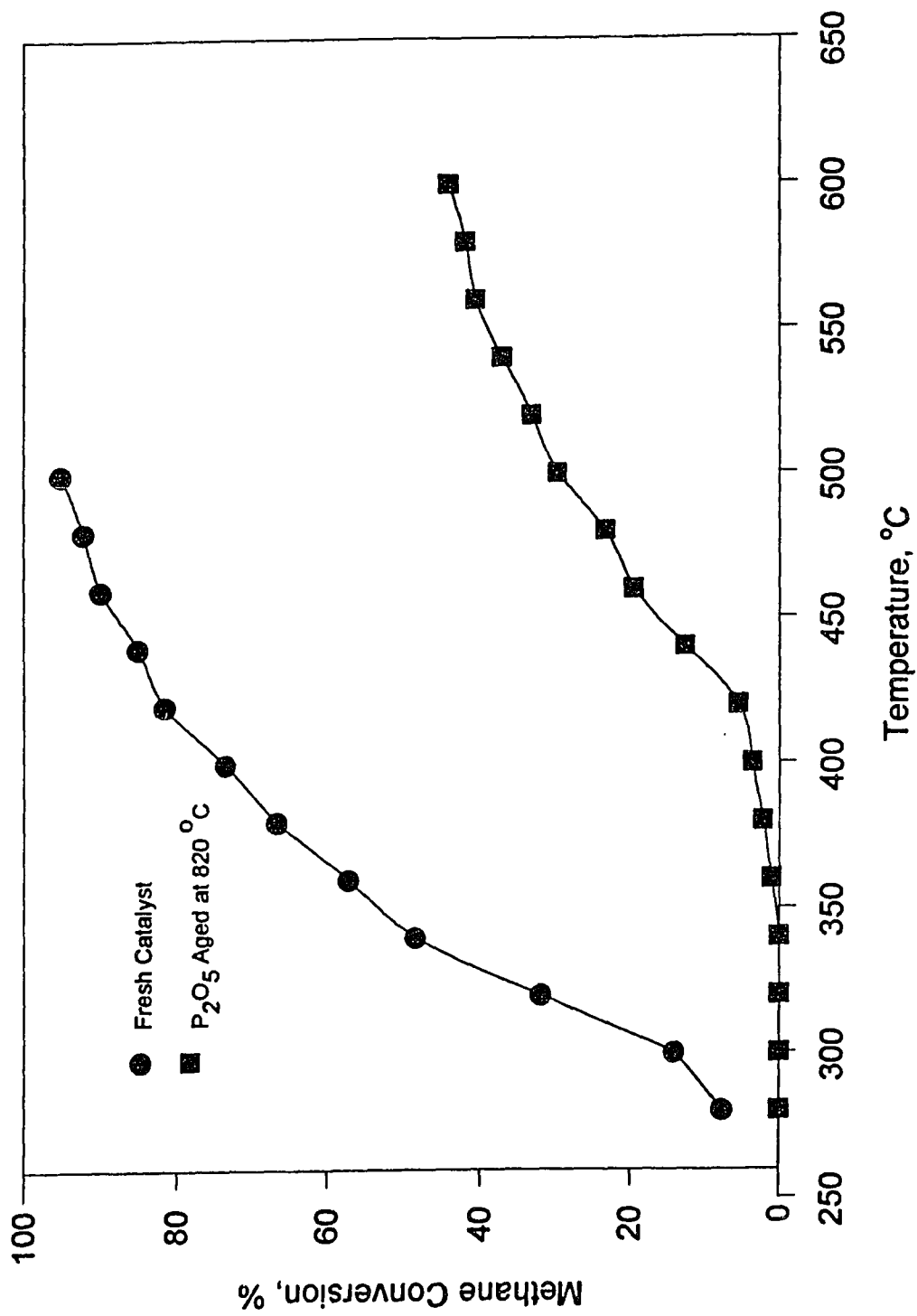
Figure 4.46 Methane Oxidation Activity as Function of Temperature over Fresh and P_2O_5 Aged Catalyst A mixture of 0.52 g P_2O_5 and 0.4 g PdO catalyst was aged for 120,000 simulated miles at 820 °C

Curve 1: TGA

File Info: yu081   Fri Mar 11 16:23:05 1994

Sample Weight: 2.433 mg

P205 in Air Atomosphere

1 P205 in Air Atomosphere

% Weight (Wt. %)

Weight (Wt. %)

120.0
110.0
100.0
90.0
80.0
70.0
60.0
50.0
40.0
30.0
20.0
10.0
0.0

0.0   200.0   400.0   600.0   800.0   1000.0

Temperature (°C)

PERKIN-ELMER
7 Series Thermal Analysis System
Thu Mar 30 13:13:07 1995

TEMP1: 20.0 C TIME1: 0.0 min RATE1: 20.0 C/min
TEMP2: 800.0 C TIME2: 0.0 min
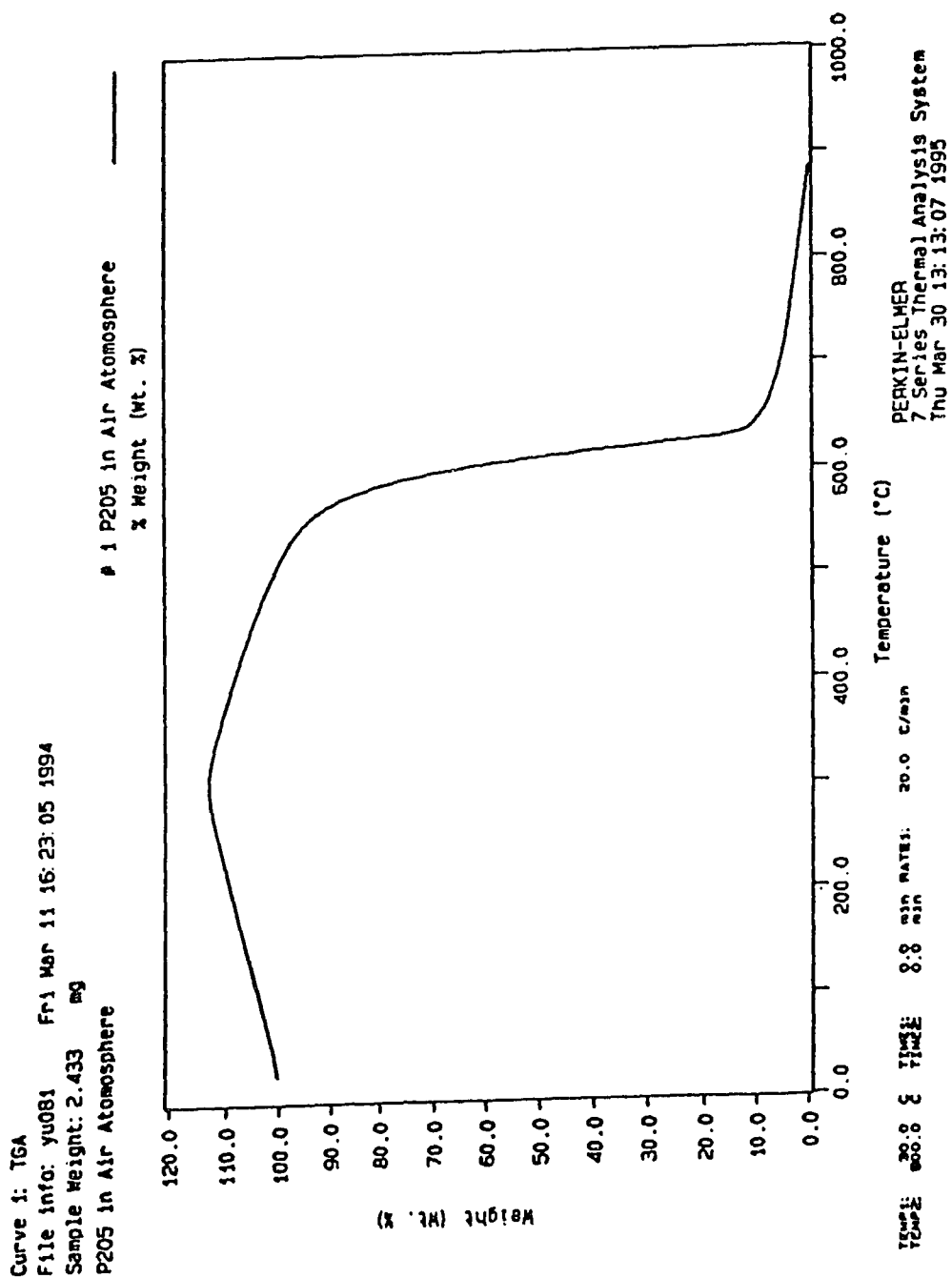
Figure 4.47 TGA Weight Change of Pure P_2O_5 in Air as a Function of Temperature.

Curve 1: TGA
File Info: yu005   Mon Feb 22 20:39:23 1993
Sample Weight: 1.091   mg
Fresh 4%PdO Catalyst

X1	25.883 °C
X2	797.283 °C
Y1	100.135 Wt. %
Y2	93.473 Wt. %
ΔY	-6.662 Wt. %

PERKIN-ELMER
7 Series Thermal Analysis System
Thu Mar 30 13:55:00 1995

Temperature (°C)

Weight (Wt. %)

ΔY
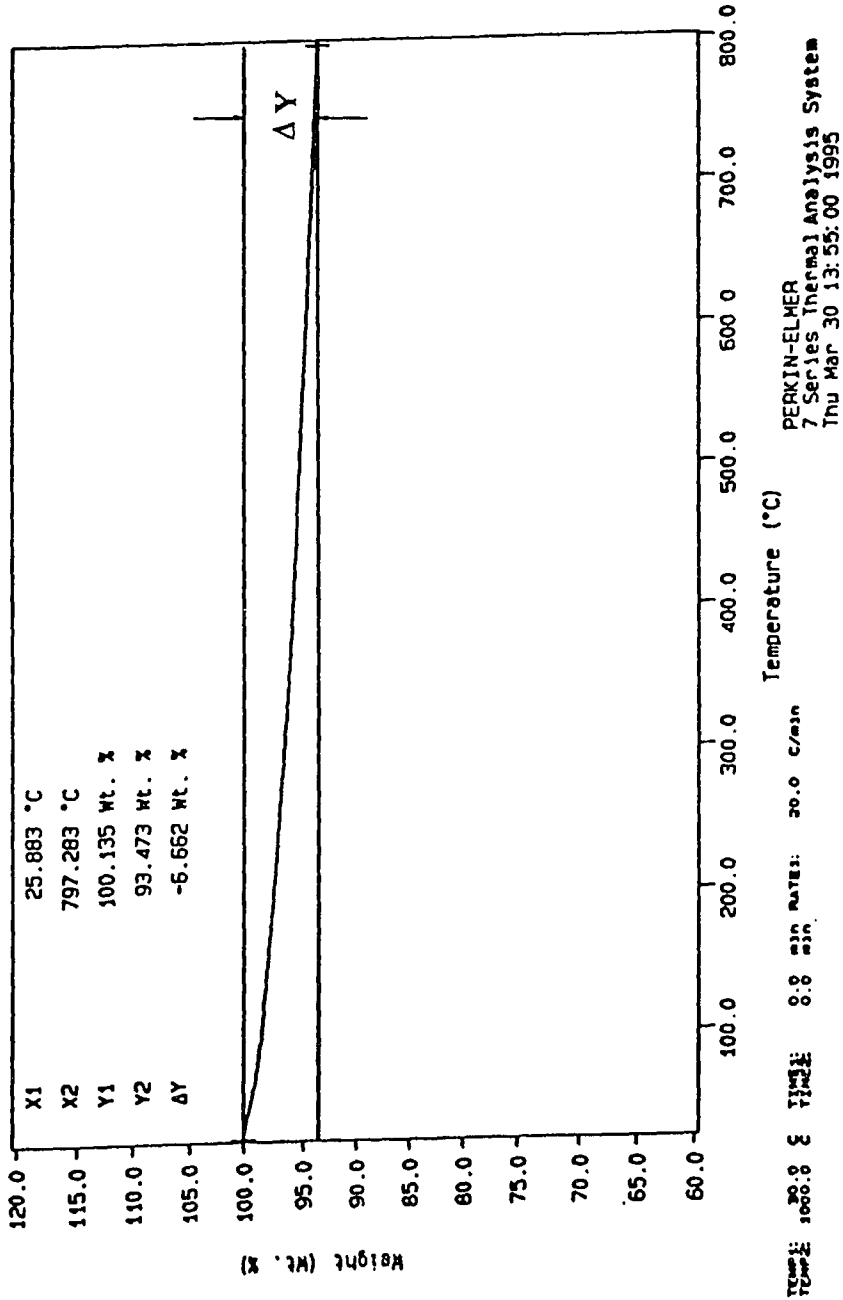
Figure 4.48 TGA Weight Change of Fresh PdO Catalyst in Air as a Function of Temperature.

Curve 1: TGA
File Info: yul09   Fri Sep 16 14:28:38 1994
Sample Weight: 12.958   mg
P205+4XP40/A1203 in Air

X1	0.000 min	
X2	36.667 min	
Y1	12.967 mg	
Y2	11.574 mg	
ΔY	-1.393 mg	

ΔY

Time (minutes)

Weight (mg)

18.0
16.0
14.0
12.0
10.0
8.0
6.0
4.0
2.0
0.0

0.0   25.0   50.0   75.0   100.0   125.0   150.0

PERKIN-ELMER
7 Series Thermal Analysis System
Thu Mar 30 13:19:25 1995

6.900 mg 4XP40/A1203
TEMP1: 30.0 C TIME1: 0.0 min RATE1: 20.0 C/min
TEMP2: 120.0 C TIME2: 120.0 min
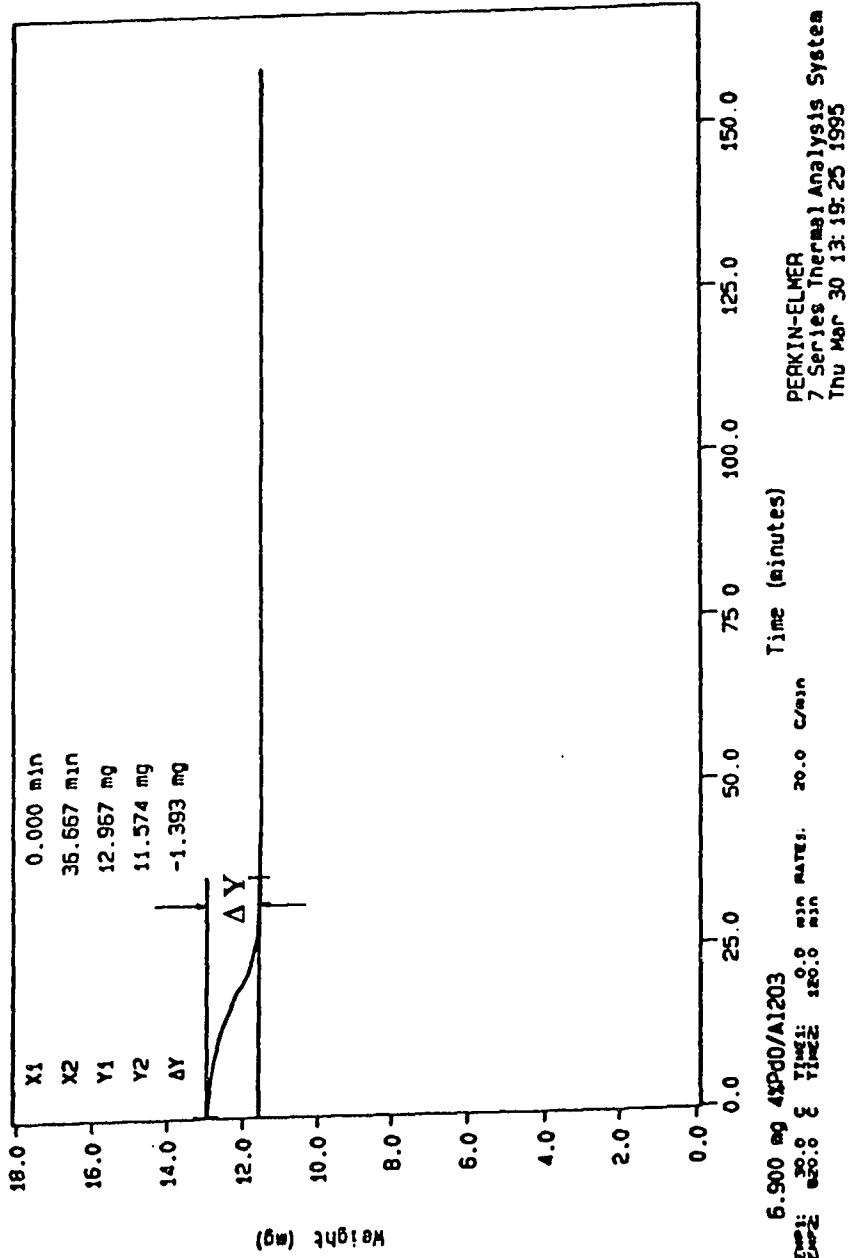
Figure 4.49 TGA Weight Change of P_2O_5 Mixed with Catalyst in Air as a Function of Time

Curve 1: TGA

File Info: yu085   Mon Mar 14 16:53:40 1994

Sample Weight: 7.073   mg

P2O5+PdO in Air

X1	25.050	°C
X2	848.666	°C
Y1	7.079	mg
Y2	6.390	mg
ΔY	-0.689	mg

Weight (mg)

Temperature (°C)

ΔY

PERKIN-ELMER
7 Series Thermal Analysis System
Thu Mar 30 13:22:05 1995

2.963 mg P2O5
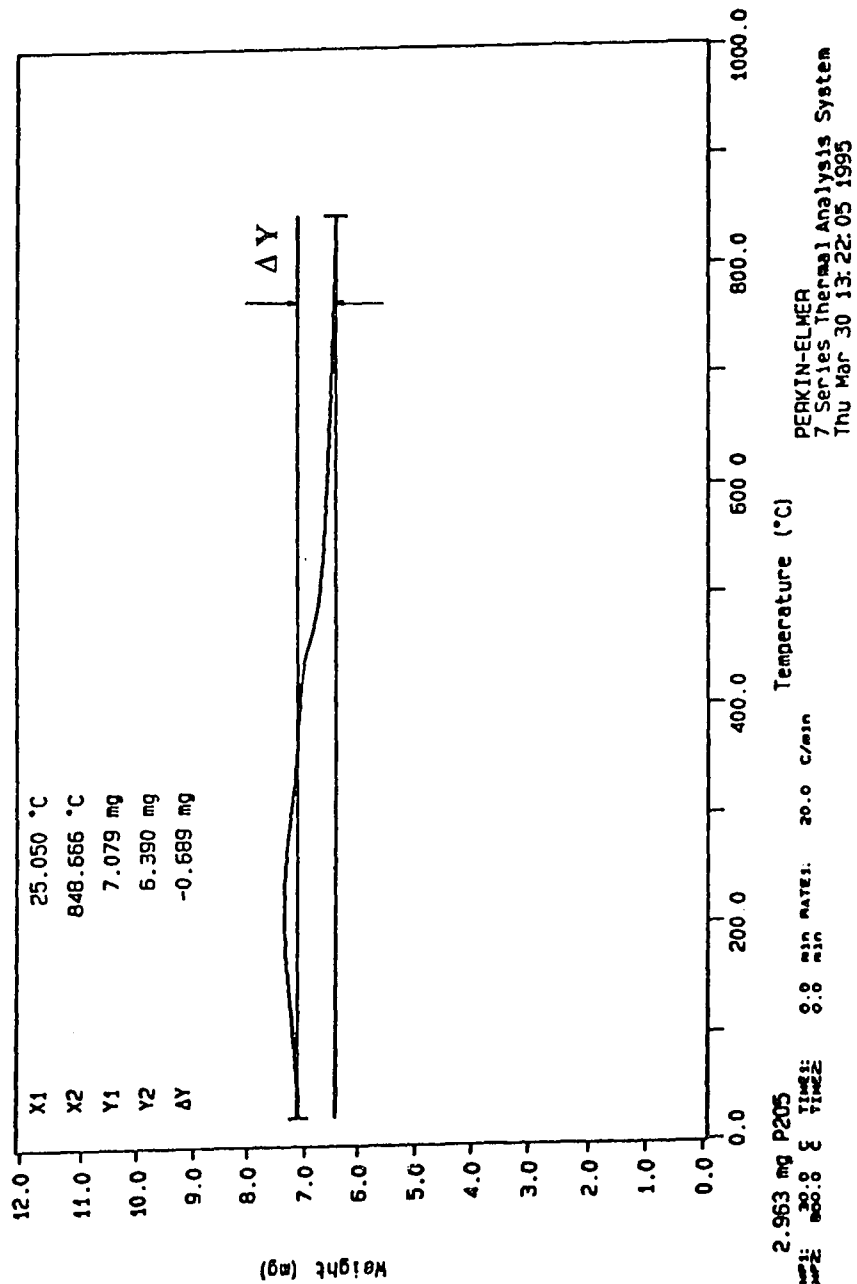
Figure 4.50 TGA Weight Change of P_2O_5 mixed with Pure PdO in Air as a Function of Temperature.

Curve 1: TGA

File Info: yu084   Mon Mar 14 12:51:36 1994
Sample Weight: 11.386   mg
P205+Al203 in Air

X1	24.966	°C
X2	848.883	°C
Y1	11.392	mg
Y2	9.717	mg
ΔY	-1.675	mg
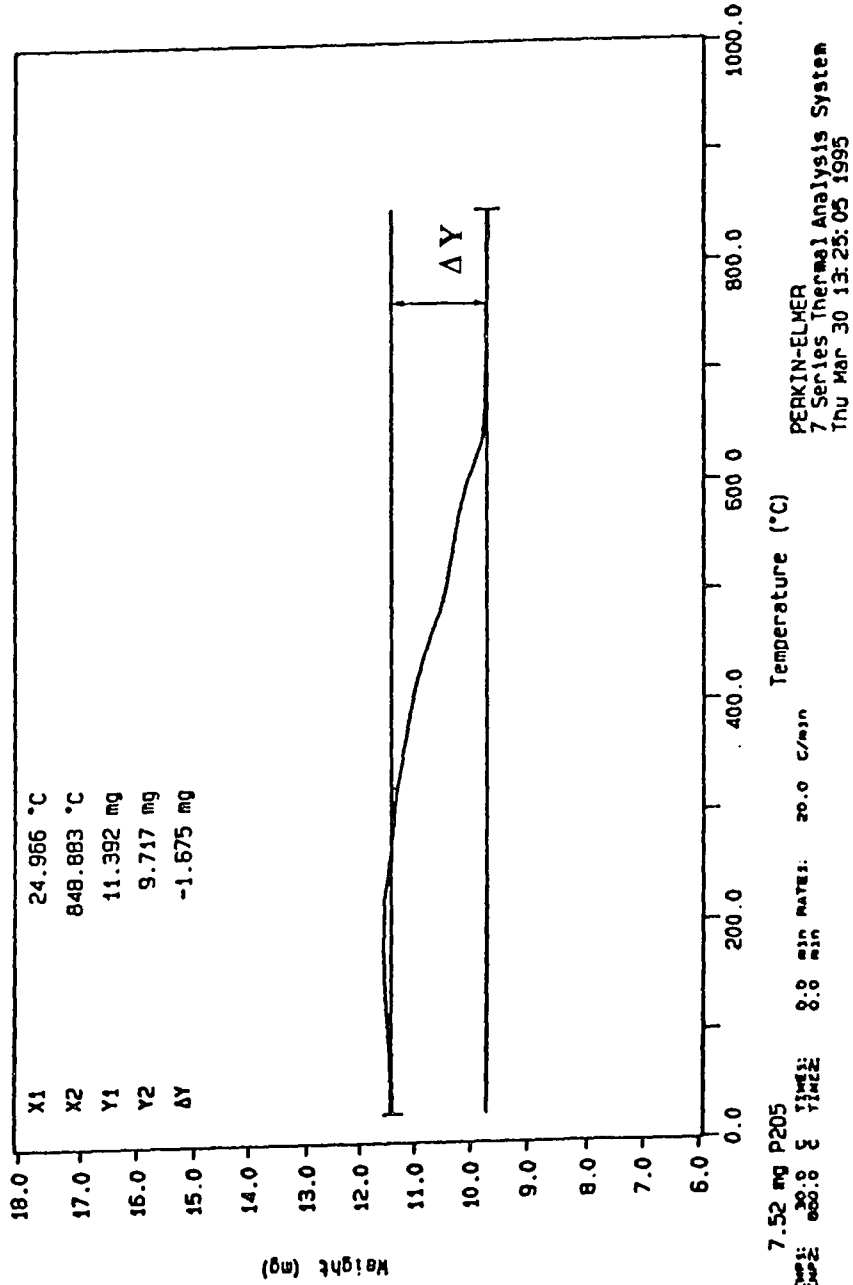
Figure 4.51 TGA Weight Change of P_2O_5 mixed with Pure γ-Alumina in Air as a Function of Temperature.
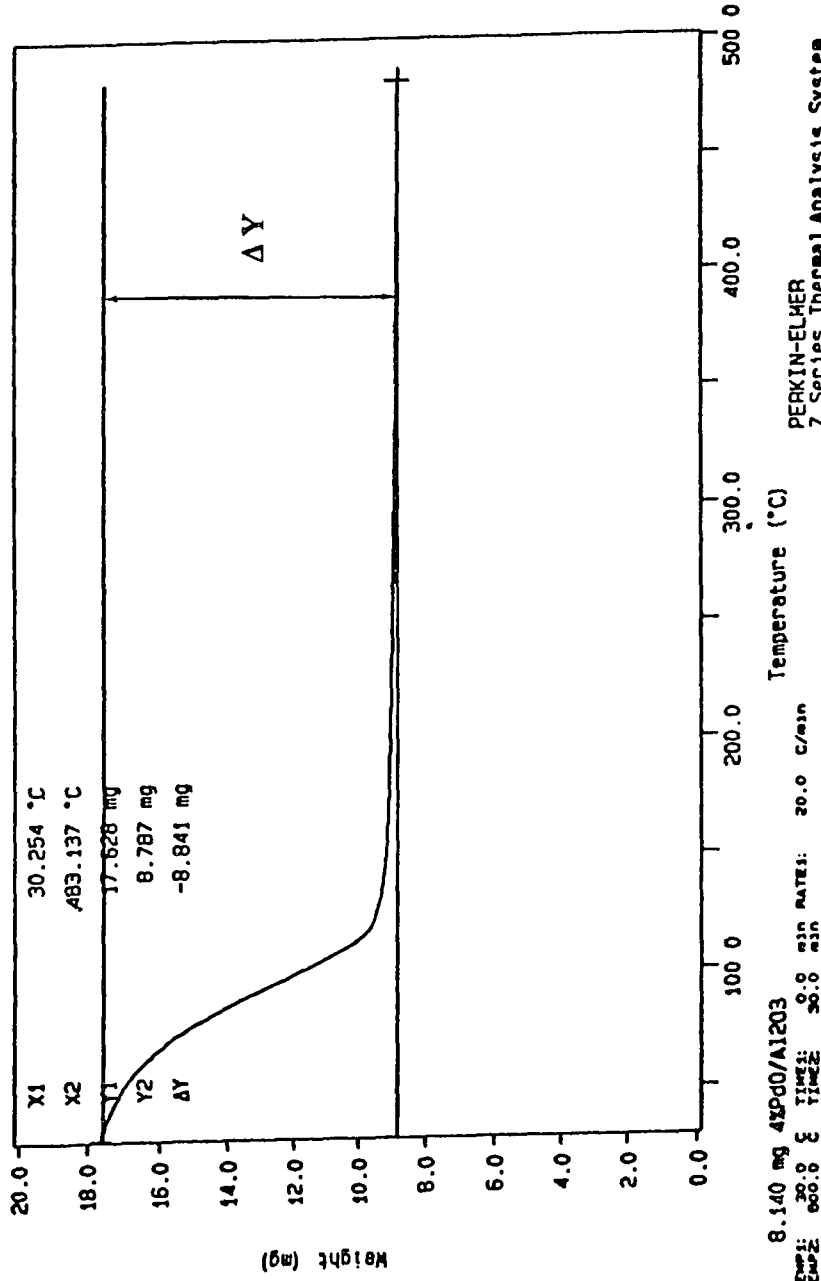
Figure 4.52 TGA Weight Change of Catalyst Prepared by Incipient Wetness of P_2O_5 Solution in Air as a Function of Temperature (to 500 °C).

Curve 1: TGA

File Info: yu112 . Mon Oct 3 10:28:15 1994

Sample Weight: 23.028 mg

11.2 wt% in H2O+ 4%Pd0/Al2O3

X1   38.420 °C

X2   791.070 °C

Y1   22.997 mg

Y2   11.607 mg.

ΔY   -11.390 mg

ΔY

Weight (mg)

Temperature (°C)

10.840 mg 4%Pd0/Al2O3

TEMP: 20.0 C TIME: 0.0 min RATE: 20.0 C/min

TEMP: 820.0 C TIME: 30.0 min
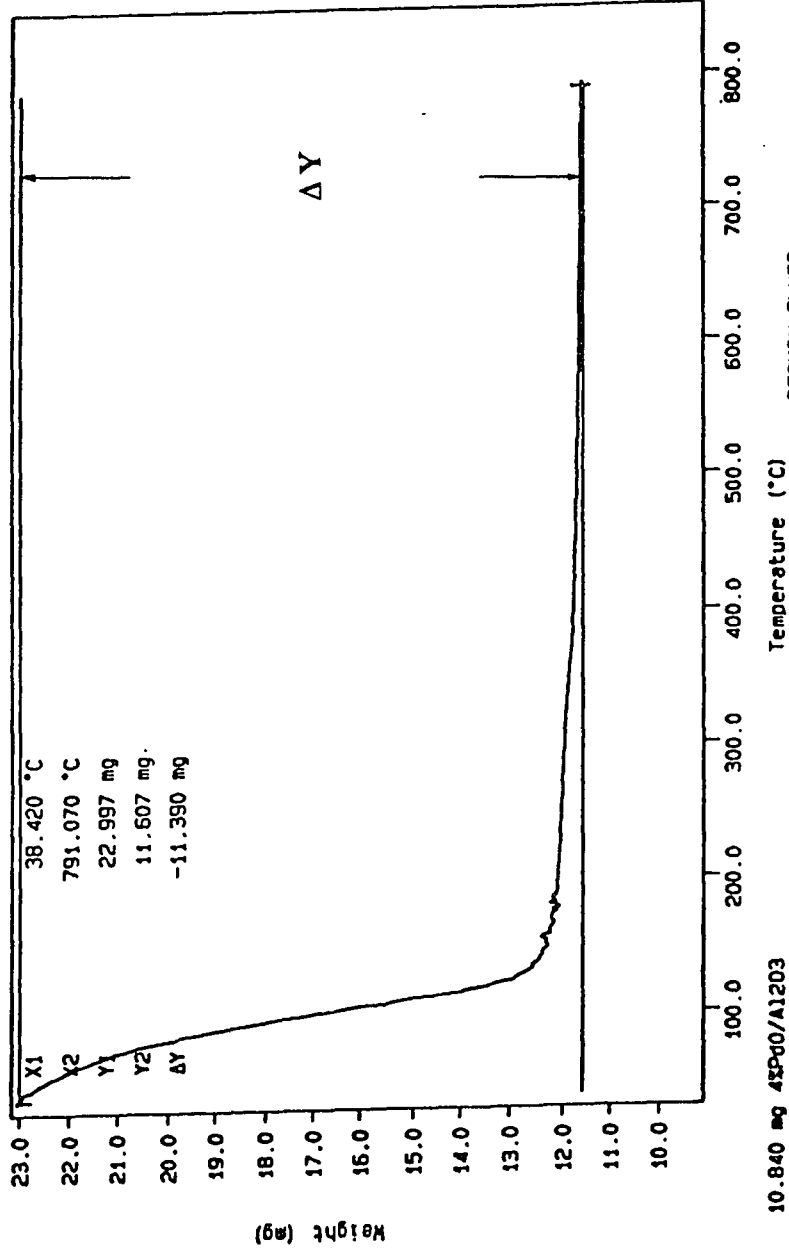
PERKIN-ELMER

7 Series Thermal Analysis System

Thu Mar 30 13:28:49 1995

Figure 4.53 TGA Weight Change of Catalyst Prepared by Incipient Wetness of P_2O_5 Solution in Air as a Function of Temperature (to 820 °C).
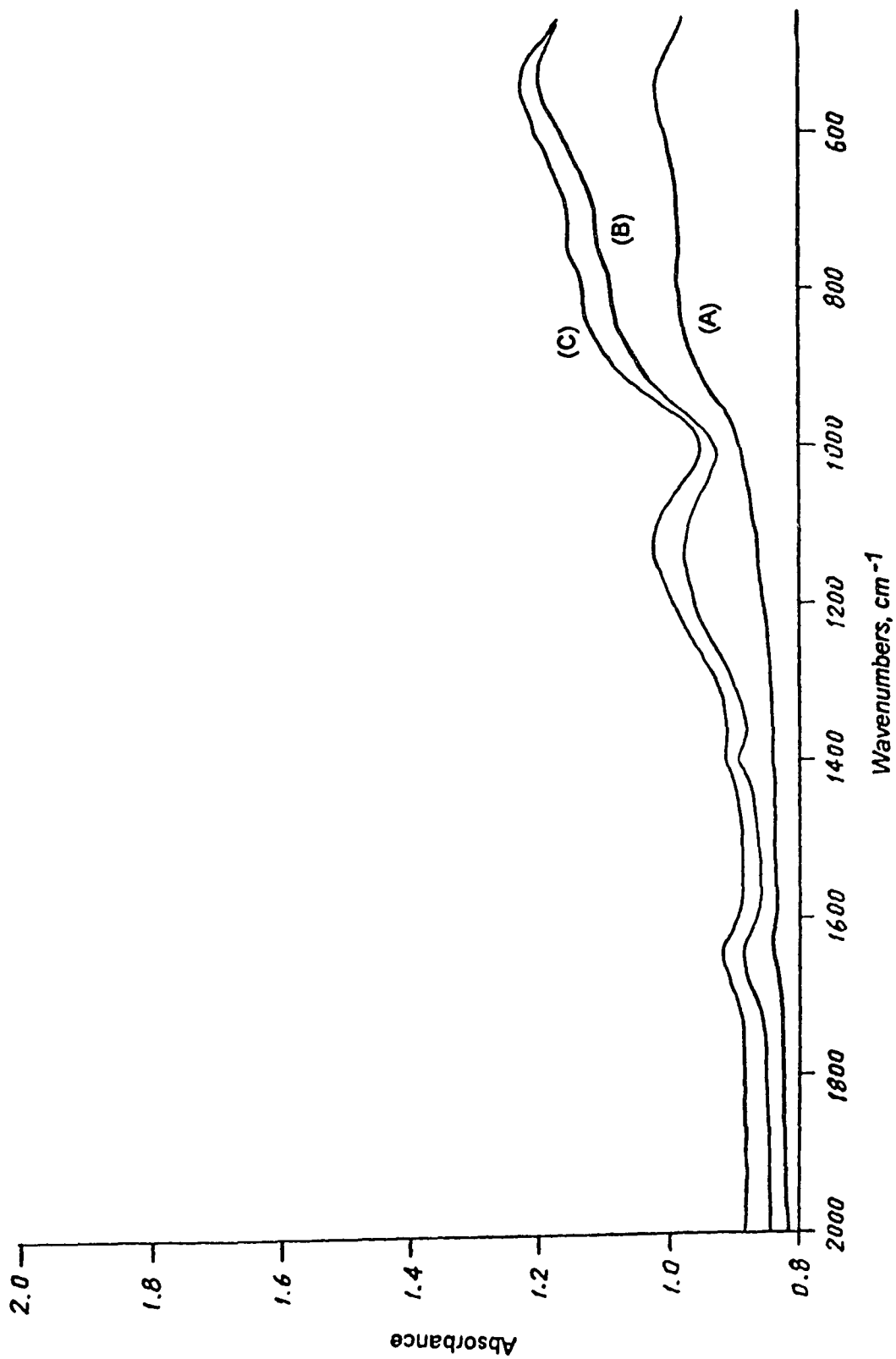
Figure 4.54 FT-IR Spectra of P_2O_5 Effect on Catalyst Deactivation as a Function of Temperature: (A) Fresh Catalyst, (B) Treatment at 500 °C, (C) Treatment at 820 °C
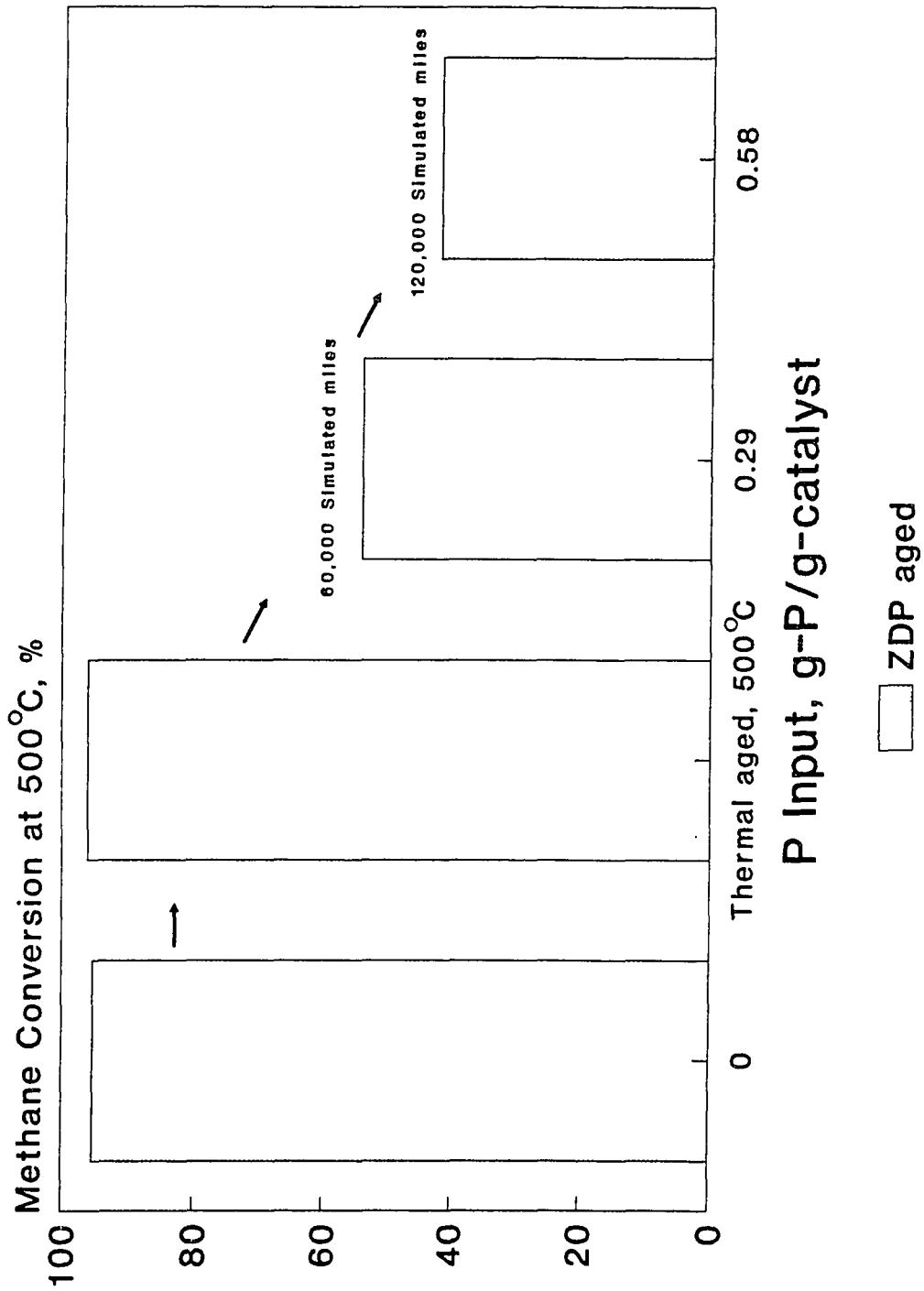
Figure 4.55 Simulation of Automotive Catalyst Poisoning Due to ZDP Effect on Methane Oxidation
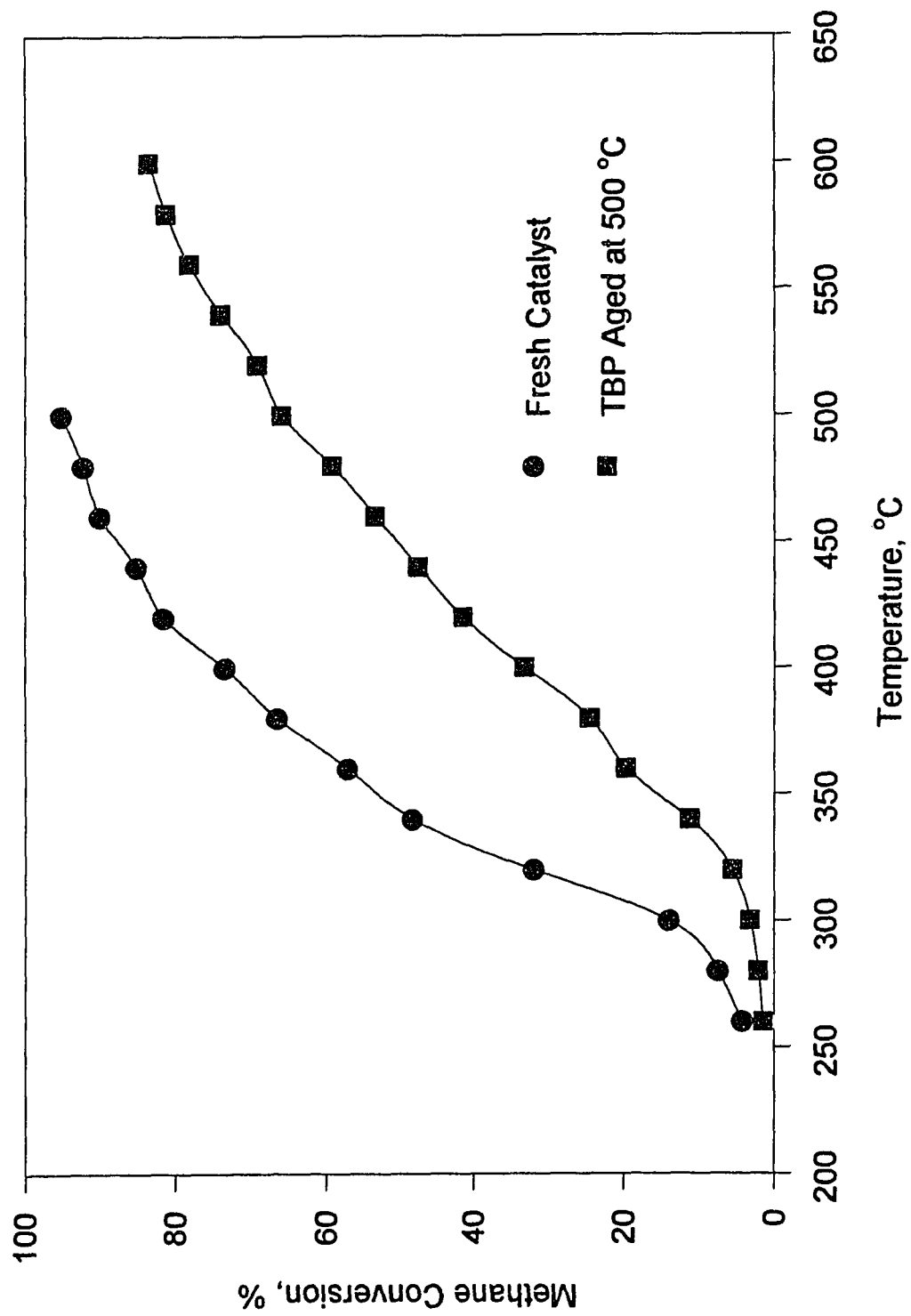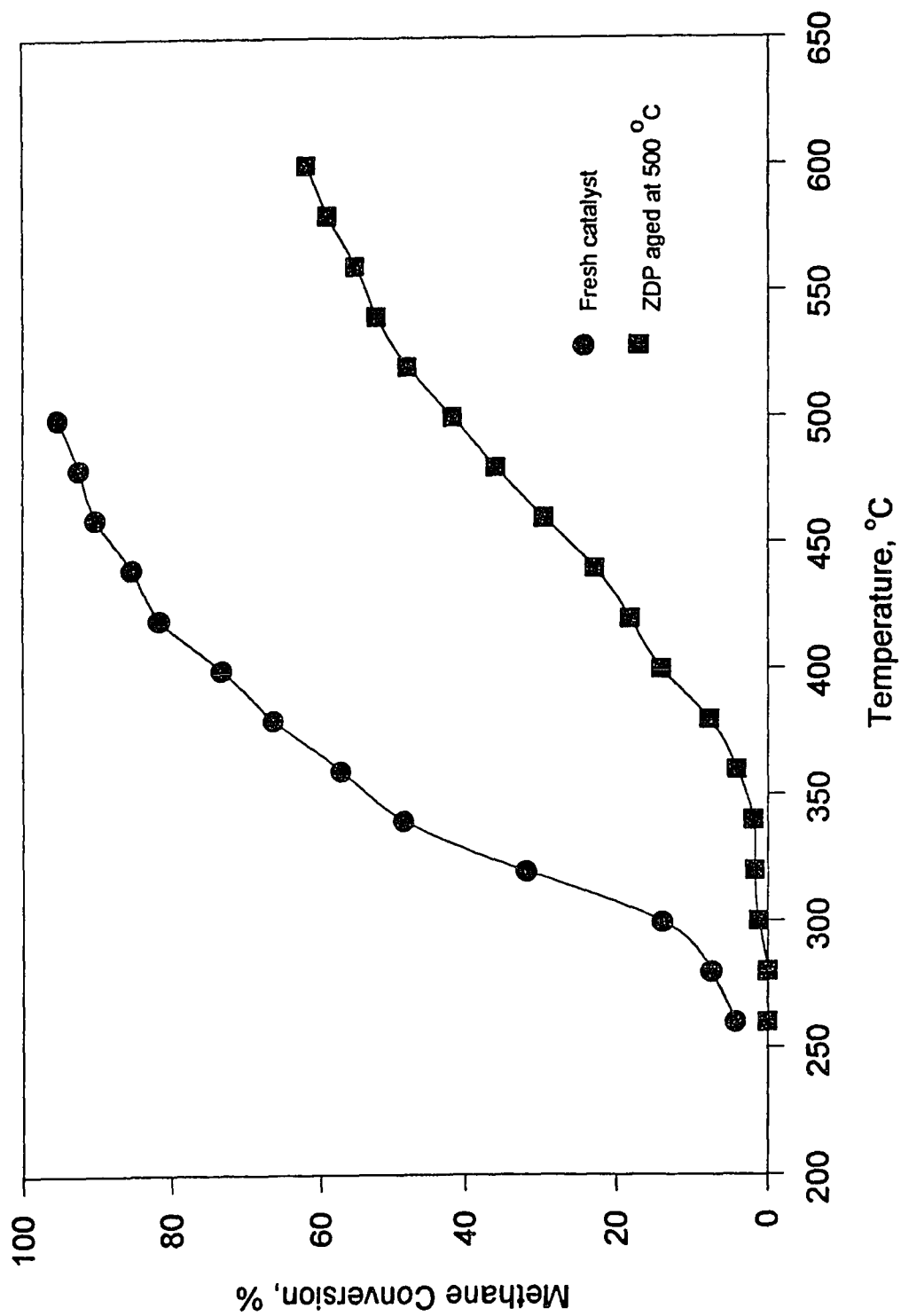
Figure 4.56 Methane Oxidation Activity as a Function of Temperature over Fresh and ZDP Aged Catalyst The Catalyst was aged by ZDP for 120,000 simulated miles
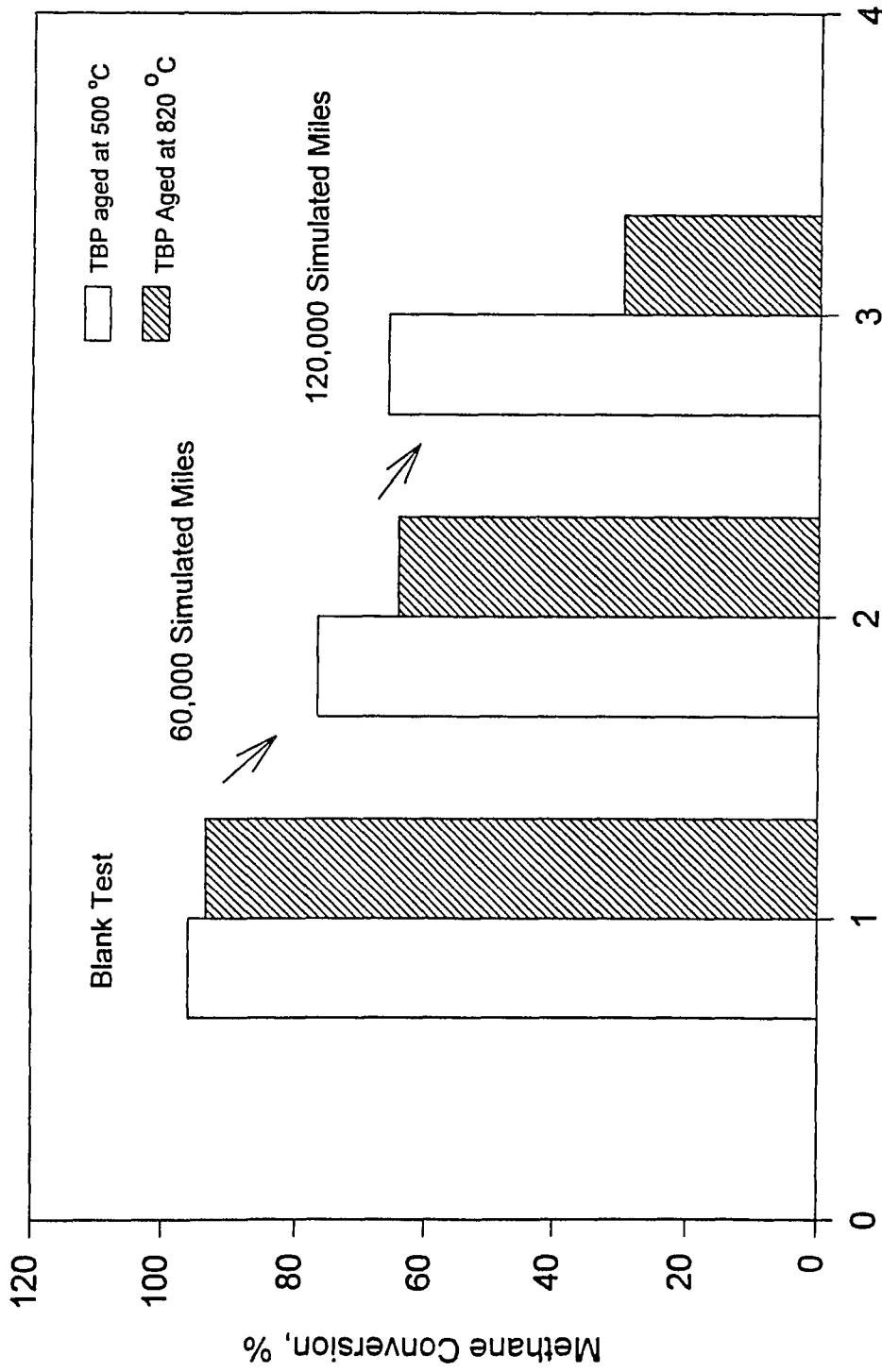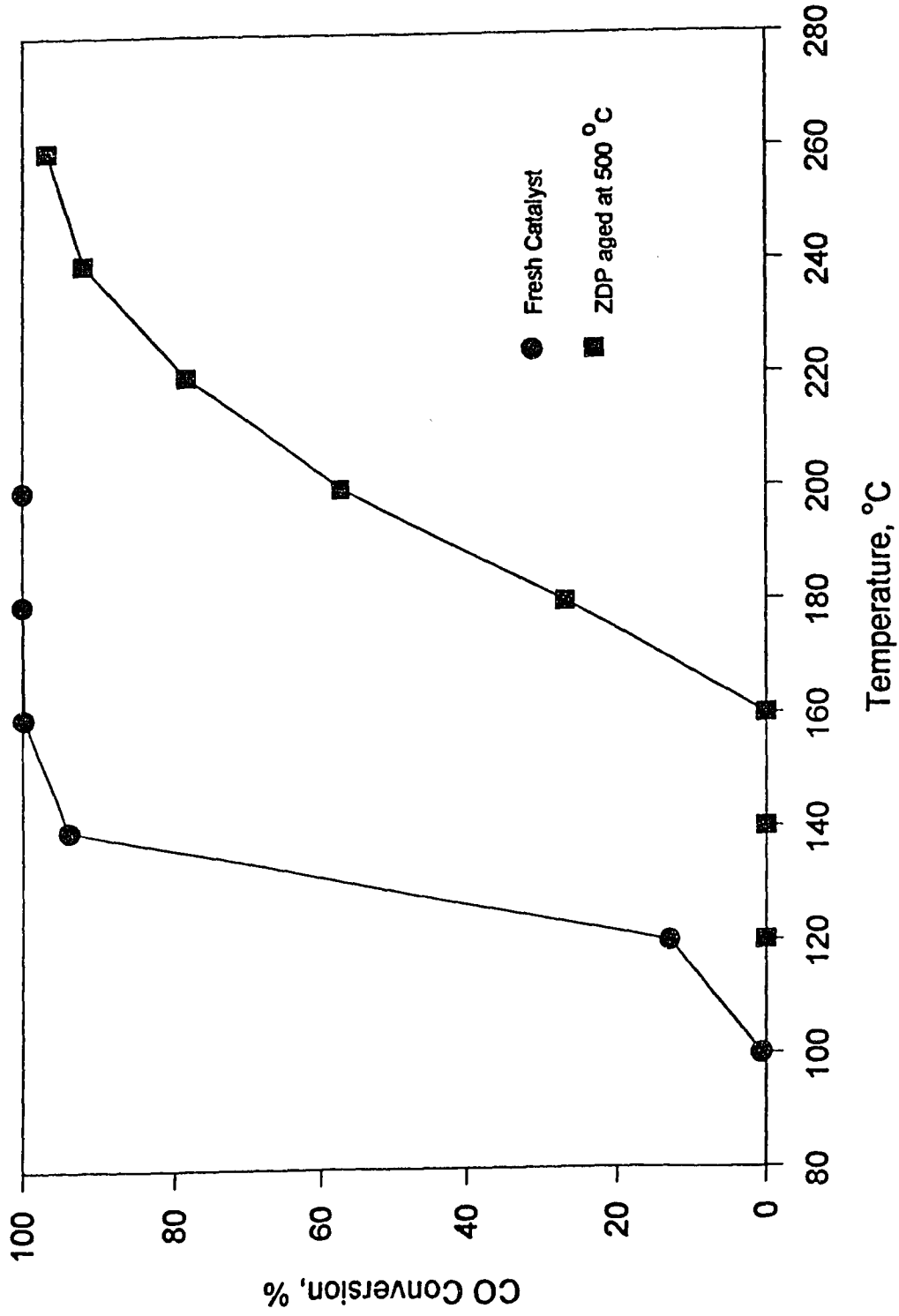
Figure 4.57 ZDP Effect on CO Oxidation over 4% PdO/γ-Alumina Catalyst as a Function of Temperature Pulsator-aged 120,000 Simulated Miles
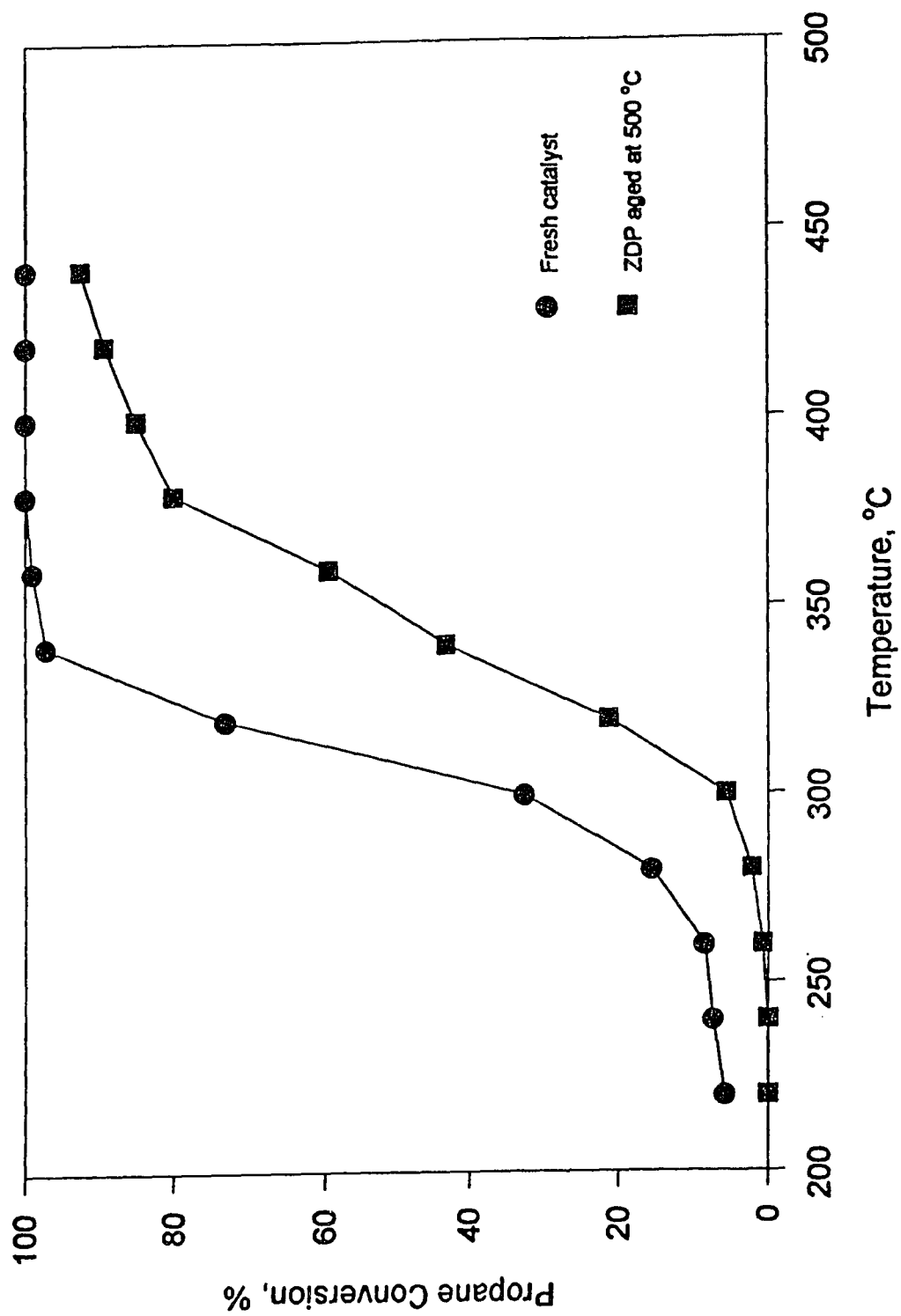
Figure 4.58 ZDP Effect on Propane Oxidation over 4% PdO/γ-Alumina Catalyst as a Function of Temperature
Pulsator-aged 120,000 Simulated Miles
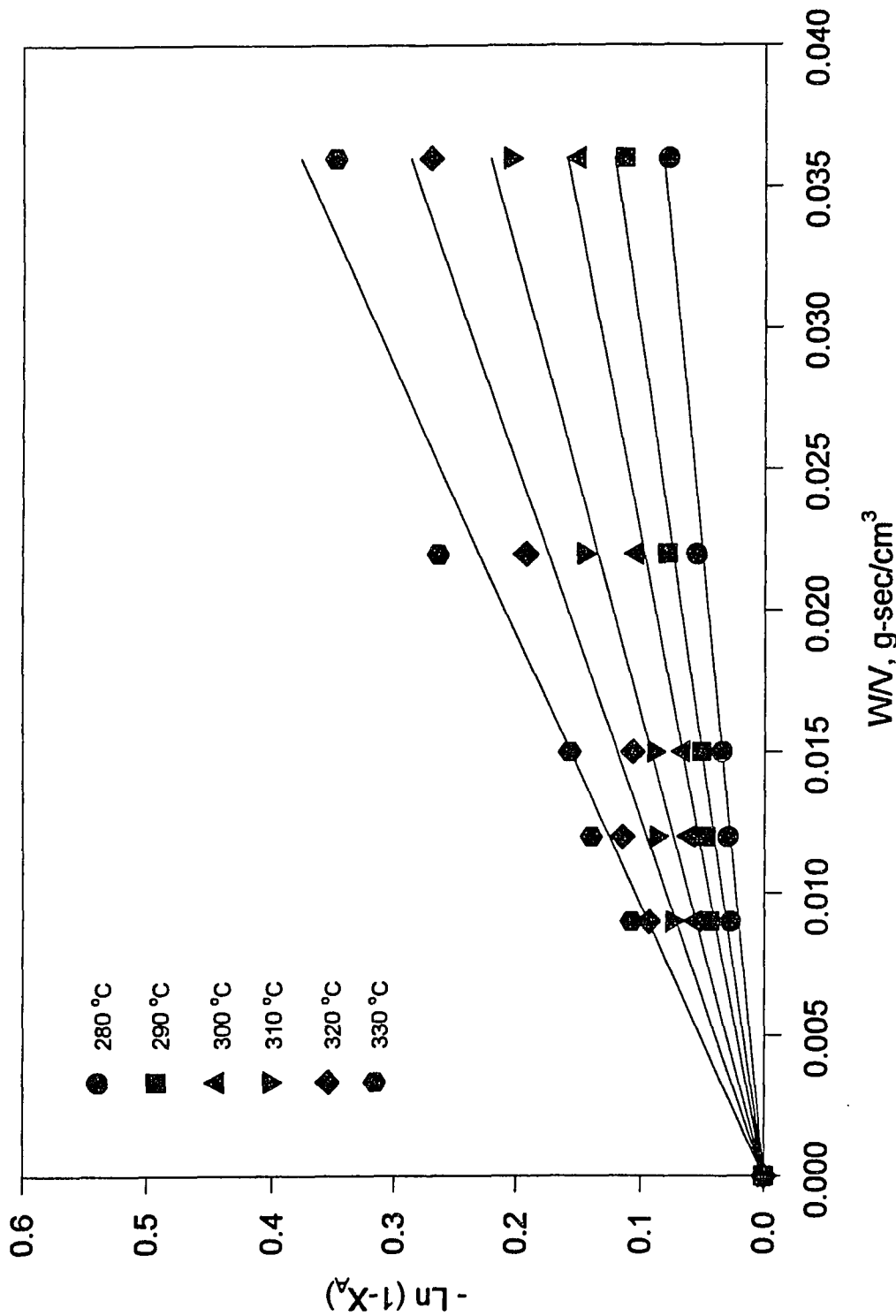
Figure 4.59 The Plots of -Ln $(1-X_A)$ versus W/V for Methane Oxidation over Fresh Catalyst
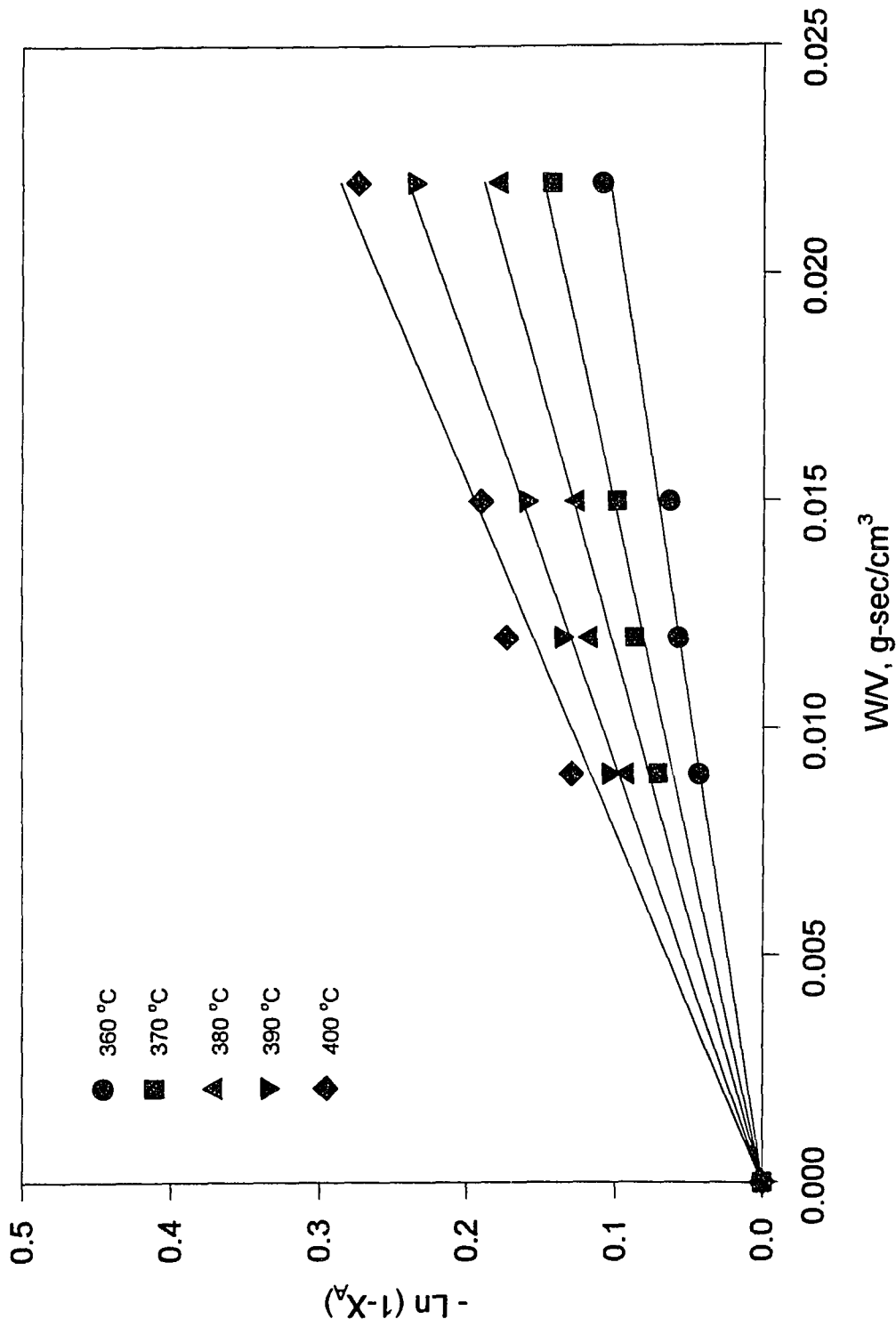
Figure 4.60 The Plots of $-\text{Ln}\,(1\text{-}X_A)$ versus W/V for Methane Oxidation over ZDP Aged Catalyst Pulsator-aged 120,000 simulated miles at 500 °C
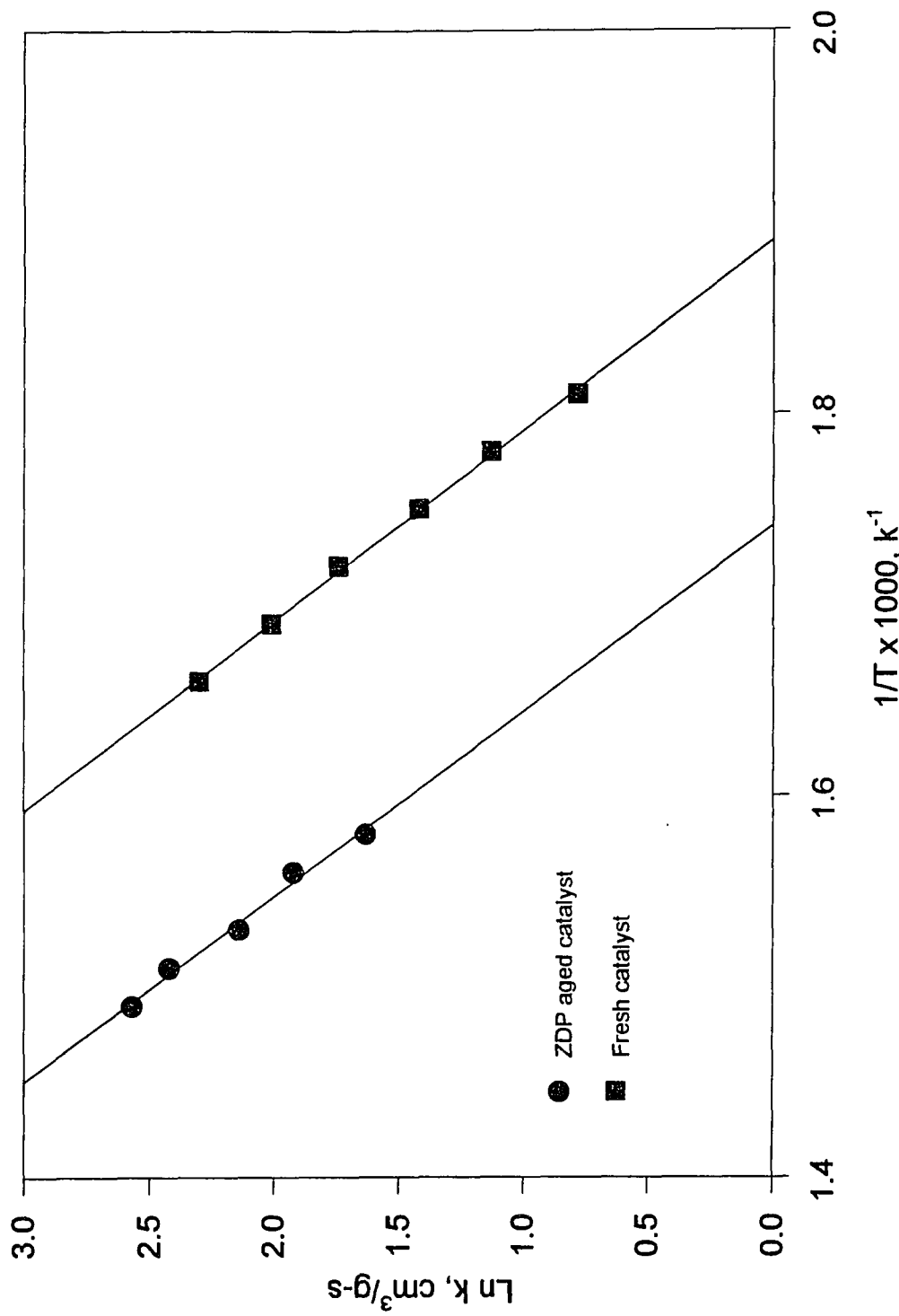
Figure 4.61 The Arrhenius Plots of Ln k versus 1/T for Methane Oxidation over Fresh and ZDP Aged Catalyst Pulsator-aged 120,000 simulated miles at 500 °C
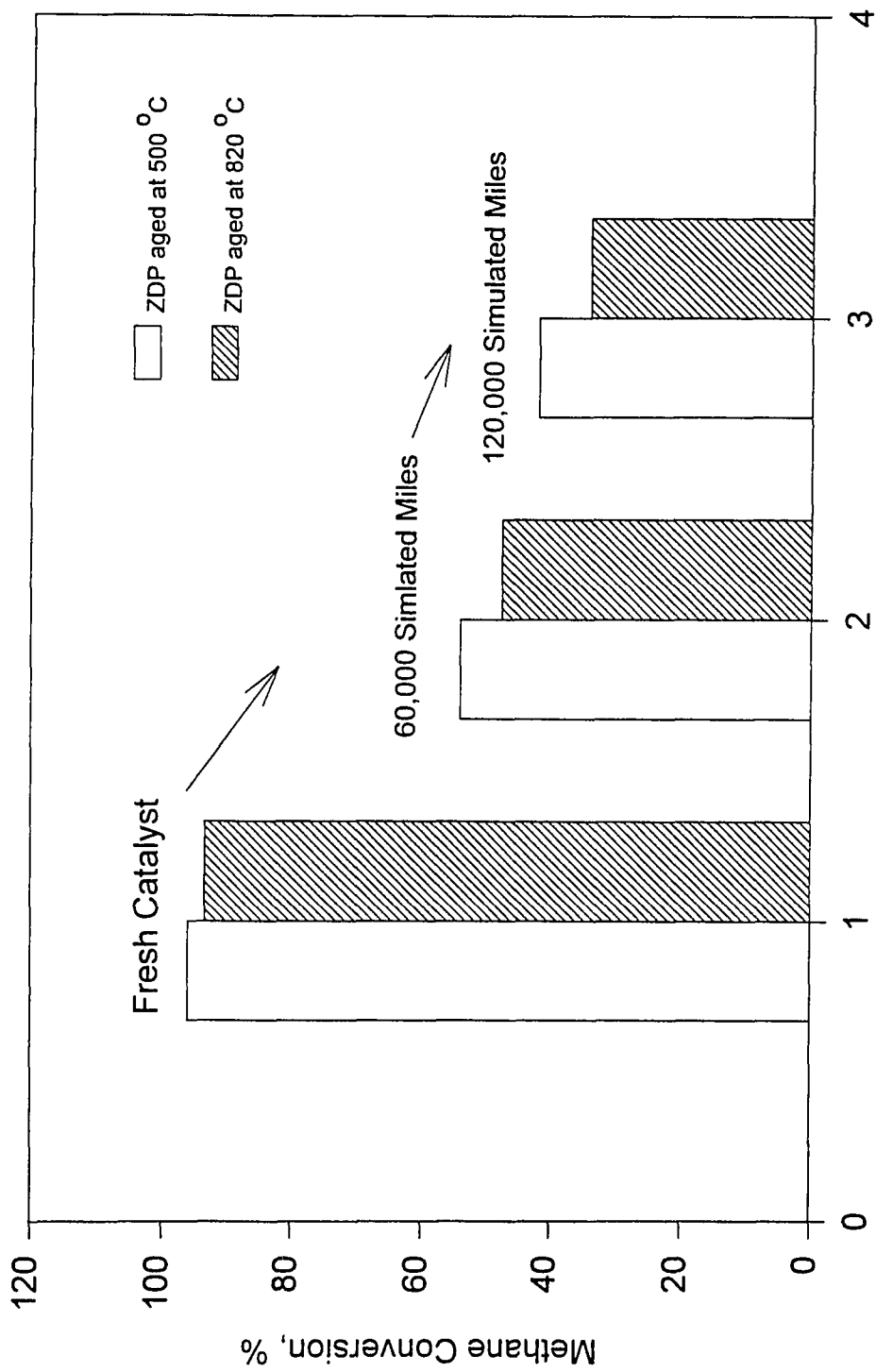
Figure 4.62 Temperature and ZDP Effects on Methane Oxidation over Palladium Catalysts

Curve 1: TGA
File Info: yu100   Fri Jul 29 09:30:10 1994
Sample Weight: 29.146   mg
ZDP Combustion in Air

1 ZDP Combustion in Air
Weight (mg)

2 ZDP/7.765mg 4%Pd0/Al2)3
Weight (mg)

35.0

30.0

25.0

20.0

15.0

10.0

5.0

0.0

Weight (mg)

0.0   200.0   400.0   500.0   800.0   1000.0

Temperature (°C)

TEMP1: 49.9 °C   TIME1: 0.0 min RATE1: 20.0 C/min
TEMP2: 800.0 °C   TIME2:

Paul
PERKIN-ELMER
7 Series Thermal Analysis System
Thu Mar 30 13:38:03 1995
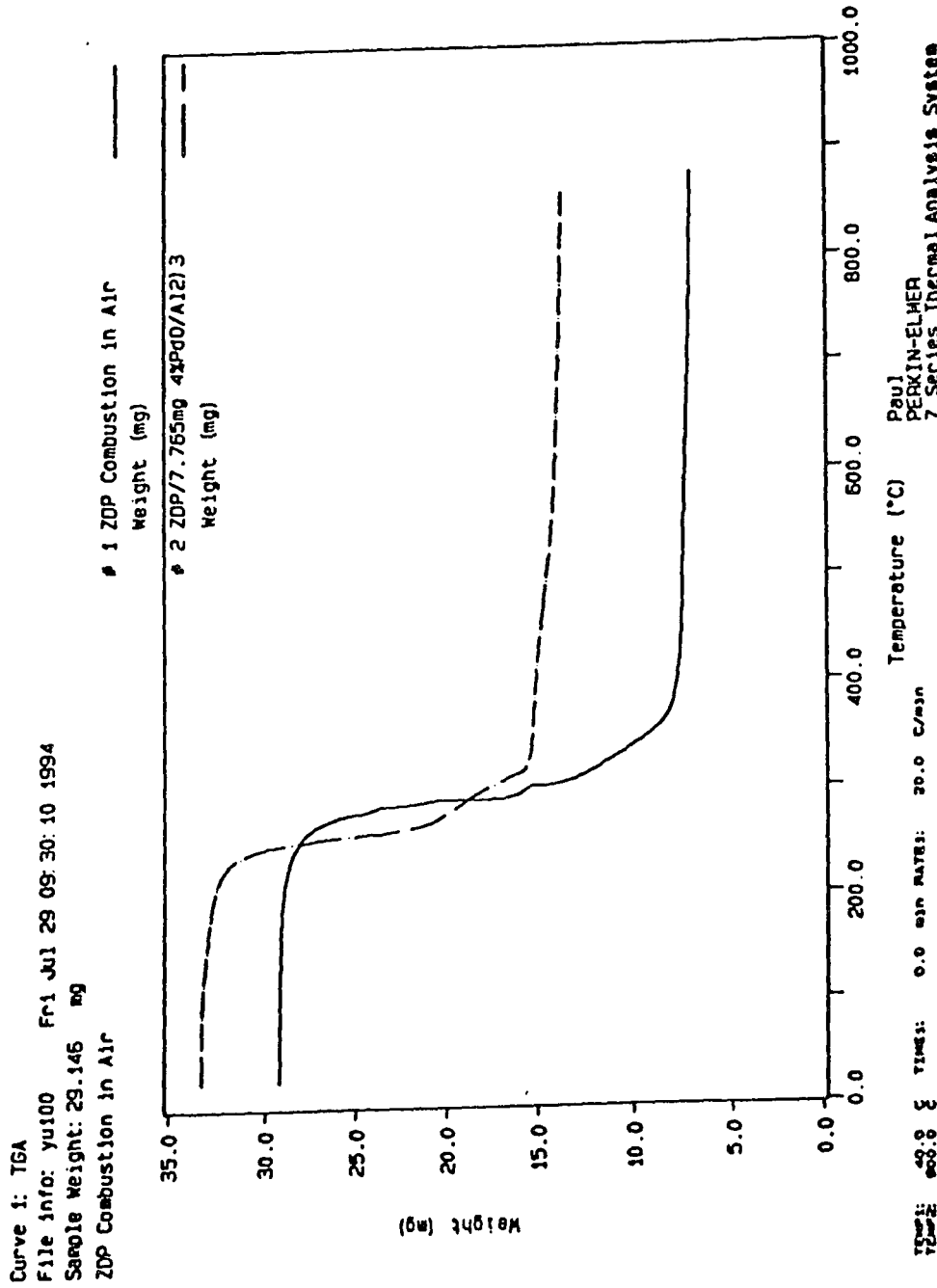
Figure 4.63 TGA Comparison of the Weight Change of ZDP Combustion in Air and over Catalyst.
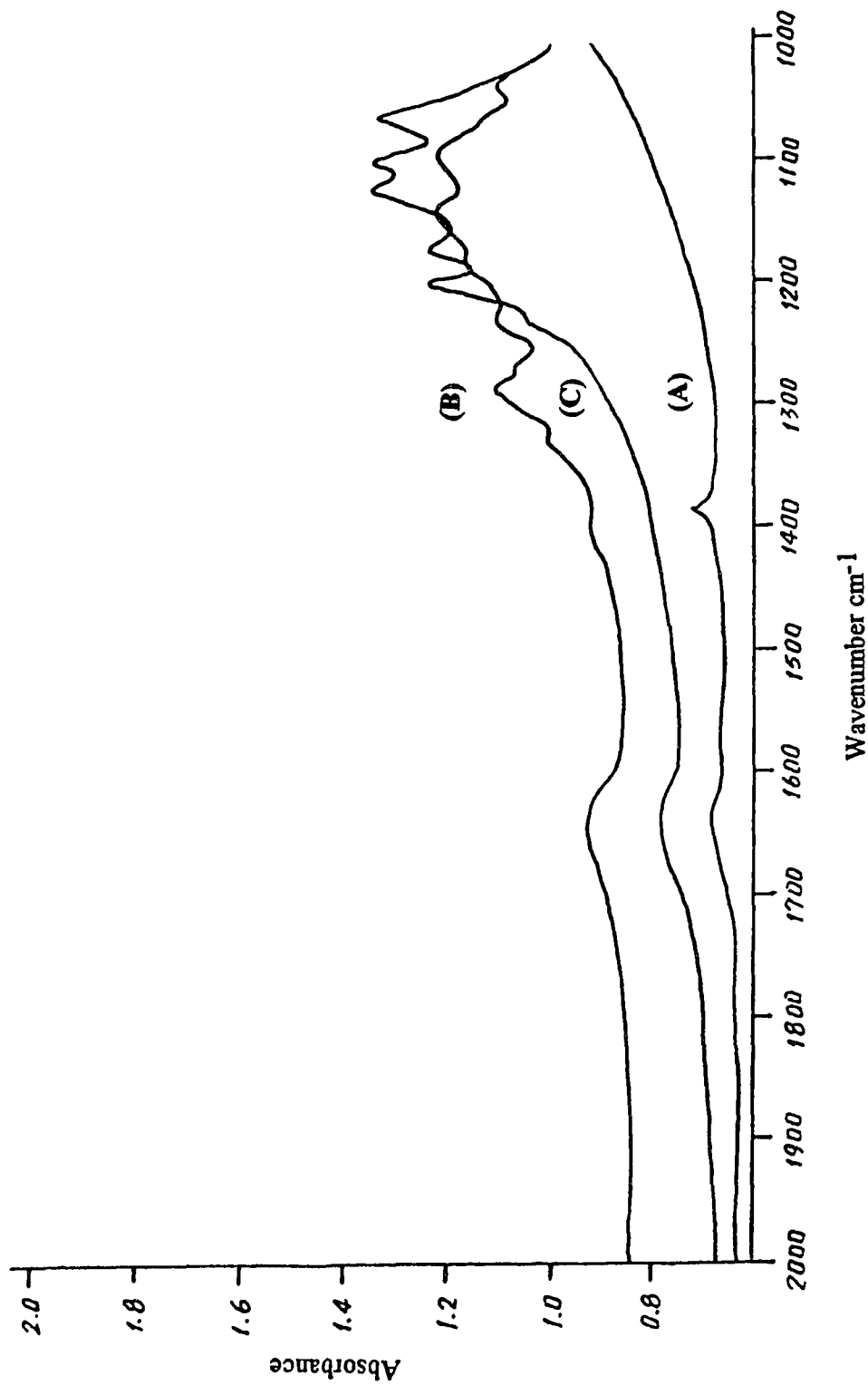
Figure 4.64 Comparison of FT-IR Spectra of the Catalyst Deactivated with ZDP at 500 °C and 820 °C (A) Fresh Catalyst, (B) Aged at 500 °C, (C) Aged at 820 °C.

ZDP820 28-44 DEG

Zinc Pyrophosphate Characteristic Patterns

2 θ	Intensity, %
29.5	100
35.2	30
42.95	25

Bragg Angle, 2θ

Intensity
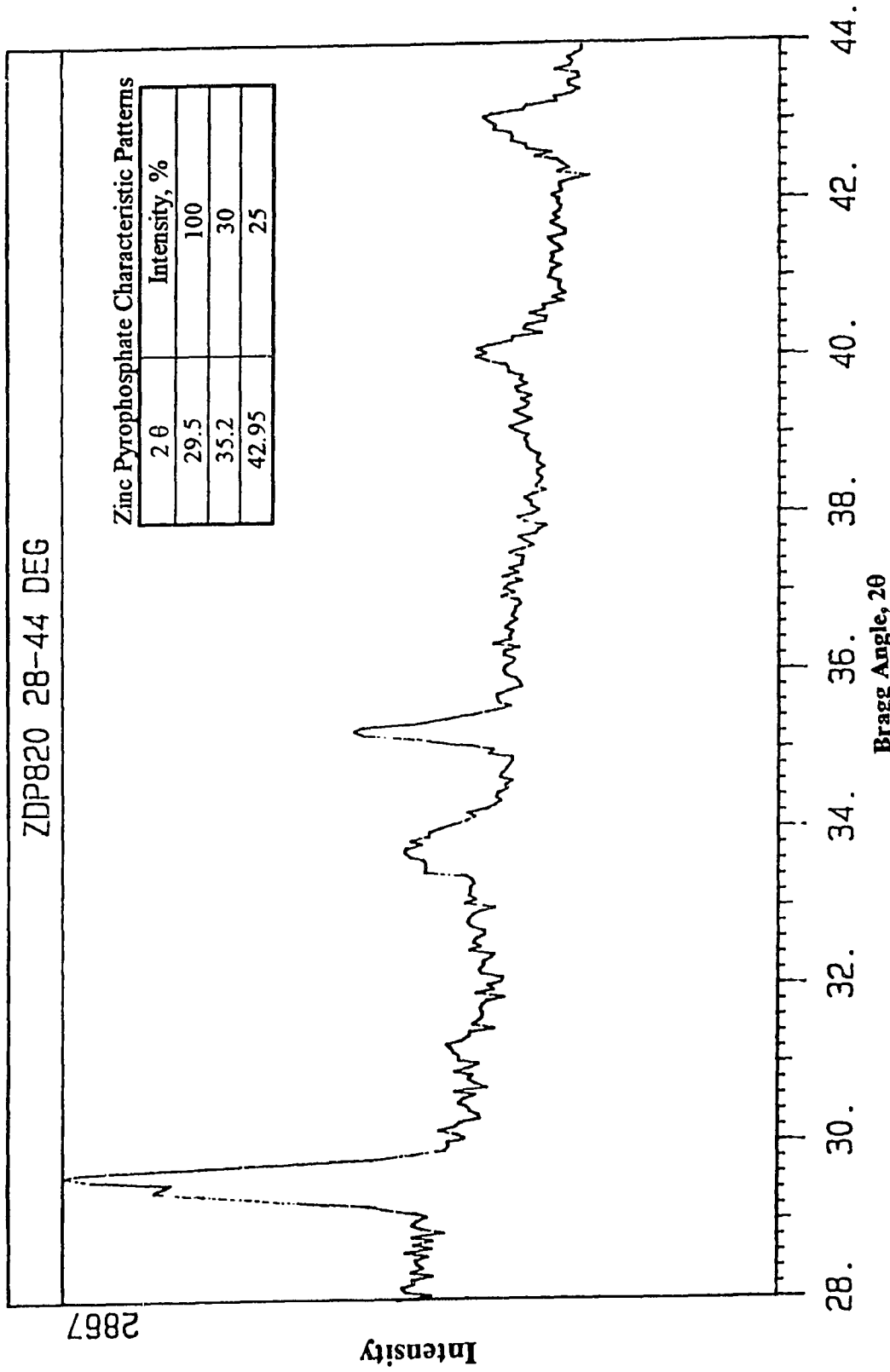
Figure 4.65 X-ray Diffraction Patterns of Catalyst Aged with ZDP at 820 °C.
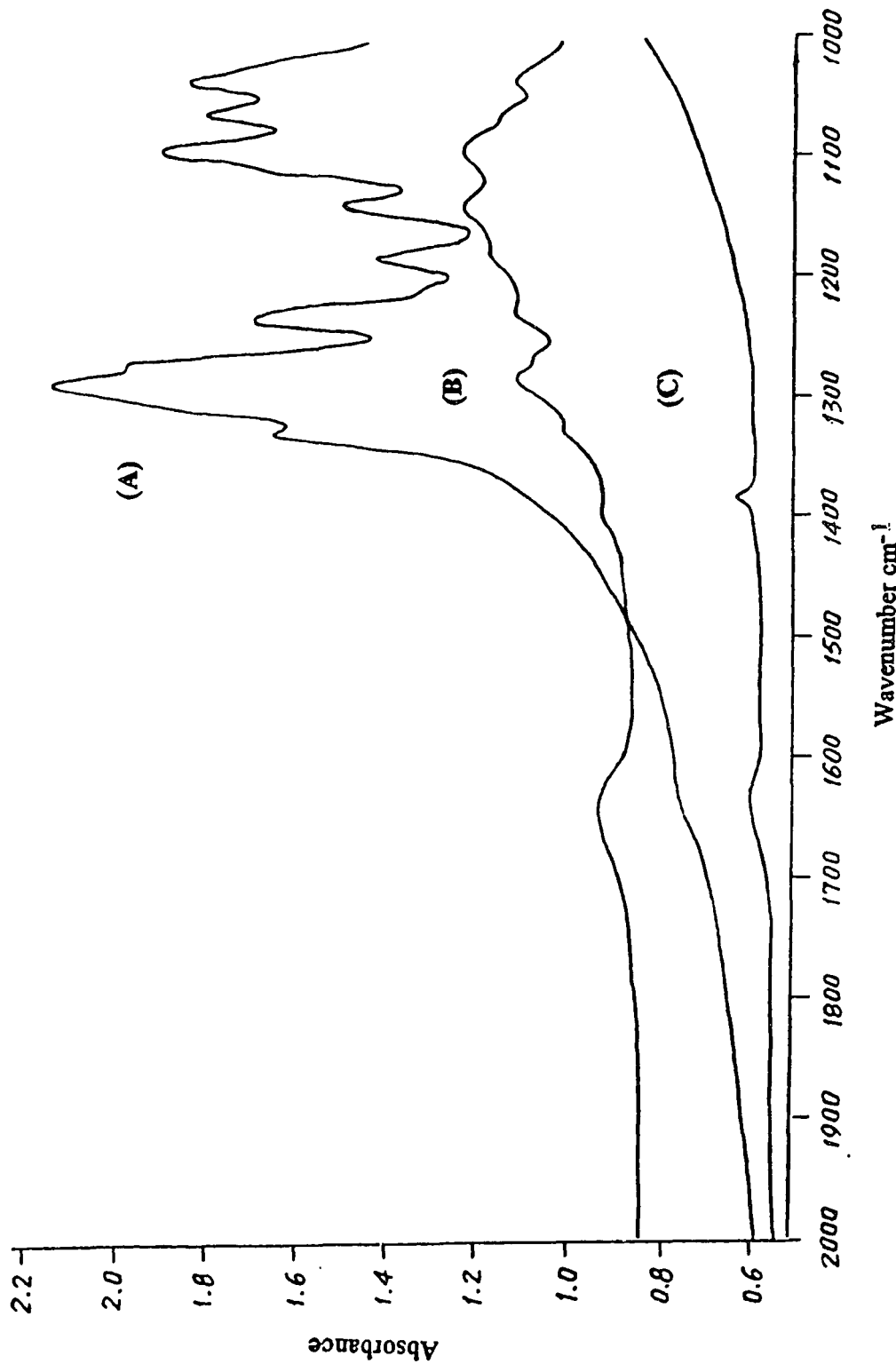
Figure 4.66 Comparison of FT-IR Spectra of the ZDP Combustion Products and the Catalyst Aged with ZDP at 500 °C: (A) ZDP Combustion Products, (B) Catalyst Aged at 500 °C, (C) Fresh Catalyst.
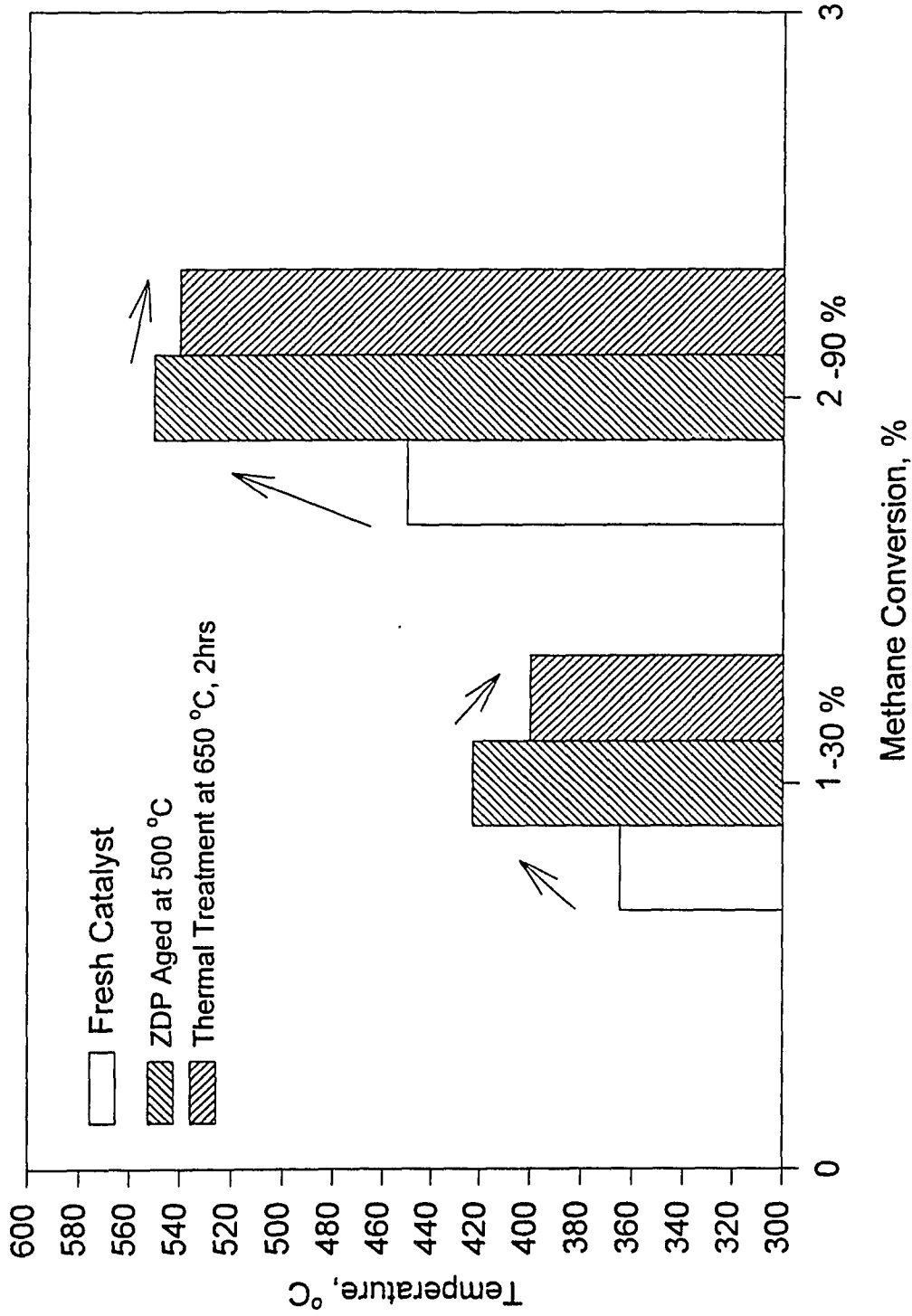
Figure 4.67 Thermal Treatment Effect on Methane Oxidation over ZDP Aged Catalyst

The Catalyst was aged with ZDP at 120,000 simulated miles.
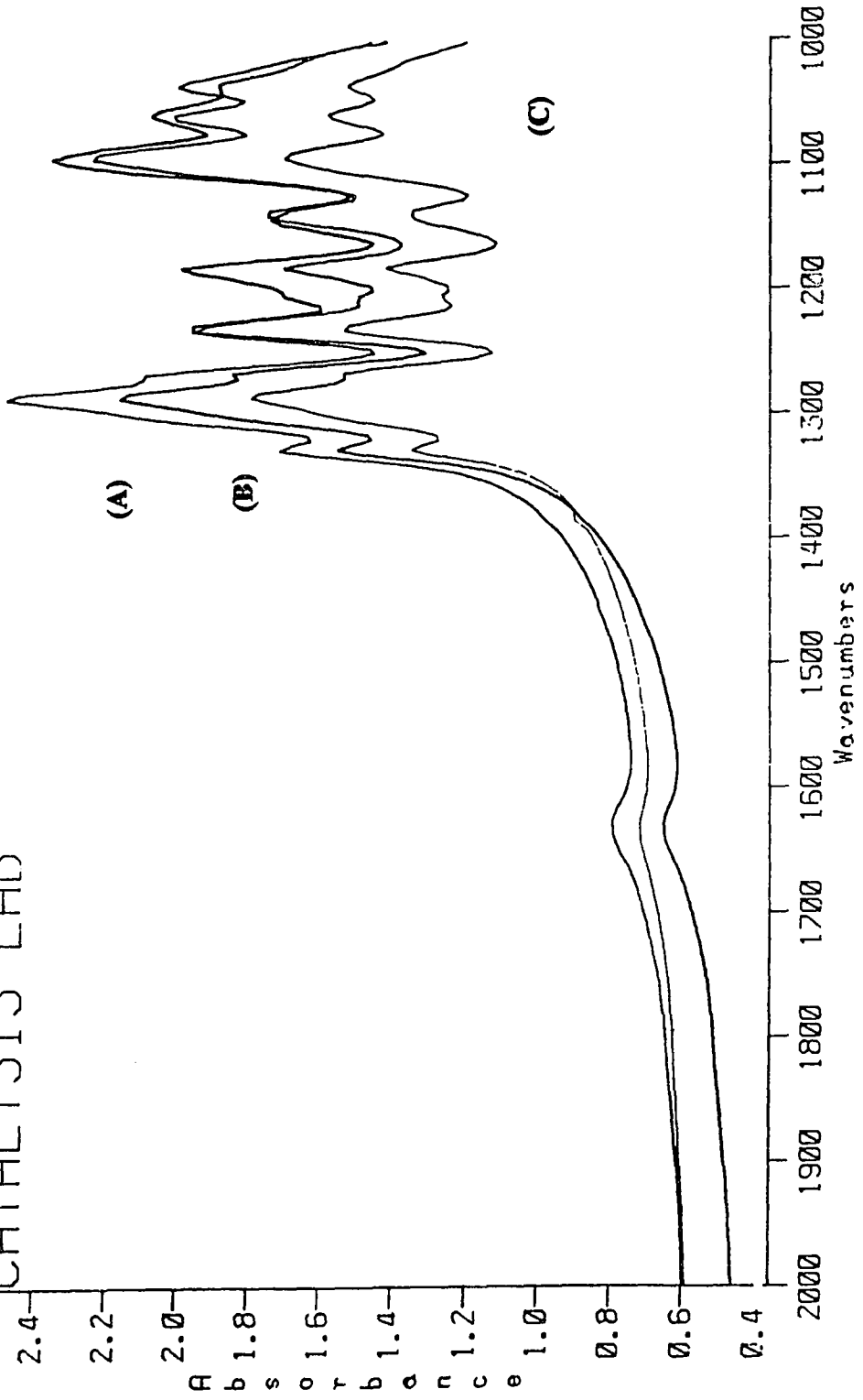
Figure 4.68 The FT-IR Spectra of Different Treatment of ZDP Aged Catalyst: (A) ZDP Aged Catalyst, (B) Thermal Treat at 650 °C, (C) H_2 Treatment at 600 °C.
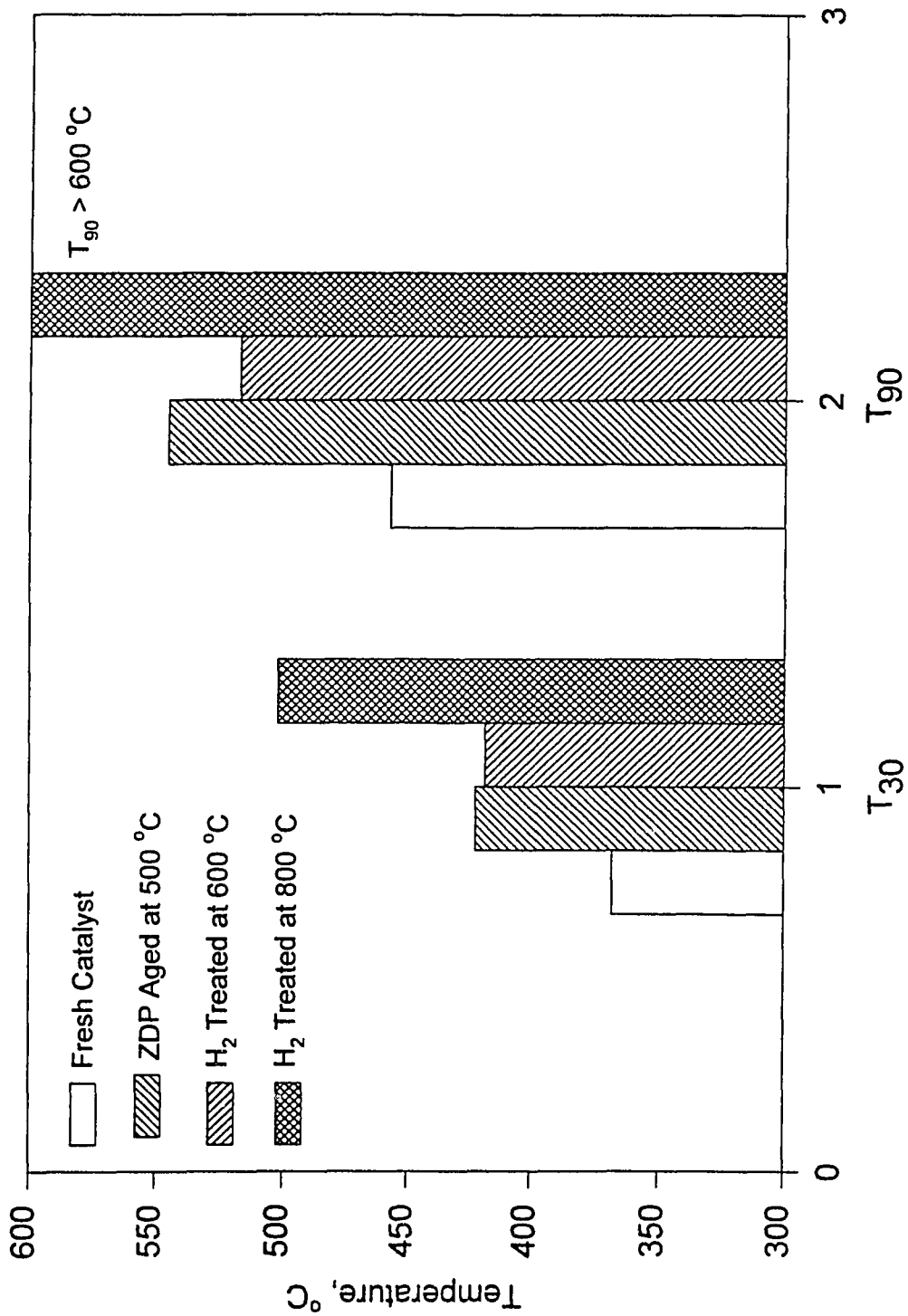
Figure 4.69 The Effects of H_2 Treatment on Methane Oxidation over ZDP Aged Palladium Catalysts

The Catalyst was aged with ZDP at 120,000 simulated miles.
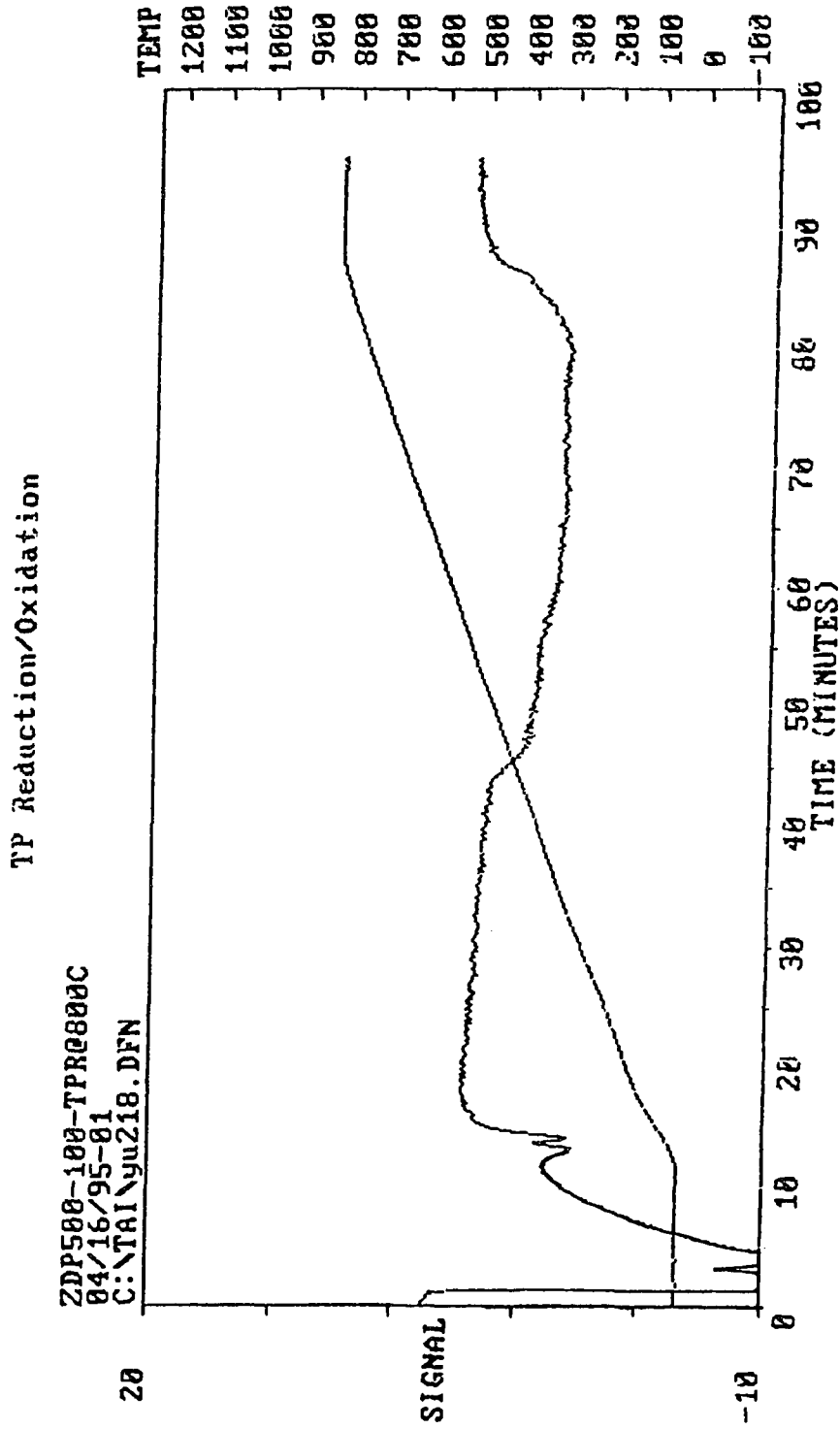
Figure 4.70 Temperature Programmed Reduction of ZDP Aged Catalyst.

CATALYSIS LAB
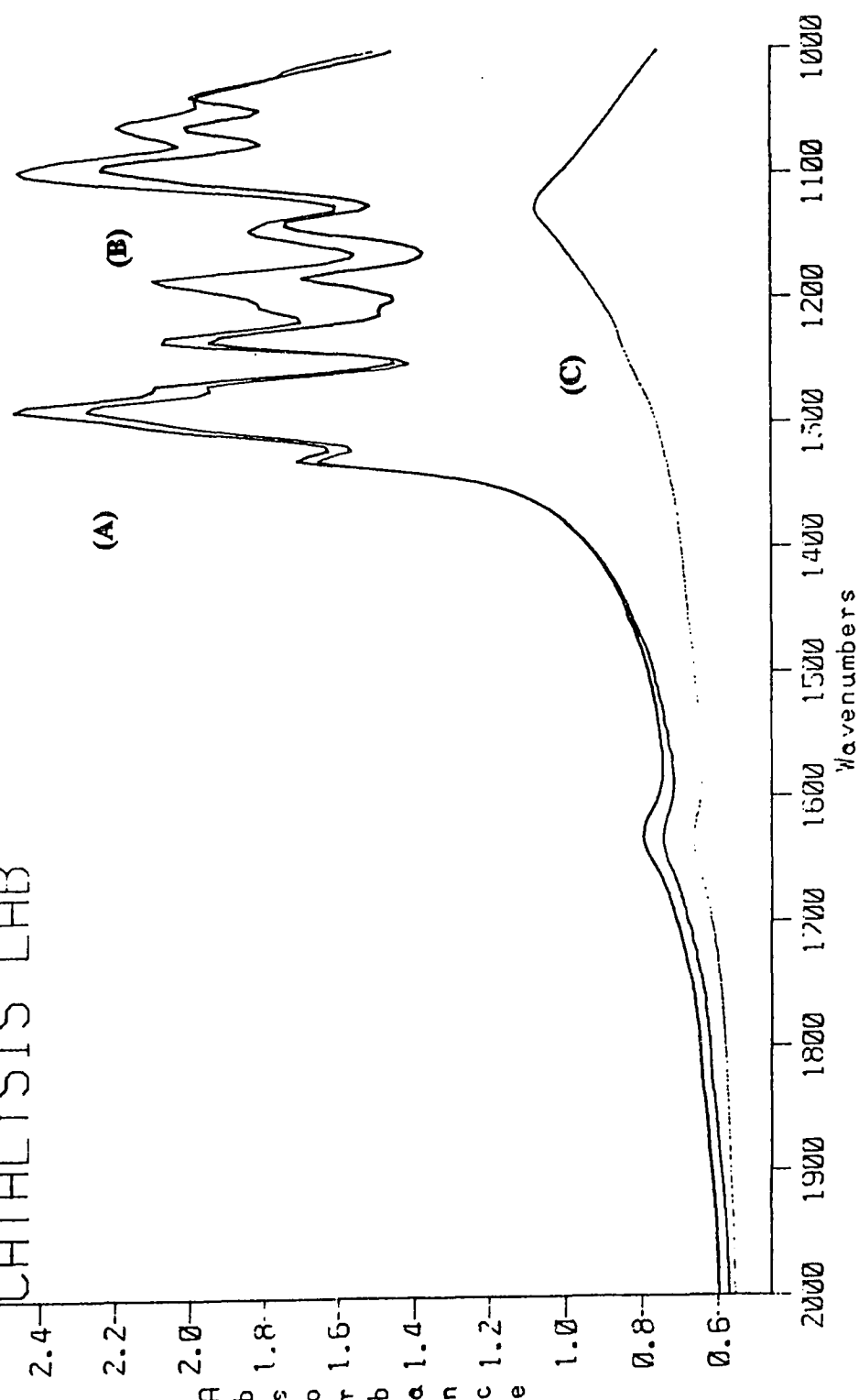
Figure 4.71 Comparison of FT-IR Spectra of Different Hydrogen Treatment Temperature Effects on ZDP Aged Catalyst: (A) ZDP Aged Catalyst, (B) H_2 Treatment at 600 °C, (C) H_2 Treatment at 800 °C.

APPENDIX C

RAW DATA FOR CHAPTER 4

Table C.1 Methane Oxidation Conversion as a Function of Temperature over Catalyst Aged by Varies Treatment at 500 °C

Temperature, °C	Fresh catalyst	1% HCl in air	Air	1.5 % H_2O in air	1% Cl_2 in air	1.5 % H_2O + 1% HCl in air
300	4.5	0	3.0	5.0	0.0	0
320	17.0	0	19.5	20.0	3.5	1.0
340	39.0	1.0	42.0	40.0	20.0	13.0
360	69.8	6.8	74.0	78.0	69.0	50.5
380	91.2	42.5	93.0	92.0	87.0	80.0
400	95.5	80.0	96.8	95.0	93.0	90.0
420	98.2	92.0	98.7	98.0	97.0	95.0
440		96.5				98.0

1. All the catalyst were aged at space velocity 44,000 v/v/hr for 24 hours.
2. The methane oxidation conversion was tested under 88,000 v/v/hr space velocity.
3. The concentration of methane was 1% methane in air.

Table C.2 H_2 Regeneration Effect on Methane Oxidation Conversion as a Function of Temperature over the Catalyst Aged by HCl at 300 °C.

Temperature, °C	Fresh catalyst	1% HCl in air	H_2 Regeneration
300	4.5	0	2.5
320	17.0	0	10.0
340	39.0	5.0	30.0
360	69.8	24.8	56.2
380	91.2	58.2	81.0
400	95.5	88.0	91.0
420	98.2	95.0	96.0
440		98.0	

1. The aged catalyst was regenerated by H_2 at 200 °C for 2 hours and oxidized by air at 500 °C for 2 hours.
2. The methane oxidation activity was tested at space velocity of 88,000 v/v/hr.

Table C.3 Water Vapor Effect on Regeneration of Catalyst Aged by HCl at 500 °C

Time, hrs	Treatment	Methane conversion, %
0	Fresh catalyst	90
15	Air calcination at 500 °C	89
16	1% HCl in air aged at 500 °C	21
17	1% HCl in air aged at 500 °C	23
40	1.5 % H_2O vapor regenerated at 500 °C	53
83	1.5 % H_2O vapor regenerated at 500 °C	54

1. The methane oxidation activity was tested at 377 °C and 88,000 v/v/hr.

Table C.4 Methane Oxidation Conversion over Fresh Catalyst as a Function of W/V

Temperature, °C	W/V= 0	W/V = 0.012	W/V = 0.024	W/V = 0.036	W/V = 0.048	W/V = 0.06
250	0	0.010	0.021	0.038	0.043	0.061
260	0	0.022	0.042	0.063	0.064	0.083
270	0	0.045	0.061	0.096	0.102	0.150
280	0	0.063	0.099	0.153	0.188	0.214
290	0	0.103	0.171	0.231	0.300	0.400
300	0	0.198	0.297	0.324	0.401	0.057

1. W/V = g-sec/cm^3

Table C.5 Catalytic Oxidation of Methane over Fresh Palladium Catalysts as a Function of Temperature

Temperature, °C	Methane Conversion, W/V= 0.036 g-sec/cm^3	Methane Conversion, W/V= 0.06 g-sec/cm^3
250	0.038	0.061
260	0.063	0.083
270	0.096	0.150
280	0.153	0.214
290	0.231	0.400
300	0.324	0.570
310	0.430	0.720
320	0.581	0.840
330	0.720	0.910
340	0.854	0.950
350	0.928	0.970
360	0.974	0.991
370	0.990	
380	0.996	

Table C.6 Methane Oxidation Conversion over H$_2$S Poisoned Catalyst as a Function of W/V

Temperature, °C	W/V= 0	W/V = 0.012	W/V = 0.024	W/V = 0.036	W/V = 0.06
280	0	0.008	0.015	0.020	0.028
300	0	0.018	0.023	0.041	0.045
320	0	0.034	0.049	0.077	0.094
340	0	0.058	0.086	0.110	0.175
360	0	0.089	0.119	0.187	0.282
360	0	0.122	0.223	0.256	0.416

1. W/V = g-sec/cm^3

2. Catalyst treated by 80 ppm H$_2$S in air at 400 °C for 24 hours

Table C.7 Catalytic Oxidation of Methane over H_2S Poisoned Palladium Catalysts as a Function of Temperature

Temperature, $^\circ$C	Methane Conversion, W/V= 0.036 g-sec/cm^3	Methane Conversion, W/V= 0.06 g-sec/cm^3
280	0.020	0.028
300	0.041	0.045
320	0.077	0.094
340	0.110	0.175
360	0.187	0.282
380	0.256	0.416
400	0.391	0.582
420	0.572	0.739
440	0.721	0.878
460	0.846	0.964
480	0.932	
500	0.979	

1. Catalyst treated by 80 ppm H_2S in air at 400 $^\circ$C for 24 hours.

Table C.8 H_2S Oxidation over 4% PdO/γ-Alumina Catalyst as a Function of Temperature

Temperature, $^\circ$C	H_2S Conversion, %
100	43.4
130	64.0
150	91.2
200	95.3
300	100
400	100

1. The initial concentration of H_2S in air was 80 ppm. The catalyst was charged 0.3 g for each reaction temperature and the flow rate of the feed stream was 260 cm^3/min.
2. The H_2S concentration was measured when the H_2S had been introduce for 20 minutes.

Table C.9 H_2S Oxidation over 4% PdO/γ-Alumina Catalyst at 200 $^\circ$C as a Function of Time

Time, hours	H_2S conversion, %	Time, hours	H_2S conversion, %
1	95.3	19	86.0
2	95.0	20	86.7
15	90.4	21	86.3
16	87.0	22	70.0
17	86.0	23	68.5
18	85.5	24	67.7

1. The catalyst was charged for 0.3 g and the flow rate of the feed stream was 260 cm^3/min in this experiment.

Table C.10 Methane Oxidation over 4% PdO/γ-Alumina Fresh and Poisoned Catalyst as a Function of Temperature

Temperature, °C	Fresh catalyst	Catalyst poisoned at 100 °C	Catalyst poisoned at 200 °C	Catalyst poisoned at 300 °C	Catalyst poisoned at 400 °C
240	4.0				
260	8.3				1.1
280	21.4	2.3			2.8
300	56.8	6.0	5.6		4.5
320	84.8	11.9	10.6	7.2	8.5
340	95.0	22.5	20.4	19.3	16.6
360	100	53.6	33.2	33.9	28.2
380		77.0	56.8	55.0	41.6
400		90.5	80.5	68.5	58.0
420		100	94.0	85.0	73.9
440			100	95.0	87.8
460				100	96.4

1. The methane oxidation activity was tested at W/V = 0.06 g-sec/cm³.
2. 0.3 g catalyst was aged at flow rate of 260 cm³/min for 24 hours.

Table C.11 H_2 Treatment Effect on Methane Oxidation over Catalyst Poisoned by H_2S at 400 °C as a Function of Temperature

Temperature, °C	Fresh catalyst	Catalyst aged at 400 °C	H_2 regeneration at 600 °C
240	4.0		
250	6.1		
260	8.3	1.1	3.0
270	15.0		5.0
280	21.4	2.8	7.2
290	40.0		14.1
300	56.8	4.5	20.9
320	84.8	8.5	50.0
340	95.0	16.6	82.7
360	99.1	28.2	94.6
380		41.6	100
400		58.0	
420		73.9	
440		87.8	
460		96.4	

1. The poisoned catalyst was regenerated by H_2 from 25 °C to 600 °C and calcined in air atmosphere at 500 °C for 2 hours.
2. The methane oxidation activity was tested at W/V = 0.06 g-sec/cm³.

Table C.12 Catalytic Oxidation of Methane over Palladium Catalysts in the Presence of H₂S.

Time, min	Methane Conversion at 300 °C	Time, min	Methane Conversion at 400 °C
0	0.246	0	0.981
30	0.188	30	0.904
60	0.126	60	0.831
70	0.086	90	0.766
80	0.084	120	0.686
90	0.067	150	0.586
120	0.027	180	0.51
180	0.009	210	0.348
		240	0.249
		300	0.155
		330	0.128
		360	0.121
		390	0.119

1. The weight residence time, W/V = 0.012 g-sec/cm³.

Table C13 Simulation of TBP and ZDP Effect on Methane Oxidation on 4% PdO/ γ-Alumina Catalyst.

Pulsator-aged simulated miles	Fresh catalyst	TBP, methane conversion, %	ZDP, methane conversion, %
0	95.2	95.2	95.2
30,000	94.1	82.6	66.0
60,000	93.8	76.7	54.0
90,000	94.0	70.7	44.5
120,000	94.1	66.0	41.9

1. The catalyst was aged at 500 °C, 44,000 v/v/hr.
2. The pump flow rate of the TBP and ZDP were 0.05 cm³/min.
3. The methane activity was tested at 500 °C, 44,000 v/v/hr.

Table C. 14 Methane Oxidation Conversion as a Function of Temperature over Fresh, TBP and ZDP Aged Catalyst

Temperature, °C	Methane conversion, % (fresh catalyst)	Methane conversion, % (TBP aged)	Methane conversion, % (ZDP aged)
260	4.3	1.5	0
280	7.5	2.1	0
300	14.0	3.2	1.2
320	31.9	5.6	1.7
340	48.4	11.3	1.9
360	57.2	19.7	4.2
380	66.6	24.5	7.8
400	73.5	33.2	14.2
420	81.6	41.5	18.3
440	95.2	47.7	23.0
460	90.1	53.5	29.7
480	92.3	59.3	36.0
500	95.2	66.0	41.9
520		69.2	48.0
540		74.0	52.3
560		78.2	55.2
580		81.3	59.1
600		83.6	62.0

1. The methane oxidation activity was tested by using 1% methane in air at 44,000 v/v/hr.

Table C.15 Heat Treatment Effect on Methane Oxidation over TBP Aged Catalyst as a Function of Temperature.

Temperature, °C	Methane conversion, % (fresh catalyst)	Methane conversion, % (TBP aged catalyst[1])	Methane conversion, % (heat treatment[2])
280	6.8		
300	12.1	7.1	7.4
320	19.9	11.4	11.7
340	34.9	18.6	19.8
360	67.3	28.7	31.1
380	83.0	41.0	50.4
400	90.3	56.3	76.0
420	96.3	85.0	93.5
440		95.8	98.1

1. The catalyst was aged by TBP in 60,000 simulated miles at 500 °C, 44,000 v/v/hr.
2. The aged catalyst was regenerated by heat treatment at 650 °C for 2 hours.
3. The methane activity was tested at 88,000 v/v/hr.

Table C.16 Methane Oxidation Conversion as a Function of Temperature over fresh and P_2O_5 Aged Catalyst.

Temperature, $^{\circ}C$	CH_4 conversion, % (fresh catalyst)	CH_4 conversion, % (P_2O_5/500 $^{\circ}C$)	CH_4 conversion, % (P_2O_5/820 $^{\circ}C$)
260	4.3	0.0	0.0
280	7.5	0.0	0.0
300	14.0	0.5	0.0
320	31.9	2.1	0.0
340	48.4	8.0	0.0
360	57.2	15.0	1.0
380	66.6	24.2	2.1
400	73.5	37.2	3.5
420	81.6	45.0	5.4
440	85.2	52.1	12.5
460	90.1	57.8	19.5
480	92.3	63.1	23.2
500	95.2	65.7	29.7
520		69.2	33.2
540		70.0	37.1
560		71.0	40.6
580		72.3	42.0
600		73.5	44.2

1. 0.4g catalysts were aged by mixing with 0.52 g P_2O_5 at 500 $^{\circ}C$ and 820 $^{\circ}C$ for 3 hours respectively. The methane activity was tested at 44,000 v/v/hr.

Table C. 17 The Data for the Plots of -Ln $(1-X_A)$ Versus W/V for Methane Oxidation over Fresh Catalyst.

W/V, g-sec/cm³	0	0.01	0.013	0.016	0.022	0.036
-Ln $(1-X_A)$/280 $^{\circ}C$	0.0	0.027	0.029	0.034	0.055	0.078
-Ln $(1-X_A)$/290 $^{\circ}C$	0.0	0.044	0.047	0.051	0.079	0.114
-Ln $(1-X_A)$/300 $^{\circ}C$	0.0	0.056	0.061	0.066	0.104	0.151
-Ln $(1-X_A)$/310 $^{\circ}C$	0.0	0.075	0.088	0.09	0.147	0.206
-Ln $(1-X_A)$/320 $^{\circ}C$	0.0	0.094	0.115	0.107	0.193	0.27
-Ln $(1-X_A)$/330 $^{\circ}C$	0.0	0.108	0.140	0.158	0.264	0.349

Table C.18 CO and Propane Oxidation Conversion as a Function of Temperature over Fresh and ZDP Aged Catalyst.

Temperature, °C	CO conversion, % (fresh catalyst)	CO conversion, % (ZDP aged)	Temperature, °C	Propane conversion, % (fresh catalyst)	Propane conversion, % (ZDP aged)
100	0.5		220	5.8	0.0
120	12.9	0.0	240	7.3	0.0
140	93.9	0.0	260	8.5	0.7
160	99.8	0.0	280	15.5	2.2
180	100	26.9	300	32.4	5.6
200	100	57.3	320	73.2	21.3
240		78.5	340	97.2	43.2
260		92.0	360	99.0	59.6
		96.8	380	100.0	80.0
			400	100.0	85.0
			420	100.0	89.3
			440	100.0	92.5

1. The CO and propane oxidation activity were tested at 44,000 v/v/hr.
2. 1% CO in air and 1% propane in air were the activity diagnostic gas.

Table C. 19 The Data for the Plots of -Ln (1-X_A) Versus W/V for Methane Oxidation over ZDP Aged Catalyst.

W/V, g-sec/cm³	0	0.009	0.012	0.014	0.021
-Ln (1-X_A)/360 °C	0.0	0.043	0.057	0.063	0.109
-Ln (1-X_A)/370 °C	0.0	0.0710	0.0920	0.105	0.130
-Ln (1-X_A)/380 °C	0.0	0.092	0.117	0.126	0.178
-Ln (1-X_A)/390 °C	0.0	0.105	0.137	0.161	0.236
-Ln (1-X_A)/400 °C	0.0	0.130	0.174	0.191	0.274

Table C.20 The Data for Arrhenius Plots of Ln k Versus 1/T for Methane Oxidation over Fresh and ZDP Aged Catalyst.

1000/T, k⁻¹	Ln k¹, cm³/g-sec	1000/T, k⁻¹	Ln k², cm³/g-sec
1.66	2.30	1.49	2.57
1.69	2.01	1.51	2.42
1.72	1.74	1.53	2.14
1.75	1.42	1.56	1.92
1.78	1.13	1.58	1.63
1.81	0.78		

1. This is for fresh catalyst logarithm rate constant.
2. This is for ZDP aged catalyst logarithm rate constant

Table C.21 Thermal Treatment Effect on Methane Oxidation over ZDP Aged Catalyst.

Temperature, °C	CH$_4$ conversion, % (fresh catalyst)	CH$_4$ conversion, % (ZDP aged)	CH$_4$ conversion, % (Thermal treatment)
320	11.5	0.0	
340	18.2	1.3	
360	26.1	5.5	9.6
380	39.2	11.0	19.0
400	59.5	16.0	30.4
420	74.6	28.0	42.9
440	86.4	37.5	56.6
460	92.9	45.8	64.8
480	96.6	57.0	70.9
500		72.8	78.2
520		82.1	83.9
540			89.1

1. The methane oxidation activity was tested at 88,000 v/v/hr.

Table C. 22 H$_2$ Treatment Temperature Effect on Methane Oxidation over ZDP Aged Catalyst.

Temperature, °C	CH$_4$ conversion, % (fresh catalyst)	CH$_4$ conversion, % (ZDP aged)	CH$_4$ conversion, % (H$_2$ treatment at 600 °C)	CH$_4$ conversion, % (H$_2$ treatment at 800 °C)
320	11.5	0.0	0.6	
340	18.2	1.3	3.2	1.0
360	26.1	5.5	8.4	1.8
380	39.2	11.0	15.5	3.6
400	59.5	16.0	23.0	4.9
420	74.6	28.0	33.0	7.4
440	86.4	37.5	44.7	11.0
460	92.9	45.8	58.0	14.4
480	96.6	57.0	72.1	22.4
500		72.8	85.3	29.8
520		82.1	93.4	35.2
540			97.0	42.1

1. The methane oxidation activity was tested at 88,000 v/v/hr.

REFERENCES

Altamira Instruction Manual, 1990. "BET Surface Area Measurement," Altamira Instruments, Inc., Pittsburgh, PA 15238, June.

Ansell, Graham P., Stanislaw E. Golunski, Helen A. Hatcher and Raj R. Rajaram, 1991. "Effects of SO$_2$ on the Alkane Activity of Three-way Catalysts," *Catalysis Letters*, **11**, 183-190.

Atkins, P. W., 1982. *Physical Chemistry, 2nd Edition*, W, H. Freeman and Company, San Francisco, CA.

Bailar Jr, J. C., 1973. *Comprehensive Inorganic Chemistry, Group VIII A, B and C*, Pergamon Press Headington Hill Hall Oxford, UK.

Baker, E. G. et al., 1989. "Catalytic Destruction of Hazardous Organics in Aqueous Waste: Continuous Reactor System Experiments," *Hazardous Waste & Hazardous Materials*, Vol. 6, No. 1.

Barbier, J., D. Bahloul and P. Marecot, 1991. "Effect of Chloride on Sintering of Pt/Al$_2$O$_3$ Catalysts," *Catalysis Letters*, **8**, 327-334.

Berg, Magnus and Sven Jaras, 1994. " Catalytic Combustion of Methane over Magnesium Oxide," Applied Catalysis A: General **114**, 227-241.

Bond, G. C., 1973. "Catalytic Destruction of Chlorinated Hydrocarbons," US Patent No. 1485735.

Bond, Geoffrey C. and Nasser Sadeghi, 1975. "Catalytic Destruction of Chlorinated Hydrocarbons," *J. Appl. Chem.* Biltechnol., **25**, 241-248.

Brunauer, S., P. H. Emmett, and E. Teller, 1938. "Adsorption of Gases in Multimolecular Layers," *J. Am. Chem. Soc.*, **60**, 309.

Burch R. and Urbano F. J., 1995. "Investigation of the Active State of Supported Palladium Catalysts in the Combustion of Methane," *Applied Catalysis* A: General **124**, 121-138.

Butt, Jonh B. and Eugene E. Petersen, 1988. *Activation Deactivation, and Poisoning of Catalysts*, Academic Press, Inc., San Diego, CA.

Chang, Charles C., 1978. "Infrared Studies of SO$_2$ on γ-Alumina", *J. of Catalysis*, **53**, 374-385.

Chen, James, Ronald M. Heck and Robert J. Farrauto, 1992. "Deactivation Regeneration and Poison-Resistant Catalysts: Commercial Experience in Stationary Pollution Abatement," *Catalysis Today*, 11, 517-545.

Corbridge, D. E. C., 1978. *Phosphorus-An Outline of its Chemistry, Biochemistry and Technology*, p. 1-3, Elsevier Scientific Publishing Co. New York, NY.

Cullis, C. F. and D. E. Keene, 1970. "Studies of the Partial Oxidation of Methane over Heterogeneous Catalysts," *J. of Catalysis*, 19, pp. 378-385.

Deng, Youquan and Thomas G. Nevell, 1993. "Sulfur Poisoning, Recovery and Related Phenomena over Supported Palladium, Rhodium and Iridium Catalysts for Methane Oxidation," *Applied Catalysis* A: General, 101, 51-62.

Drury, Carol and Scott Whitehouse, 1994. "The Effect of Lubricant Phosphorus Level on Exhaust Emissions in a Field Trial of Gasoline Engine Vehicles," *SAE* Paper No. 940745.

Exxon Chemical Americas, PARANOX 15 MSDS No. 81850000, 1995. "Lube Oil Additive Containing Zinc Salt of Diakyldithiophosphoric Acid in oil," Houston, TX.

Farratuto, Robert J. and John J. Mooney, 1992. "Effects of Sulfur on Performance of Catalytic Aftertreatment Devices," *SAE* Paper No. 920557.

Farrauto, R. J., M. C. Hobson, T. Kennelly, E. M. Waterman, 1992. "Catalytic Chemistry of Supported Palladium for Combustion of Methane," *Applied Catalysis, A:* General, 81, 227-237.

Farrauto, Robert J., 1974. "Determination and Applications of Catalytic Surface Area Measurements," *AIChE, Symposium Series*, Vol. 70, No. 143.

Farrauto, Robert J., Ronald M. Heck, and Barry K. Speronello, 1992. "Environmental Catalysts," Special Report, *C&EN*, Sep. 7, 34-44.

Fogler, H. Scott, 1986. *Elementals of Chemical Reaction Engineering*, Prentice-Hall, Inc., Englewood, NJ.

Gandhi, H. S. and M. Shelef, 1991. "Effects of Sulphur on Noble Metal Automotive Catalysts," *Applied Catalysis*, 77, 175-186.

Gandhi, H. S., A. G. Piken, M. Shelef and R. G. Delosh, 1976. "Laboratory Evaluation of Three-Way Catalysts," *SAE* Paper No. 760201.

Hartley, F. R., 1973. *The Chemistry of Platinum and Palladium*, John Wiley and Sons, New York, NY.

Heck, Ronald M. and Robert J. Farrauto, 1995. *Catalytic Air Pollution Control: Commercial Technology*, Van Nostrand Reinhold, New York, NY.

Hepburn, Jeffrey S., Ken S. Patel, Mario G, Meneghel, Haren S. Gandhi, Engelhard Three Way Catalyst Development Team and Johnson Matthey Three Way Catalyst Development Team, 1994. "Development of Pd-only Three Way Catalyst Technology," *SAE* Paper No. 941058.

Hicks, Robert F., Haihua Qi, Michael L. Young, and Raymond G. Lee, 1990. "Structure Sensitivity of Methane Oxidation over Platinum and Palladium," *J. of Catalysis* **122**, 280-294.

Hoyos, Luis Jacier, Michel Primet and Helene Praliaud, 1992. "Sulfur Poisoning and Regeneration of Palladium-based Catalyst: Part 1-Dehydrogenation of Cyclohexane on Pd/Al$_2$O$_3$ and Pd/SiO$_2$-Al$_2$O$_3$ Catalysts," *Chem. Soc. Faraday Trans.*, **88**(1), 113-119.

Hoyos, Luis Jacier, 1993. "Catalytic Combustion of Methane over Palladium Supported on Alumina and Silica in Presence of Hydrogen Sulfide," *Applied Catalysis* A: General, **98**, 125-138.

Hubbard, C. P., K. Otto, H. S. Gandhi, and K. Y. S. Ng, 1993. "Effects of Support Material and Sulfation on Propane Oxidation," *J. of Catalysis*, **144**, 484-494.

Hucknall, D. J., B. M. Willatt and R. J. Hockham, 1980. "Studies of the Deactivation of Supported Palladium Catalysts by Halogenocarbons," *Catalyst Deactivation*, Elsevier, 213-232.

Inoue, Kiyoshi, Takao Kurahashi, Tatsuo Negishi, Kenyu Akiyama, Kazutaka Arimura, and Kazuyoshi Tasaka, 1992. "Effects of Phosphorus and Ash Contents of Engine Oils on Deactivation of Monolithic Three-Way Catalysts and Oxygen Sensors", *SAE* Paper No. 920654.

Lester, George R., 1990. "Catalytic Destruction of Organohalogen Compounds," International Patent BOID 53/36, BOIJ 23/64, A62D3100, International Publication No. WO 90/13352.

Levenspiel, Octave, 1972. *Chemical Reaction Engineering*, John Wiley and Sons, Inc. New York, NY.

Li, Yuejin and John N. Armor, 1994. "Catalytic Combustion of Methane over Palladium Exchanged Zeolites," *Applied Catalysis* B: Environmental, **3**, 275-282.

Lisitsyn, A. S., S. V. Gurevich, A. L. Chuvilin, A. I. Boronin, V. I. Bukhtiyarov and V. A. Likholobov, 1989. "Reaction Kinetics," *Catalysis Letter*, **38**, 109.

Marecot, P., A. Fakche, B Kellali, G. Mabilon, M. Prigent and J. Barbier, 1994. "Propane and Propene Oxidation over Platinum and Palladium on Alumina: Effects of Chloride and Water," *Applied Catalysis* B: Environmental 3, 283-294.

Mendyka, Bozina, Anna Musialik-Piotrowsks and Krystyna Syczewska, 1992. "Effect of Chlorine Compounds on the Deactivation of Platinum Catalysts," *Catalysis Today*, 11, 597-610.

Miciukiewicz J., 1989. "The Effect of Phosphorous-Alumina on Hydrotreatment Catalysts," *Applied Catalysis*, 49, 261-271.

Mouaddib, Najat, Christiane Feumi-Jantou, Edouard Garbowski and Michel Primet, 1992. "Catalytic Oxidation of Methane over Palladium Supported on Alumina: Influence of the Oxygen to Methane Ratio," *Applied Catalysis* A: General, 87, 129-144.

New Jersey Department of Health, 1986. "Hazardous Substance Fact Sheet: Trichloroethylene," Trenton, NJ 08625.

Novinson, T., 1989. "Chemical Detoxification of Polychlorinated Biphenyls (PCBs)," US Patent 4804779, Feb. 14.

Nyquist, Richard A. and Ronald O. Kagel, 1971. *Infrared Spectra of Inorganic Compounds*, Academic Press, Inc., New York, NY.

Oh, S, H., P. J. Mitchell and R. M. Siewert, 1991. " Methane Oxidation over Alumina-Supported Noble Metal Catalysts with and without Cerium Additives," *J. of Catalysis* 132, 287-301.

Oh, S. H., P. J. Mitchell and R. M. Siewert, 1992. "Methane Oxidation over Noble Metal Catalysts as Related to Controlling Natural Gas Vehicle Exhaust Emissions," *ACS Symposium Series* 495, 12-25.

Olfenbuttel, R., 1991. "New Technologies for Cleaning up Contaminated Soil and Groundwater," A Battelle Special Report on Soil Remediation.

Otto, K, 1989. "Methane Oxidation over Pt on Gamma-Alumina: Kinetics and Structure Senstivity," *Langmuir* 5, 1364-1369.

Pope, D., D. S. Walker and R. L. Moss, 1978. "Evaluation of Platinum-Honeycomb Catalysts for the Destructive Oxidation of Low Concentrations of Odorous Compounds in Air," *Atm. Environ.*, Vol. 12, 1921-1927.

Ramanathan, K., J. J. Spivey, 1989. "Catalytic Oxidation of 1,1-Dichloroethane," *Combustion Sci. & Tech.*, 63, 247-255.

Satterfield, Charles N., 1980. *Heterogeneous Catalysis in Practice*, McGraw-Hill Book Co., New York, NY.

Senken, S. M., W. D. Chang and S. B. Karra, 1986. "A Detailed Mechanism for the High Temperature Oxidation of C_2HCl_3," *Combustion Sci. & Tech.*, Vol. 47, 229-237.

Shaw, Henry, Jun Du, and Anthony E. Cerkanowicz, 1991. "The Oxidation of Methylene Chloride Over Manganese Dioxide Catalyst," Presented as Paper 60a at the AIChE Pittsburgh National Meeting.

Shaw, Henry, T-C. Yu, Y. Wang and Anthony E. Cerkanowicz, 1993. "Catalytic Oxidation of Trichloroethylene and Methylene Chloride," *ACS Symposium Series*, 518: 358-379.

Shaw, Henry, 1974. "The Effect of Water, Pressure, and Equivalence Ratio in Nitric Oxide Production in Gas Turbines," Trans. ASME, Series A, *Journal of Engineering for Power*, 96, 240-246.

Simone, Dianne O., Teresa Kennelly, Nancy L. Brungard and Robert J. Farrauto, 1991. "Reversible Poisoning of Palladium Catalysts for Methane Oxidation," *Applied Catalysis*, 70, 87-100.

Spivey, John and John Butt, 1992. "Literature Review, Deactivation of Catalysts in the Oxidation of Volatile Organic Compounds," *Catalysis Today*, 11:465-500.

Sreeramamurthy, R., P. G. Menon, 1974. "Oxidation of H_2S on Active Carbon Catalyst," *Journal of Catalysis*, 37, 287-296.

Summers, J. C., J. F. Skowron, W. B. Williamson, and K. I. Mitchell, 1992. "Fuel Sulfur Effects on Automotive Catalyst Performance," *SAE* Paper 920588.

Summers, Jerry C., John E. Sawyer and A. C. Frost, 1992. "The 1990 Clean Air Act and Catalytic Emission Control Technology for Stationary Sources," *ACS Symposium Series*, 45: 98-114.

Thermogravimetric Analyzer, 1992. *TGA 7 Users Manual*, Permin Elmer, Norwalk, CT.

Ueda, Fumio, Shinichi Sugiyama, Kazutaka Arimura, Shigeki Hamaguchi and Kenyu Akiyama, 1994. "Engine Oil Additive Effects on Deactivation on Monolithic Three-Way Catalysts and Oxygen Sensors," *SAE* Paper No. 940746.

Wang, Yi, Henry Shaw and Robert, J. Farrauto, 1992. "Catalytic Oxidation of Trace Concentrations of Trichloroethylene over 1.5% Pt on γ-Al_2O_3," *ACS Symposium Series*, 45 :125-140.

Williams, Frank L., and Kenneth Baron, 1975. "Lead, Sulfur and Phosphorous Interactions with Platinum and Palladium Metal Foils," *J. of Catalysis*, 40, 108-116.

Williamson, W. B., J. Perry, R. L. Goss, G. S. Gandhi and T. E. Beason, 1984. "Catalyst Deactivation Due to Glaze Formation from Oil-Derived Phosphorus and Zinc," *SAE* Paper No. 841406.

Williamson, W. B., H. S. Gandhi, M. E. Heyde and C. A. Zawacki, 1979. "Deactivation of Three Way Catalysts by Fuel Contaminants: Lead, Phosphorus and Sulfur," *SAE* Paper No. 790942.

Williamson, W. B., J. Perry, H. S. Gandhi and J. L. Bomback, 1985. "Effects of Oil Phosphorus on Deactivation of Monolithic Three Way Catalysts," *Applied Catalysis*, 15, 277-292.

Windawi, H., and M. Wyatt, 1993. "Catalytic Destruction of Halogenated Volatile Organic Compounds: Mechanisms of Platinum Catalyst Systems," *Platinum Metals Rev.*, 37, (4), 186-193.

Wise, Edmund M., 1968. *Palladium, Recovery, Properties and Uses*, Academic Press, New York, NY.

Xu, S., 1994. "Catalytic Oxidation of Chlorinated Hydrocarbons over Powder Transition Metal Oxide," M. S. Thesis, New Jersey Institute of Technology, Newark, NJ, May.

Yao, H. C., H. K. Stepien and H. S. Gandhi, 1981. "The Effects of SO_2 on the Oxidation of Hydrocaarbons and Carbon Monoxide over Pt/γ-Al_2O_3 Catalysts," *J. of Catalysis*, 67, 231-236.

Yu, Tai-Chiang, Henry Shaw and Robert, J. Farrauto, 1992, "Catalytic Oxidation of Trichloroethylene over PdO Catalysts," *ACS Symposium Series*, 45:141-152.

Yu, Tai-Chiang, 1991. "Catalytic Oxidation of Chlorinated Compounds over PdO/Al_2O_3 on a Monolith," Master Thesis, New Jersey Institute of Technology, Newark, NJ, May.

Zeldovitch, J., 1946. "The Oxidation of Nitrogen in Combustion and Explosives," *Acta. Physicochimica*, vol. 21, P.577, USSR.